

Enclosure 1

July 28, 1987

DISTRIBUTION
Central Files
DRPR R/F
GLainas
JThoma
KEccleston
ERubenstein
LEngle ✓
SVarga
SRPR R/F

MEMORANDUM FOR: Albert Gibson, Director
Division of Reactor Safety
Division of Reactor Projects, RII

FROM: Gus C. Lainas
Assistant Director for Region II Reactors
Division of Reactor Projects 1/II
Office of Nuclear Reactor Regulation

SUBJECT: TIA - NORTH ANNA UNIT 1 STEAM GENERATOR TUBE FAILURE EVENT

The purpose of this memorandum is to present our interface agreement relative to the recent North Anna Unit 1 steam generator tube failure event.

The following actions and responsibilities are designated in consideration of the enclosed memorandum, "Dircks to Regional Administrators, dated April 13, 1982," Steam Generator Problem.

1. RII to restrict restart of unit and issue CAL. (RII complete)
2. RII to form and dispatch an AIT team to the site with NRR technical and PM assistance. (RII complete) concurrence.
3. AIT Report to be reviewed by RII and NRR prior to issuance. (RII/NRR)
4. Adequacy of SG repairs for North Anna for restart. (NRR/DEST)
5. Generic implications of event. (NRR/DEST)

The contact for the above actions will be L. Engle, who can be reached on FTS 49-29795.

LS
Gus C. Lainas
Assistant Director for Region II Reactors
Division of Reactor Projects 1/II
Office of Nuclear Reactor Regulation

Enclosure:
As stated

cc: T. Murley
J. N. Grace
L. Reyes
J. Sniezek
F. Miraglia
R. Starostecki
J. Richardson

PD11-PPM
LEngle
7/28/87

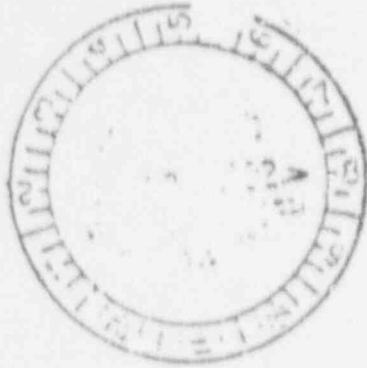
ERubenstein
7/28/87

AD11/DRPR
GLainas
7/28/87

DRPR
SVarga
7/28/87

870731.0173 XA - *XX*
IP

ATTACHMENT



APR 13 1982

Distribution:

- DL R/F
- DGEisenhut
- RAPurple
- HRDenton
- WJDircks
- RVollmer
- RMattson
- SHanauer
- HThompson
- RDeYoung
- EDO Read File
- MSK LLO JWP/ELK

MEMORANDUM FOR: Regional Administrators

FROM: William J. Dircks
Executive Director for Operations

SUBJECT: STEAM GENERATOR PROBLEMS

As have been discussed in the weekly conference calls, there are an increasing number of problems with PWR steam generators. Our responses are compounded by the wide diversity of causes of steam generator tube degradation (foreign objects, denting, cracking, wastage, etc.) and the resulting variety of appropriate remedial actions (plugging, sleeving, water chemistry changes, leak specifications, wastage limits, inspection intervals, etc.). It is essential that the NRC response to these problems be technically correct, regionally consistent, and integrated with ongoing studies and research.

We need a central point for dealing with these technical issues. Accordingly, as I understand you have discussed, for any future steam generator problem that you judge requires substantive NRC technical review, I would like you to transfer responsibility for NRC action to NRR.

This transfer should be accomplished by memorandum to the Director of Licensing, NRR. The memorandum should transmit as much information about the problem as you initially have available.

You will, of course, retain cognizance over any potential enforcement actions that may be related to a steam generator problem (e.g., failure to report, management control weaknesses, violation of tech specs, etc.).

(Signed) William J. Dircks

William J. Dircks
Executive Director for Operations

RD-722

~~8245170187~~
4/13/82

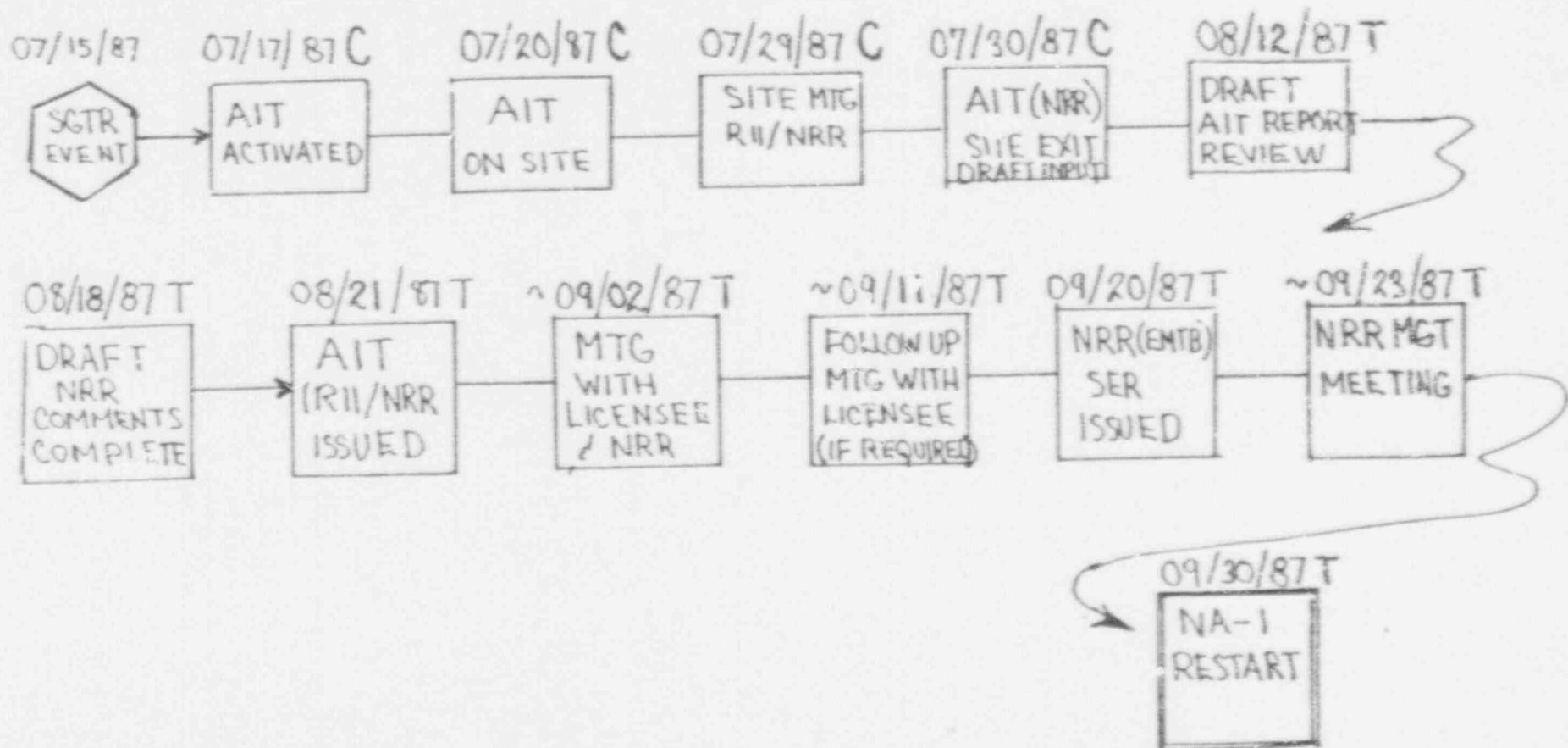
OFFICE	DL R/F	DGEisenhut	HRDenton	WJDircks		
NAME	RAPurple	DGEisenhut	HRDenton	WJDircks		
DATE	4/8/82	4/13/82	4/13/82	4/13/82		

NA-1 SGTR EVENT
MILESTONES

ENCLOSURE 2

NRR/EMTB AIT & SER INPUT - PRIOR TO RESTART

NORTH ANNA TAC 65791



WCAP-11602

NORTH ANNA UNIT 1
STEAM GENERATOR TUBE RUPTURE
AND
REMEDIAL ACTIONS TECHNICAL
EVALUATION
SEPTEMBER 1987

0/5/

Westinghouse Energy Systems



~~2110050084~~
20788

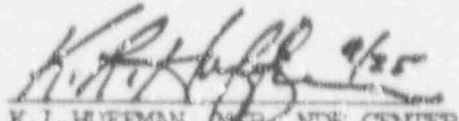
D/5/

WCAP-11602

NORTH ANNA UNIT 1
STEAM GENERATOR TUBE RUPTURE
AND
REMEDIAL ACTIONS TECHNICAL
EVALUATION
SEPTEMBER 1987

0/5/

APPROVED


K. L. HUFFMAN, NRC NDE CENTER
AND STD PROGRAMS

WORK PERFORMED UNDER SHOP ORDER VECD-14016

WESTINGHOUSE ELECTRIC CORPORATION
NUCLEAR ENERGY SYSTEMS
P. O. BOX 355
PITTSBURGH, PA 15230-0355

TABLE OF CONTENTS

SECTION	TITLE
1.0	Introduction/Summary
1.1	Introduction
1.2	Summary
2.0	Failed Tube Evaluation
2.1	Tube Pull
2.2	Examination of the Pulled Tube
2.3	Failure Analysis Results
3.0	Failure Cause and Leakage Correlation
3.1	Leaking Tube Analysis
3.2	Cyclic Life Analysis
4.0	Causative Mechanism and Corrective Action
4.1	Mechanisms Discussion
4.2	Steam Generator Modifications
4.3	Post Modification Leakage Consideration
4.4	Stabilization of Row 9 Column 51
4.5	Downcomer Flow Resistance Plate
5.0	References

1.0 INTRODUCTION/SUMMARY

1.1 Introduction

The purpose of this report is to document the evaluations of the North Anna Unit 1 Steam Generator "C" Row 9 Column 51 tube rupture event and the steam generator modifications which will be made to minimize the requisite conditions for future occurrence of a similar event.

The evaluations include those from nondestructive testing of the tube before removal from the steam generator, those from the laboratory destructive and nondestructive tests conducted on the removed tube and those associated with the necessary loading conditions acting on the tube leading to the rupture of the tube. Also included here are evaluations of the extent of those conditions in the steam generator which may provide the loading which could lead to a similar occurrence during continued operation of the North Anna Unit 1 steam generators. Finally the report documents the modifications which will be performed to minimize those conditions which are judged necessary for future occurrences and evaluates the effectiveness of these modifications.

1.2 Summary

On July 15, 1987, a steam generator tube rupture event occurred at the North Anna Unit 1 plant. The ruptured tube was determined to be Row 9 Column 51 in steam generator "C". The location of the opening was found to be at the top tube support plate on the cold leg side of the tube and was circumferential in orientation with a 360 degree extent. -

In order to confirm steam generator tube integrity at North Anna 1, evaluation of the conditions in the steam generator have been assessed leading to a definition of the cause of the tube rupture, the details of the mechanism leading to the rupture, the prerequisite conditions necessary for the mechanism and the modifications appropriate to minimize prerequisite conditions for future occurrence. As a supplemental element, leak-before-break conditions have been established. Detailed studies of these elements form the majority of this report and are in many cases interdependent. A logic diagram connecting fundamental results from the studies is shown as Figure 1.2-1. The overall conclusions of the evaluation are summarized as follows.

The cause of the tube rupture has been determined to be high cycle fatigue. The source of the loads associated with the fatigue mechanism has been determined to be a combination of a mean stress level σ in the tube and a superimposed alternating stress. The mean stress has been determined to be the result of denting of the tube at the top tube support plate and the alternating stress due to out-of-

plane deflection of the tube above the top tube support caused by flow induced vibration. These loads are consistent with a lower bound fatigue curve for the tube material in an AVT water chemistry environment. The vibration mechanism has been determined to be fluidelastic, based on the magnitude of the alternating stress.

The most significant contributor to the occurrence of excessive vibration is the reduction in damping at the tube to tube support plate interface caused by the denting. The absence of antivibration bar (AVB) support has been concluded to be required for requisite vibration to occur, together with the reduction in damping. The presence of AVB support will restrict tube motion and thus preclude the deflection amplitude required for fatigue. Row 11 tubes are the minimum requirement for antivibration bar (AVB) support in the original design configuration. Inspection data shows that an AVB is not present for the Row 9 Column 51 tube but that the actual AVB installation depth exceeded the minimum requirements in all cases with data for AVB's at many other Row 9 tubes. Also contributing to the level of vibration, and thus loading, is the local flow field associated with the detailed geometry of the steam generator. The tube which ruptured is considered to have a worst case combination of loading conditions and fatigue properties.

The prerequisite conditions derived from the evaluations were concluded to be:

<u>Fatigue Requirements</u>	<u>Prerequisite Conditions</u>
Mean stress	Denting
Alternating stress	Tube vibration <ul style="list-style-type: none">- Dented support- Flow excitation- Absence of AVB
Material fatigue properties	AVT environment <ul style="list-style-type: none">- Lower range of properties

The modifications to the steam generator have been defined to address the prerequisite conditions. Criteria have been established to effectively eliminate the cause or to establish sufficiently conservative limits that a high confidence level is achieved that the combined actions reduce the potential for tube fatigue in the future to a very small level. For those prerequisite conditions associated with the inherent tube condition, worst case assumptions have been made. All tubes are assumed to be dented sufficiently to provide mean stress levels associated with tube yielding at the tube support. All tubes are assumed to have reduced damping associated with denting at the top tube support sufficient to result in a clamped condition. The material fatigue properties have been assumed to be the lower bound for

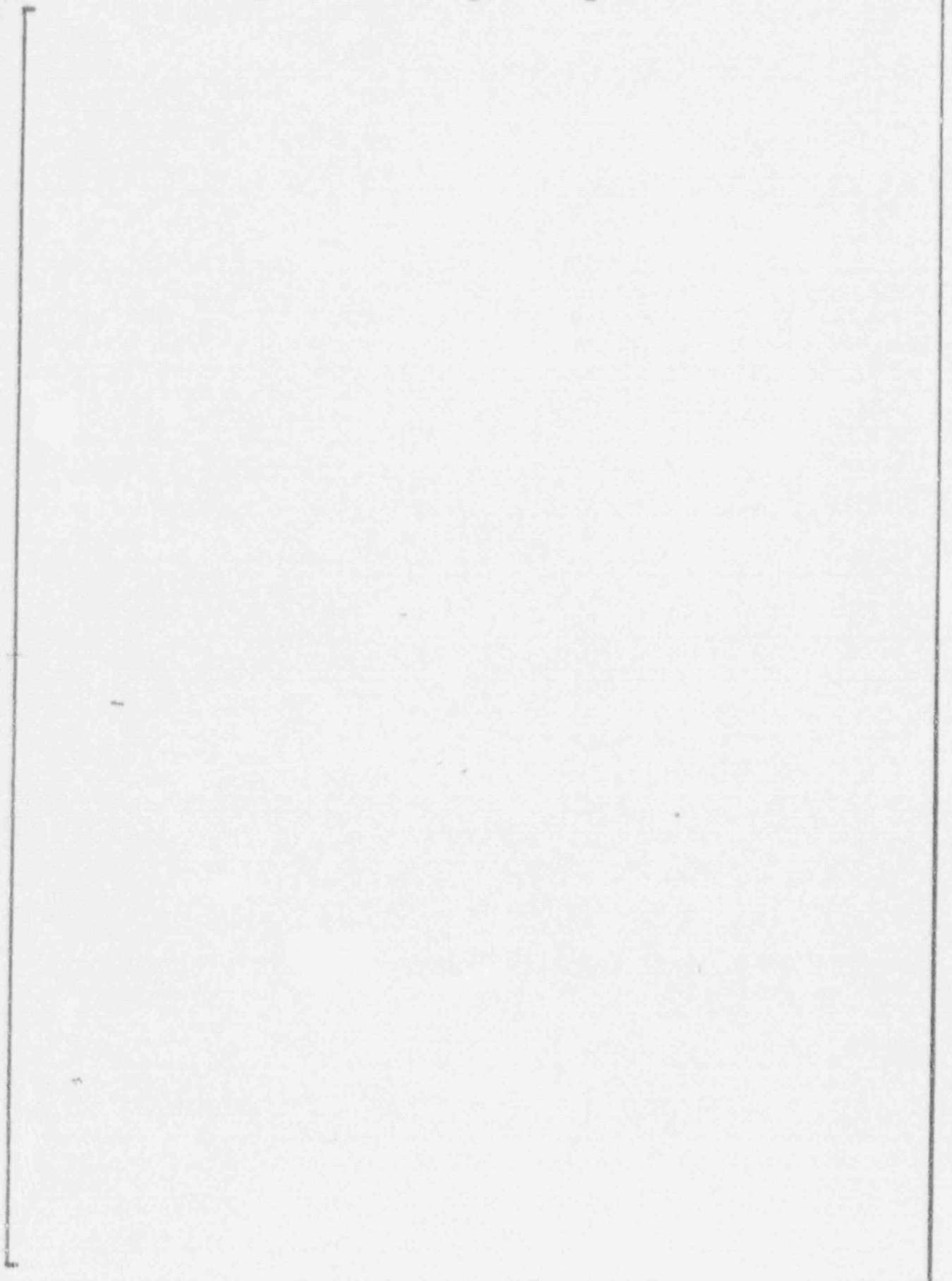
AVT water chemistry conditions. The location of AVB's has been conservatively defined from inspection data for each of the tubes in the three steam generators. The goal for level of improvement of the flow excitation required to avoid significant future fatigue accumulation has been conservatively selected based upon the range of possible initiating alternate stress for the worst case tube during continued operation.

To achieve the flow excitation reduction, a modification to reduce the circulation through the steam generator and thus reduce the hydrodynamic loads acting on the tubes will be installed. This modification is called a downcomer flow resistance plate (DFRP) and has been previously used in many steam generators. The adjustment to the circulation will be to a level where significant operating experience exists in other steam generators. This modification alone is sufficient to account for vibration associated with a very low tube damping level. To account for the combined effect of both reduced damping and high flow conditions, tubes in high flow areas will be conservatively removed from service. A tube plug which allows a controlled level of leakage will be utilized so that leakage in the tube wall can be readily detected.

As a result of the modifications, it is expected that the potential for large leakage occurrences will be eliminated based on multiple criteria of which each significantly reduces the probability of occurrence of tube fatigue. Supplemental to the steam generator modifications, the practicality of leak-before-break was established based on a correlation of plant leakage data not normally used to monitor primary to secondary leakage and the tube rupture analysis. These results show that leakage was present before the tube rupture and that leak-before-break was present.

Figure 1.2-1 Logic Diagram

A, C



2.0 FAILED TUBE EVALUATION

Tube R9C51 in steam generator C of North Anna Unit 1 was observed, by in-plant Endoscope examination to have separated circumferentially immediately above the seventh cold leg support plate. A tube pull removed the cold leg segment of the tube from the tubesheet bottom to the fracture face at the top edge of the seventh support plate. The removed tube was examined in the laboratory by a variety of techniques and it was determined that the tube degradation occurred as a result of fatigue. The presence of fatigue striations confirmed the fatigue mechanism. Measurement of the striation spacing and observation of the general topographic features permitted determination of the stress intensity present at various stages of crack propagation. There was no indication of significant wall penetration occurring by other mechanisms such as stress corrosion cracking or intergranular attack. Details of these efforts appear in the following report sections 2.1 - 2.3.

2.1 Tube Pull

The cold leg tube segment was removed with 0.9 inches of elongation occurring during the tube pull. The elongation was observed to be confined to above the third support plate and to increase with increasing elevation. Between the sixth and seventh support plates, 0.8% elongation occurred resulting in a reduction of the average tube OD from 0.871-0.872 to approximately 0.867 inches. The pull forces required to remove the tube were as follows: 103.6 ksi to break the tube free; 62-65 ksi after 4 feet of removal; 41.4 ksi after 8 feet; 6.9 ksi after 21 feet; and less than 0.8 ksi thereafter. These data suggest that support plate denting in the upper cold leg support plate restrained the tube during the tube pull. (Field eddy current measurements also showed significant denting at these locations as shown in Figure 3.1-7.) Table 2.1-1 and Figure 2.1-1 summarize measurements made on the pulled tube.

One of the more prominent features on the fracture face of the pulled tube is the region subsequently labeled as the "tab". The small local protrusion on the fracture was clearly visible during the in-plant endoscope examinations. The intradon region of the U-bend could also be determined by noting the position of the endoscope support cable during the photography. This information, coupled with viewing the location of seventh tube support plate flow holes, permitted orientation of the fracture face with respect to the plane of the U-bend. The plane of the U-bend was accordingly positioned at approximately 45° to the general tab position.

2.2 Examination of the Pulled Tube

The following section summarizes the findings of the failure analysis. In general the results established that the tube had the intended mechanical properties and otherwise displayed the expected characteristics of Alloy 600 in the mill annealed condition. Some specific details follow.

2.2.1 Physical and Metallurgical Properties

From a region of the tubing where no tube pulling elongation occurred, two room temperature tensile specimens were obtained and pulled. Results from these tests agreed closely with 1971 tubing certification data for Heat 44B3 which is the heat in location R9C51 (Table 2.2-1). These mechanical property values are considered typical of tubing in North Anna Unit 1. Chemistry data for Heat 44B3 are shown in Table 2.2-2. These values are also considered typical of North Anna Unit 1 tubing although it should be noted that the carbon concentration of 0.05 weight percent is on the high side of normal. Figure 2.2-1 shows a metallographic cross section obtained on the cold leg tube segment. The microstructure appears typical of mill annealed Alloy 600 in North Anna Unit 1.

2.2.2 NDE Examination of the Seventh Support Plate Region

Radiography, consisting of double wall radiographs taken at 4 rotations 90° apart and of a single wall radiograph using a rotisserie technique, revealed no indications in the seventh support plate region other than the fracture at the top edge of the support plate location.

Eddy current examinations were also conducted on the seventh support plate region using bobbin, 8 x 1, RPC, and OD pencil probes. No indications were observed below the fracture face in the support plate region.

2.2.3 Visual and Macroscopic Examinations of Seventh Support Plate Region

Figures 2.2-2, -3, and -4 provide macrophotographs of the seventh support plate region and the fracture face. With the orientation system chosen, the plane of the U-bend is located at 45° . Minimal OD surface deposits were observed although demarcation of the support plate edges was clearly observed on the OD surface of the tubing. As will be demonstrated later, multiple site fracture initiation occurred between approximately 90° and 180° . The tubing between 90° and 180° is determined to have protruded approximately 0.07 inches above the top edge of the support plate (0.82 inches above the bottom edge of the support plate demarcation). This location is the fracture region

closest in elevation to the top edge of the support plate. The highest elevation of the fracture is located at 315° and is approximately 0.17 inches above the top edge of the support plate. On the fracture face a dark deposit was noted from approximately 90° to 150° . Typically the deposit extends from the OD to $3/4$ through-wall, although it may have touched the ID locally. Figure 2.2-2 shows a photograph of the fracture face in which the deposit is observed, and Figure 2.2-4 shows a sketch of the deposit boundary. An analysis of these deposits showed that they had a composition similar to adjacent OD deposits and that they contain elements which would be expected from secondary side water-borne deposits (Tables 2.2-3 and -4). Later it will be shown that fatigue cracks initiated in this location. The significance of these deposits is that they show the shape of the early macro-crack before faster crack growth rates occurred. From the shape of the deposit, it is believed that the macro-crack initially broke through-wall over an approximately 40° crack front that extended from approximately 100° to 140° . Fatigue striation orientation data, presented later, also support this hypothesis.

Visual examinations and macroscopic examinations of the fracture surface and the OD surface adjacent to the fracture surface were conducted to determine the surface condition and to determine crack origins and paths of crack propagation. The salient features observed during these examinations are summarized in Figure 2.2-5 and consist of the following:

1. Tab-shaped area near region marked 0° has a rough fracture texture and orientation consistent with final overload fracture.
2. Region from about 90° to 155° is generally flat (orientation: normal to wall) throughout most of wall except for small portions that have shear orientations (45° to wall) adjacent to the OD and ID surfaces.
3. Most of the remainder of the fracture is oriented at about 45° to the wall surface except for a flat area surrounding a minor crack origin at about the 190° location.
4. The fracture occurred by multiple initiation - all on the OD surface. A number of "origins" were identified from fracture surface markings (tear ridges) and contour on OD surface with four principal initiation sites found at approximately 110° , 120° , 135° and 150° . Figure 2.2-6 shows a photograph of these locations after the deposit had been partially removed by cathodic descaling.
5. Fracture Texture:
 - a. Within flat region: fine texture.
 - b. Counterclockwise from 90° : fine texture.

- c. Clockwise from 180° : initially fine. Texture becomes rougher with herringbone pattern evident near 270° region indicating an accelerating rate of crack propagation.
- d. Within the region from about 280° through 360° to 15° : rough texture (fractographic examination revealed dimpled rupture in this region) indicative of overload fracture.

2.2.4 SEM Fracture Face Examination

SEM fractographic examinations of the fracture surface confirmed the conclusions of the optical-macroscopic examinations that the crack origins were located on the OD surface. At low to intermediate magnifications, as illustrated in Figure 2.2-7, the fracture (in the 30° to 210° portion of the fracture) has a transgranular, feathery, cleavage-like faceted appearance. The feathery appearance results from microscopic tear ridges (which, like macroscopic tear ridges, run in the direction of local crack propagation) and small regions of ductile fracture (produced by ductile cutting) which interconnect multi-level, finger-like plateaus and sub-regions on those plateaus. Dimpled rupture (the predominant mechanism of ductile, overload fracture) was found only in the final portion of the fracture (from about 310 through 360° to the 15° portion of the fracture). At higher magnifications (also illustrated in Figure 2.2-7 frequent variations in the direction of local crack propagation of nearly $\pm 45^{\circ}$ (both vertically and horizontally), could be noted as indicated by changes in the orientation and direction of the plateaus. Crack growth occurred simultaneously along facets at different levels so that tear ridges and undercutting of one facet by another was a common occurrence. Such phenomena are common to fatigue crack propagation.

One definitive feature of fatigue cracks that is often observed is the presence of numerous, usually evenly spaced, striations that run perpendicular to the direction of local crack propagation. The striations develop as a consequence of repeated blunting and resharpening of the crack tip during the cyclic applications of load; each striation, therefore, marks the position of the crack tip at the time it was formed.

Striation-like markings could be seen at very high magnifications during the SEM fractography. The striations appear like those that occur in fatigue fractures inasmuch as they run perpendicular to the direction of local crack propagation; however, the resolution by SEM was not adequate to determine if the spacing is uniform or random or to determine the striation spacing.

The appearance of the crack origin at approximately 110° is shown in Figure 2.2-8. In the top photograph the fracture surface is shown as viewed from above. Note the crack propagation line fanning out from the origin region. In the middle photograph the specimen has been tilted to show both the fracture surface the OD surface of the tubing. The presence of the shallow polishing marks are still visible

on the tube. The presence of some surface disturbance on the tube in this region is also visible. These disturbed areas are quite shallow and of unknown mechanical or corrosive origin. The lower photograph of the OD of the tube again shows the polishing marks and also some scrape marks that likely occurred during the tube pulling operation.

No intergranular cracking was found at any position in the fracture. This total absence of intergranular cracking, eliminates the possibility that cracking initiated as or propagated by intergranular stress corrosion cracking.

2.2.5 TEM Fractographic Examination

TEM fractographic examinations were performed to provide the extra resolution to definitively determine if the striation-like markings observed during SEM fractography were indeed fatigue striations and to provide quantitative data pertaining to the spacing of the striations. Two-stage carbon replicas were utilized for this examination. The first stage consists of a cellulose acetate replica of the entire fracture surface. The second stage consists of making small carbon replicas (usually referred to as grids, since small metallic grids are used to support the fragile carbon replica) from selected areas of the cellulose acetate replica. Replicas were made both before and after Endox cleaning (cathodic descaling of oxide deposits) of the fracture surface.

The salient features observed during the TEM fractographic examination are schematically shown in Figure 2.2-9 and summarized below:

1. Oxidation and/or fretting, observed on most of the fracture surface, is most severe at about the 135° position, heavy throughout the region containing most of the crack origins and of diminishing severity at locations proceeding in the clockwise direction from about 170° and counter clockwise from about 70° . This suggests that the oldest portion of the crack occurred at about the 135° position.
2. Fine fatigue striations are observed near the crack origins. Striation spacing (see Table 2.2-5) increased from about 1.0 micro-in. near the OD surface to nearly 2.0 micro-in. near the ID surface.
3. Fine to coarse fatigue striations occur at locations from about 190° to 250° and from about 30° to 70° as shown in Table 2.2-5. The fatigue striation spacing increased (indicating higher propagation rates) as the crack propagated around the circumference of the tube in a clockwise direction from about the 190° position and counter clockwise from about the 70° position. Higher propagation rates in the 190 to 300° positions than in the 70 to 15° regions indicates eccentric loading or a component of torsional loading.

4. Parabolic dimples with internal necking between dimples were the predominant fractographic features at about the 270° position. These features are indicative of very high fatigue propagation rates. This position is within the regions of herringbone pattern and coarse texture observed during visual examinations.
5. Equiaxed dimples indicative of the overload portion of the fracture were observed at about the 310° position. These fractographic features, coupled with the macroscopic features, indicate that the overload fracture occurred throughout the region from about 300° through 360° to 15° .
6. Damage to the fracture, most probably imposed by peening and fretting, was fairly common. The most severe peening was observed at the 290° position, but some amount of surface peening occurred throughout the fracture surface.

2.2.6 Metallography of Seventh Support Plate Region*

A series of longitudinal metallographic sections was made from below the bottom edge of the seventh support plate through the crevice region up to the fracture face. In the key fatigue initiation zone from approximately 90° to 180° , the region from 130° to 165° , which included two major initiation sites and at least one minor initiation site, was cut by five equispaced longitudinal sections. Minor OD intergranular penetrations, as well as minor ID intergranular penetrations, were found in isolated, small zones within the support plate crevice region. The penetrations were typically 0.3 mils deep and approached a maximum depth of 1.0 mil. See Figure 2.2-10. The closest distance to the fracture face, in which an intergranular penetration approached the fracture face, was 4 mils. See Figure 2.2-11. It is judged most likely that intergranular penetrations, based primarily on the extensive SEM examination performed on the fracture face, were not present at the exact fatigue initiation locations. There still remains the possibility that this could have occurred; however, that possibility would not change the observed data which support fatigue initiation and propagation.

*Note: Prior to metallographic mounting the sample section containing the fracture face was plated with nickel. This provides an extended surface area for the grinding and polishing steps and reduces edge rounding of the tubing segments.

2.2.7 Summary of Pulled Tube Examination

Fatigue was found to have initiated on the OD surface of Tube R9C51 CL immediately above the 7th cold leg support plate. No indications of significant accompanying intergranular corrosion was observed on the fracture face or on the immediately adjacent OD surfaces. Multiple fatigue initiation sites were found with major sites located at 110°, 120°, 135° and 150°. The plane of the U-bend is located at 45° with the orientation system used or approximately 85° from the geometric center of the initiation zone. High cycle fatigue striation spacings approached 1 micro-inch near the origin sites. The early crack front is believed to have broken through-wall from approximately 100° to 140°. From this time on, crack growth is believed (as determined by striation spacing, striation direction, and later observations of parabolic dimples followed by equiaxed dimples) to have accelerated and to have changed direction with the resulting crack front running perpendicular to the circumferential direction.

TABLE 2.2-3

DEPOSIT ANALYSIS

N. ANNA 1 TUBE R9-C51 CL

AS-RECEIVED FRACTURE SURFACE

SEMIQUANTITATIVE SEM-EDS ANALYSES (w/o)

Z >10 (Na), 75 MILS² MID-WALL AREA SCANS

ELEMENT	zone of heavy deposit				
	0°	90°	150°	180°	270°
Mg	9.7	16.3	---	16.3	10.7
Al	---	---	---	---	---
Si	8.7	14.3	9.1	9.9	11.2
S	0.6	1.0	---	---	---
Ca	---	0.2	---	---	0.2
Ti	---	---	---	---	0.2
Cr	16.8	9.0	12.5	11.8	9.9
Mn	1.6	---	2.5	---	0.5
Fe	42.2	11.8	11.5	8.4	10.4
Ni	17.5	37.2	54.3	45.4	38.6
Cu	8.6	6.3	7.7	5.8	7.6
Zn	6.3	3.9	2.3	1.5	7.6
Mo	---	---	---	---	2.9
Pb	---	---	---	---	0.1

TABLE 2.2-4

DEPOSIT ANALYSIS

N. ANNA 1 TUBE R9-R51 CL

AS-RECEIVED ON SURFACES IN MIDDLE OF 7TH TSP

SEMIQUANTITATIVE SEM-EDS ANALYSES (w/o)

Z >10 (Na), 75 MILS² AREA SCANS

<u>ELEMENT</u>	<u>0°</u>	<u>90°</u>	<u>180°</u>	<u>270°</u>
Mg	---	---	---	---
Al	1.5	0.9	3.1	1.3
Si	4.4	3.8	6.5	8.2
S	---	---	---	1.4
Ca	0.3	---	---	0.7
Ti	0.4	0.4	---	0.2
Cr	16.8	15.5	12.3	15.0
Mn	---	---	---	---
Fe	13.2	11.8	21.1	17.3
Ni	51.3	56.9	38.8	39.8
Cu	6.0	8.0	7.8	8.6
Zn	4.4	2.9	9.4	7.4
Mo	1.7	---	1.2	---

TABLE 2.2-5

SUMMARY OF STATION SPACING MEASUREMENTS

<u>GRID</u>	<u>DISTANCE FROM O.D. SURFACE, IN.</u>	<u>AVERAGE SPACING #-IN.</u>
A		8.24
B		3.39
C	0.014	1.00
	0.036	1.58
	0.046	1.85
E	0.024	1.60
	0.031	1.53
F		20.7

Figure 2.1-1

DIMENSIONS OF PULLED TUBE R9-C51CL FROM N. ANNA 1 S/G C

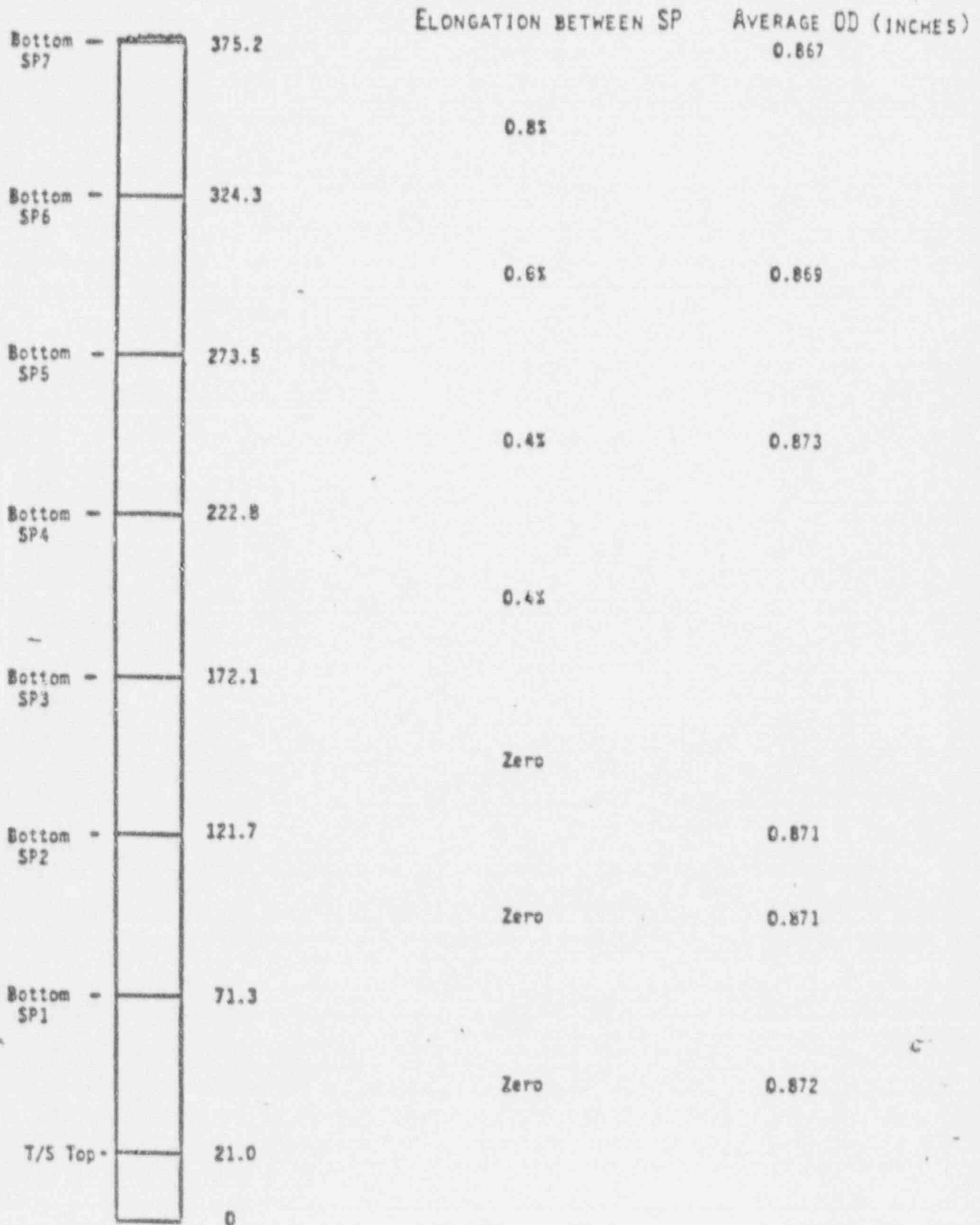
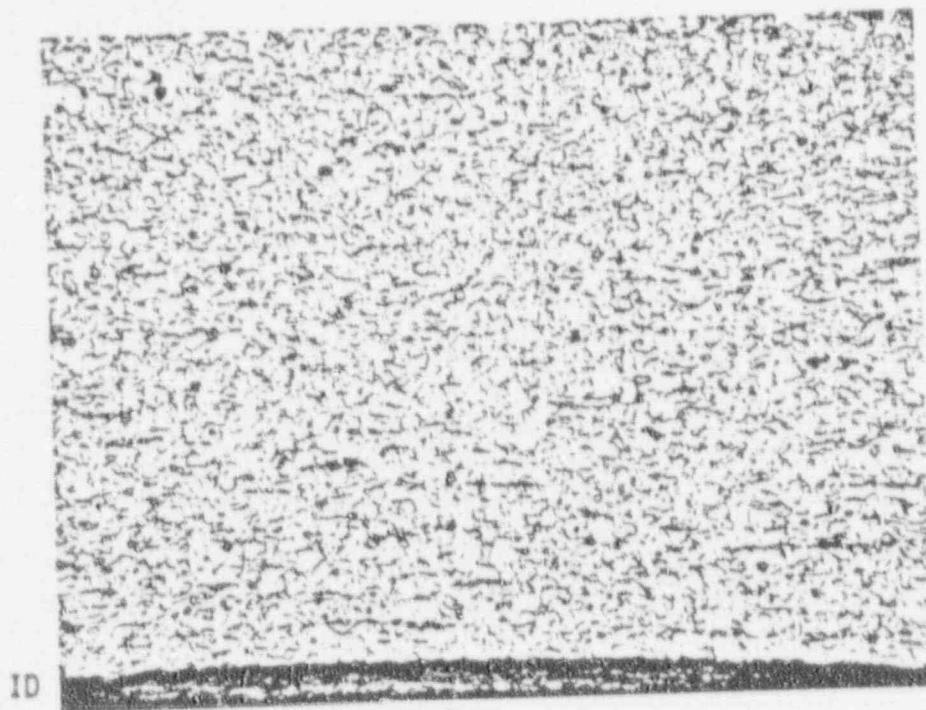
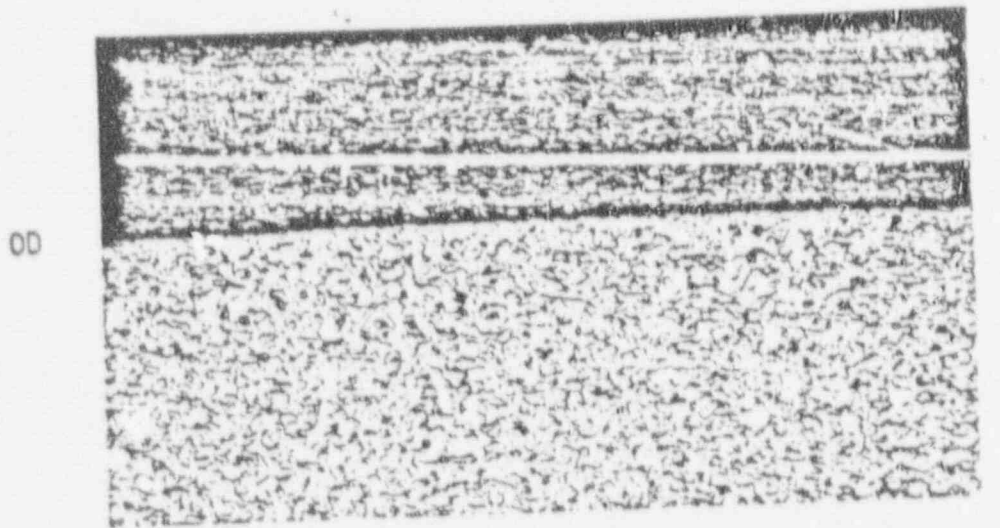


Figure 2.2-1

TRANSVERSE METALLOGRAPHY -5 INCHES BELOW FRACTURE FOR TUBE R9-C54 CL



100X

ASTM G.S. -9.5

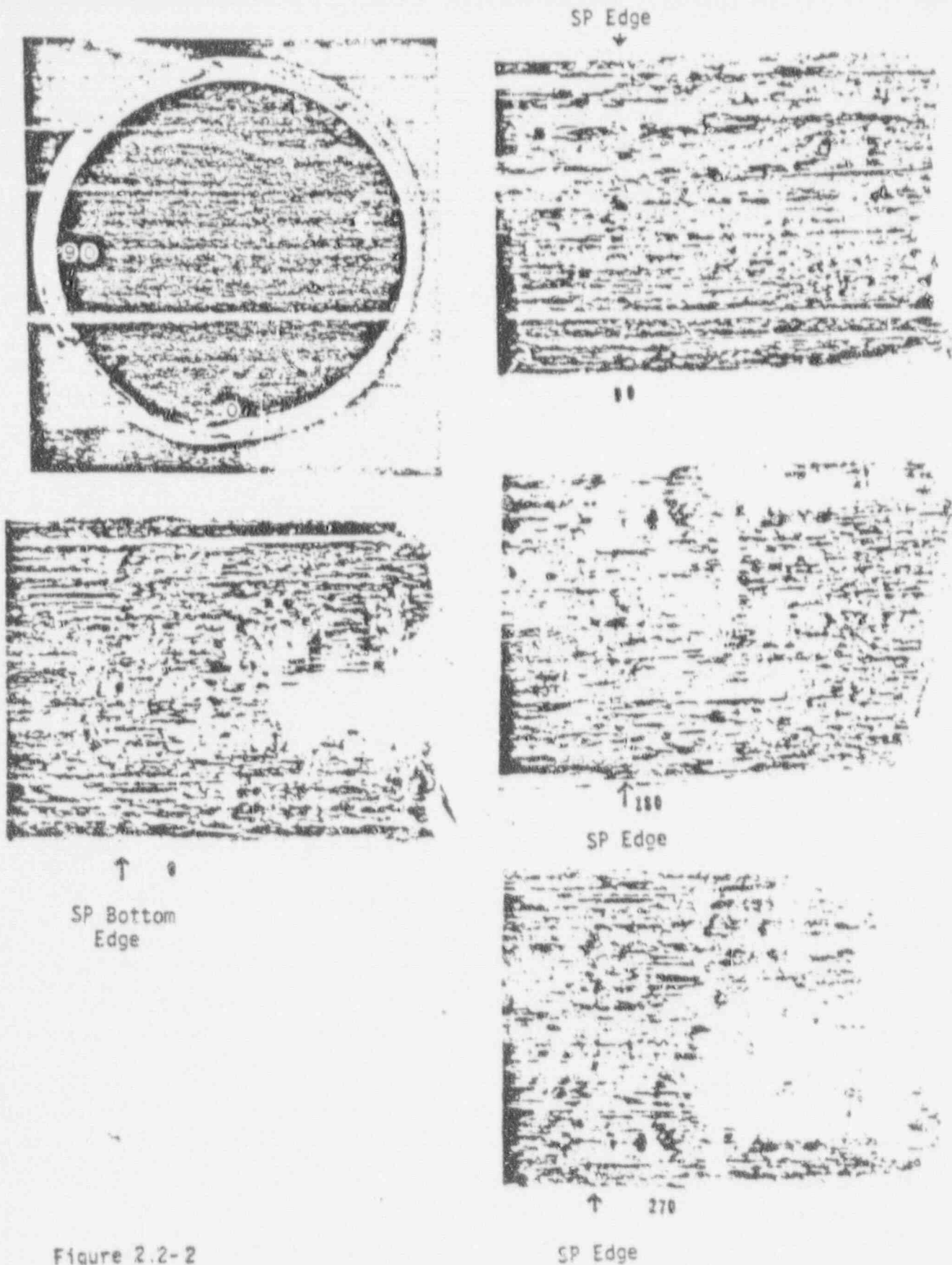


Figure 2.2-2

End and side views of circumferential separation at 7th TSP (cold leg)
 Tube R9-C51, North Anna Unit 1.

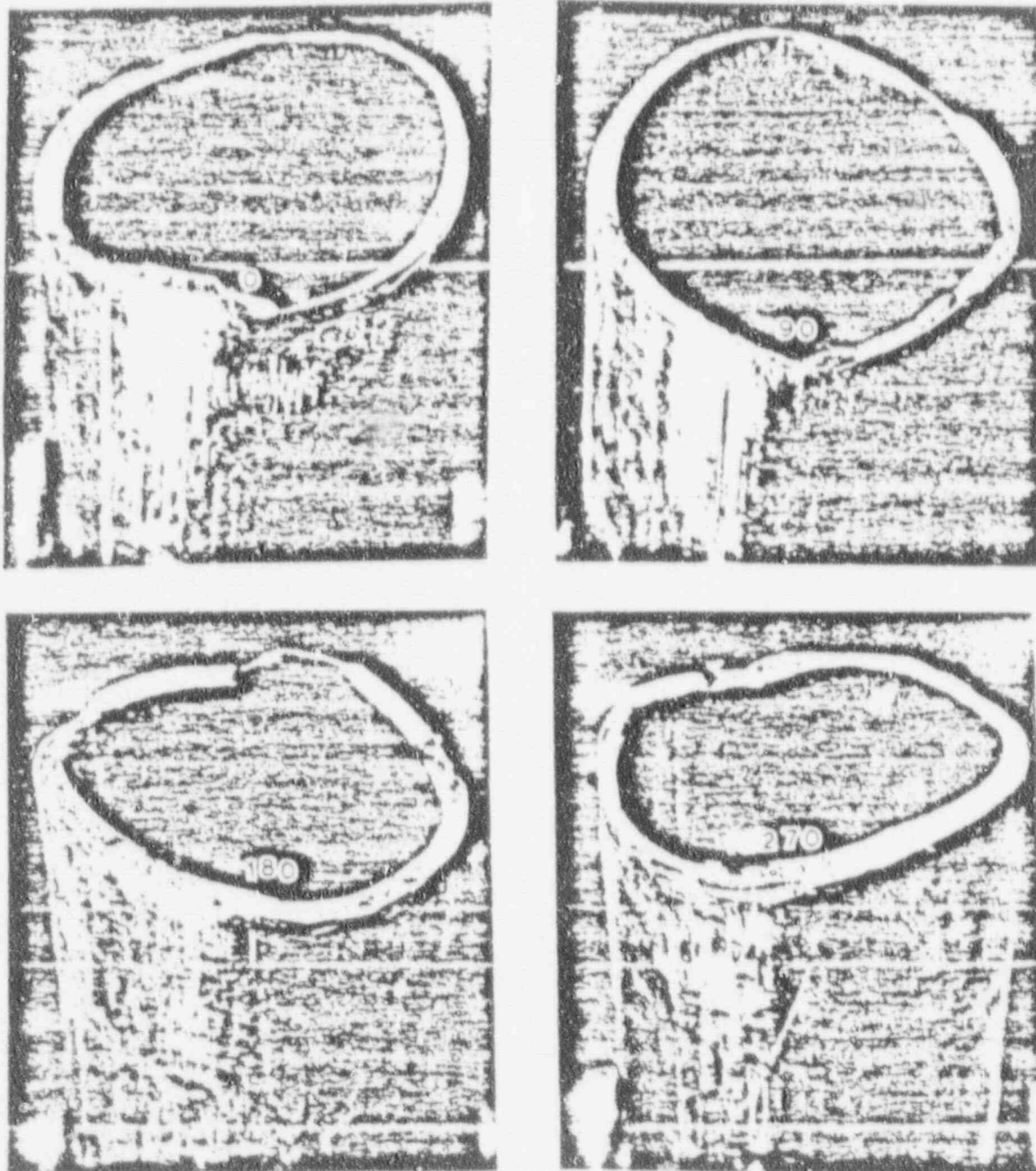


Figure 2.2-3

Views of circumferential separation at 7th TSP (cold leg) of Tube R9-C51, North Anna Unit 1.

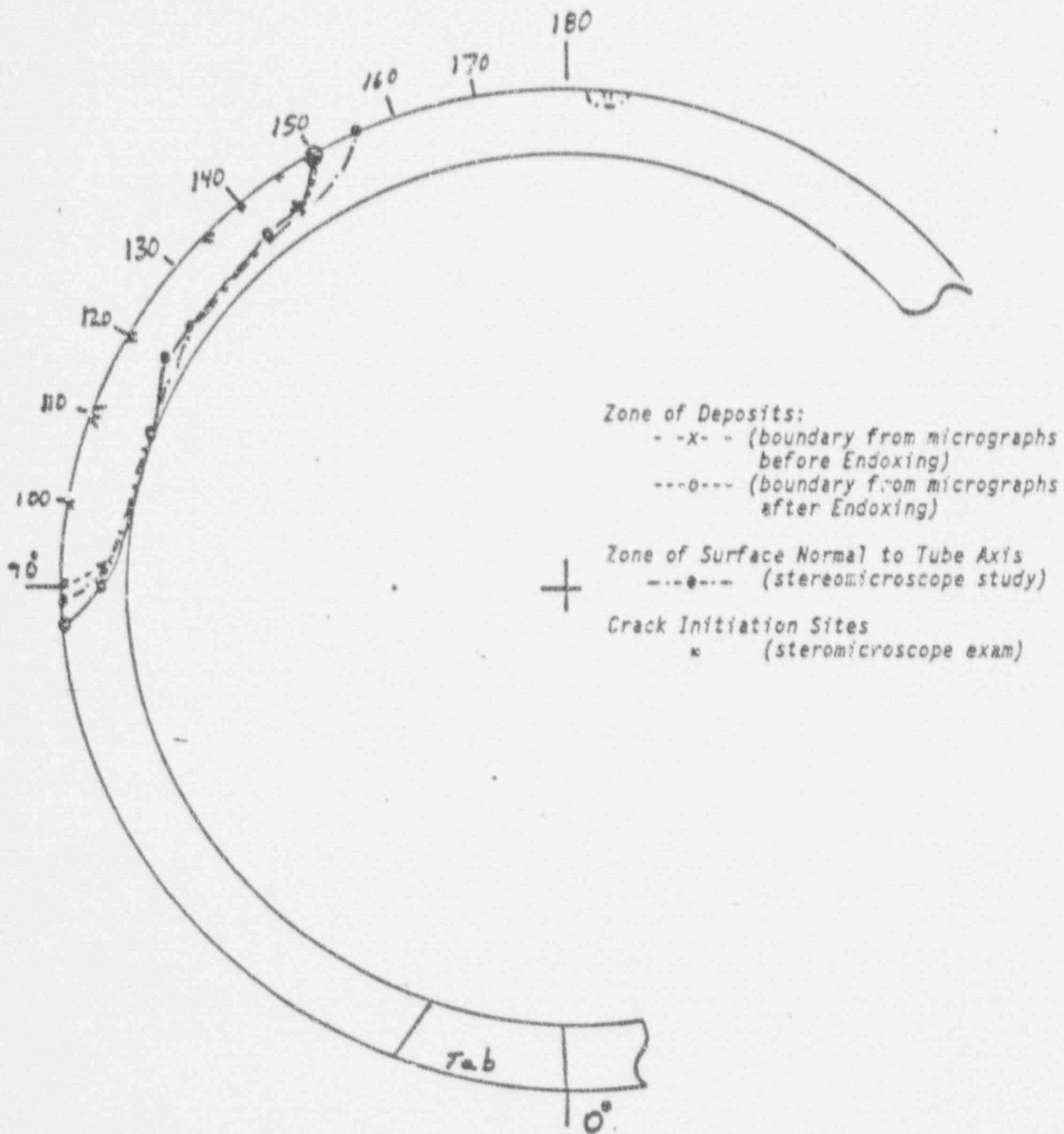


FIGURE 2.2-4 Schematic of fracture face region which was covered by deposits

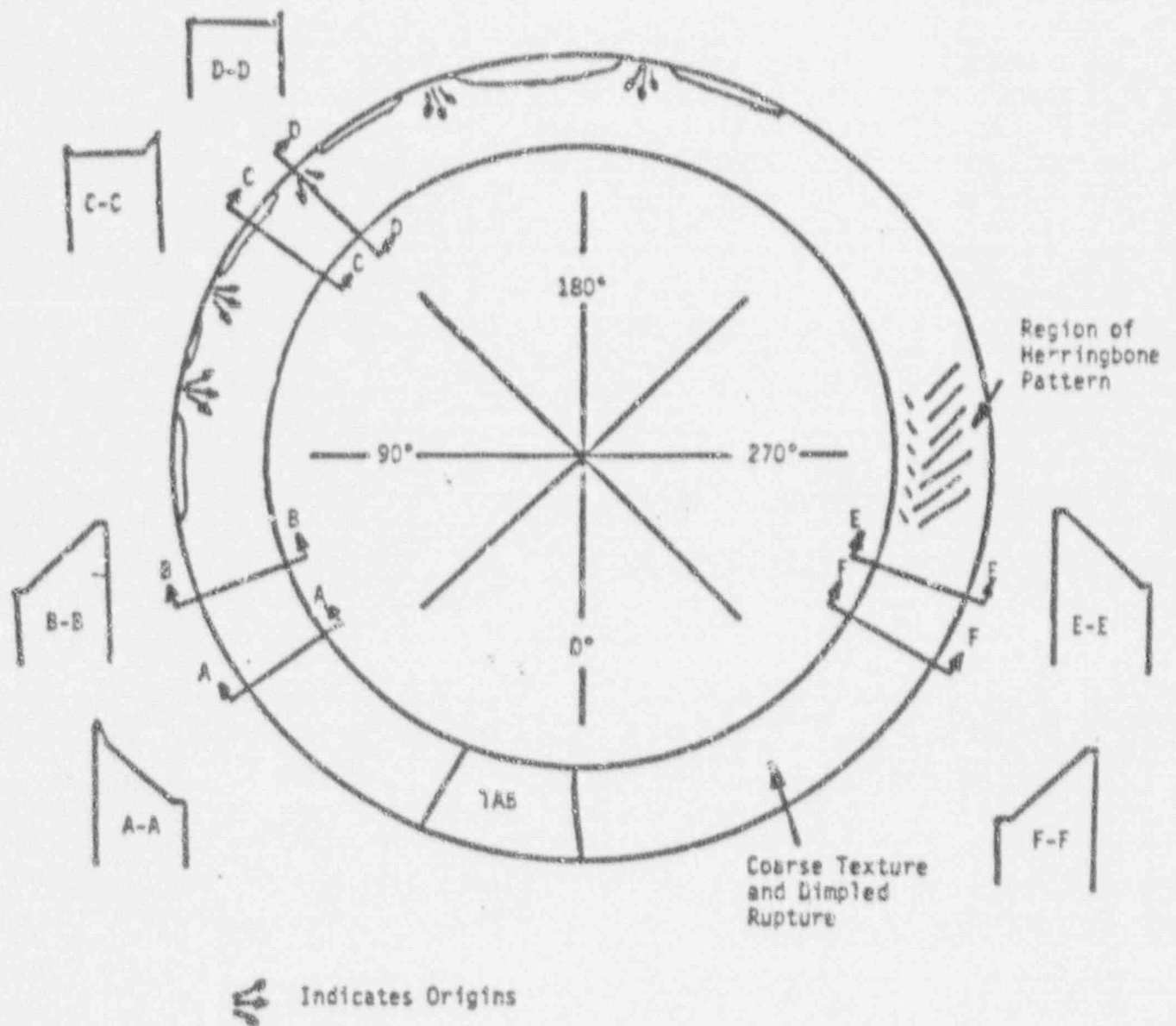


FIGURE 2.2-5 Approximate Mapping of Fracture Surface of Tube R9C51, S/G "C" Cold Leg.

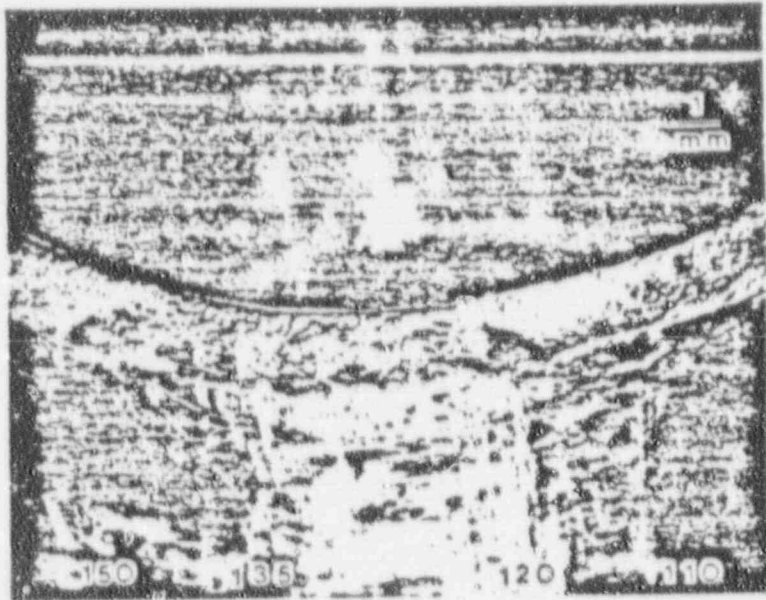


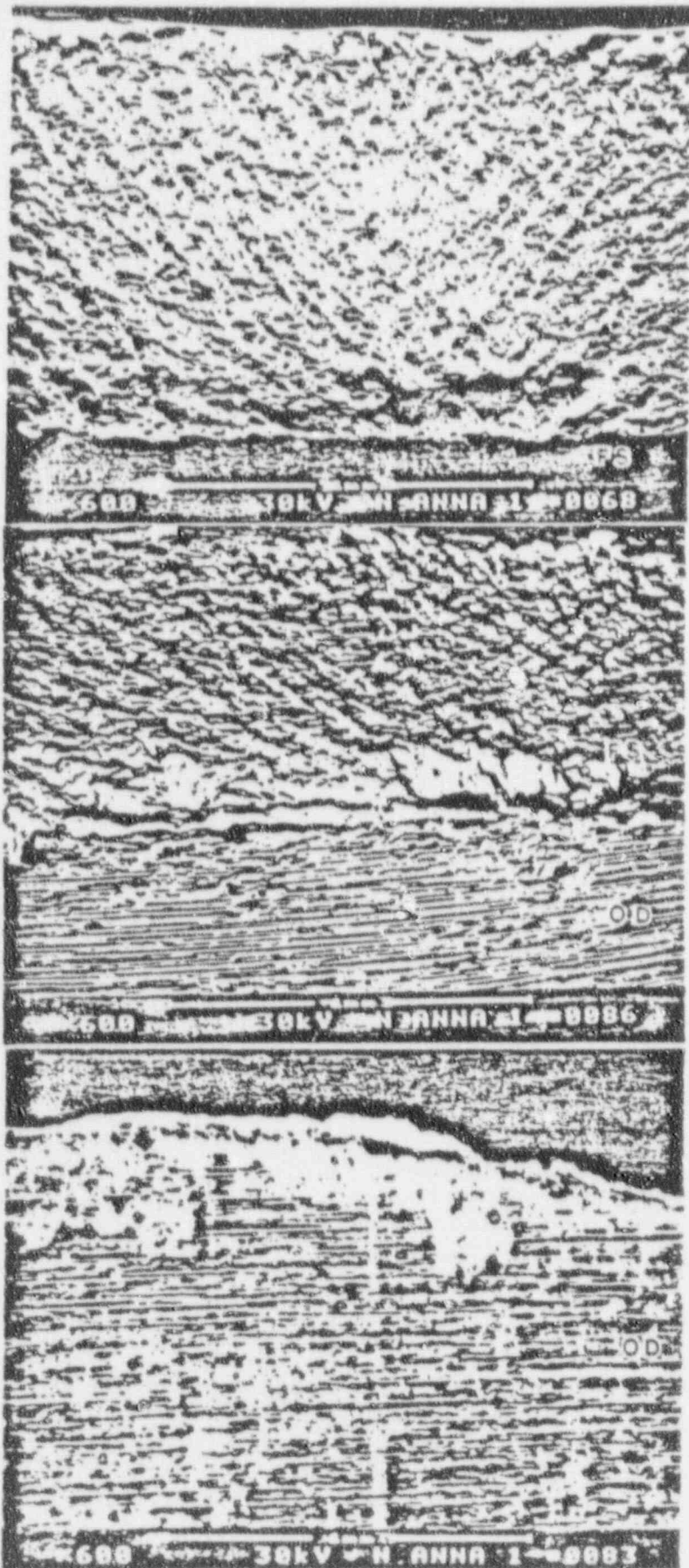
FIGURE 2.2-6

Light photograph indicating multiple origins of cracks on the OD of FS on Piece 9B2 after cathodic cleaning.



FIGURE 2.2-7

SEM micrographs at various locations near the 135° crack origin on the FS of Piece 9B2.



SEI

← Fracture Surface

← Fracture Surface

FIGURE 2.2-8
Crack origin at 110°
on FS of Piece 9B2.

← Tube Wall Showing
Polishing Marks

← Tube Wall

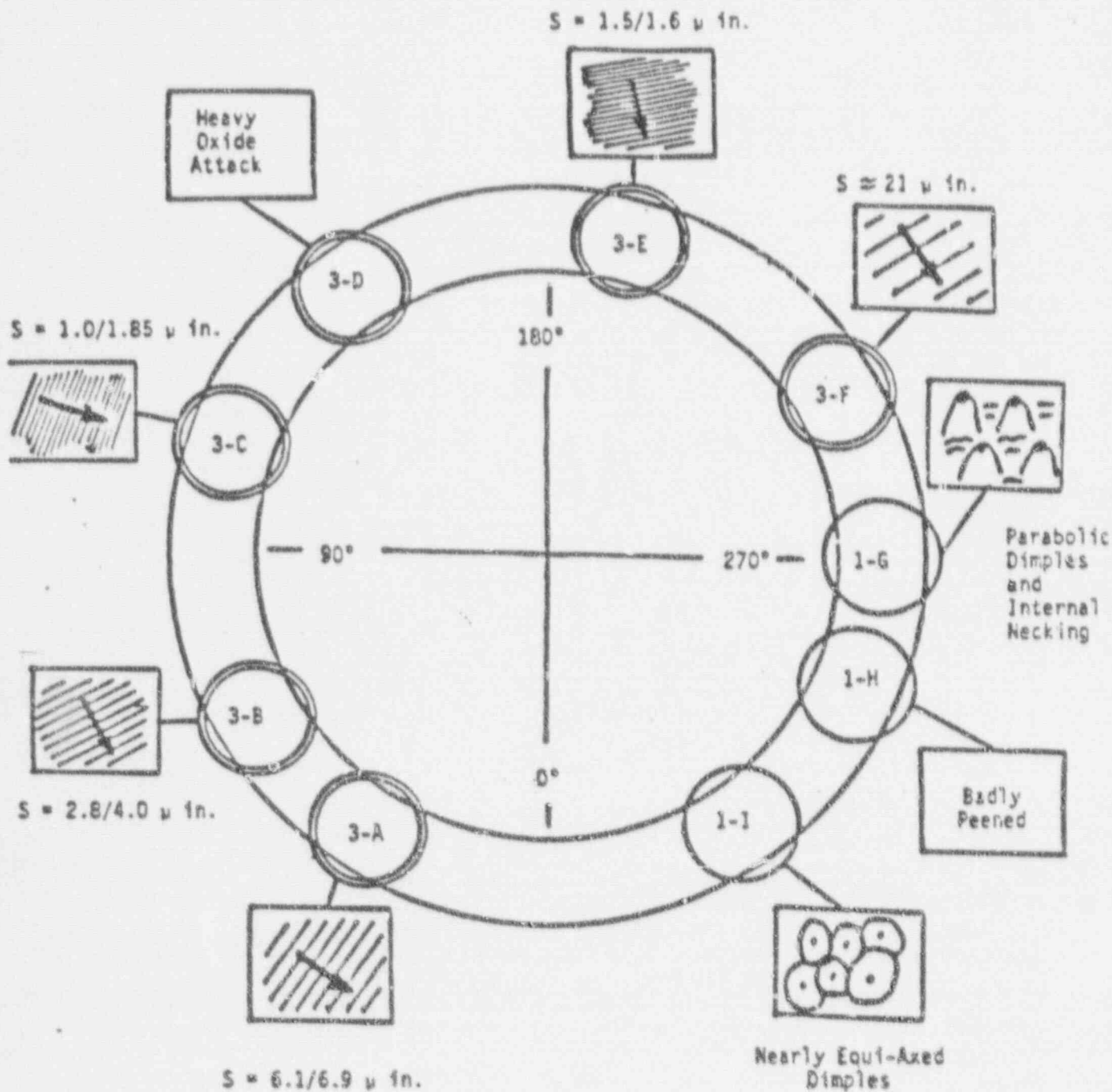
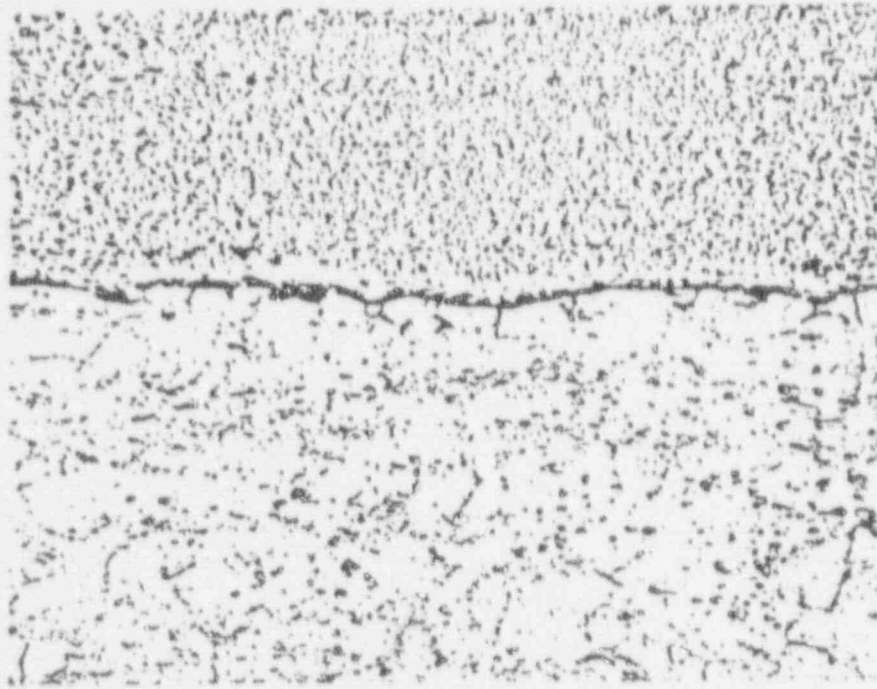


FIGURE 2.2-9 Note: Arrows Indicate Direction of Fracture Propagation

Schematic Representation of Features Observed During TEM Fractographic Examination of Fracture Surface of Tube R9C51, S/G "C" Cold Leg.

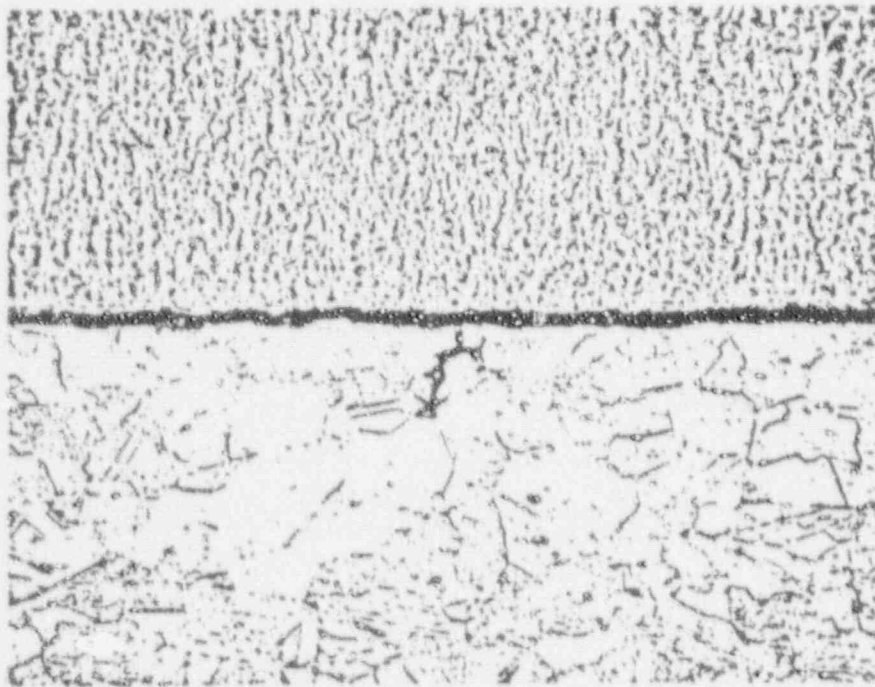


Nickel Plating

ID surface
at 165°
(typical penetration)

Alloy 600

0.002"
51 μm



Nickel Plating

OD surface
at 155°
(maximum penetration)

Alloy 600

0.002"
51 μm

Figure 2.2-10 Longitudinal metallography of intergranular penetrations of ID and OD surfaces within seventh support plate crevice at 165° and 155°.

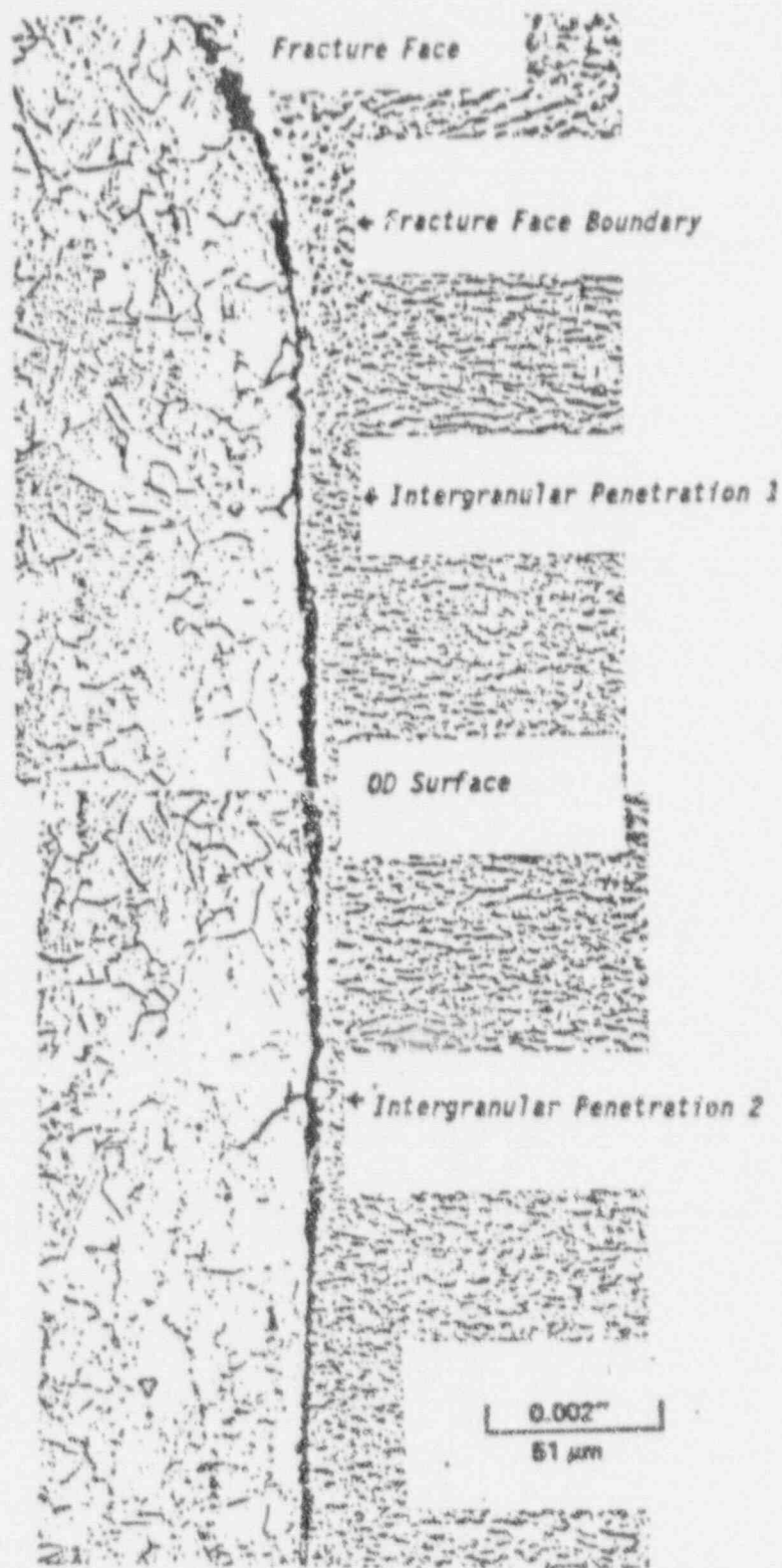


FIGURE 2.2-11 Longitudinal metallography of OD intergranular penetrations nearest fracture face at 155°.

2.3 Failure Analysis Results

The tube examination results, as presented in the previous section, show that fatigue cracks initiated at multiple sites on the OD of the tube at a location slightly above the tube support plate. These cracks joined together, progressed through the tube wall and then grew around the circumference of tube. This section begins a more quantitative analysis of the tube fatigue fracture.

One definitive feature of fatigue cracks that is often observed is the presence of numerous, usually evenly spaced, striations that run perpendicular to the direction of local crack propagation. The striations develop as a consequence of repeated blunting and resharpening of the crack tip during the cyclic applications of load, so each striation marks the position of the crack tip at the time it was formed. The striation spacing provides a rough estimate of the crack growth rate per cycle. More importantly, in the context of the present discussion, there is a demonstrated correlation between the striation spacing and the cyclic stress intensity factor range, (ΔK) . If one makes the reasonable assumption that the overall vibrational loading of the tube is not significantly changed by the development and early growth of small fatigue cracks then (ΔK) levels indicated from striation spacings can be used to determine the cyclic stress range that began the fatigue process.

Replicas of the fracture surface were examined in a transmission electron microscope (TEM). These TEM fractographic examinations were performed to provide the resolution needed to definitively determine if the striation-like markings observed during SEM fractography were indeed fatigue striations and to provide quantitative data pertaining to the spacing of the striations. Two-stage carbon replicas were made for these examinations. The first stage consists of a cellulose acetate replica of the entire fracture surface. The second stage consists of making small carbon replicas, usually referred to as grids, from selected areas of the cellulose acetate replica. Three sets of replicas were made, two before Endox cleaning of the fracture surface and the third after Endox cleaning of the fracture surface. The locations of the grids relative to the fracture surface are illustrated in figure 2.3-1. Grids 3-E, 3-D and 3-C are in the area of the multiple crack initiation sites. Grids 3-B, 3-A and 3-F are in the regions of circumferential growth of the macroscopic fatigue crack.

A summary of striation spacing measurements is presented in Table 2.3-1. Average spacings are listed for various grids and thus locations around the fracture surface. In grids C and E, where the fatigue crack growth direction is essentially through the tube wall, striation spacings are listed for several distances from the tube OD. Indicated (ΔK) levels from the Bates-Clark correlation are also listed.

Estimates of cyclic stress levels can be made from indicated (ΔK) levels as the crack grows through the wall and at relatively short through wall crack lengths. For the case of growth through the tube wall it must be recognized that the tube was dented from corrosion products in the tube support plate crevice. As shown in another section, the denting was of sufficient magnitude to cause plastic

3.1 LEAKING TUBE ANALYSIS

This section provides the stress analysis basis for Row 9 Column 51 at the top of the seventh tube support plate, the effect of denting on mean stress in that region, the tube dynamic characteristics with a propagating crack, the crack propagation analysis matching the fracture surface striations, and the resulting leakage versus time for correlation with the best estimate of actual plant, measured leakage progression.

The fracture surface evaluation of Section 2.0 has shown the failure mechanism to be high cycle fatigue. To address a fatigue mechanism and identify the cause of the loading, any loading condition that would cause cyclic stress or steady mean stress must be considered. The analysis of Normal, Upset and Test conditions described below indicates a relatively low total number of cycles involved and a corresponding low fatigue usage, even with accounting for the dented tube condition at the plate. This analysis does show an axial stress contribution at the tube OD a short distance above the plate from pressure and temperature, thus providing a contribution to mean stress. In addition, combining the effects of denting deflection on the tube demonstrates a high mean stress at the failure location. The vibration analysis for the tube develops the characteristics of first mode, cantilever response of the dented tube to flow induced vibration for the uncracked tube and for the tube with an increasing crack angle, beginning at 90° to the plane of the tube and progressing around on both sides to 180° opposite.

The crack propagation analysis utilizes the results of the analyses just described to match cyclic deformation with the stress intensities and striation spacings indicated by the fracture inspection and analysis. A review of applicable fatigue data with consideration of mean stress provides the basis for probable initial stress amplitudes in the range of 4.0 ksi to 10.0 ksi. Leakage data and crack opening analysis provide the relationship between leak rate and circumferential crack length. Leakage versus time is then predicted from the crack growth analysis and the leakage analysis with initial stress amplitude of 5, 7, and 9 ksi. The comparison to the best estimate of plant leakage (performed after the event) shows a very good agreement. This confirms that flow-induced vibration of the tube with dented supports (providing fixity and mean stress) was the cause for the crack initiation and the subsequent crack propagation and failure of the Row 9 Column 51 tube at the top of the seventh support plate at the cold leg.

3.1.1 Tube Fatigue Analysis

The purpose of this analysis is to determine the fatigue usage for the outside surface of the R9C51 tube at the top support plate resulting from Normal, Upset and Test conditions. The tube is assumed to be round with no gap between the tube and support plate hole. The loading conditions considered include internal pressure, interference loads resulting from differential radial expansion between the tube and support plate, and thru-wall thermal gradient in the tube. The analysis considers all transient conditions defined in the Series 51 Design Specification for North Anna. A summary of the conditions considered is provided in Table 3.1-1. The number of transient cycles is presented for both 9 and 40 years of operation.

The temperatures and pressures for the transient conditions are based on the curves provided in the design specification. The primary-side water temperature at the top support plate is taken to be the average of the T_{hot} and T_{cold} values. Secondary side pressures are determined from steam tables at the saturation temperatures shown in the design specification curves. The tube support-plate temperature is taken to be at the secondary side steam temperature. Summaries of the transient pressures and temperatures are provided in Tables 3.1-2 and 3.1-3. A summary of the primary-to-secondary pressure drop, the tube/support plate relative radial interference, and the thru-wall temperature gradient for each of the transient conditions is provided in Table 3.1-4.

The tube stresses are calculated using the axisymmetric finite element model shown in Figure 3.1-1. Symmetry about the support-plate centerline is utilized to reduce the size of the finite element model. Outside of the support plate, a sufficient length of the tube is modeled to eliminate any end effects from the calculated stresses. Reference pressure and interference load cases are applied to the model, and the results are then scaled based on the actual transient conditions. Stresses for the thru-wall temperature gradient are calculated using conventional analysis techniques. Boundary conditions for the finite element model at the tube/support plate interface assume the tube to be unable to move radially inside the support plate. An axial load is also applied to the tube for the pressure case to account for pressure end-cap loads.

Plots showing the axial stress distribution for the tube inside and outside surfaces for the pressure and radial interference cases are provided in Figures 3.1-2 to 3.1-4. These stresses correspond to a pressure drop across the tube wall of 1000 psi and a tube/support plate interference of 1.0 mil.

For each of the transient conditions, the stress components from the three loading mechanisms are scaled and combined. These stresses are converted to principal stresses and then to stress differences for performing the fatigue analysis. A summary of the resulting stress

differences for the tube outside surface are presented in Table 3.1-5. Prior to performing the fatigue analysis, these stresses are reduced to the set of umbrella conditions summarized in Table 3.1-6. The results of the subsequent fatigue analysis for the tube outside surface is provided in Table 3.1-7. These results show the fatigue usage for an operating period of 40 years to be 0.0396. On a pro-rated basis, the usage for 9 years of operation is 0.009. These results show the fatigue usage from operating conditions to be insignificant with regard to the tube failure.

TABLE 3.1-1
DUTY CYCLE SUMMARY

TRANSIENT	Cycles 40 years	Cycles 9 years
PLANT HEAT UP / COOLDOWN	200	45
PLANT LOADING / UNLOADING	18,300	4118
SMALL STEP LOAD INCREASE	2,000	450
SMALL STEP LOAD DECREASE	2,000	450
LARGE STEP LOAD DECREASE	200	45
HOT STANDBY OPERATION	18,300	4118
LOSS OF LOAD	80	18
LOSS OF POWER	40	9
LOSS OF FLOW	80	18
REACTOR TRIP	400	90
FEEDWATER CYCLING	18,300	4118
PRIMARY SIDE HYDRO	5	1
SECONDARY SIDE HYDRO	5	1
STEAM LINE BREAK	1*	
LOSS OF COOLANT ACCIDENT	1*	
FEED LINE BREAK	1*	

* NOT CONSIDERED IN THE FATIGUE ANALYSIS

TABLE 3.1-2
TRANSIENT PRESSURES

TRANSIENT	TIME	PRIMARY PRESSURE	SECONDARY PRESSURE	PRESSURE GRADIENT
1 PLANT HEAT UP	0.0	0	0	0
	300.0	2250	1020	1230
2 PLANT COOLDOWN	0.0	2250	1020	1230
	300.0	0	0	0
3 PLANT LOADING	0.0	2250	1020	1230
	1200.0	2250	850	1400
4 PLANT UNLOADING	0.0	2250	850	1400
	1200.0	2250	1020	1230
5 SMALL STEP LOAD INCREASE	0.0	2250	850	1400
	25.0	2320	962	1358
	150.0	2125	886	1239
6 SMALL STEP LOAD DECREASE	0.0	2250	850	1400
	25.0	2190	746	1444
	180.0	2310	798	1512
7 LARGE STEP LOAD DECREASE	0.0	2250	850	1400
	50.0	2350	1180	1170
	540.0	1975	1106	869
	1200.0	2200	1089	1111
8 LOSS OF LOAD	0.0	2250	850	1400
	10.0	2600	1228	1372
	100.0	1630	1228	402
9 LOSS OF POWER	0.0	2250	850	1400
	10.0	2070	1238	832
10 LOSS OF FLOW	0.0	2250	850	1400
	140.0	1875	1047	828
11 REACTOR TRIP	0.0	2250	850	1400
	100.0	1870	1106	764
12 FEEDWATER CYCLING	0.0	2250	1020	1230
	540.0	2250	811	1439
13 PRIMARY HYDROTEST	---	3106	0	3106
14 SECONDARY HYDROTEST	---	0	1356	-1356

PRESSURES HAVE UNITS OF PSI
TIME HAS UNITS OF SECONDS

TABLE 3.1-3
TRANSIENT TEMPERATURES

TRANSIENT	TIME	PLATE TEMP	HOT LFG TUBE TEMP	CLD LEG TUBE TEMP
1 PLANT HEAT UP	0.0	70	70	70
	300.0	547	547	547
2 PLANT COOLDOWN	0.0	547	547	547
	300.0	70	70	70
3 PLANT LOADING	0.0	547	547	547
	1200.0	525	568	548
4 PLANT UNLOADING	0.0	525	568	548
	1200.0	547	547	547
5 SMALL STEP LOAD INCREASE	0.0	525	568	548
	25.0	540	579	560
	150.0	530	570	549
6 SMALL STEP LOAD DECREASE	0.0	525	568	548
	50.0	510	558	536
	180.0	518	567	544
7 LARGE STEP LOAD DECREASE	0.0	525	568	548
	60.0	565	590	572
	540.0	547	556	548
	1200.0	555	543	540
8 LOSS OF LOAD	0.0	525	568	548
	10.0	570	593	574
	100.0	570	560	555
9 LOSS OF POWER	0.0	525	568	548
	10.0	571	578	545
10 LOSS OF FLOW	0.0	525	568	548
	45.0	550	523	523
11 REACTOR TRIP	0.0	525	568	548
	100.0	557	544	542
12 FEEDWATER CYCLING	0.0	547	547	547
	540.0	520	534	534
13 PRIMARY HYDROTEST	---	70	70	70
14 SECONDARY HYDROTEST	---	70	70	70

TEMPERATURES ARE IN DEGREES FAHRENHEIT
TIME HAS UNITS OF SECONDS

TABLE 3.1-4
SUMMARY OF TRANSIENT LOAD PARAMETERS

TRANSIENT	TIME	PRESSURE GRADIENT	INTER-FERENCE	THRU-WALL DT
1 PLANT HEAT UP	0.0 300.0	0 1230	[]	a, b, c
2 PLANT COOLDOWN	0.0 300.0	1230 0		
3 PLANT LOADING	0.0 1200.0	1230 1400		
4 PLANT UNLOADING	0.0 1200.0	1400 1230		
5 SMALL STEP LOAD INCREASE	0.0 25.0 150.0	1430 1358 1239		
6 SMALL STEP LOAD DECREASE	0.0 25.0 180.0	1400 1444 1512		
7 LARGE STEP LOAD DECREASE	0.0 60.0 540.0 1200.0	1400 1170 869 1111		
8 LOSS OF LOAD	0.0 10.0 100.0	1400 1372 402		
9 LOSS OF POWER	0.0 10.0	1400 872		
10 LOSS OF FLOW	0.0 45.0	1400 828		
11 REACTOR TRIP	0.0 100.0	1400 764		
12 FEEDWATER CYCLING	0.0 540.0	1230 1439		
13 PRIMARY HYDROTEST	---	3106		
14 SECONDARY HYDROTEST	---	-1356		

THRU-WALL DT (PRIMARY - SECONDARY) HAS UNITS OF DEGREES FAHRENHEIT
PRESSURES HAVE UNITS OF PSI
INTERFERENCE HAS UNITS OF MILS

TABLE 3.1-5
SUMMARY OF STRESS DIFFERENCES
TUBE OUTSIDE SURFACE

CASE NO	TRANSIENT	TIME	SIG 1-2	SIG 2-3	SIG 3-1
1	PLANT HEAT UP	0			
2		300			
3	PLANT COOL DOWN	0			
4		300			
5	PLANT LOADING	0			
6		1200			
7	PLANT UNLOADING	0			
8		1200			
10	SMALL STEP LOAD INCREASE	0			
11		25			
12		150			
13	SMALL STEP LOAD DECREASE	0			
14		5			
15		180			
16	LARGE STEP LOAD DECREASE	0			
17		60			
18		540			
19		1200			
20	LOSS OF LOAD	0			
21		10			
22		100			
23	LOSS OF POWER	0			
24		10			
25	LOSS OF FLOW	0			
26		10			
27	REACTOR TRIP	0			
28		10			
29	FEEDWATER CYCLING	0			
30		540			
31	PRIMARY HYDRO	---			
32	SECONDARY HYDRO	---			

STRESSES HAVE UNITS OF PSI
TIME HAS UNITS OF SEC

TABLE 3.1-6
SUMMARY OF UMBRELLA EVENTS
TUBE OUTSIDE SURFACE

CASE NO	TRANSIENT	CYCLES	SIG 1-2	SIG 2-3	SIG 3-1
1	PLANT HEAT UP	200			
5	PLANT LOADING	18300			
6					
8	PLANT UNLOADING	18300			
10	SMALL STEP LOAD INCREASE	2000			
12					
15	SMALL STEP LOAD DECREASE	2000			
19	LARGE STEP LOAD DECREASE	200			
22	LOSS OF LOAD	80			
24	LOSS OF POWER	40			
26	LOSS OF FLOW	80			
28	REACTOR TRIP	400			
29	FEEDWATER CYCLING	18300			
30					
31	PRIMARY HYDRO	5			

a, c

STRESSES HAVE UNITS OF PSI

TABLE 3.1-7
 SUMMARY OF FATIGUE CALCULATIONS
 TUBE OUTSIDE SURFACE

LOAD COND	Sr	Sa	K x Sa	n	N	n / N
1 - 15						
31						
15 - 22						
15 - 24						
15 - 28						
15 - 26						
15 - 19						
32						
15 - 5						
5 - 6 - 8						
29 - 30						
10 - 12						

$$\text{DAMAGE FOR 9 YEARS} = \frac{9}{40} (0.0396) = 0.009$$

$$\text{YOUNG'S MODULUS RATIO} = 26.0 / 29.0 = 0.897$$

$$K = 0.897$$

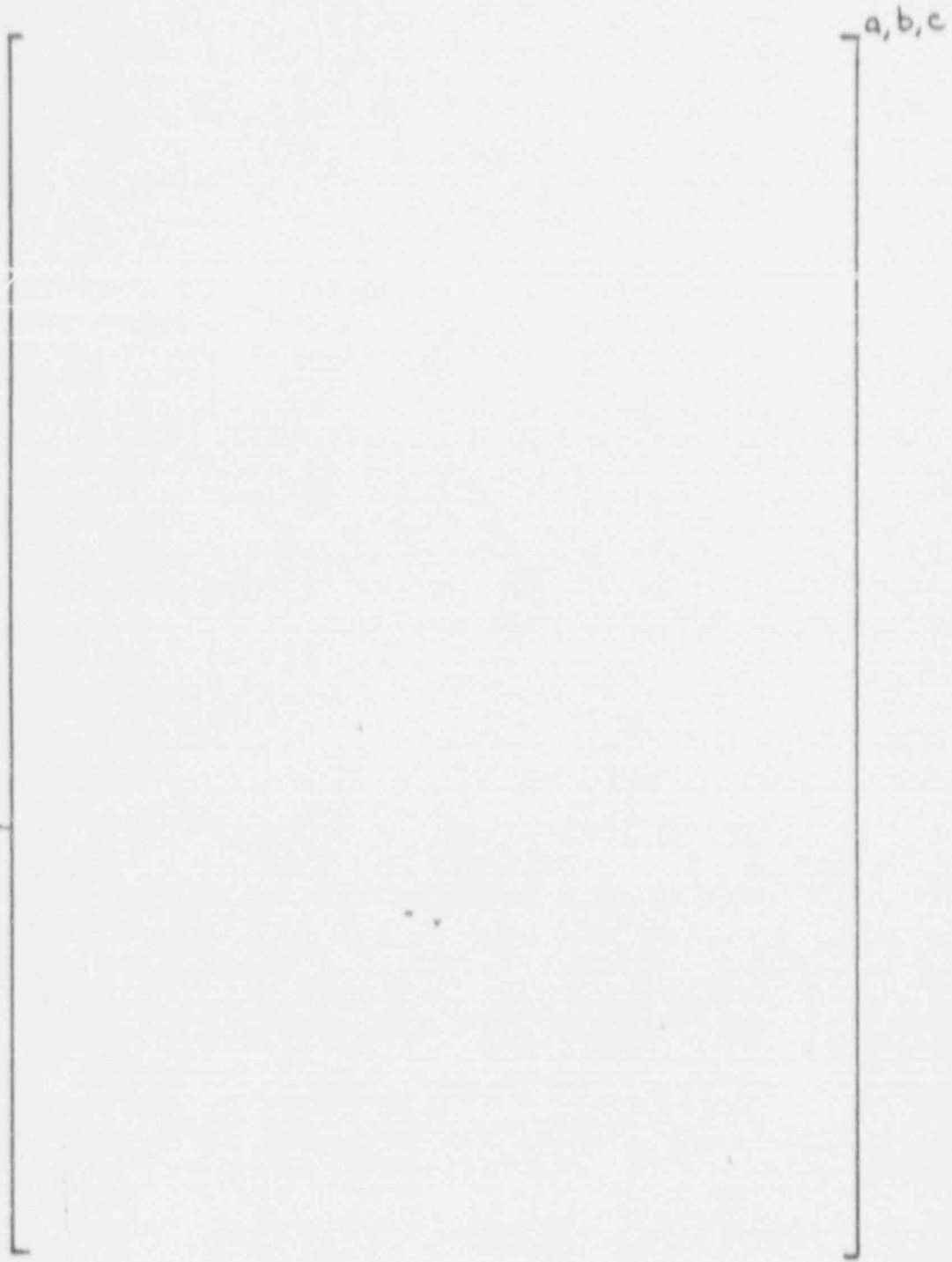


FIGURE 3.1-1 AXISYMMETRIC FINITE ELEMENT TUBE MODEL

DENTED TUBE STRESS DISTRIBUTIONS
PRESSURE LOAD ON TUBE
PRESSURE = 1000 PSI
INSIDE SURFACE

a,b,c

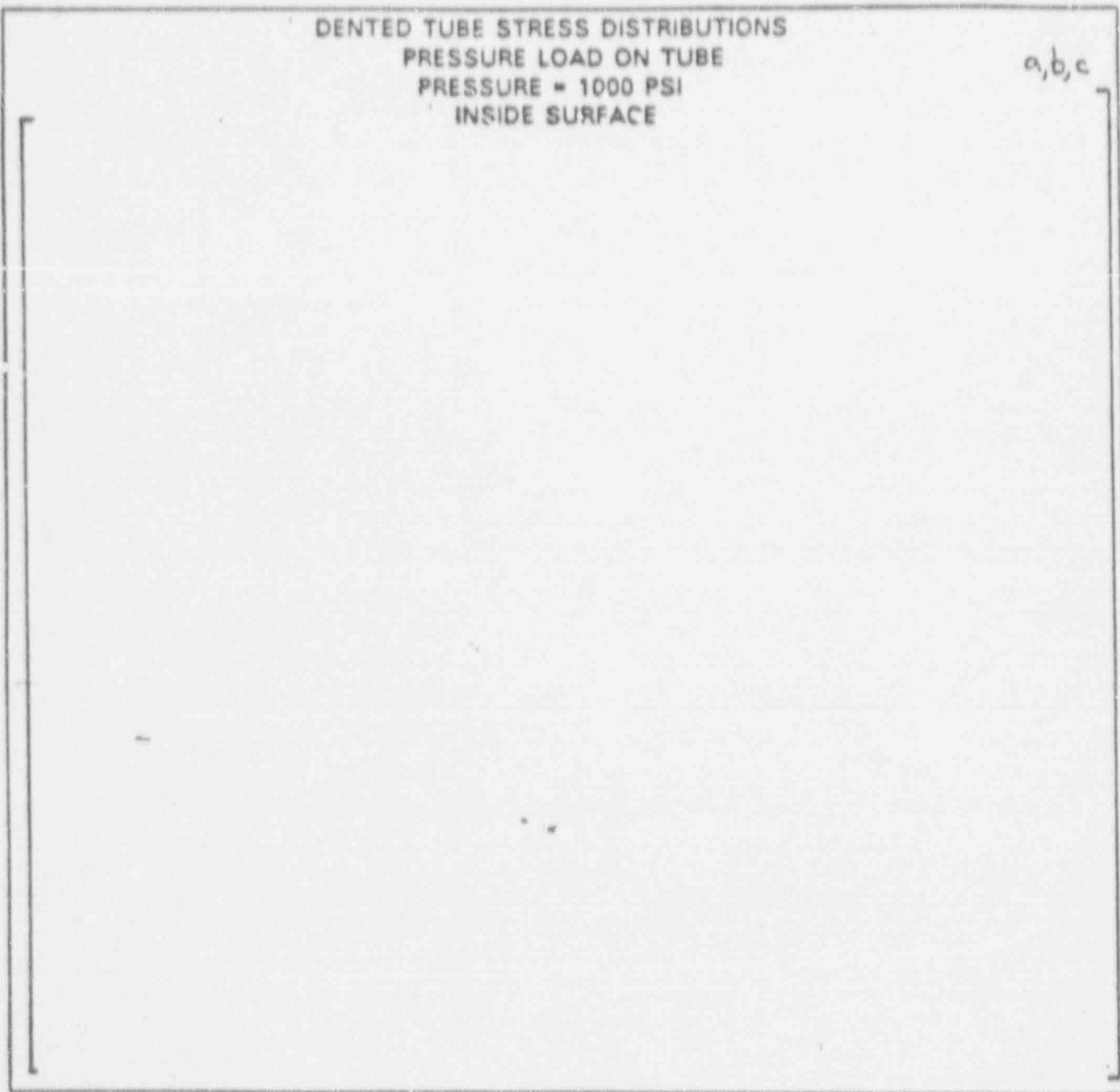


FIGURE 3.1-2 DENTED TUBE STRESS DISTRIBUTIONS
PRESSURE LOAD ON TUBE
INSIDE SURFACE

DENTED TUBE STRESS DISTRIBUTIONS
PRESSURE LOAD ON TUBE
PRESSURE = 1000 PSI
OUTSIDE SURFACE

a,b,c

FIGURE 3.1-3 DENTED TUBE STRESS DISTRIBUTIONS
PRESSURE LOAD ON TUBE
OUTSIDE SURFACE

DENTED TUBE STRESS DISTRIBUTIONS
INTERFERENCE LOAD ON TUBE
1 MIL RADIAL INTERFERENCE
INSIDE SURFACE

a, b, c

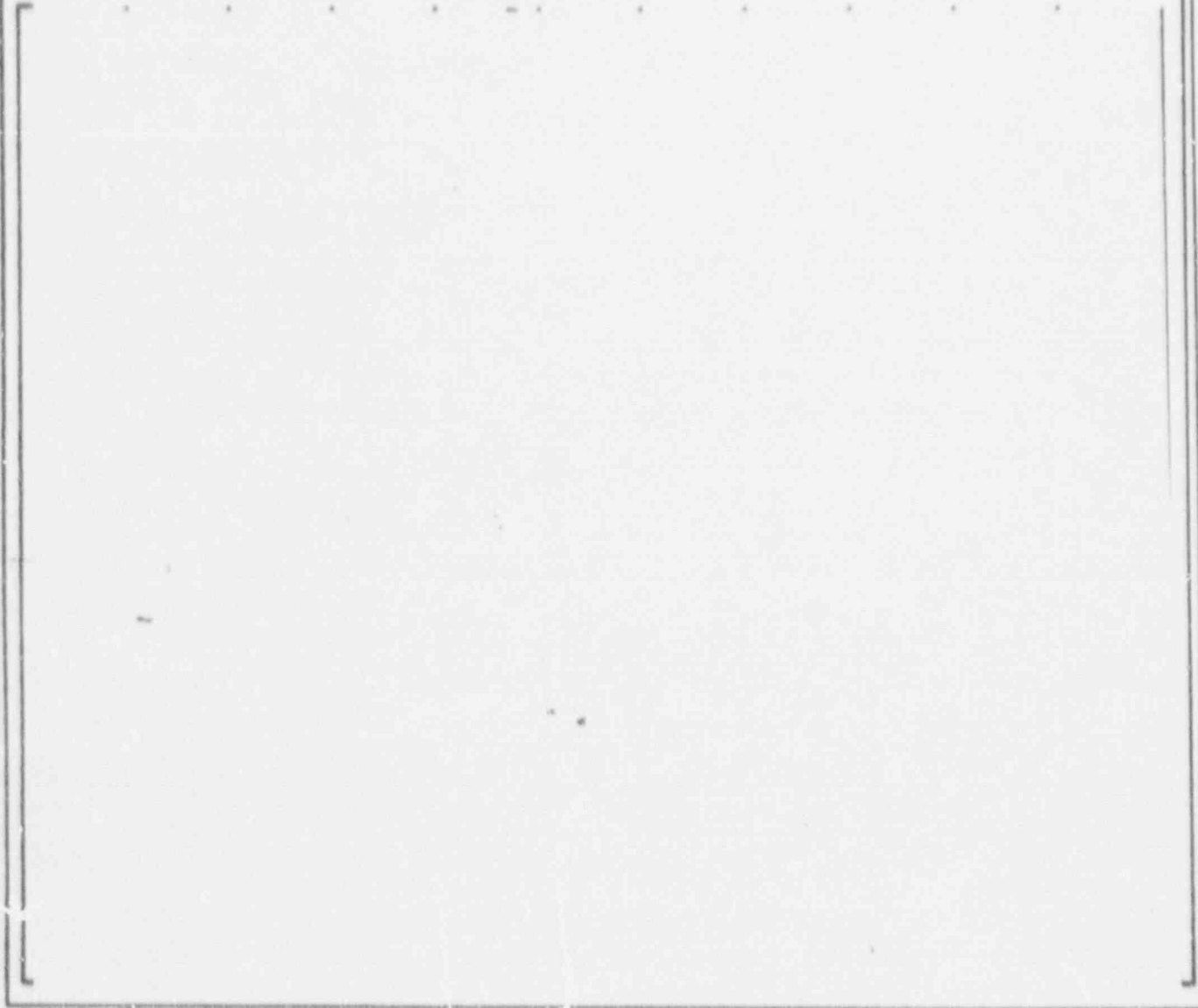


FIGURE 3.1-4 DENTED TUBE STRESS DISTRIBUTIONS
INTERFERENCE LOAD ON TUBE
INSIDE SURFACE

DENTED TUBE STRESS DISTRIBUTIONS
INTERFERENCE LOAD ON TUBE
1 MIL RADIAL INTERFERENCE
OUTSIDE SURFACE

a, b, c

FIGURE 3.1-5 DENTED TUBE STRESS DISTRIBUTIONS
INTERFERENCE LOAD ON TUBE
OUTSIDE SURFACE

3.1.2 Tube Axisymmetric Denting Analysis

This section describes the analysis used to obtain the stresses in the tube produced by an axisymmetric dent at the top tube support plate. Included are a discussion of the basis for the dent profile, a description of GAPL-3, the computer program used to calculate the stresses, the finite element model and boundary conditions, and the results of the analysis.

Profilometry data was obtained for the severed tube. However, the look-ahead feature of the instrumentation was overloaded by the break in the tube and, as shown in Figure 3.1-6, gave spurious results for the tube profile in the upper half of the TSP. Consequently, profilometry data for an adjacent tube was used as the basis for the dent profile, scaled to match the depth of the dent observed in the severed tube in the bottom half of TSP 7. Figure 3.1-7 shows the dent profiles for the severed tube and an adjacent tube. The analysis described in this section uses the dent profile of the adjacent tube, but with a maximum radial deflection of 2.67 mils. This figure includes the 2.5 mils indicated by data for the severed tube plus 0.17 mils due to differential thermal expansion between the TSP and tube. The inelastic stress analysis of the dented tube was performed using the computer program GAPL-3. This program performs an elastic-plastic, large deflection analysis of thin plates or axisymmetric shells with pressure loading and deflection restraints. It is particularly appropriate when nonlinear material or geometric effects are important. Among its distinguishing features are:

1. Large deflection theory based on the current, updated geometry is used
2. Either the deformation or incremental theory of plasticity may be specified
3. Elastic-plastic material properties are used
4. A wide range of boundary conditions may be considered
5. The rigid deflection restraint may take any shape and orientation
6. GAPL-3 has been confirmed by experiment to provide accurate solutions for plastic strains up to 10-15%.

GAPL-3 uses a two-layered system of finite elements. A body is first divided into elements along its length called strain regions, where interpolating polynomials are used to express deflections within these regions in terms of deflection parameters at the ends. Each strain region is then sub-divided into stress elements, in which stresses are found as functions of the strains in the element.

For this analysis, a section of the tube from the middle of the top TSP to 0.875 inches above the top TSP is considered. This section of tube is divided into 30 strain regions with up to 15 stress elements through the thickness as shown in Figure 3.1-9.

The stress-strain curve used for the tube is shown in Figure 3.1-13. This was obtained by adjusting the stress-strain curve for SB-163 at 550°F to give a 0.2% offset yield stress of []^{2,4,C}

Boundary conditions consist of symmetry conditions at the center of the TSP (left end) and zero rotation plus an end cap force at the right end. An internal pressure of 1400 psi is also applied to represent the difference between the primary and secondary side pressures. The rigid deflection restraint is used to impose the denting profile on the tube within the TSP. This is done in several steps to insure that solution convergence is maintained.

Figures 3.1-8 through 3.1-12 show the results of this analysis. The deflection of the tube mid-surface is shown in Figure 3.1-10. On this figure the cross-hatched area is the deflection restraint, the dashed line is the initial position of the tube, and the solid line is the final deflected position of the tube. The next two figures give the axial and hoop stresses along the inside and outside surfaces of the tube. The axial stress contours within the tube are given in Figure 3.1-12.

The maximum axial stress at the outside surface is 46.4 ksi. This includes the effects of the dent, differential thermal expansion between the TSP and tube, and the tube through wall temperature gradient.

FIFTH ANNA SEVERED TUBE PROFILE

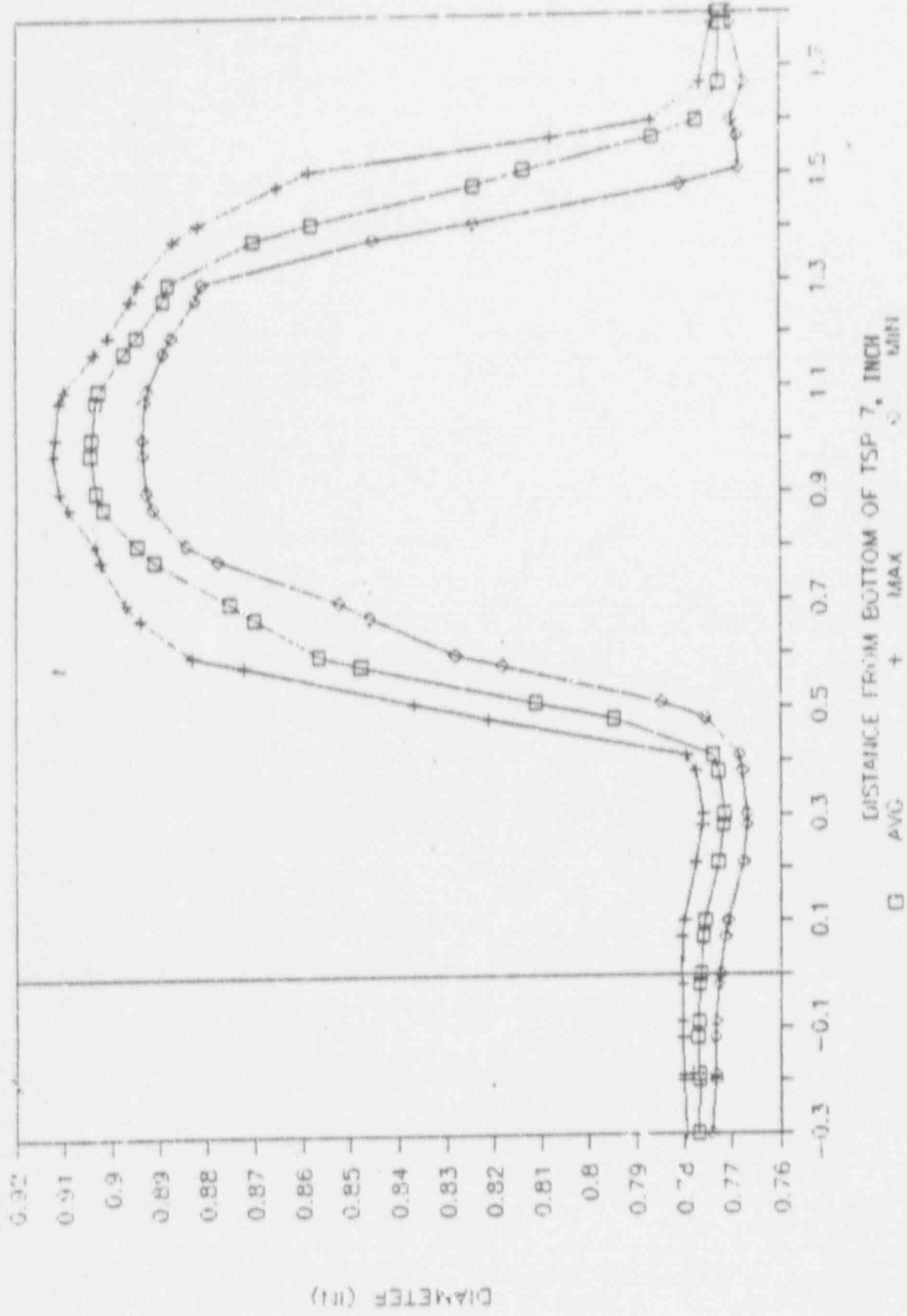


FIGURE 3.1-6 Severed Tube Profilometry Data

a, b, c



FIGURE 3.1-7 Comparison of Dent Profiles for Severed and Adjacent Tubes

a,b,c

FIGURE 3.1-8. DENTED TUBE SURFACE HOOP STRESSES

a, b, c

FIGURE 3.1-9 GAPL-3 Finite Element Model (Not to Scale)

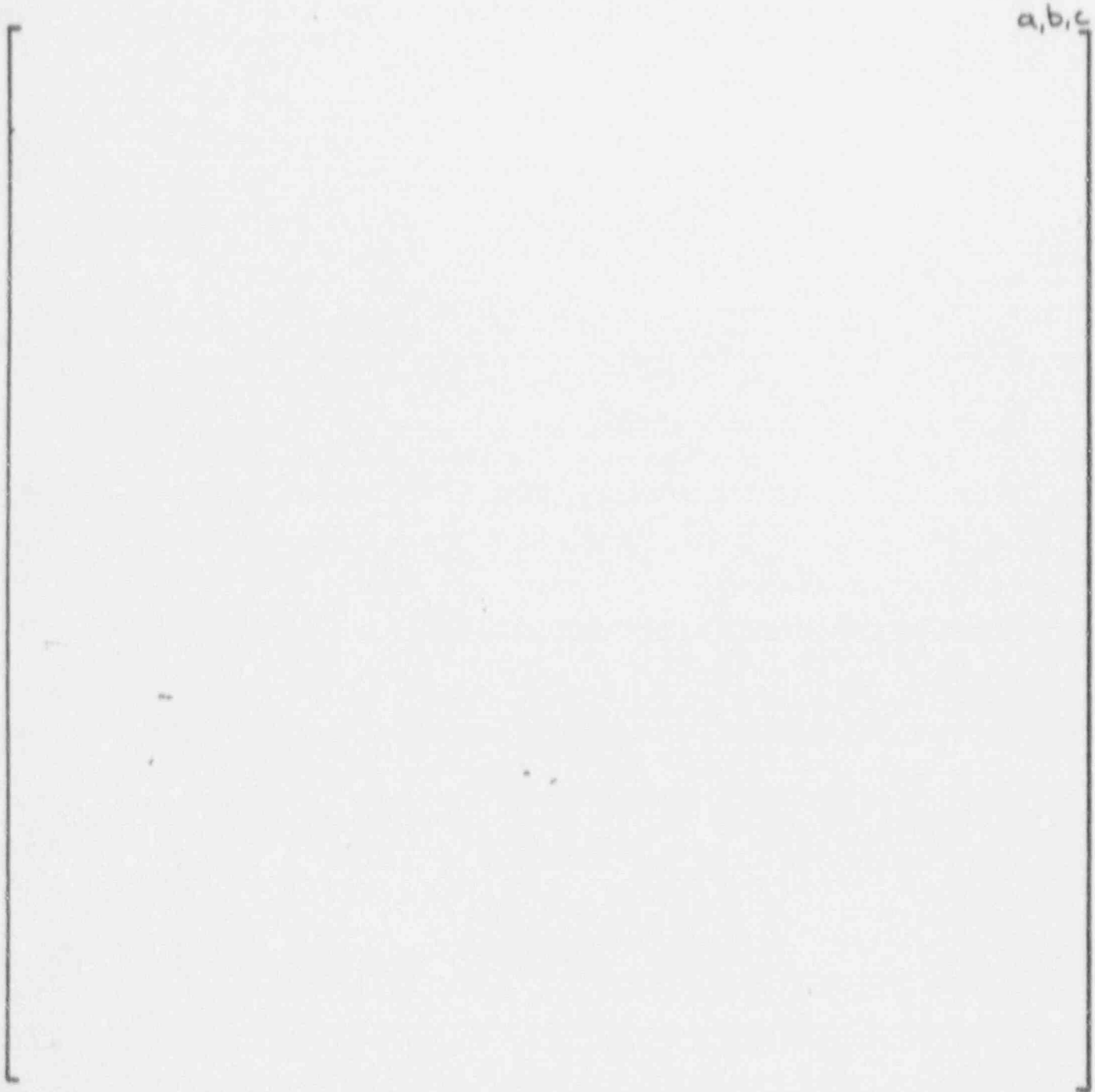


FIGURE 3.1-10 Deflection of Dented Tube Mid-Surface

a,b,c

FIGURE 3.1-11. CENED TUBE SURFACE AXIAL STRESSES

a, b, c

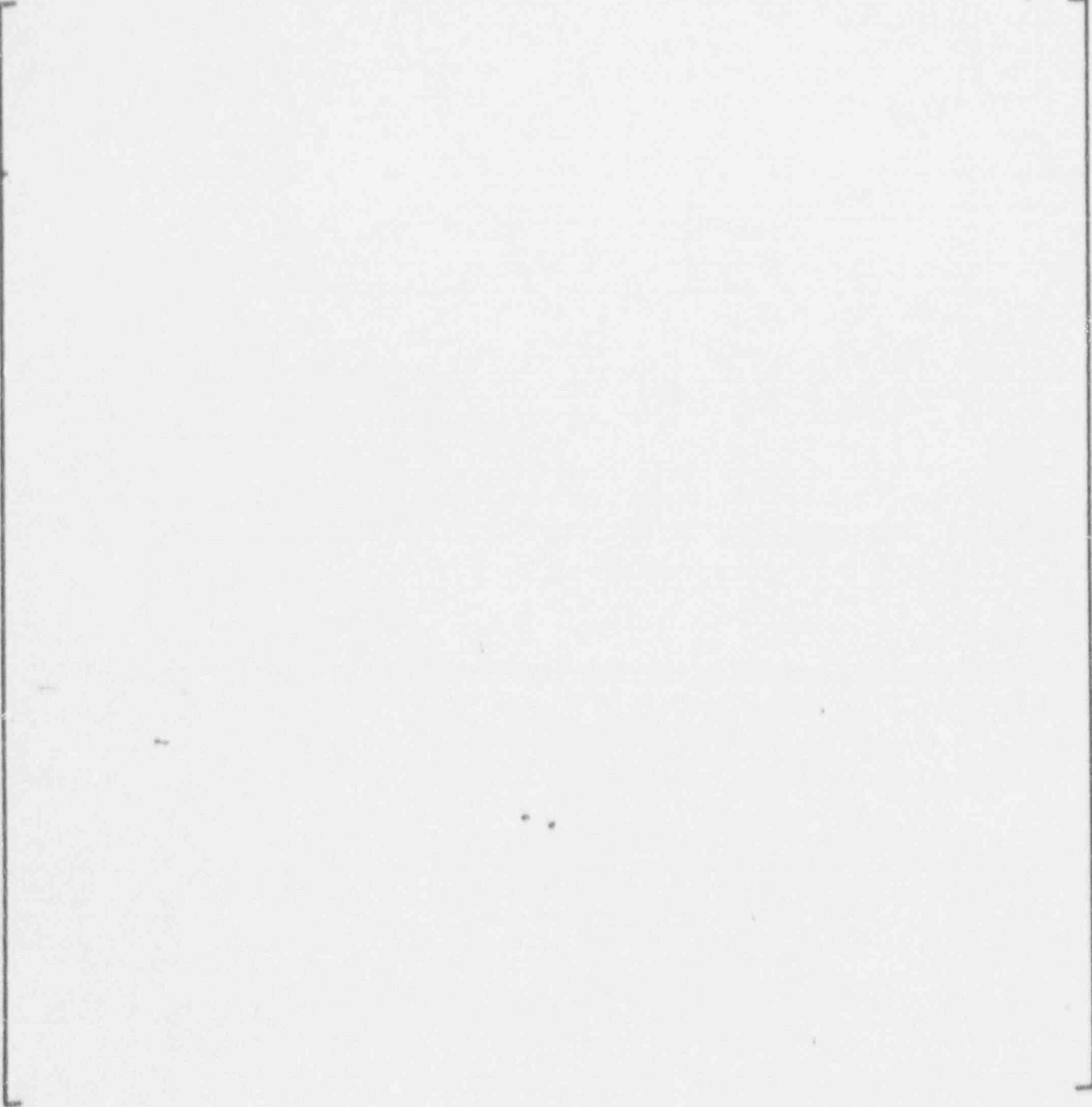


FIGURE 3.1-12 Dented Tube Axial Stress Contours

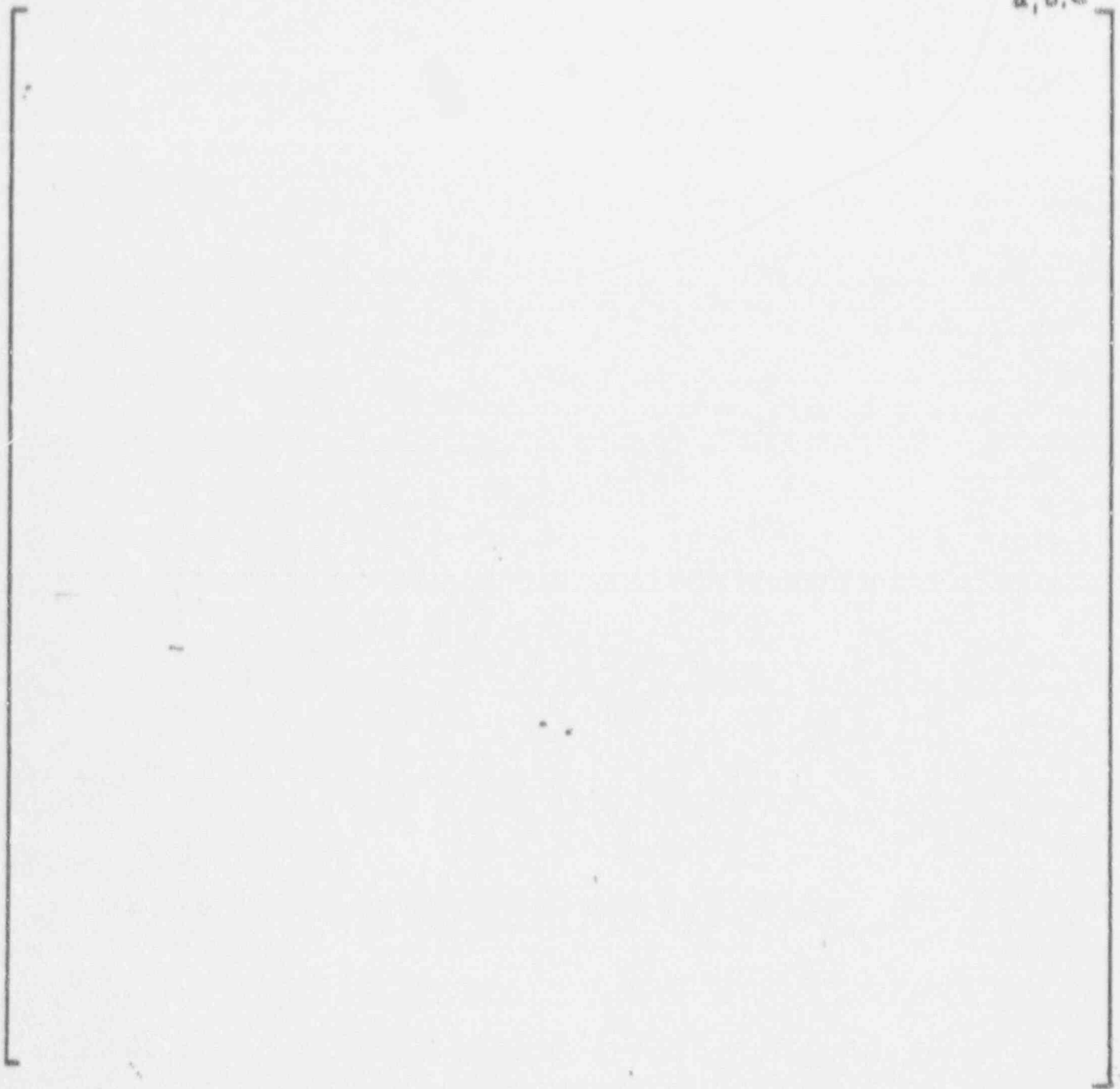


FIGURE 3.1-13 ENGINEERING STRESS - STRAIN CURVE FOR $S_y = KSI$

3.1.3 Tube Vibration Analysis

This section contains the results and procedures used to describe the effect on the tube of a crack developing and growing in steam generator C at North Anna 1. The region of interest is located at the top tube support plate in row 9 column 51 with the crack occurring on the cold leg side. The analysis is performed using FLOVIB, a Westinghouse proprietary computer code coupled with closed form techniques. The methodology is described in further detail along with the results of the analysis in the following paragraphs. The analysis forms the basis to describe the events leading to the tube rupture once the through wall crack had developed.

The results presented in this section indicate that with increased crack size, an increase in the propensity of the tube to become fluidelastically unstable would result. Increased tube stress and tube displacement would also occur.

The tube was modeled using FLOVIB, a Westinghouse proprietary finite element based computer code. This code was written to predict the response of steam generator tubing exposed to a given fluid velocity and density profile. The program calculates the tube natural frequencies and mode shapes using a linear finite element model of the tube. The fluidelastic stability ratio U_e/U_c (the ratio of the effective velocity to the critical velocity), the vibration amplitudes caused by turbulence, and the resulting dynamic forces and moments generated at the tube support locations are calculated for a given velocity/density field and tube support condition. The velocity and density distributions for a given row and column are determined using the ATHOS computer code. Also input to the code are: node locations, element conductivity, material and section properties. Additional input to the code consists of boundary conditions, fluid elastic stability constants, turbulence constants and damping. All of these quantities are required to obtain a solution using FLOVIB.

Figure 3.1.3-1 contains a plot of the FLOVIB model used to determine the response of the tube with various size cracks included in the model. Note that the model represents the full tube with both straight leg and U-bends included. However because the tubes are [

J. A. C

The hot leg is the left most portion and the cold leg is the right most portion of the model as indicated in the figure. The crack has been modeled on the cold leg side |

are contained in a subsequent subsection.]^a The results of this process

The crack was incorporated into the FLOVIB model by [

] ^{a, c}

[

] a, c

Figure 3.1.3-3 contains a plot of I_2 vs. half crack angle (GAMMA). As can be observed in the figure, the moment of inertia rapidly drops off with increased crack size indicating that even small cracks can effect the rotational stiffness of the tube. This plot can be compared to a case where the additional rotation due to the crack has been not been included. Figure 3.1.3-4 contains a plot of the moment of inertia without the crack. As can be observed in the figure, the moment of inertia (and also rotational stiffness) does not drop off nearly as fast as when the crack opening is specifically included. Comparing these two plots indicates that [

] Therefore all of the analysis performed with cracks present in the tube have used the information contained in Figure 3.1.3-3 in the modeling process. 5

The methodology discussed above was used on a parametric basis to describe the effect on the row 9 column 51 tube with various sized cracks. This was performed by running FLOVIB with the section properties (at the crack elevation) modified according to Figure 3.1.3-3 for half crack angles (GAMMA): 0, 30, 65, 90, 110, 145 and 175 degrees. Note that the results presented in this section are relative with damping and beta held constant at 1.0 percent and 5.2 respectively.

A measure of the propensity of the tube to experience more fluidelastic excitation is to look at the normalized critical velocity vs. GAMMA. Figure 3.1.3-5 contains this plot where the critical velocity has been normalized with critical velocity with GAMMA set to 0 degrees. As can be observed in the figure (and would be expected) the critical velocity decreases with increased GAMMA. This indicates that the fluid velocity required for the tube to be excited fluidelastically decreases with increased crack angle. Figure 3.1.3-6 contains a plot of first mode natural frequency vs. GAMMA. This figure also correlates with the expected response of the tube due to a decrease in tube stiffness, i.e., with decreased stiffness a decrease in natural frequency would occur. The reduction in frequency coupled with the reduction in critical velocity is an expected correlation. Critical velocity must change with a frequency change because all of the other relevant parameters do not, i.e. Beta, Zeta, fluid profile and density profile.

FLOVIB also calculates tube displacement due to turbulence for a given set of boundary conditions. Figure 3.1.3-7 contains a plot of tube displacement vs. GAMMA. Both the maximum displacement and displacement at the Ubend apex are included in this plot. As can be observed in the plot the displacements increase with increasing GAMMA. Note that the apex displacement and maximum displacement have the same value when the half crack angle is small (indicating symmetrical displacement about the apex). An additional observation is that as the crack angle increases the maximum displacement value increases at a greater rate than the apex displacement value indicating that the tube displacement is becoming more and more unsymmetrical. This trend can be observed in Figure 3.1.3-8 where the location of maximum displacement is plotted against GAMMA. As can be observed in the figure the location of maximum displacement moves closer to the crack with increased crack angle.

The dynamic bending and torsion moments at the crack can also be calculated in FLOVIB. Figure 3.1.3-9 contains a plot of bending moment and torsion values vs. GAMMA. This figure indicates that both the bending moment and torsion values are fairly constant over a substantial portion of the range of GAMMA before the values begin to change. These fairly constant values of torsion and bending moment along with the decrease in section modulus (due to the crack) will result in an increase in stress with increased crack angle.

Specific values of stress and turbulent amplitude were calculated for use in subsequent analysis. It was determined that the RMS modal vibration amplitude is [] for an uncracked (GAMMA = 0) row 9 column 51 tube. The resulting bending stress amplitude is 50 psi for this RMS displacement. Allowing for peak amplitudes and certainties in turbulence input would still result in a stress amplitude of less than 1000 psi. It was also determined (for fluidelastic excitation) that the bending stress amplitude for the first mode of vibration is

] A, B, C

As cracking progresses around the tube circumference, the vibration amplitude of the tube will increase since the tube stiffness is decreasing and the critical velocity is decreasing. For this analysis, BETA and damping have been held constant and therefore the drop in critical velocity is the result of the frequency change.

The crack growth analysis develops growth that is consistent with the K stress intensity implied by the striation spacing. A tube stress and the implied displacement is required for the uncracked tube for initiation and the correct displacement must be obtained at a crack half angle of 90 degrees that gives a K = 50 ksi-root inch. That displacement is [] The relation between the initiation displacement and the displacement at 90 degrees is specified as an nth order function of frequency, i.e., critical velocity.

The relation is :

$$\left[\dots \right]^{A, B, C}$$

where $n = \left[\dots \right]^{A, B, C}$ For an initial displacement of [] and the resulting plot of displacement versus [] crack half angle is shown in Figure 3.1.5-10.

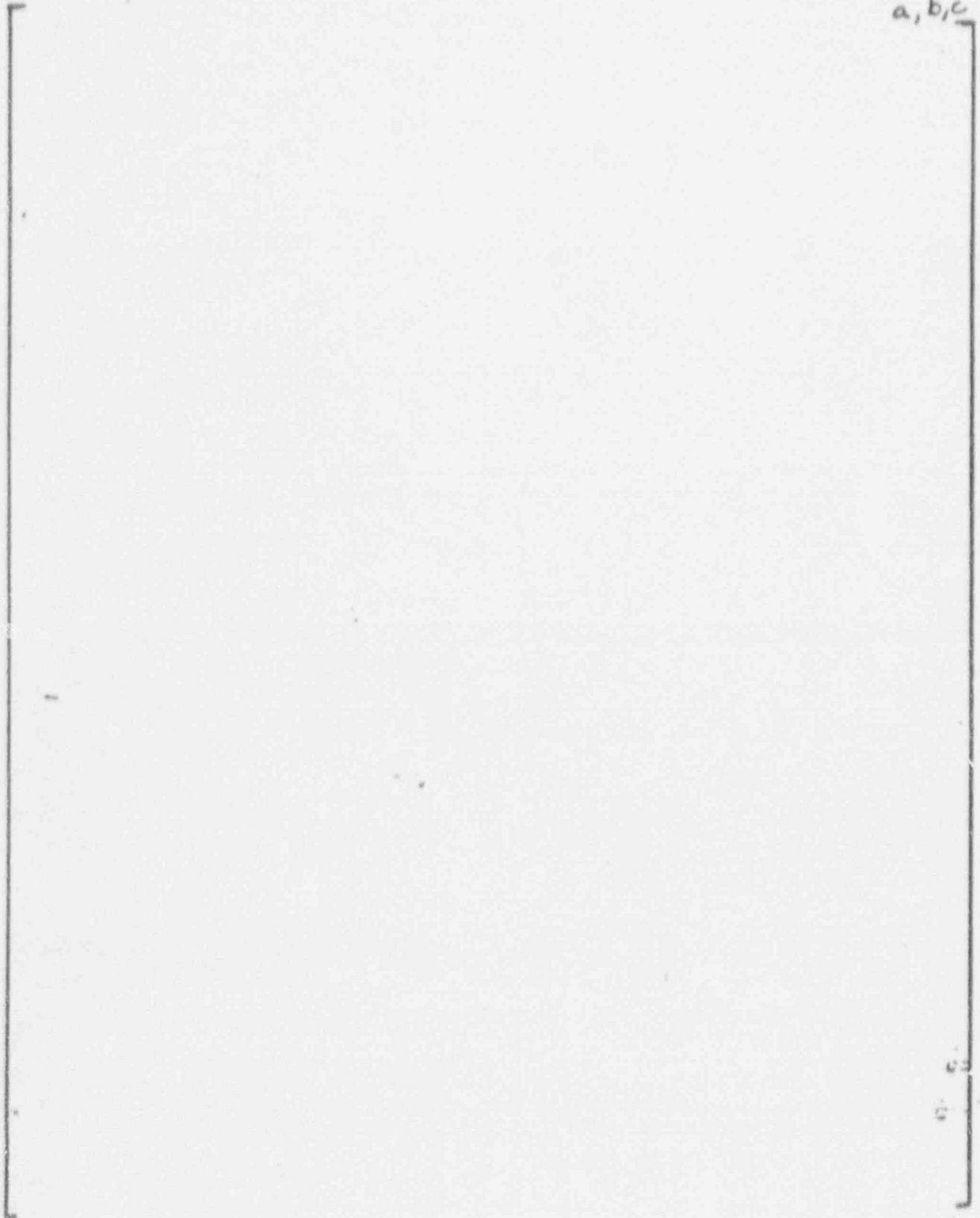


FIGURE 3.1.3-1: FLOVIB MODEL OF STEAM GENERATOR TUBE



FIGURE 3.1.3-2: CRACK MODEL PARAMETER DESCRIPTION

a, b, c

MOMENT OF INERTIA VS. HALF CRACK ANGLE

FIGURE 3.1.3-3

MOMENT OF INERTIA VS CRACK ANGLE

a,b,c



FIGURE 3.1.3-4

NORMALIZED 'CRITICAL VELOCITY

a_{cr}/c

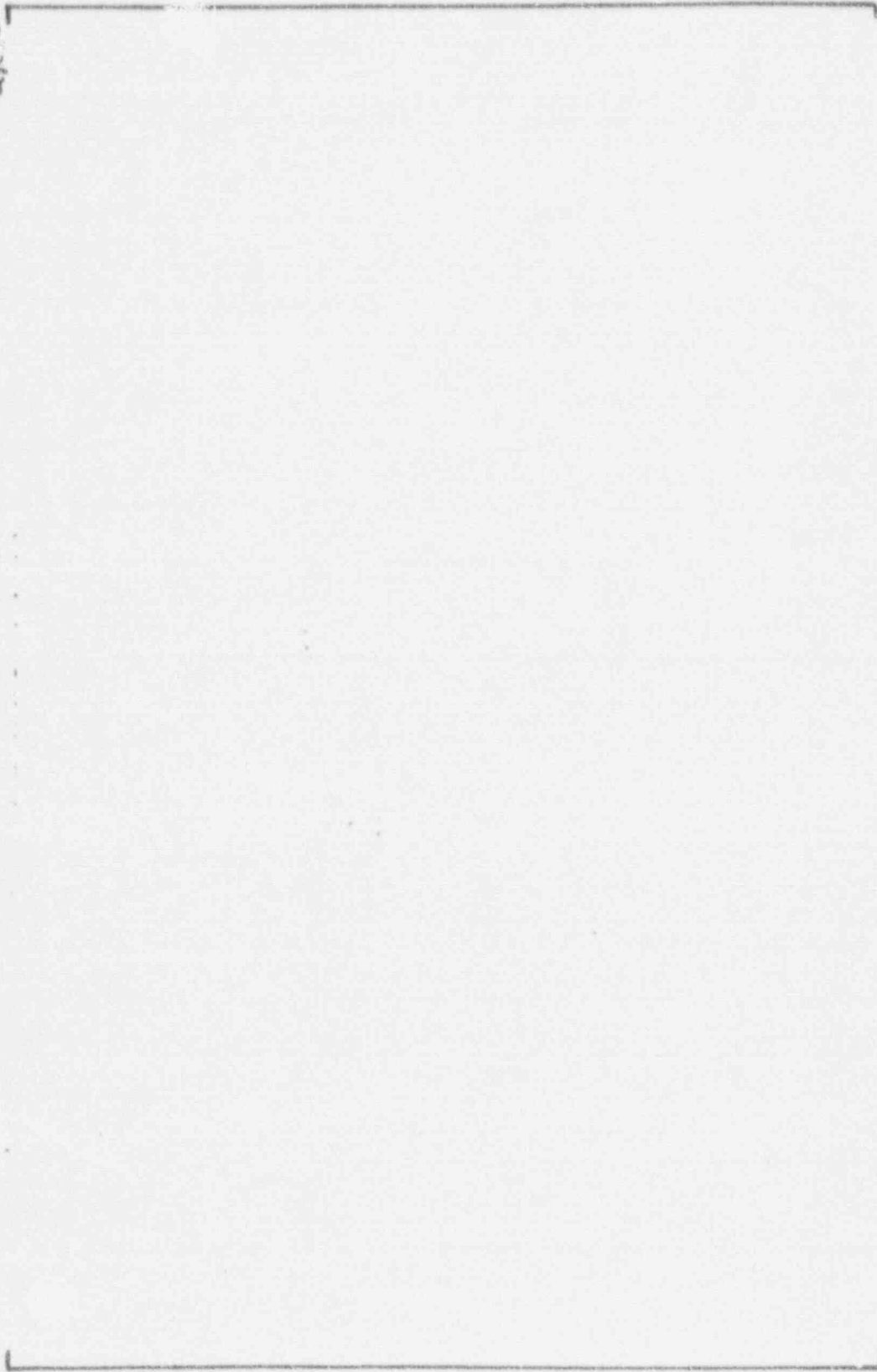


FIGURE 3.1.3-5

FREQUENCY VS. HALF CRACK ANGLE

a,b,c

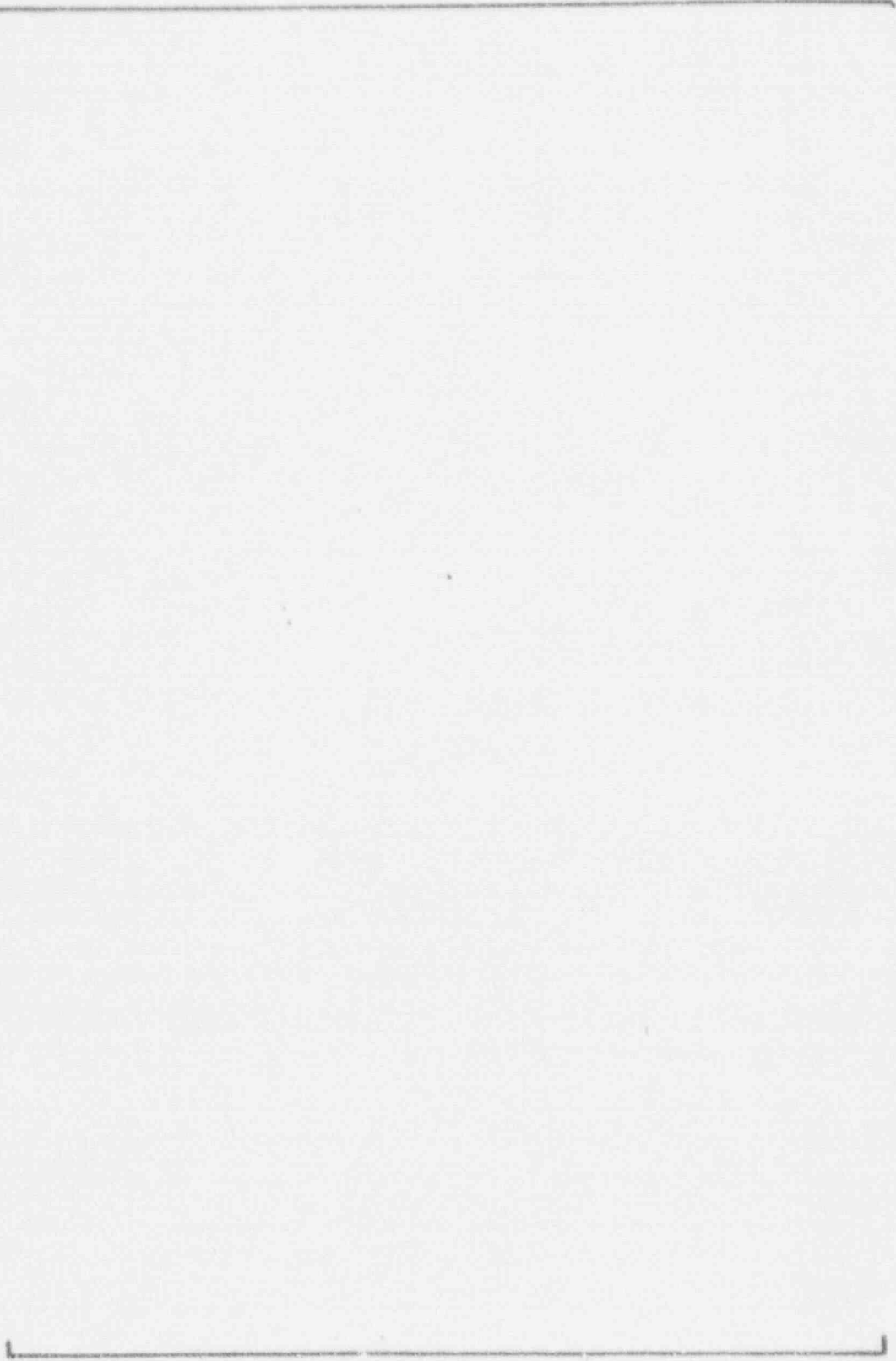


FIGURE 1.3-6

TUBE DISPLACEMENT VS. HALF CRACK ANGLE

a.b.c

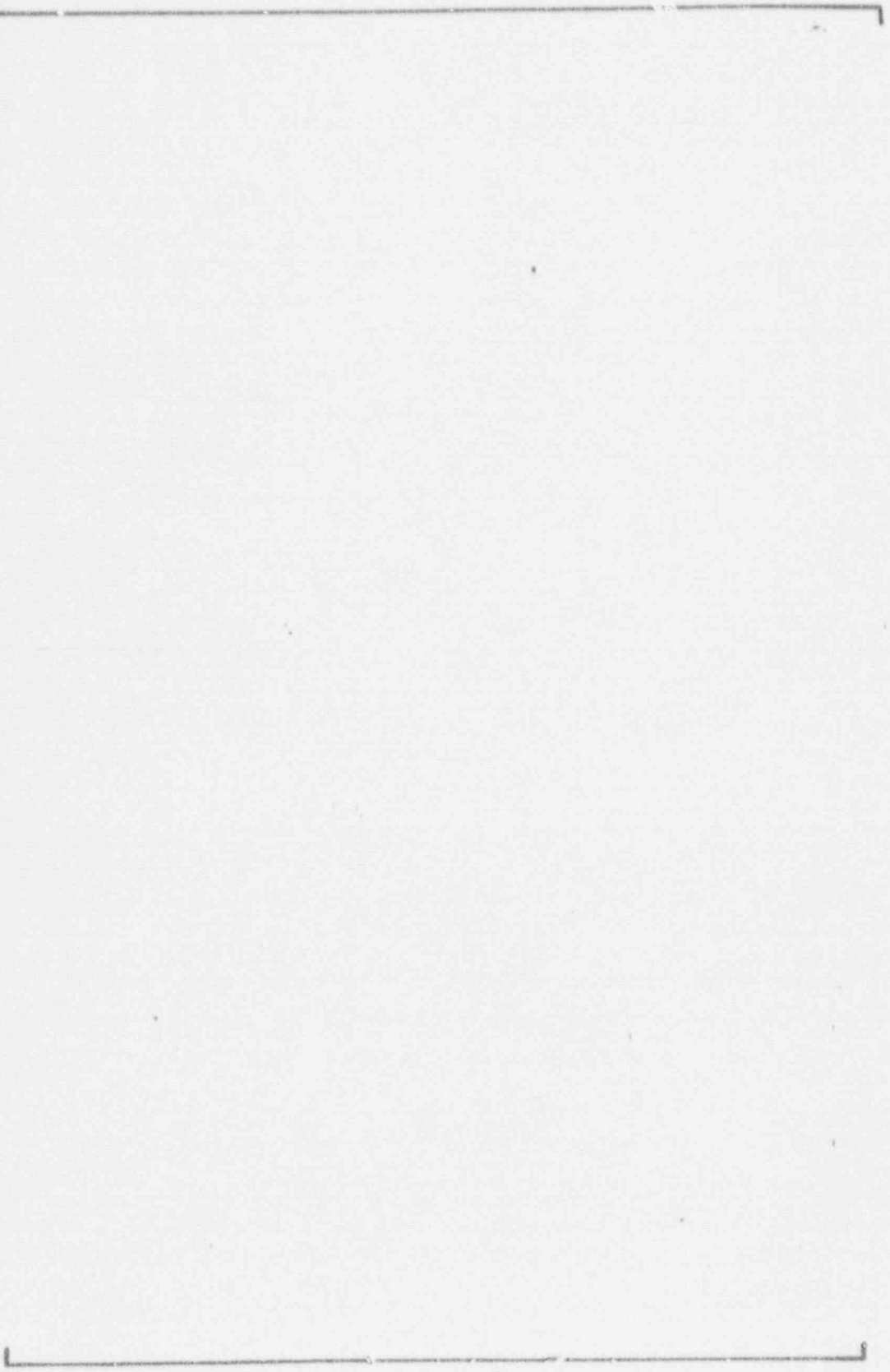


FIGURE 3.1.3-7

MAX DISPL. LOC. VS. HALF CRACK ANGLE

a,b,c

FIGURE 3.1.3-8

MOMENT AND TORSION VS. HALF CRACK ANGLE a/bc

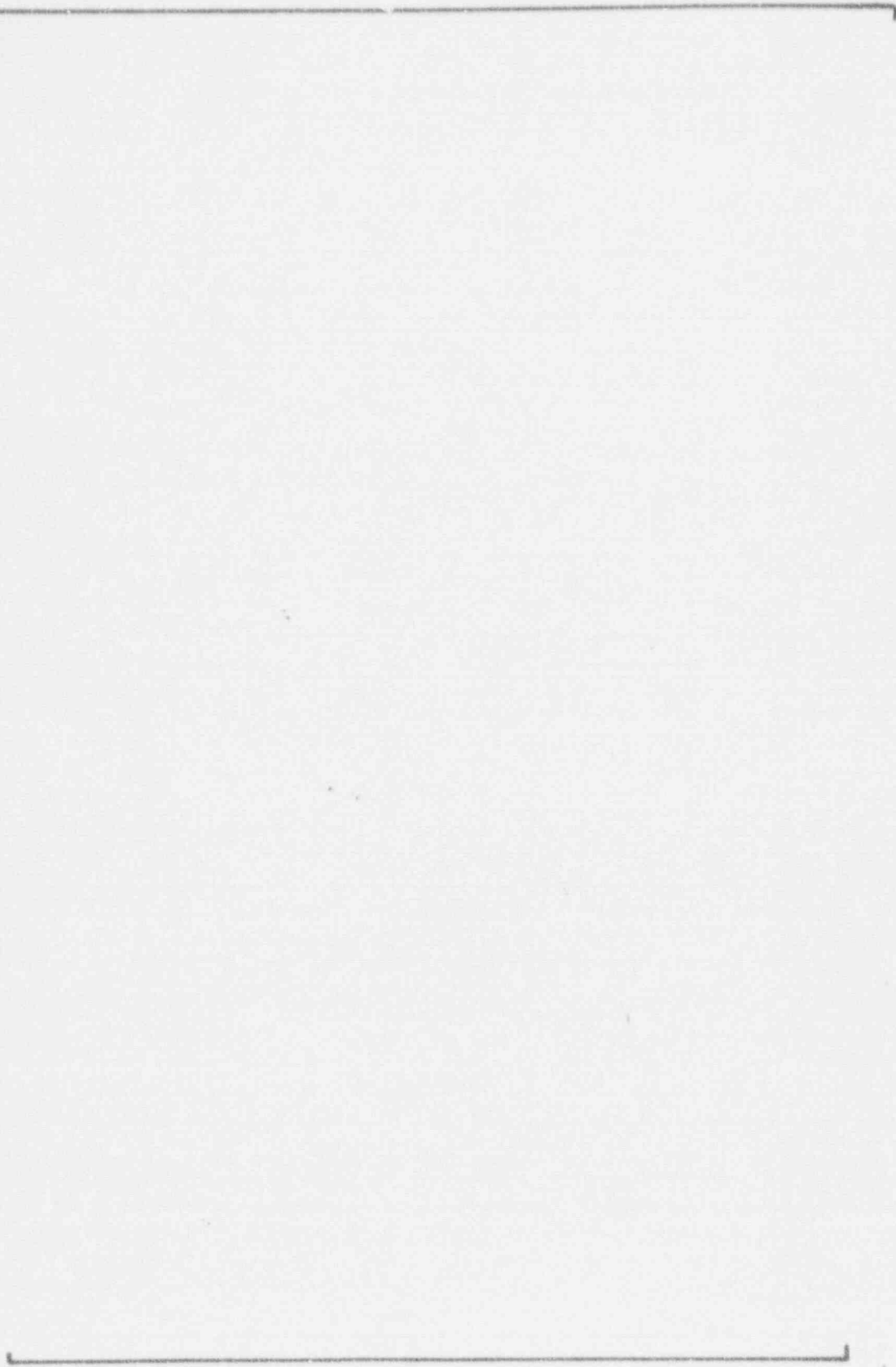


FIGURE 3.1.3-9

a, b, c



FIGURE 1.1.3-10

3.2 Cyclic Life Analysis

A cyclic life analysis of the severed tube is presented in the following paragraphs. Fatigue initiation is considered first, then crack growth across the wall thickness and finally circumferential growth of the through wall crack leading to tube rupture. Leak rates through the growing circumferential crack are calculated and compared to field observations.

The fatigue crack initiation analysis begins with the selection of the appropriate S-N curve. Ideally, data on high carbon, mill annealed Alloy 600 tubing in a secondary water environment is desired. Information of this nature is available from the work of Jacko. Figure 3.2.1 is a plot of fatigue strength versus cyclic life for mill annealed Alloy 600 tubing in AVT water at 600 F. The carbon content and yield strength of the test material 0.049% C and [] are close matches to the fractured tube. The fatigue strength is expressed as the cyclic stress amplitude for fully reversed loading. The calculated lower three sigma fatigue strength is plotted, that is, the calculated average fatigue strength minus three standard deviations. Since the natural frequency of vibration of uncracked row 9 U-bends is [] the total number of cycles experienced by the ruptured tube is estimated as about $3.5E+9$ cycles. From figure 3.2.1, the fatigue strength for fully reversed loading at this cyclic life is estimated as 20 ksi. Since the fractured tube was dented, a mean stress effect must be considered. The previous section has shown that denting, of the magnitude experienced by the fractured tube, is sufficient to cause plastic yielding of the tube wall in the vicinity of the tube support plate. Axial stresses at essentially yield point levels are produced. These stresses vary rapidly in the vicinity of the top of the tube support plate changing from compression to tension as distance increases from the top of the plate. The fatigue crack initiation sites are considered to be located at the position of high tensile stress. Cyclic bending of the tube and shakedown to elastic action thus leads to tension-tension cyclic stresses with a maximum stress at the yield point level on the OD of the tube. The yield stress of the fractured tube at temperature is judged to be []. The data presented by Jacko indicates that the cyclic and monotonic strengths of the ruptured tube should be about equal.

A number of approaches describing mean stress effects on fatigue strength are available. []

[] The equation simply states that the product of cyclic stress amplitude and maximum stress in the cycle is a constant. On this basis, cyclic stress amplitude versus maximum stress is plotted in figure 3.2.2 for a cyclic life of $3.5E+9$ cycles for Alloy 600 in 600 F AVT water. Entering the maximum stress as [], the yield point of the ruptured tube at temperature, leads to a cyclic stress amplitude required for failure on the order of 7 ksi. This cyclic stress amplitude is in

reasonable agreement with estimates of cyclic stress amplitudes in the range of 4 to 10 ksi from striation spacing measurements. Fatigue loading at these amplitudes in the presence of a mean tensile stress produced by denting is judged to be a reasonable requirement to produce fatigue crack initiation in the presence of nominal bulk AVT water chemistry for cyclic lives in the vicinity of $3.5E+9$ cycles. Figure 3.2.2A shows the successful application of the Smith-Watson-Topper correlation to empirical data which includes the influence of environmental effects on fatigue behavior.

At some point in the crack initiation process, crack growth begins to approach rates related to macroscopic cracks describable in terms of fracture mechanics parameters. As will be seen shortly, the fatigue life of the ruptured tube was overwhelmingly devoted to the process of crack initiation. In the vicinity of several mils to 10 mils in crack depth, after a relatively lengthy period of development, fatigue crack growth rates approached measured striation spacings on the order of one micro-inch per cycle. Since the tube wall thickness is 50,000 micro-inches, a rough estimate of the cycles required for penetration of the tube wall is 50,000 cycles. At 60 hertz this would be rapidly accomplished.

Once the dynamic analysis of row 9 U-bend vibration is available, the analysis of the propagation of a through wall fatigue crack around the circumference of the tube is relatively straightforward. [

Since leak rates versus time are of much greater practical interest, crack growth calculations are expressed in this fashion. The relationship of leak rates to crack opening areas was established empirically. Measurements of leak rates through axial fatigue cracks in Alloy 600 tubing have been performed at Westinghouse for over 15 years. A constant relating leak rates at 550 F at a differential pressure of 1250 psi to crack opening areas was determined. This constant used to compute leak rates through circumferential cracks.

Comparison of limited recent measurements of leak rates through circumferential fatigue cracks with calculated values was excellent. This constant was adjusted to the slightly higher differential pressure of 1400 psi by the ratio of the square root of the pressure differential.

Since the natural frequency of the U-bend vibration depends on the crack angle, this relationship was included to convert the cycle count to a time count.

Leak rate versus time calculations are illustrated in figure 3.2.2. Three cyclic stress amplitudes are included 5, 7 and 9 ksi. Initial U-bend apex displacements were selected to produce these outer fiber stresses in an uncracked tube. As the crack grew, the displacement was increased to produce a cyclic stress stress intensity range of 50 ksi in^{1/2} at a total crack arc of 180 degrees. This is in agreement with striation spacing measurements and a transition in the macroscopic fracture appearance from flat to slant fracture. The macroscopic fracture mode transition in fatigue occurs approximately when the cyclic plastic zone size is equal to the tube wall thickness. Calculations were begun when the initial through wall total crack arc was 20 degrees. This is about the minimum arc expected for a single initiation site. The leak rate expected for a [

] A reasonable match of [

] This value places the crack growth rates at the lower edge of the scatter band of measured values. The predicted leak rate versus time curves of figure 3.2.3 provide a reasonable bound to expected leak rates from possible tube fatigue events without any action to reduce vibration amplitudes. As actions are taken to lessen vibrational amplitudes, additional tube fatigue events become very unlikely and the expected time to respond to this unlikely event increases.

a, b, c

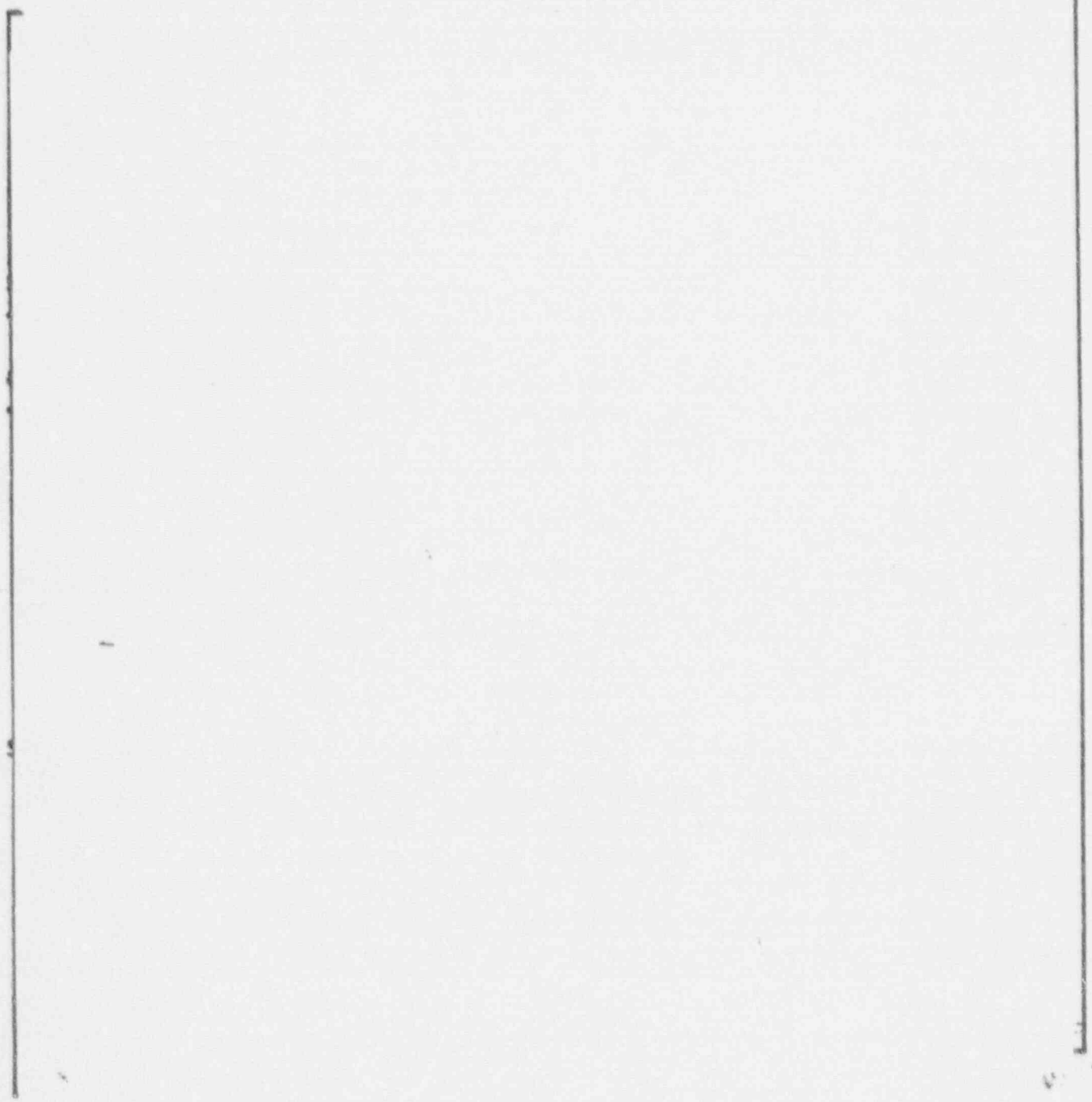


FIGURE 2.3.1
Sketches of TEM grid locations on fracture surface and striation
spacing measurements.

FIGURE 3.2.1

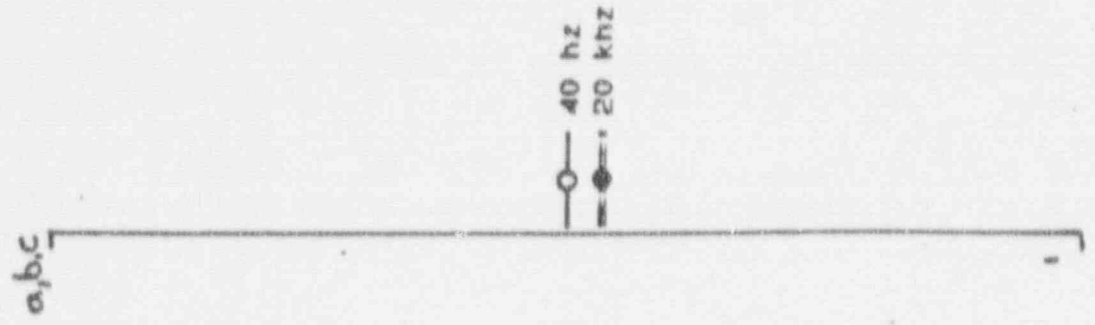


FIGURE 3.2.2

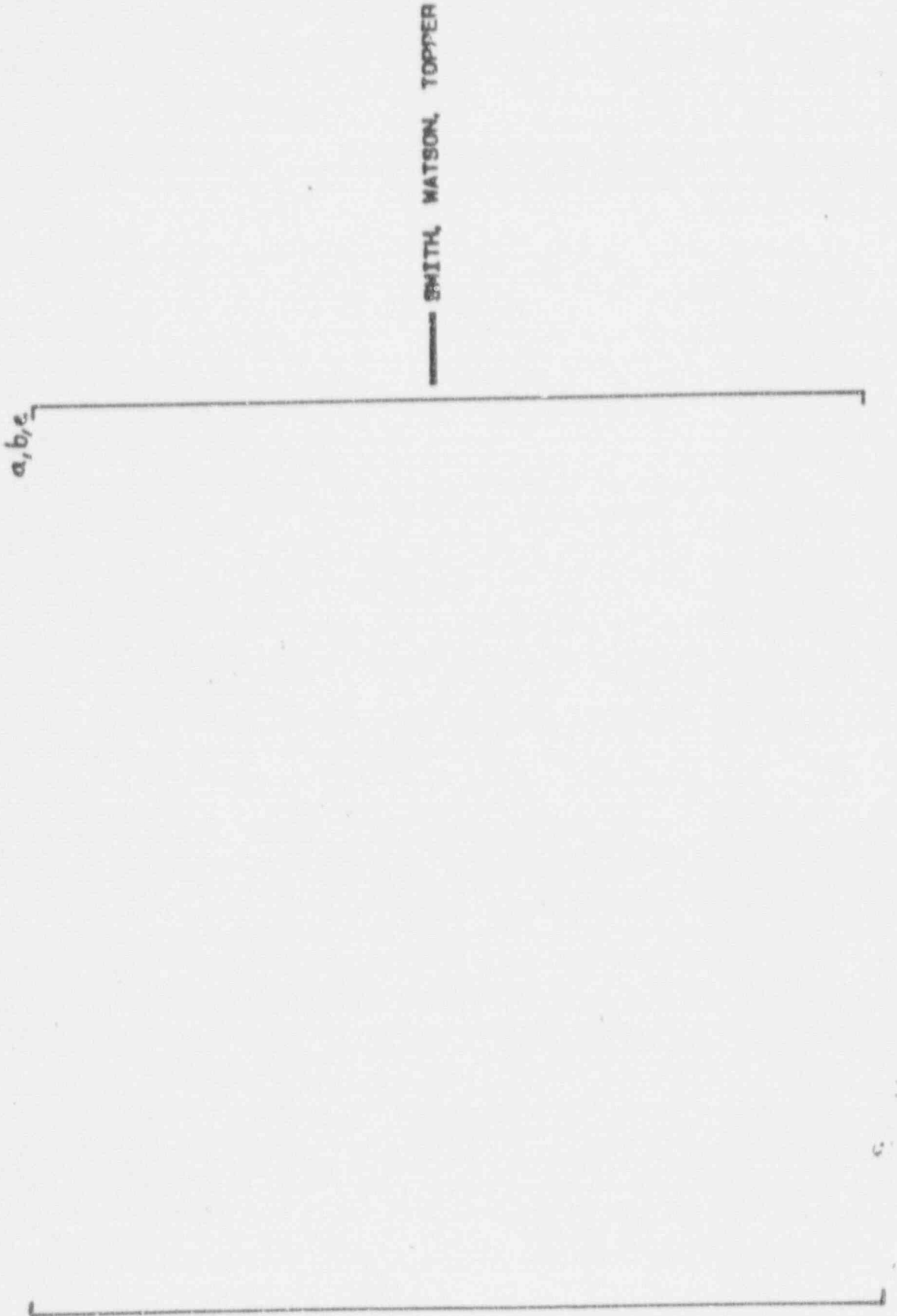
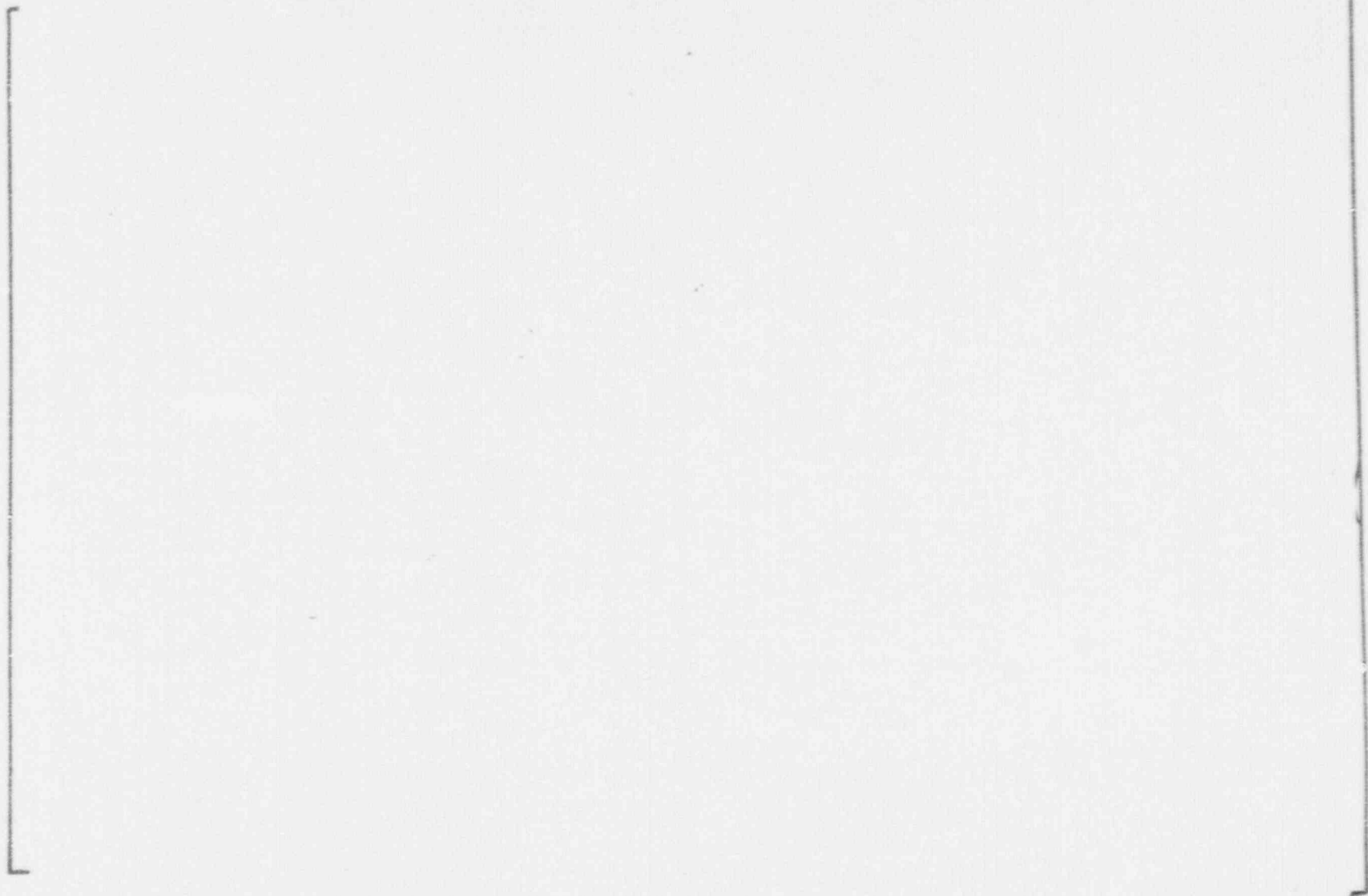


FIGURE 3.2.3

Calculated and observed leak rates versus time.
Observed values based on gaseous species condenser
air ejector

a, b, c



UNIVERSITY OF TORONTO LIBRARY

abc

Front 3.2.2 A

4.0 CAUSATIVE MECHANISM AND CORRECTIVE ACTION

4.1 MECHANISMS DISCUSSION

4.1.1 Summary

The failure surface of R9C51 at the top of the seventh tube support plate has been analyzed and concluded to be a fatigue failure from initiation through propagation (Section 2.3). It is further concluded that the number of cycles involved exceeded 10^5 cycles. The propagation and leakage evaluation of Section 3.0 further demonstrated that a first mode vibration at the tube's natural frequency [*d,c*] is consistent with leakage rates calculated after the event. In order for initiation to have occurred at the stress amplitudes predicted, a significant steady-state mean stress is also required. The range of stress amplitude needed for initiation is concluded to be 4.0 ksi to 10 ksi. This range of stress amplitude could occur from normal, upset and test conditions, but it has been shown in Section 3.1 that the cumulative fatigue usage from those conditions is insignificant.

Based on these results, it follows that the predominant loading mechanism that would be responsible is a flow-induced, tube vibration loading mechanism. It is shown in this section that of the two possible flow-induced vibration mechanisms, turbulence and fluidelastic instability, that fluidelastic instability is the most probable cause. Due to the range of expected initiation stress amplitude (4.0 ksi to 10.0 ksi), the fluidelastic instability would be limited in displacement to a range of approximately 0.032 inch to 0.080 inch. This is less than the distance between tubes at the apex, [*d,c*]. It is further confirmed that displacement prior to the failure was limited since no indication of tube U-bend damage was evident in the eddy current signals for adjacent tubes.

Given the probable cause of limited displacement, fluidelastic instability, a means of establishing the change in displacement, and corresponding change in stress amplitude, is developed for a given reduction in stability ratio (SR). Since the failure is a fatigue mechanism, the change in stress amplitude resulting from a reduction in stability ratio is converted to a fatigue usage benefit through the use of the fatigue curve recommended in Section 3.2. Mean stress effects are included due to the presence of denting. Both 2 sigma and 3 sigma lower bound fatigue curves (with maximum effect of mean stress) are used to establish the change in SR required to reduce the fatigue usage per year to an acceptable level. Table 4.1-1 shows the results of the evaluation. The results indicate that a 10% reduction in SR is needed (considering the range of possible initiation stress amplitudes) to reduce the fatigue usage per year to less than 0.02 for a Row 9 tube similar to Column 51. This same change would reduce fatigue usage per year to less than 0.005 for a Row 8 tube with similar flow conditions.

TABLE 4-1

FATIGUE USAGE PER YEAR RESULTING FROM
STABILITY RATIO REDUCTION

TUBE	SR, % REDUCTION	PER YEAR	FATIGUE CURVE	STRESS BASIS (1)
R9C51	-5.	0.0207	3 sigma	9 yrs to fail
	10.	0.0168	3 sigma	1 yr to fail
	5.	0.0107	2 sigma	9 yrs to fail
	10.	0.0053	2 sigma	Max stress amplitude
R8C51	5.	0.0054	3 sigma	Max stress amplitude

(1) This gives the basis for selection of the initial alternating stress.

4.1.2 Flow Induced Vibration

Fluid flowing over heat exchanger tubes has been shown, by tests as well as field experiences, to be a source of potential mechanical degradation. Tubes can be excited by numerous flow related vibration mechanisms. The list of mechanisms which have, or may have, caused field tube degradation includes cross-flow turbulence, vortex shedding and fluid-elastic instability.

It is noted that since the failure occurred in the U-bend region, where the flow is highly two-phase (liquid and gas), this brings into concern a potential "slug-flow" mechanism. This mechanism could excite a tube at low frequencies and higher amplitudes than those associated with "normal" two-phase cross flow turbulence.

A review of the information which is available and related to each mechanism is presented to evaluate the potential for the above mechanisms to have caused the tube to fail. This information base includes results from field experiences, tests and analyses. It is important to recognize that much of the test data described below is particularly relevant because it was obtained from highly prototypical two-phase (steam-water) flow tests at the relevant pressures and temperatures and for tubes of approximately the same size as the failed tube.

The prototypical tests just described, as well as tests by other investigators, have shown that [

] A,C

Additionally, these latest tests show that [

] A,C

Westinghouse has performed an extensive evaluation of the turbulence response of U-bends using nonlinear, finite element, dynamic (time-history) methods. In addition, an extensive consideration of possible support conditions at the anti-vibration bars was incorporated by way of Monte Carlo techniques.

[

]

], c

As can be seen from the above equations, the important input parameters are the stability constant (beta), the damping values and $\sqrt{\rho} * U$.

The beta values used for these analyses are based on an extensive data base comprised of both Westinghouse and other experimental results. In addition, previous field experiences are considered.

Motions developed by a tube in the fluidelastically unstable mode are quite large in comparison to the other known

mechanisms. The maximum modal displacement (at the apex of the tube) is linearly related to the bending stress in the tube just above the cold leg top tube support plate. This relationship applies to any vibration (turbulence or fluidelastic) in that mode. Thus, it is possible for an unstable, fixed boundary condition tube to move an amount which will produce fatigue inducing stresses when the bending stress to displacement relation is [as it is for the undegraded Row 9 Column 51 (failed) tube with denting.

From the above discussions it is judged highly unlikely that vortex shedding or slug-flow played an important role in the failure of the North Anna tube R9C51.

Further, turbulence induced vibration amplitudes for R9C51 are predicted to be on the order of less [at the tube apex. This order of amplitude would cause maximum stresses (at the top of the uppermost tube support plate) for peak to peak amplitudes (with uncertainties) of less than 1000 psi.

Because of the potentially large response displacements (and stresses) inherent in an unstable tube condition, and because the above discussions eliminate or limit the stresses associated with all other known mechanisms, it is judged that the failed tube is most likely a result of its having been fluidelastically unstable.

The major features of the fluidelastic mechanism are illustrated on Figure 4.1.1. This Figure shows, in a conceptual manner, the logarithm of the displacement response (LOG D) of a tube as the logarithm of velocity (LOG V) increases.

Log-log plots are used by experimentors [

] a, c

The above described method was applied to the R9C51 tube case. However, rather than use an arbitrary reference velocity, all velocities were normalized to the reference instability velocity. This normalization is done on a linear basis, that is, not on log coordinates. Thus, the new independent variable becomes V/V_{cr} , which, as described previously, is the fluidelastic stability ratio, SR.

The results from this application of the method are illustrated on Figure 4.1-2. Note that the point in this Figure corresponding to point 3 in Figure 4.1-1 has a LOG (V/Vcr) value of zero indicating that it is at the instability condition where $V = V_{cr}$ and $V/V_{cr} = SR = 1.0$ (LOG (1) = 0.0).

Figure 4.1-2 can be used to infer the stability ratio of the failed tube assuming a slope of 10. This inferred stability ratio is the anti-log of the LOG (V/Vcr) [or LOG (SR)] associated with the point on the Figure corresponding to point 2 of Figure 4.1-1. This suggests that the stability ratio associated with operating conditions of the R9C51 tube, before initiation of the failure, was in the range of 1.22 (slope of 20) to 1.56 (slope of 10), with an initial displacement of 0.057 inch.

The reduction in response obtained from a stability ratio reduction is of great concern when addressing other tubes. The fluidelastic curve of Figure 4.1-2 can be expressed by the following equation:

$$[\quad]^{a,c}$$

where D_2 and SR_2 are the known values at the point corresponding to point 2 of Figure 4.1-1 and D_1 and SR_1 are values corresponding to any point lower on this curve. Therefore, this equation can be used to determine the reduction in displacement response for any given reduction in stability ratio.

A study of this equation shows that there is a tremendous benefit derived from even a very small percentage change in the stability ratio. It is this very significant reduction in displacement for a quite small reduction in stability ratio that forms the basis for the fatigue life benefit evaluated in the next section.

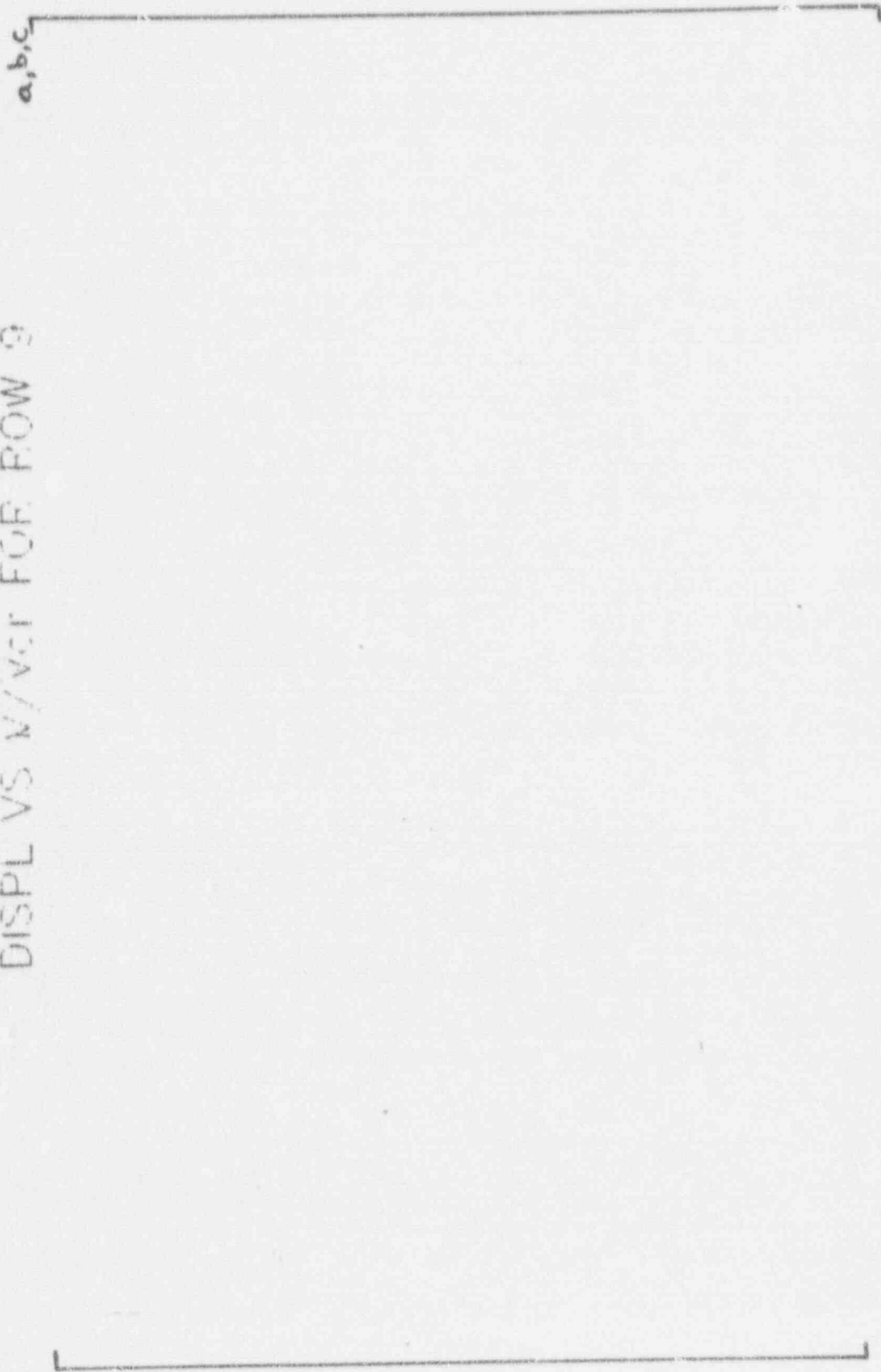
a,b,c



FIGURE 4.1-1

FIGURE 4.1-2

DISPL VS V/\sqrt{C} FOR ROW 9



4.1.3 Fatigue Evaluation

The fatigue curve recommended in Section 3.2 is [

$$\text{Thus,} \\ \left[\quad \quad \quad \right]^{a,c}$$

where σ'_a is the equivalent stress amplitude to σ_a that accounts for a maximum stress of S_y , the yield strength. The 3 sigma curve with mean stress effects is shown in Figure 4.1-3 and is compared to the ASME Code Design Fatigue Curve for Inconel 600 with the maximum effect of mean stress. The curve utilized in this evaluation is clearly well below the code curve reflecting the effect of AVT water testing and the Smith-Watson-Tupper technique that applies to materials in a corrosive environment.

The assessment of a reduction in stability ratio begins with the relationship between stability ratio and deflection developed in Section 4.1.2. The displacement change is directly proportional to change in stress so that stress has the same relationship with stability ratio,

$$\left[\quad \quad \quad \right]^{a,c}$$

The slope in this equation can range from 6 to 20 on a log scale, as discussed in Section 4.1.2, depending on the amplitude of displacement. Knowing the stress [

per year is then determined assuming continuous cycling at the natural frequency of the tube, [] for Row 9 and [] Hz for Row 8. The initial stress must be considered to be in the range of 4.0 to 10.0 ksi, consistent with the conclusion of Section 3.2.]^{a,c} fatigue usage

Using the 3 sigma fatigue curve with mean stress effects, initial stress amplitudes in this range are obtained by making an assumption of time to failure of Row 2 Column 51. With a 75% availability and at [] one year would result in 1.419×10^9 cycles and nine years in 1.277×10^{10} cycles. A 40 year continuous cycling would result in 5.68×10^{10} cycles. Making an assumption of failure in 1 year yields a corresponding stress amplitude of 8.7 ksi, Figure 4.1-4. Similarly, an assumption of failure in 9 years yields a stress amplitude of 5.6 ksi, Figure 4.1-5.

For the 8.7 ksi, 1 year case, the corresponding displacement is 0.069 inch. Above 0.040 inch, a slope of 10.0 is used to assess the effect of a change in SR, whereas below 0.040 inch, a slope of 6.0 is used. A reduction of 5.3% reduces the displacement to 0.040 with the slope of 10. Another 4.7%, totally 10%, reduces the displacement to 0.030 inch and a corresponding stress amplitude of 3.78 ksi. The cycles to failure associated with this stress amplitude is 8.43×10^{10} cycles. Based on the [] frequency, the fatigue usage per year would be reduced to 0.0168. See Figure 4.1-4.

In a similar fashion, the 9 year, 5.6 ksi case is found to provide a usage per year of 0.0207 for a 5% reduction in SR. See Figure 4.1-5.

On a 2 sigma basis, the one year assumption provides a stress amplitude that exceeds 10 ksi, outside the predicted range. The upper bound case for the 2 sigma basis is therefore based on the maximum stress back-calculated from the fracture analysis which gave an 0.098 inch displacement to cause 50 ksi - root inch at a crack half angle of 90° . Using a conservative linear relationship with frequency between initiation displacement and propagation displacement, the maximum initiatic displacement is



The corresponding maximum stress is 9.5 ksi. In the same way then, the fatigue usage per year is obtained to be 0.0053 for a 10% reduction in SR. See Figure 4.1-6.

The 9 year failure assumption yields a stress of 7.0 ksi on the 2 sigma curve. A 5% change in SR drops this to 4.5 ksi yielding a usage per year of 0.0107. See Figure 4.1-7.

Therefore, for a tube similar to the failed tube at Row 9 Column 51, a 10% reduction in SR results in a fatigue usage per year of less than 0.017 using the highest initial stress amplitude assumptions. Also, the 2 sigma curve results in greater benefits from the same SR change than does the 3 sigma curve.

For a neighboring tube such as Row 8 Column 51, the benefit of a similar reduction can be estimated knowing the SR comparison between the two tubes. The Row 8 SR is 0.86 times the SR of Row 9. Thus, the max stress for Row 8 Column 51 would be

$$\left[\quad \quad \quad \right]^{d,c}$$

$$= 9.5 (0.405) = 3.85 \text{ ksi}$$

A 5% reduction in SR for Row 8, Column 51 would yield a new stress amplitude of 2.83 ksi and a fatigue usage per year of 0.0054 using the 3 sigma curve. See Figure 4.1-8.

a, b, c

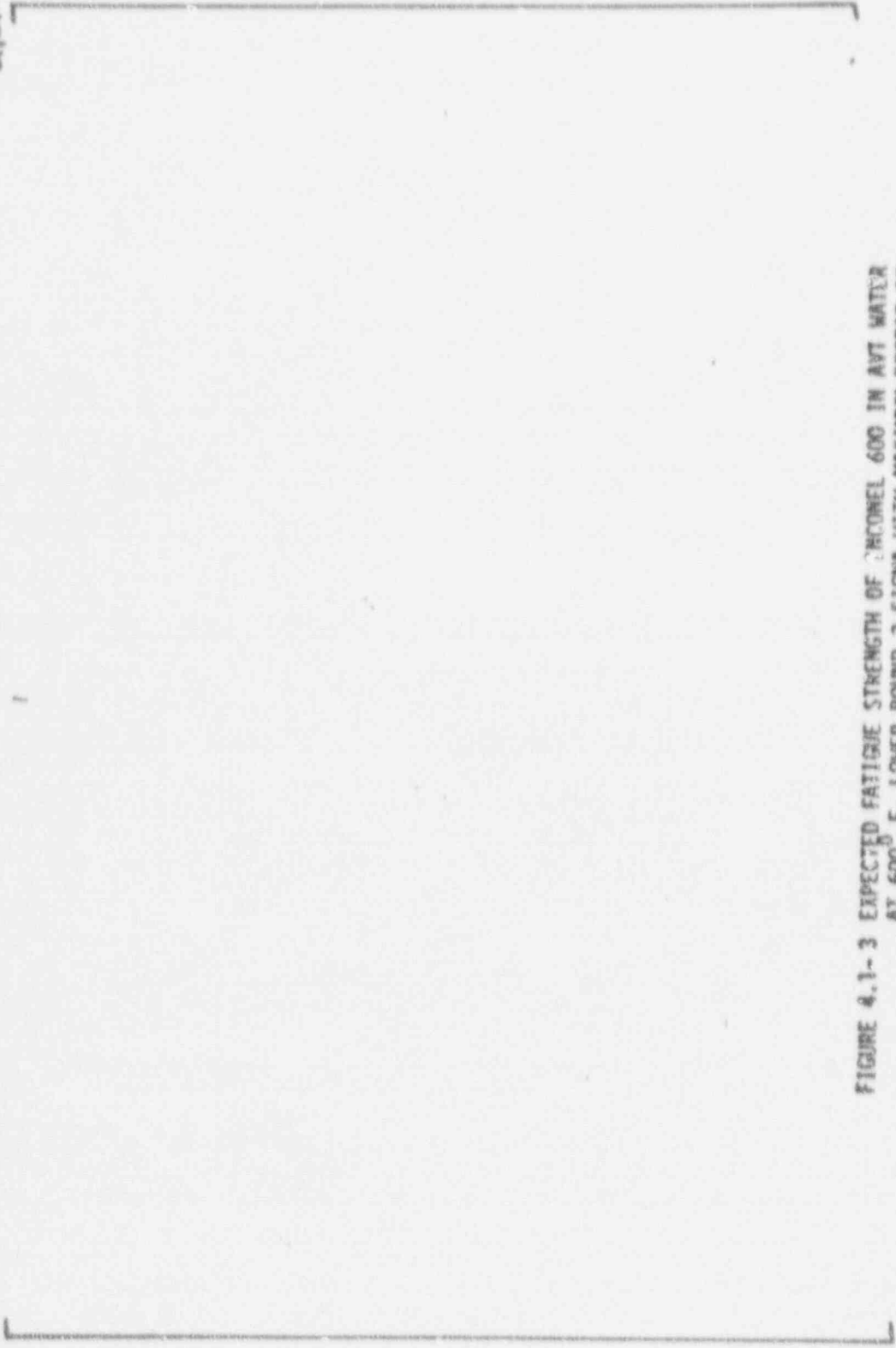


FIGURE 4.1-3 EXPECTED FATIGUE STRENGTH OF INCONEL 600 IN AWT WATER AT 600 F, LOWER BOUND 3 SIGMA WITH MAXIMUM EFFECT OF MEAN STRESS (SYMBOLS DO NOT REPRESENT DATA POINTS) WITH A COMPARISON TO THE ASME CODE DESIGN CURVE.

a,b,c

FIGURE 4.1-4 INCREASE IN FATIGUE LIFE FROM A STRESS AMPLITUDE CONSISTENT WITH FAILURE IN 1 YEAR, DUE TO A 10% DROP IN STABILITY RATIO (3 SIGMA LOWER BOUND). ROW 9 COLUMN 51.

a, b, c



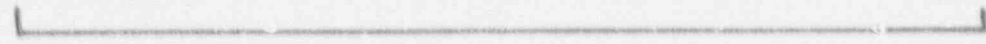
FIGURE 4.1-5 INCREASE IN FATIGUE LIFE FROM A STRESS AMPLITUDE CONSISTENT WITH FAILURE IN 9 YEARS, DUE TO A 5% DROP IN STABILITY RATIO (3 SIGMA LOWER BOUND). ROW 9 COLUMN 51.

61 c.

$\sigma_{b,c}$



FIGURE 4.1-6 INCREASE IN FATIGUE LIFE FROM THE MAXIMUM EXPECTED STRESS AMPLITUDE, DUE TO A 10% DROP IN STABILITY RATIO (2 SIGMA LOWER BOUND). ROW 9 COLUMN 51.



a, b, c




FIGURE 4.1-7 INCREASE IN FATIGUE LIFE FROM A STRESS AMPLITUDE CONSISTENT WITH A 9 YEAR FAILURE, DUE TO A 5% DROP IN STABILITY RATIO (2 SIGMA LOWER BOUND), ROW 9 COLUMN 51.

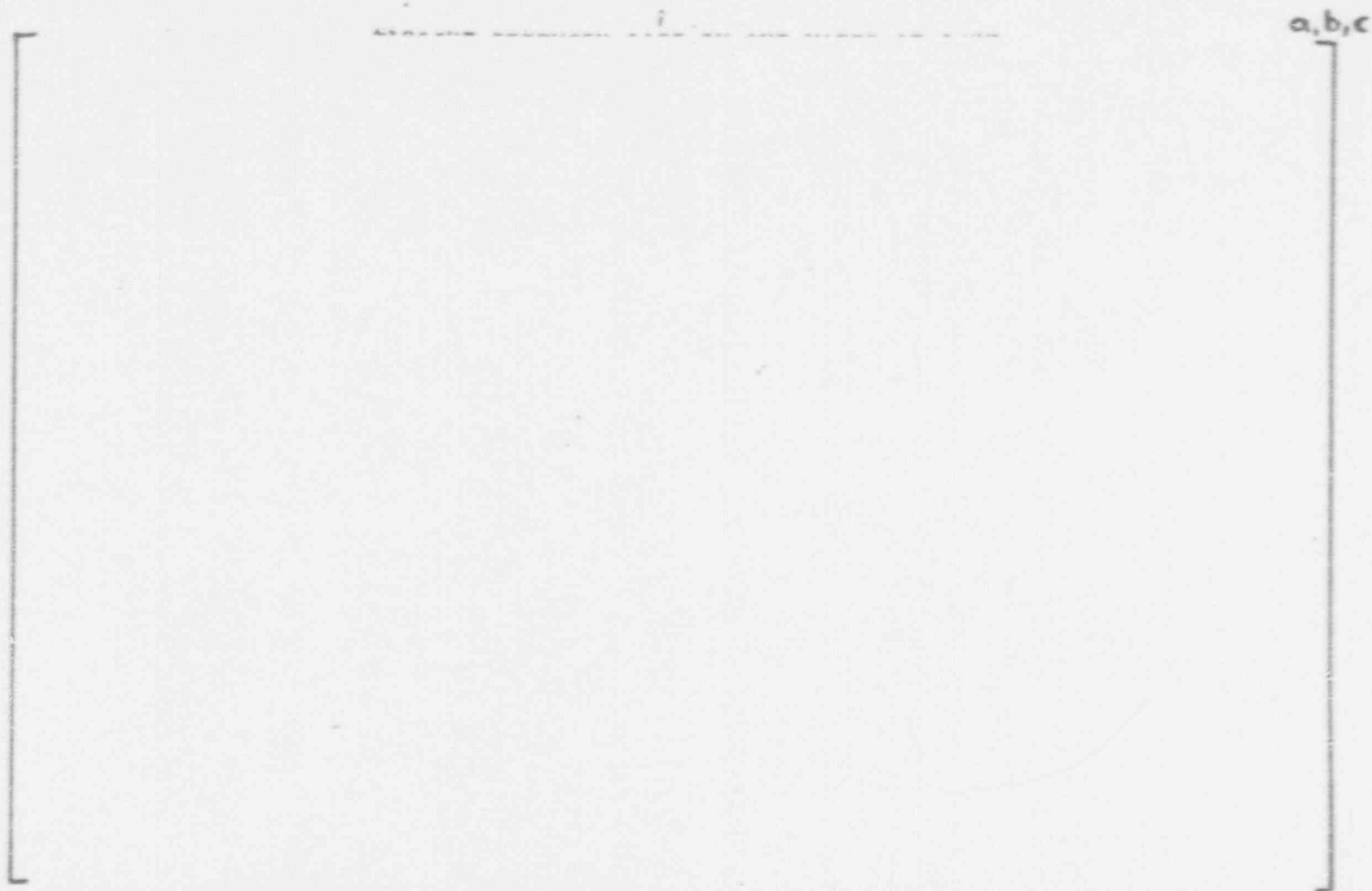


FIGURE 4.1-8 INCREASE IN FATIGUE LIFE FROM THE MAXIMUM ESTIMATED STRESS AMPLITUDE FOR ROW 2 COLUMN 51, DUE TO A 5% DROP IN STABILITY RATIO (3 SIGMA LOWER BOUND).

4.2 Steam Generator Modifications

4.2.1 Introduction

This section describes the downcomer flow resistance plate modification being implemented in the North Anna Unit 1 steam generators. The improvement criteria for the modification as developed in Section 4.1 is a 10% decrease in the stability ratio for tubes without AVB's in Rows 9 and 10. Tubes in lower rows are expected to meet the 10% criteria without the modification but will also benefit from it. Tubes in Row 11 have AVB's. The improvement evaluated from the modification is in the range of 8-22%, with an expected level of 13-15%. The range of improvement evaluated results from sensitivity analysis of pertinent vibration parameters. The expected level of improvement results from the reflection of field observations in the choice of vibration parameters likely. Since it is possible to identify conditions in which the improvement criteria would not be met, tubes which could be affected will be removed from service as a conservative measure. Section 4.2.2 discusses the modification requirements and the modifications being implemented including installation of Downcomer Flow Resistance Plates and preventative tube plugging. Results of fluidelastic instability analyses for both the pre-modification and post-modification conditions are given in Section 4.2.3. Data on AVB insertion depths are provided in Section 4.2.4 and tube plugging considerations for local flow variations are given in Section 4.2.5. In Section 4.2.6, it is shown that stability ratios decrease with reduced load and there are no part load conditions that need to be avoided during plant operation.

4.2.2 Modification Requirements and Summary Implementation

The results from the R9C51 failure analyses (Section 2.3) and the causative mechanism evaluations (Section 4.1) developed the required conditions for tube cracking initiation at the top support plate. These required conditions are summarized in Table 4.2.2-1. These necessary conditions include tube denting at the top support plate, no AVB support, stability ratios close (within 10% or higher) to that of the failed R9C51 tube and off-nominal conditions of local flow peaking and/or low tube damping.

The North Anna 1 modification to eliminate tube cracking at the top support plate addresses the elimination of some of the required conditions as summarized in Table 4.2.2-2. The required conditions for tube crack initiation are directly addressed in the following manner by the modifications including installation of a Downcomer Flow Resistance Plate (described in Section 4.5) and selective preventative tube plugging:

CONDITION FOR TUBE CRACK INITIATION

MODIFICATION

No AVB support

Preventative tube plugging of tubes without AVB support in regions of local high flow velocity.

Identification of tubes without AVB support through evaluation of eddy current inspection data.

Stability ratios within 10% of Tube R9C51 or higher

DFRP results in 15-22% stability ratio reductions for tubes with very low damping.

DFRP results in - 8% reductions for tubes with nominal damping.

Off-nominal, local high velocity regions

Preventative tube plugging used to augment lower bound 8% DFRP improvement.

Off-nominal low tube damping

DFRP modification

High Mean Stress from tube denting conditions

Denting progression demonstrated to be stopped.

The overall objective for the modification is to exceed the requirement developed in Section 4.1 for the 10% reduction in stability ratios which provides for a steam generator 40 year design life. As noted above, this objective is satisfied by the combined DFRP modification and preventative tube plugging. The overall stability ratio improvements for the DFRP are developed in Section 4.2.3.6. The eddy current results to identify tubes without AVB supports are described in Section 4.2.4 and tube plugging considerations for local flow variations are described in Section 4.2.5.

4.2.3.1 Stability Constant, β , for Stability Analyses

The stability constant, β , for calculation of critical velocities (See Section 4.1) has been measured for full length, U-bend tubes in prototypic steam/water environments. In addition, measurements in U-bend air models have been made with both no AVB and variable AVB supports. These data are summarized in Figure 4.2.3.1-1. The lowest measured β for tubes without AVB's was []^{d,c}. This value has been used in all stability ratio analyses in this report.

To help minimize the uncertainties in ATHOS flow predictions on stability analyses, the Model Boiler (MB-3) tests performed at Mitsubishi Heavy Industries (MHI) in Japan were analyzed using ATHOS velocity data to calculate β from the flow conditions at the measured critical velocity. These analyses support the β value of []^{d,c}.

Figure 4.2.3.1-1A is a plot of instability constant, β , as a function of frequency obtained for severed tubes from wind tunnel tests.

4.2.3.2 Tube Damping Values

To identify the potential minimum damping for tubes typical of a Row 9 U-bend, measurements were made of mechanical damping in air using a U-bend shaker test facility. The tube tested was a 7/8 inch diameter, Alloy 600 tube prototypic of North Anna tubing. The U-bend shaker test facility is illustrated in Figures 4.2.3.2-1A, B and C. The results of these tests are shown in Figure 4.2.3.2-1. Additional test results are shown in Figures 4.2.3.2-1D through 4.2.3.2-1F. For []

[]^{d,c} With a tendency to increase slightly with vibration amplitude. This value is used as a lower bound value of damping for the present report and to adjust other data for mechanical damping as noted below. It can be noted from the Figure 4.2.3.2-1 data that the mechanical damping increases substantially as the clamped-clamped support conditions are progressively relaxed to preloaded pinned-pinned support conditions. The latter value of 1.1% can be considered to be typical of U-bend steam generator conditions without denting for which the tubes have a high likelihood of preloaded, pinned supports at the top support plate.

[] Tube damping values under steam/water flow conditions were measured by []

[]^{d,c} to the measured []^{d,c} mechanical damping noted above for the Row 9, U-bend tube measurements. This process is equivalent to using the two phase fluid damping of []^{d,c} and the Westinghouse measured mechanical damping for a Row 9 tube. The []

[]^{d,c} in this report.

Tube damping values [

] A.C

TABLE 4.2.3.3-2

STABILITY RATIO RANGE FOR R9C51 INCLUDING UNCERTAINTIES

	STABILITY RATIO
Nominal Stability Ratio	[] ^{A,C}
<ul style="list-style-type: none"> o Calculated flow conditions without local velocity peaks o Lower range of stability constant from U-bend tests o Average value of damping for clamped supports 	
Including Uncertainties from β , f_n and Average Flow - 15%	0.74
<ul style="list-style-type: none"> o This uncertainty would not significantly influence a ratio (SR_2/SR_1) of stability ratios as used to evaluate modification improvement factors 	
Including Local Velocity Peaking Factors - 10 to 20%	0.81 to 0.89
<ul style="list-style-type: none"> o Preliminary estimate on effects of non-uniform AVB insertion depths 	
Including Damping Uncertainties for Dented Tubes	
<ul style="list-style-type: none"> o 50% uncertainty which reduces damping from 0.82 to 0.41 - 41% increase in stability ratios o Lower bound on damping as mechanical damping of []^{A,C} - Would yield a factor of 2 increase in stability ratios 	1.15 to 1.26

TABLE 4.2.2-1

REQUIRED CONDITIONS FOR TUBE CRACKING INITIATION

Tube Denting at Top Support Plate

- o Leads to High Mean Stress and Associated Reduction in Fatigue Properties
- o Necessary for Maximum Bending Stress to Occur at the Top Support Plate
- o Results in Reduced Tube Damping

No AVB Support

- o Tubes without AVB support are a required condition for the high vibration amplitudes needed to achieve the stress range necessary for fatigue crack initiation
- o Based on inspection data, the presence of AVB's has been established to lower Row numbers than the original design minimum (Row 11)

Stability Ratios Within 10% of Ruptured Tube R9C51 or Higher

- o Lower stability ratios would result in vibration amplitudes too small to initiate fatigue cracking - see Section 4.1 for development

Off-Nominal Conditions for Fluidelastic Excitation

- o Nominal Stability Ratio Calculations Lead to the Expectation that Tubes in Row 10 or Lower Would be Stable (Section 4.2.3.3)
- o Either or Both of the Following Conditions are Necessary for Fatigue Cracking in Addition to the Above Conditions
 - Local High Flow Velocity Regions
 - Tube Damping Below Test Measurements, Approaching Mechanical Damping Only

TABLE 4.2.2-2

SUMMARY OF REQUIRED CORRECTION ACTIONS

Tube Locations Requiring No Corrective Action

- o Tubes in Row 8 or Lower
 - Stability Ratios are 14% Lower than Tube R9C51 and Meet 10% Lower Requirement
- o Tubes with AVB Support
 - AVB's Limit Vibration Amplitudes
 - Depths of AVB penetration into Tube Bundles are Obtained from Eddy Current Inspection Map

Corrective Actions Required

- o Tubes with Low Tube Damping
 - The DFRP Modification Reduces Stability Ratios by 15-22% Under the Low Tube Damping Assumption (Low Void Fraction Dependence) and meets 10% Lower Requirement
- o Tubes with Local High Velocities
 - The DFRP Modification Reduces Stability Ratios by - 8% with Nominal Tube Damping (Significant Void Fraction Dependence)
 - Preventative Tube Plugging at Tube Locations with Potentially High Local Flow Velocities
 - o Required Only for Tubes in Row 9 or Higher without AVB Support
 - The Combined DFRP Modification and Preventative Tube Plugging Reduce Stability Ratios of Operational Tubes by More than 10%

4.2.3.3 Pre-Modification Stability Ratios

The ATHOS3 computer code is used in the evaluation of the detailed thermal and hydraulic performance of PWR steam generators. The code was developed for the Electric Power Research Institute (EPRI) by Cham of North America, Inc. Independently, ATHOS has been verified against both field steam generator instrumentation data and to test data. Since its introduction in 1981, it has been used extensively by both steam generator vendors and the electric utilities in the design and analysis of new steam generators and in the resolution of field problems. Figures 4.2.3.3A, 4.2.3.3B and 4.2.3.3C represents plan and elevation views of the ATHOS calculational model.

Figure 4.2.3.3-1 provides velocity and density distributions for the Row 9 Column 51 tube in the North Anna 1 steam generator C. The distributions cover both the straight leg regions of the hot and cold legs for this tube (as a function of axial length along the tube) and the U-bend (as a function on angular location). Both the velocity normal to the tube and the secondary coolant mixture density are shown in the figure.

The distributions of Figure 4.2.3.3-1 are used together with the stability constant and damping data to calculate stability ratios utilizing the stability ratio expression given in Section 4.1.2.

The pre-modification stability analyses represent the North Anna 1 operating conditions at the time of the R9C51 tube failure. The calculated stability ratios are given in Table 4.2.3.3-1. The expected stability ratio for R9C51 is [] based on the nominal or test based damping values for clamped tube supports. Thus the tube would be considered to be stable with a significant margin. The following section addresses potential uncertainties relative to the low stability prediction for R9C51. A summary of the uncertainty estimates and their associated increase in the R9C51 stability ratio are given in Table 4.2.3.3-2. The principal uncertainty is that associated with tube damping values for dented tube conditions. Changes in damping values within realistic uncertainties have the dominant influence for higher stability ratios. Local flow peaking at R9C51 due to non-uniform insertion depths could have added to the instability and, together with low damping, led to the vibration amplitudes for the tube failure.

Results for a low damping assumption are included in the table. This low damping assumption of 0.34% for R9C51 is based on the damping value that would increase the stability ratio from 0.64 to 1.0. The low damping value stability ratios are provided to assess modifications based on the judgment that low tube damping is the primary contributor to the instability for tube R9C51. For assessing void fraction effects which are small for this low damping value, a linear approximation for the damping is made with 0.34% at 86% void fraction and []^{a,c} (mechanical damping only) at 95% void fraction. ④

Figures 4.2.3.3-1A, B and C provide a comparison of the stability ratio with/without void dependent damping between North Anna Unit 1 and other operating steam generators. This shows that the North Anna 1 steam generators before modifications have the highest fluidelastic stability ratio of the units evaluated.

4.2.3.4 Stability Ratio Uncertainty Considerations

Figure 4.2.3.4-1 summarizes an assessment of potential uncertainties influencing the predicted stability ratios. It is concluded that the most significant factors influencing the stability ratios are the local flow field and the tube damping uncertainties. The basis for these conclusions are discussed below:

Average Flow Field, Stability Constant and Frequency Uncertainties

Reviews of eddy current data for Model 51 steam generators available at Westinghouse, exclusive of North Anna, indicate that tube wear at the top support plate is negligible in the Row 8-10 data which were reviewed and that tube wear at AVB's is typically detected in Rows 14 or larger. The predicted stability ratio for a tube with pinned supports using the best estimate damping (Figure 4.2.3.2-2) for pinned conditions is similar to the clamped support conditions. For example, R9C51 stability ratios are [] with clamped or dented supports and [] with pinned supports.

Uncertainties in the average flow field, stability constant and frequencies are essentially the same for units with dented or non-dented top support plates. If these errors were large, similar instabilities would be expected in the non-dented units with resulting wear at either the top support plate or inner row AVB's. Since such tube wear has not been identified in Rows 8 to 10 in operating steam generators without denting, it can be expected that the factors leading to R9C51 are unique to dented units. Thus an uncertainty estimate of about 15% for the combined effects of average flow field, stability constant and frequency appears to be reasonable. To further minimize the impact of these uncertainties, the modification is evaluated as a percentage or ratio improvement so that constant error factors are eliminated.

Local Flow Field Uncertainties

In Section 4.2.5, a preliminary estimate of a 15% velocity peaking factor has been obtained for R9C51 in steam generator C based on non-uniform AVB insertion depths for this tube. Eddy current data indicate tube wall thinning in a few Row 8 to 10 tubes in the North Anna 1 units. These indications could result from tube wear due to fluidelastic induced vibration. For some of these tubes, the adjacent AVB insertion depths are uniform compared to R9C51. Thus it appears that non-uniform AVB's are not the dominant factor for instability although this effect at a 15% magnitude could have had a major influence on the R9C51 failure. Pending further evaluation of the effects of non-uniform AVB's, a 10-20% uncertainty factor for local flow effects appears to be reasonable.

Tube Damping Uncertainties

Very little data is available to define the tube damping for clamped tube supports in steam/water conditions. Prototypic U-bend testing has been performed under conditions leading to pinned supports. The data of [] in Figure 4.2.3.3-2 provides the principal data for clamped tube conditions in steam/water and was performed for cross flow across straight tubes. Uncertainties are not defined for these test data. In general, tests show large variability in measured tube damping values.

Based on the apparent differences in tube wear at AVB's between North Anna 1 and other Model 51 steam generators, the conditions for instability are unique to dented tube conditions. The effects of denting on tube damping would thus appear to be the major uncertainty factor leading to the tube instabilities in the dented condition. Uncertainties of the order of 50% on tube damping for dented conditions appears to be a reasonable estimate.

Overall Assessment

It is concluded that low tube damping below the average of test data for clamped tube supports is the principal contributor to the instability conditions for R9C51. Local flow peaking likely contributed further to the instability and associated increased vibration amplitude.

4.2.3.5 Eddy Current Wall Thinning Indications at AVB's in Rows 8 to 12

As part of the inspection of the steam generators, tubes in Rows 8 to 12 in each steam generator were eddy current inspected for wall thinning indications at AVB's. The results of this inspection for tubes with indications at AVB's are given in Table 4.2.3.5-1. Wall thinning indications, which may be indicative of tube wear due to tube vibration, were found in Row 8 and higher. The indication depths are generally small and include efforts to identify potential indications of less than 20% depth.

A possible causative mechanism for these indications is wear due to fluidelastic induced vibration with displacement limited by the AVB's. Based on AVB insertion depths described in Section 4.2.4, most of these indications occur at locations for which AVB insertion depths are not significantly staggered between adjacent columns. In this case, local flow peaking would not be expected to be a major contributor to fluidelastic instability. Based on the assessment of Section 4.2.3.4, it appears that low tube damping would be the principal contributor to fluidelastic instability for the tubes with wear at AVB's. c

As noted in Sections 4.2.3.4 and 4.2.3.5, the low damping conditions are estimated to be the principal contributor to fluidelastic instability. Under these conditions, the stability ratio reductions are 15-22% and significantly exceed the 10% requirement.

TABLE 4.2.3.6-1

REDUCTIONS IN STABILITY RATIOS FROM
THE DFRP MODIFICATION

TUBE DAMPING ASSUMPTION	STABILITY RATIO REDUCTION
Low tube damping independent of void fraction	22%
Low tube damping with associated linear dependence on void fraction	13-15%
Nominal tube damping with test based dependence on void fraction	8%

4.2.4 AVB Insertion Depths

The presence of an AVB adjacent to a tube can be detected by eddy current inspections using the standard bobbin coil. This method can be used to detect the depth of insertion for the lower AVB based on the lowest row number in each tube column that the presence of an AVB can be detected. Each unplugged tube in Rows 8 to 12 were inspected for the presence of AVB's. The results of these inspections are shown in Figure 4.2.4-1.

It is possible for the eddy current inspection to miss the presence of an AVB due to contaminants such as copper or other high noise level conditions. However, detection of an AVB is considered to be a firm indication of the AVB on at least one side of the inspected tube. Figure 4.2.4-2 identifies logic used where interpretation of the data is necessary. Laboratory and mockup tests using a bobbin coil probe show that the tube to AVB gaps are over estimated but that the distance for detectability of an AVB under limiting conditions exceeds maximum potential tube to AVB gaps. Consequently, the data is used to simply establish the presence of an AVB.

Figure 4.2.4-3 provides the AVB positions developed from the eddy current data in the vicinity of tube R9C51 in steam generator C. It can be noted that AVB insertion depths are more variable between tube columns near R9C51 than for most other tube locations. The AVB pattern near R9C51 appears to be sufficiently staggered to potentially lead to locally higher flow velocities at R9C51. Thus it is possible that flow peaking conditions contributed to the R9C51 fluidelastic instability.

4.2.5 Local Flow Variations Due to Non-Uniform AVB Insertion Depths

A preliminary assessment of a velocity peaking factor for tube R9C51 has been made based on the non-uniform path of flow resistance due to the presence of an AVB. The non-uniform resistance yields a local velocity perturbation. Based on Figure 4.2.4 for AVB depths near R9C51, the lower AVB insertion depths and associated increased flow resistance at adjacent tube columns (between columns 49-50, 52-53, and 53-54) tend to divert flow toward the tube gaps adjacent to R9C51. Based on small perturbation considerations, a preliminary estimate indicates the magnitude of a 15% increase in tube gap velocities for R9C51. Based on those results, tubes with a velocity peaking geometry would be candidates for preventative tube plugging.

4.2.6 Dependence of Stability Ratio on Load

The influence of thermal load on fluidelastic stability ratio in the U-bend is discussed below. A discussion of the general trend is followed by that for a partial load range of 30-50% power.

4.2.6.1 General Trend

The steam flow rate from the steam generator is strongly dependent on thermal load. As the load increases the steam flow rate increases. The maximum steam flow rate occurs at full load.

Since most of the vapor generation occurs in the straight leg portion of the tube bundle, when the secondary flow passes through the U-bend the total vapor flow is nearly equal to the steam flow from the steam generator. The vapor velocity in the U-bend is thus proportional to the steam flow rate. As steam flow rate increases with load, the circulation ratio decreases. The total mass flow rate (liquid plus vapor) through the tube bundle is nearly constant and is independent of load above 60% load. However, since the specific volume of vapor is 20 to 30 times higher than that of the liquid, the volumetric flow rate increases with increase in load. Thus the velocity in the U-bend increases and the density of the two phase mixture decreases with increase in load.

The fluidelastic stability ratio is proportional to $\sqrt{\rho V^2}$. The net effect on the stability ratio from the flow conditions alone is an increase with load. Figure 4.2.6-1 shows the effect of load on the $\sqrt{\rho V^2}$ component of the stability ratio. This figure provides post modification reduction factors relative to full load operating conditions prior to the installation of the downcomer flow restrictor as a function of thermal load. Note that this figure is based on aggregate flow rates and circulation ratios. Although it does not account for detailed distributions of velocity and density along the tubes, it is a good means of comparing the influence of load since the detailed distributions will have only a secondary effect.

A decrease in load is accompanied by a decrease in void fraction. Thus a decrease in load would increase tube damping and further reduce stability ratios. For tube with low damping, this contribution would be small. However, the reductions in stability ratio with reductions in load would be equal to or greater than the factors shown in Figure 4.2.6-1.

4.2.6-2 Stability Ratio at 30-50% Power

At 50% of full load, the effects on stability ratios from velocity and density alone are to reduce the stability ratio by a factor of two relative to full load prior to the modification. Further, this will be accompanied by a reduction in void fraction of over 10%. The reduction in void fraction, if considered, would further reduce the stability ratio. At 30% of full load, the stability ratio is further reduced due to the lower $\sqrt{\rho} V^2$ level and reduced void fraction.

FIGURE 4.2.3.1-1

Instability Constant - β

U-Bend Test Data

- MB-3 Tests
 - β values of []^{a,b,c}
- MB-2 Tests
 - β of []^{a,b,c}
- Air Model Tests
 - β of []^{a,b,c} without AVBs
 - Tendency for β to increase in range of []^{a,b,c} with inactive AVBs (gaps at AVBs)
 - Tendency for β to decrease toward a lower bound of []^{a,b,c} with active AVBs

Verification of Instability Conditions

- Flow conditions at critical velocity from MB-3
- Measured damping for the specific tube
- Calculated velocities from ATHOS 3D analysis
- β determined from calculated critical velocities
 - Good agreement with reported β values
- ATHOS velocity data with β of []^{a,b,c} and known damping should not significantly underestimate instability for regions of uniform U-bend flow

a, b, c

FIGURE 4.2.3.1-1A- Instability constants, β , obtained for curved tubes from wind tunnel tests on the 0.214 scale U-bend model

a,b,c

FIG. 1.3.3.2-1A
SHALOR TEST FACILITY

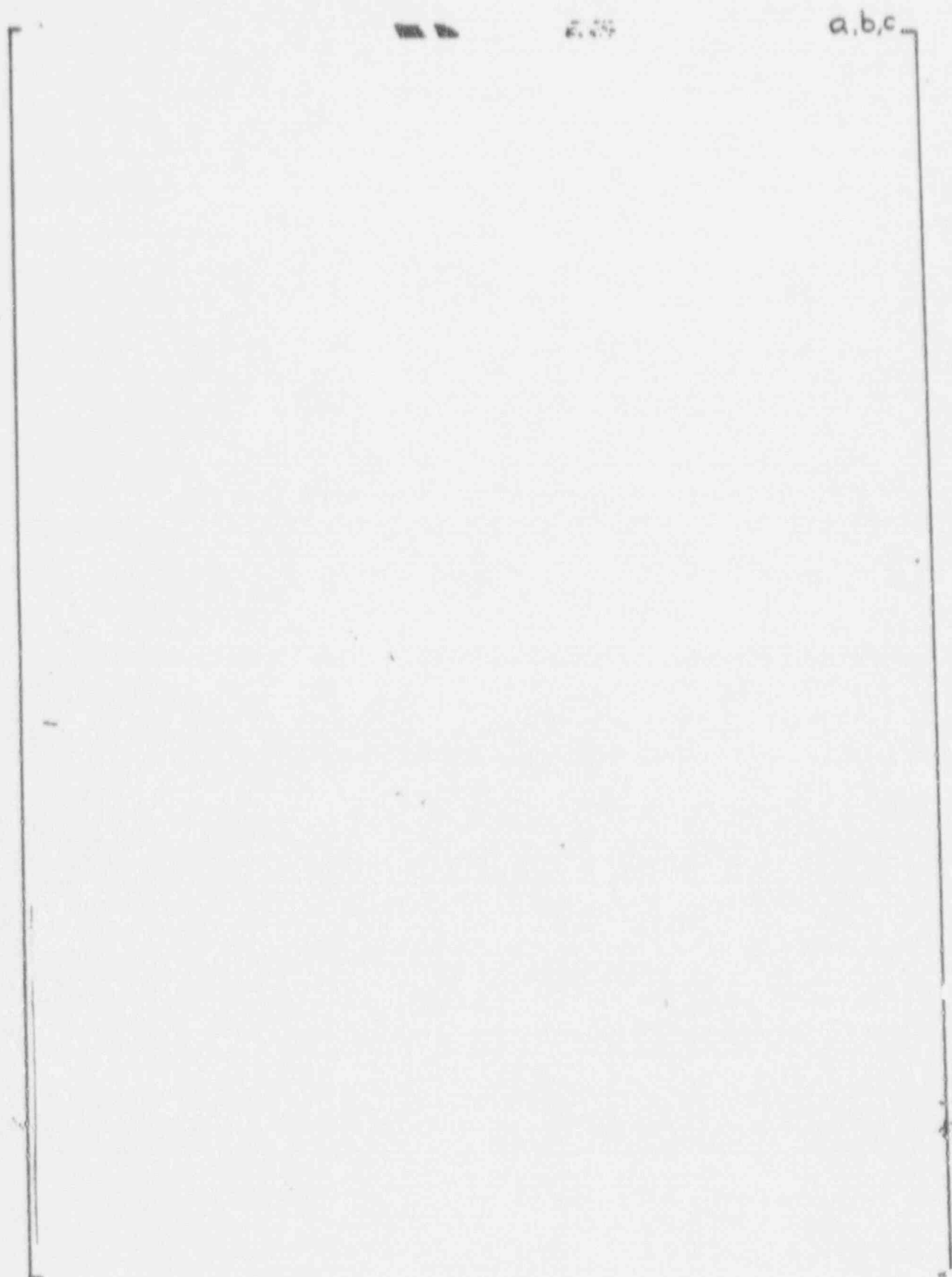


FIGURE 4.2.2.2-1C SMOOR TRSF FACILITY (CONT)

NORTH ANNA
SHAKER TESTS
ORIGINAL TUBE

○	CLAMPED-CLAMPED	68.8 Hz
●	CLAMPED-PINNED	46.6 Hz
□	PINNED-PINNED	34.6 Hz

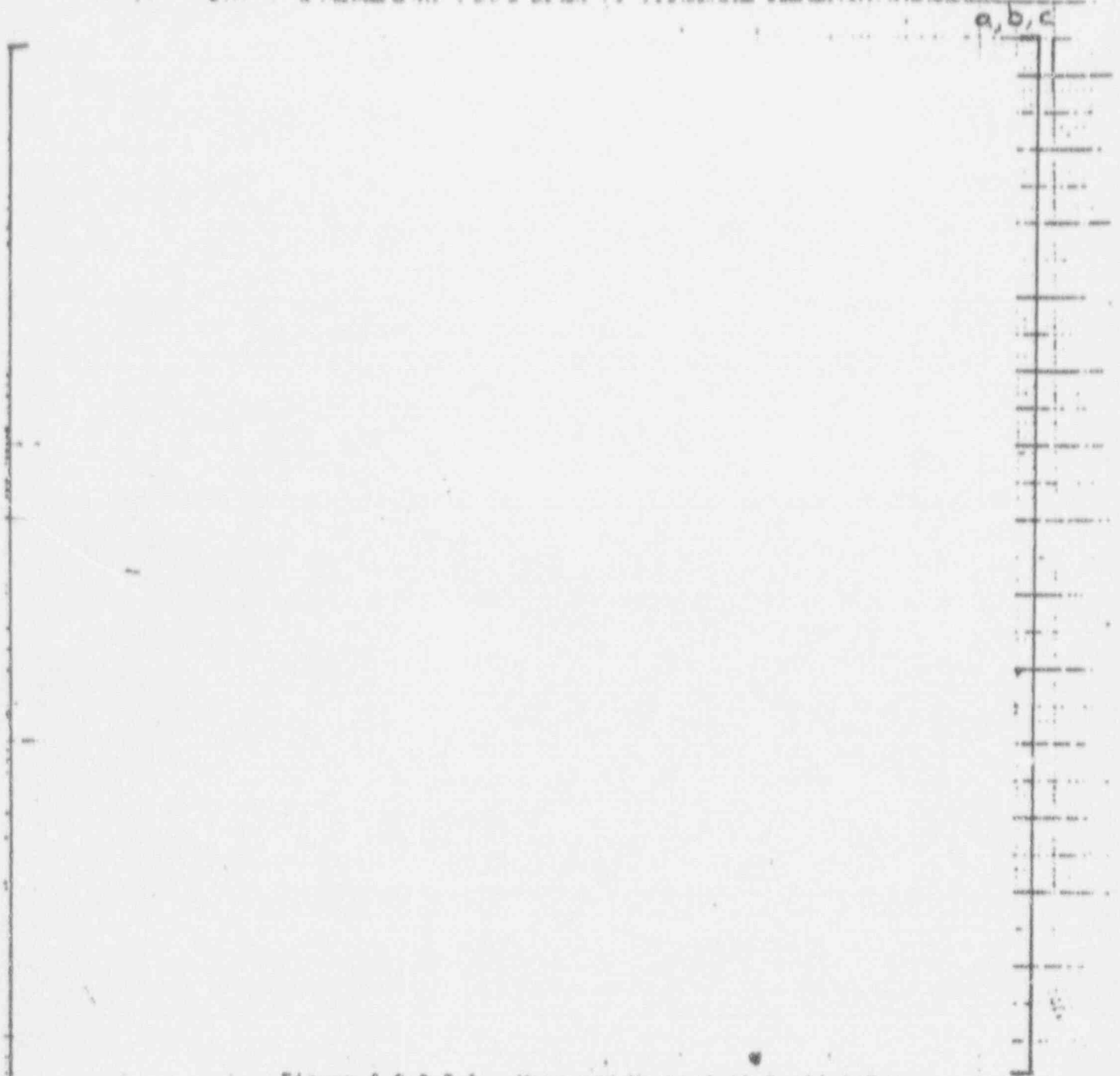


Figure 4.2.3.2-1. Measured Mechanical Damping For a
Row 9 U-Bend Tube in Air

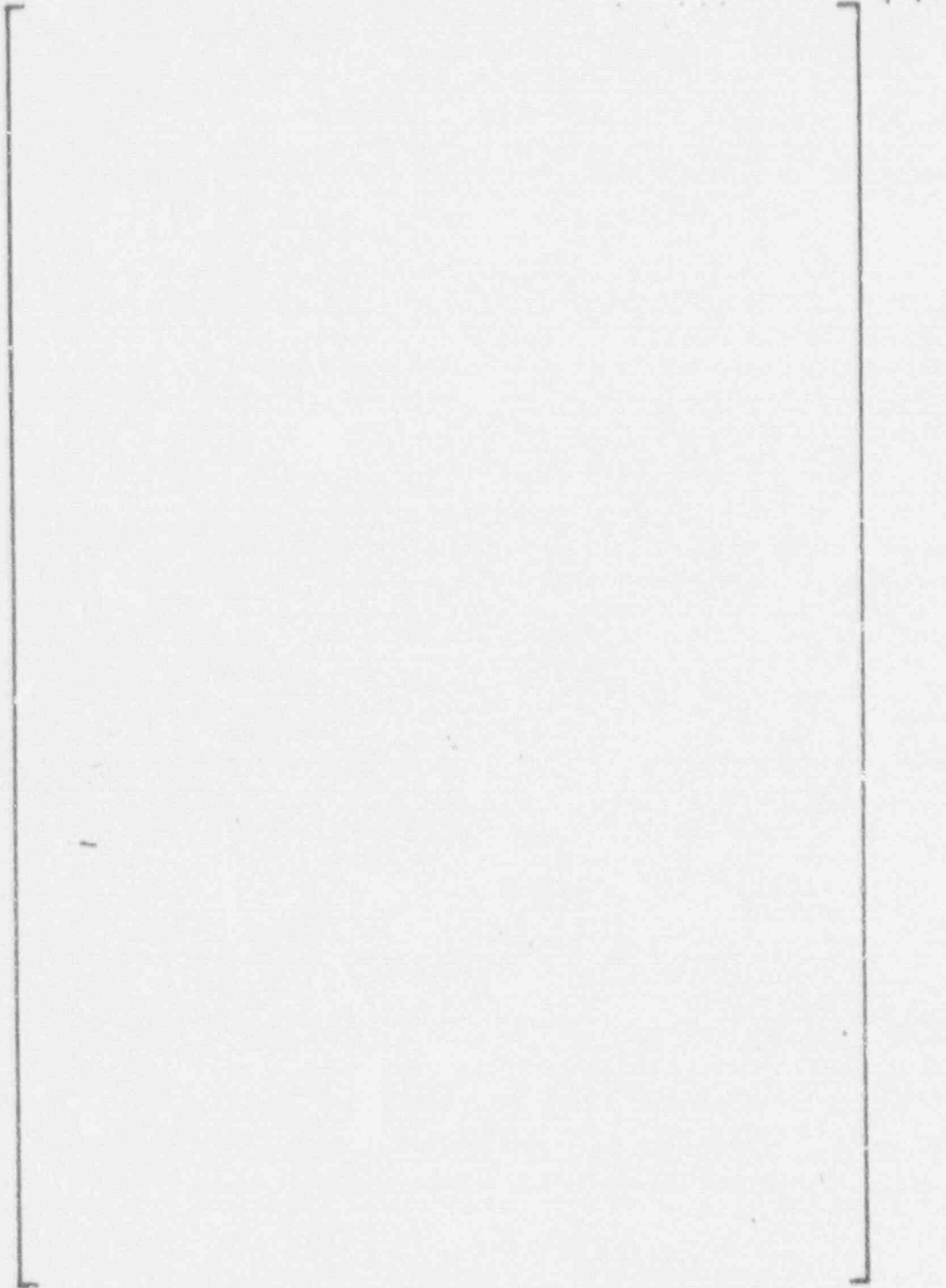


FIGURE 4.2.3.2-1 D -Rnis strain gage output (proportional to vibration amplitude, $401 \mu g = 1$ inch) for out-of-plane vibration of R11C2 with AVBS removed

ANALYTICAL (FLOVIB & NLH) TURBULENCE FORCE SPECTRUM BASES

a,b,c

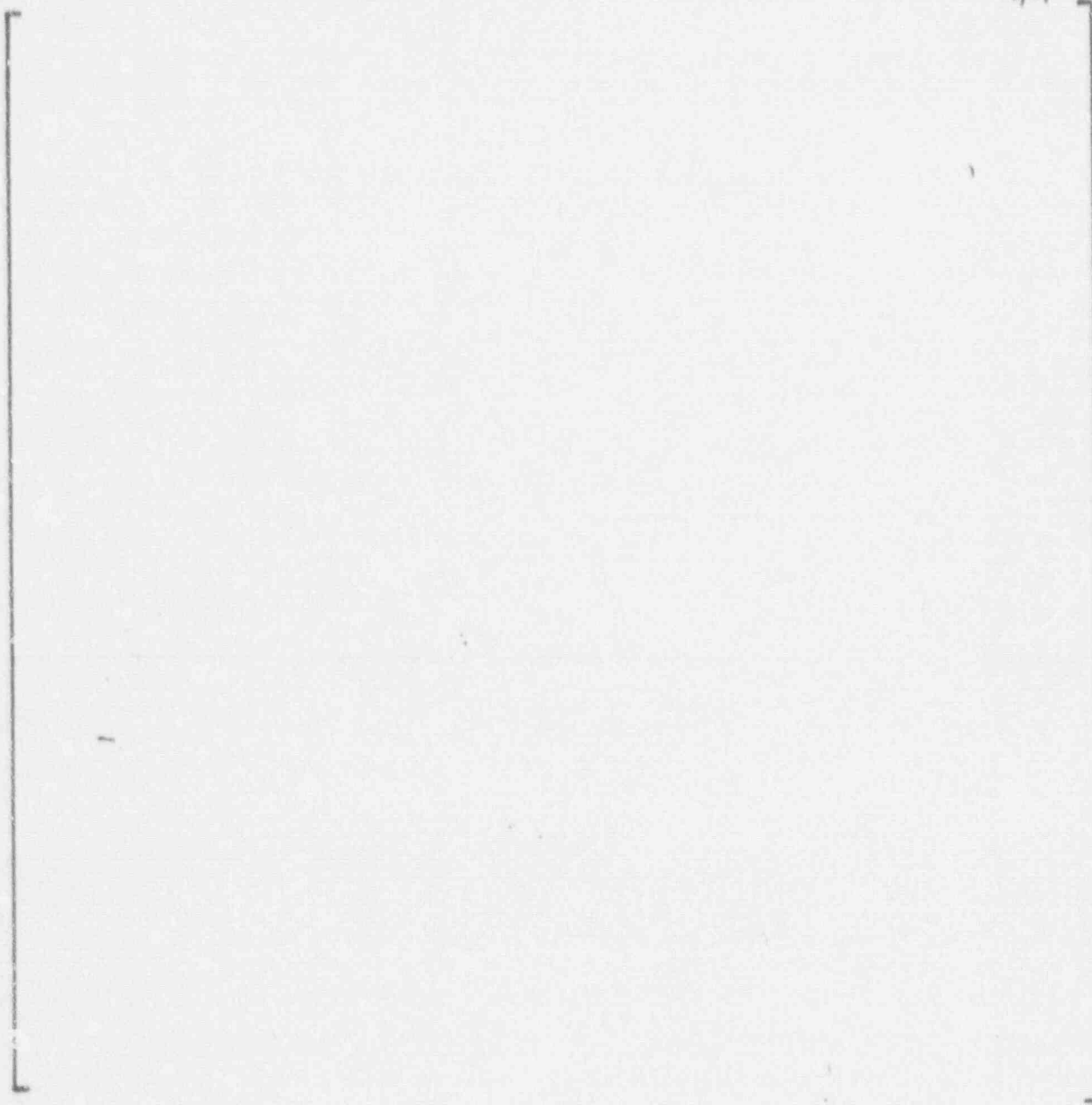


FIGURE 4.2.3.2-1E

ANALYTICAL TURBULENCE FORCE SPECTRUM
BASES RESULTS

Curve 14/1.74-4 a,b,c

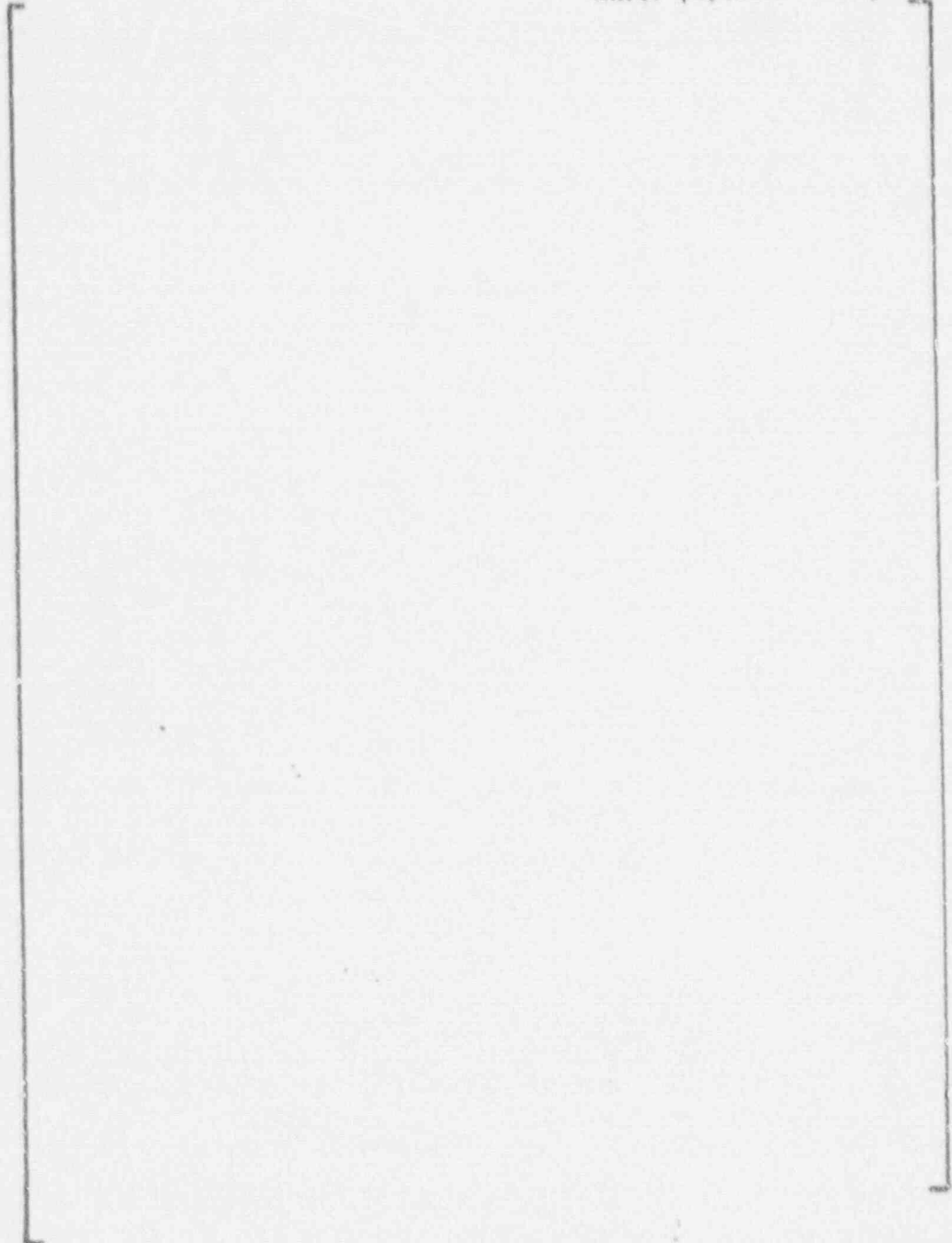


FIGURE 4.2.3.2-1F - Measured and predicted rms vibration amplitudes in the out-of-plane direction versus effective flow for Tubes R13C2 and R13C3 with AVB5 Installed

Fig 4.2.3.3.1-2
a, b, c

Damping vs Slip Void Fraction



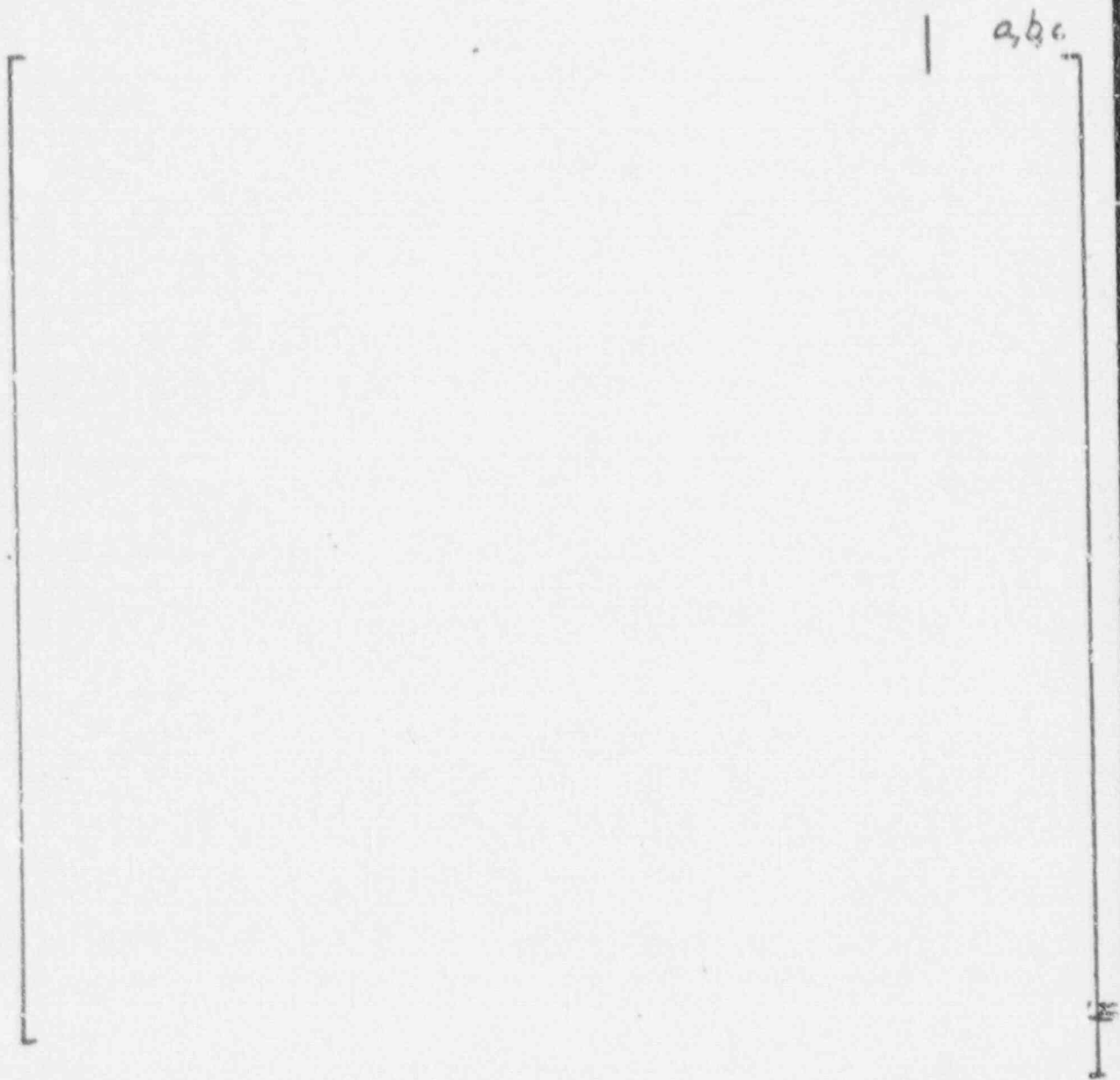


FIGURE 4.2.8.3A PLAN VIEW OF MODEL



MS1 NORTH ANNA /

X PLANES - 1 AND 16 Z PLANES - 1 THRU 25

a,b,c

FIGURE 4.2.9.3B ELEVATION VIEW OF MODEL

a,b,c

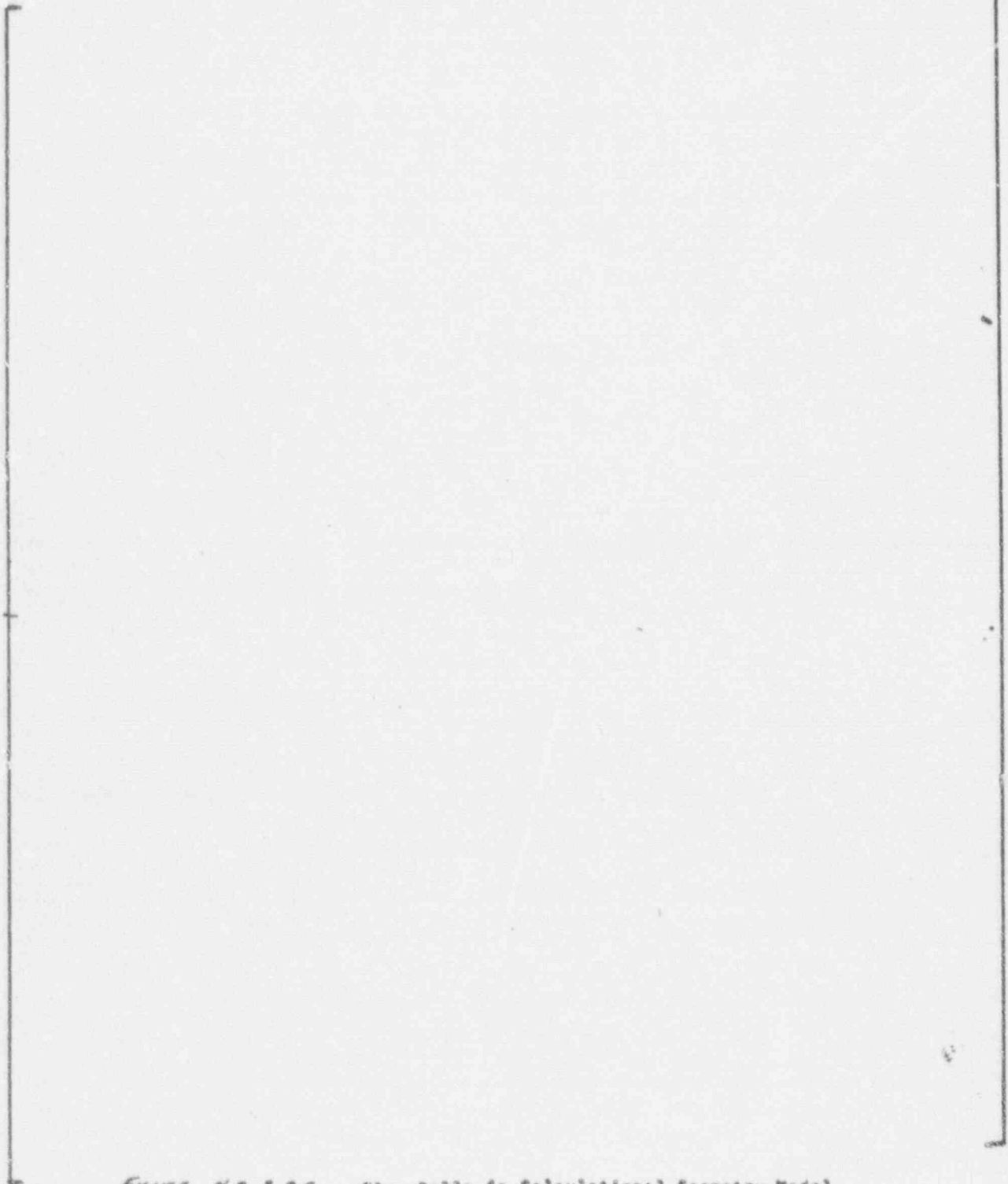


FIGURE 4.2.2.3C - Flow Cells in Computational Geometry Model

a,b,c

Figure 4.2.3.3-1. North Anna 1, Tube R9C51 Tube Gap Velocity and Density Distributions

TABLE 4.2.3.3-2

STABILITY RATIO RANGE FOR R9C51 INCLUDING UNCERTAINTIES 4.2.3.4

	STABILITY RATIO
Nominal Stability Ratio	[] ^{A,C}
<ul style="list-style-type: none"> o Calculated flow conditions without local velocity peaks o Lower range of stability constant from U-bend o Average value of damping for clamped supports 	
Including Uncertainties from , n and Average Flow - 15%	0.74
<ul style="list-style-type: none"> o This uncertainty would not significantly influence a ratio (SR₂/SR₁) of stability ratios as used to evaluate modification improvement factors 	
Including Local Velocity Peaking Factors - 10 to 20%	0.81 to 0.89
<ul style="list-style-type: none"> o Effects of non-uniform AVB insertion depth o Additional analyses in process to establish enhanced confidence on this effect 	
Including Damping Uncertainties for Dented Tubes	
<ul style="list-style-type: none"> o 50% uncertainty reducing damping from 0.82 to 0.41 	1.15 to 1.26
<ul style="list-style-type: none"> - 41% increase in stability ratios 	
<ul style="list-style-type: none"> o Lower bound on damping as mechanical damping of 0.2% 	
<ul style="list-style-type: none"> - Would yield a factor of 2 increase in stability ratios 	

RELATIVE FLUIDELASTIC STABILITY RATIO COMPARISON

- METHOD OF COMPARING RELATIVE SUSCEPTIBILITY TO FLUIDELASTIC INSTABILITY
- PLANT-TO-PLANT SUSCEPTIBILITY REFERENCED TO STABILITY RATIO (SR) FOR NORTH ANNA 1 (VRA)
- SR = FLUIDELASTIC STABILITY RATIO

$$= \frac{U_{\text{EFFECTIVE}}}{U_{\text{CRITICAL AT ONSET OF INSTABILITY}}}$$

$$\bullet \left(\frac{SR_{\text{plant}}}{SR_{\text{VRA}}} \right) = \left(\frac{(\rho v^2)^{1/2}_{\text{plant}}}{(\rho v^2)^{1/2}_{\text{VRA}}} \right) * \left(\frac{(m_{\text{VRA}})^{1/2}}{(m_{\text{plant}})^{1/2}} \right) * \left(\frac{f_n \text{ VRA}}{f_n \text{ plant}} \right) * \left(\frac{(\delta_{\text{VRA}})^{1/2}}{(\delta_{\text{plant}})^{1/2}} \right)$$

• WHERE:

ρ, v = AVERAGE U-BEND DENSITY AND RADIAL GAP VELOCITY
 = F (TUBE BUNDLE GEOMETRY, P_s , W_s , CIRC RATIO)

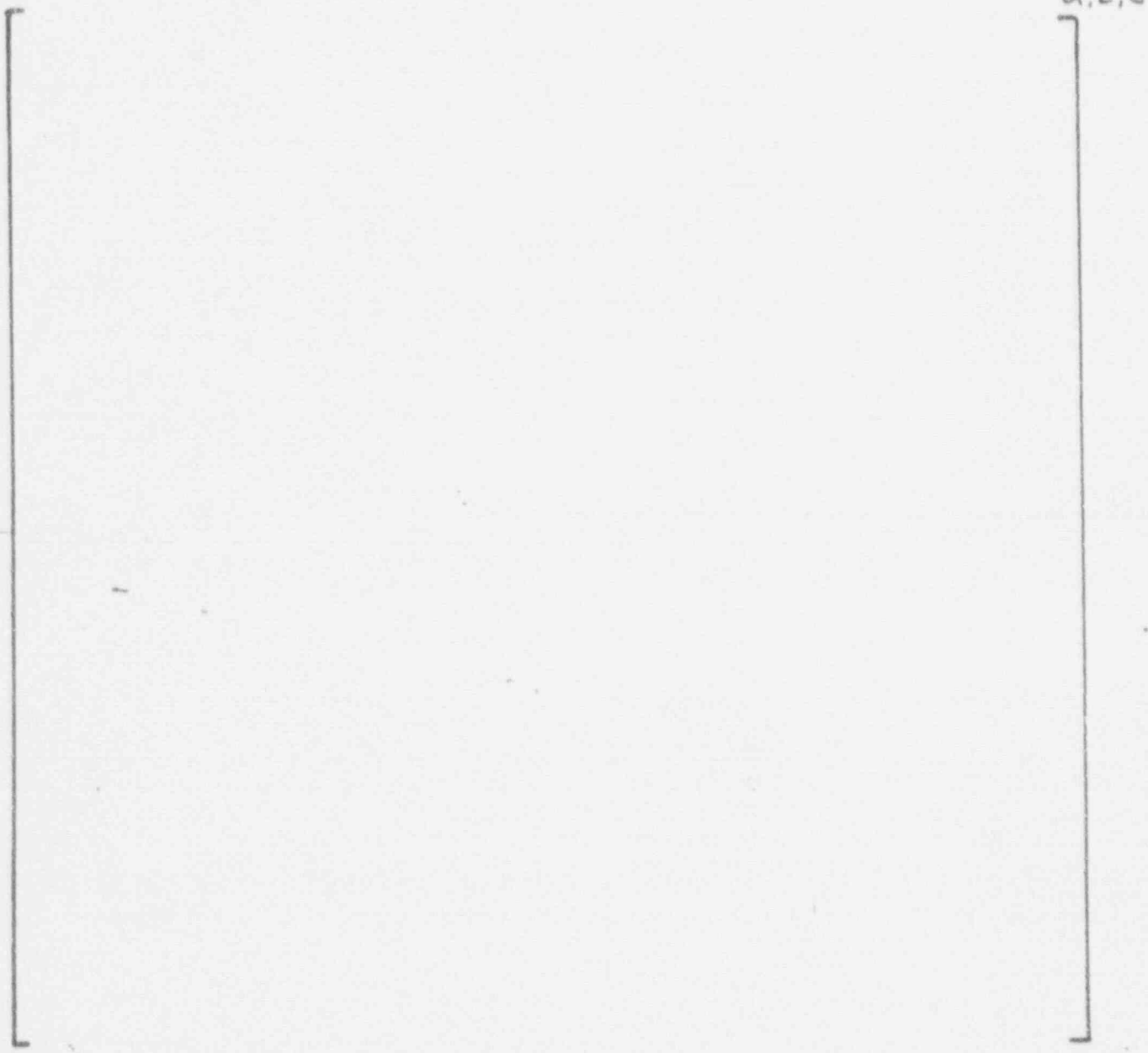
m = TUBE INCREMENTAL MASS
 = $(M_{\text{TUBE}} + M_{\text{PRIMARY}} + M_{\text{SECONDARY}})/\text{LENGTH IN A UNIT CELL}$

f_n = TUBE NATURAL FREQUENCY CALCULATED FOR CLAMPED CONDITION

δ = DAMPING PARAMETER
 = $2\pi\xi$ WHERE ξ = DAMPING RATIO

FIGURE 4.2.3.3-1B

RELATIVE FLUIDELASTIC STABILITY RATIOS



STEAM GENERATOR MODEL

■ - Dented Top TSP, □ - Nondented

FIGURE 4.2.3.3-1C

RELATIVE FLUIDELASTIC STABILITY RATIOS WITH CONSTANT DAMPING

a,b,c

STEAM GENERATOR MODEL

All Model D's have Normalized S.R. Less than 0.7
with Constant Damping

■ - Dented Top TSP, □ - Nondented

Figure 4.2.3.4-1: Fluidelastic Instability Uncertainty Assessment

a,b,c

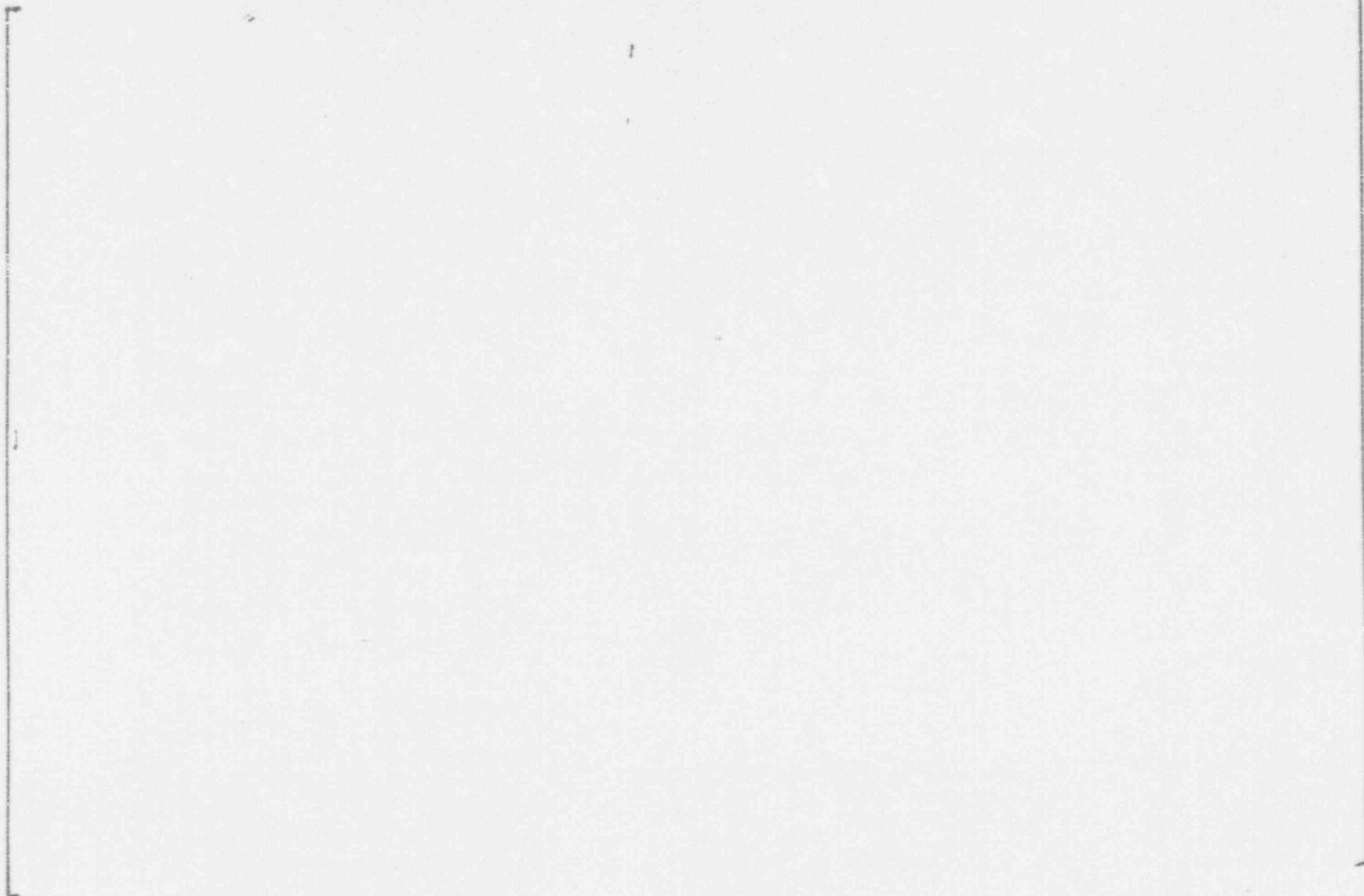


Figure 4.2.3.5 - 1

N. Anna - 1
 EC Indications for Tube Wall Thinning at AVBs
 for Rows 8 Through 12

S/G	Row	Column	AVB *	Depth (%)
A	9	87	1	<20
B	9	24	4	<20
B	8	28	4	21
B	11	35	2	23
B	12	39	2	31
B	12	46	4	24
B	10	50	1	25
B	8	61	1	26
B	8	65	1	22
B	8	65	4	<20
B	8	66	4	<20
B	8	68	1	<20
B	9	70	1	<20
B	9	70	4	21
B	12	71	1	24
B	12	71	4	26
B	12	72	4	<20
B	12	74	1	<20
B	11	75	1	21
B	11	75	4	22
B	12	77	4	<20
B	11	80	1	20
C	12	11	2	20
C	12	11	3	25
C	12	58	3	17
C	9	70	2	12

* AVB Number : 1 = Lower AVB, Hot Leg;
 2 = Upper AVB, Hot Leg; 3 = Upper AVB, Cold
 Leg; 4 = Lower AVB, Cold Leg

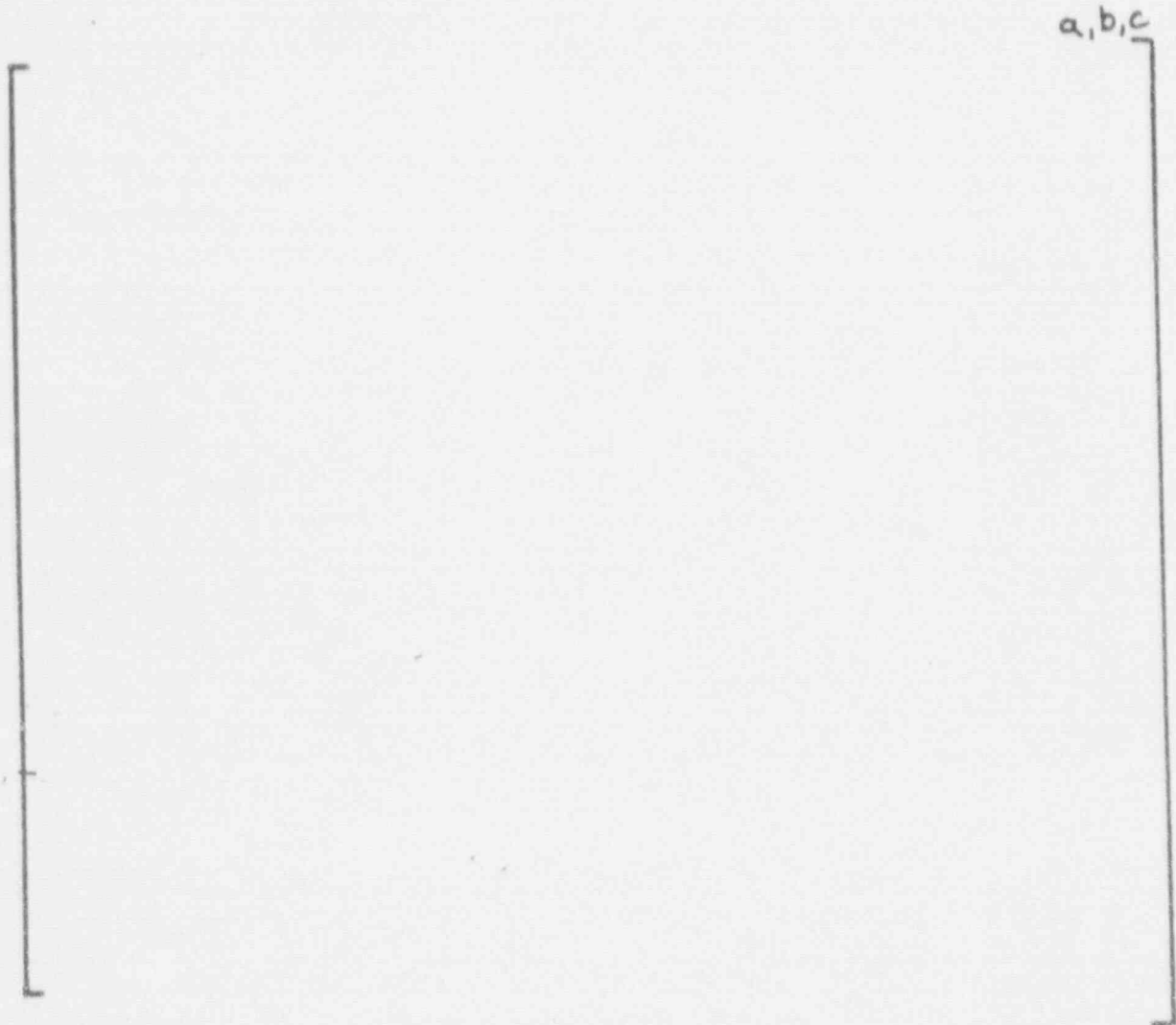
a,b,c

Figure 4.2.3.6-1. North Anna 1, with DFRP Modification,
Tube R9C51 Tube Gap Velocities and
Density Distributions

a, b, c

FIGURE 4.2.4 A LOCAL VELOCITY PEAKING FACTOR IN U-BEND OF NORTH ANNA 1 STEAM GENERATORS (TYPE I AND XI ARE INSERTION)

FIGURE 4.2.4B FLUIDELASTIC AMPLITUDE WITH NON-UNIFORM GAPS



4.2.4B

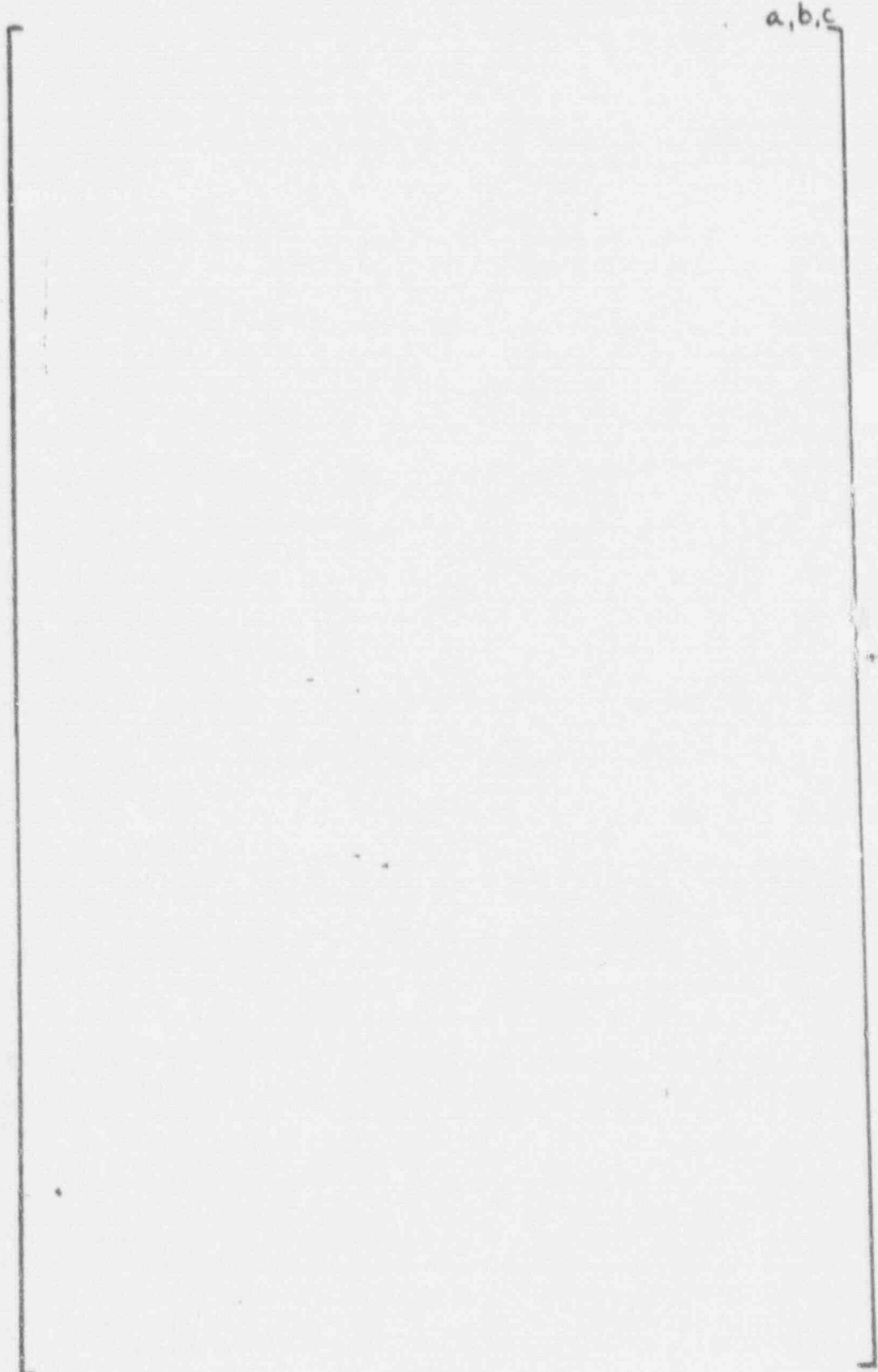


FIGURE 4.3.4C Cantilever Tube Wind Tunnel Model

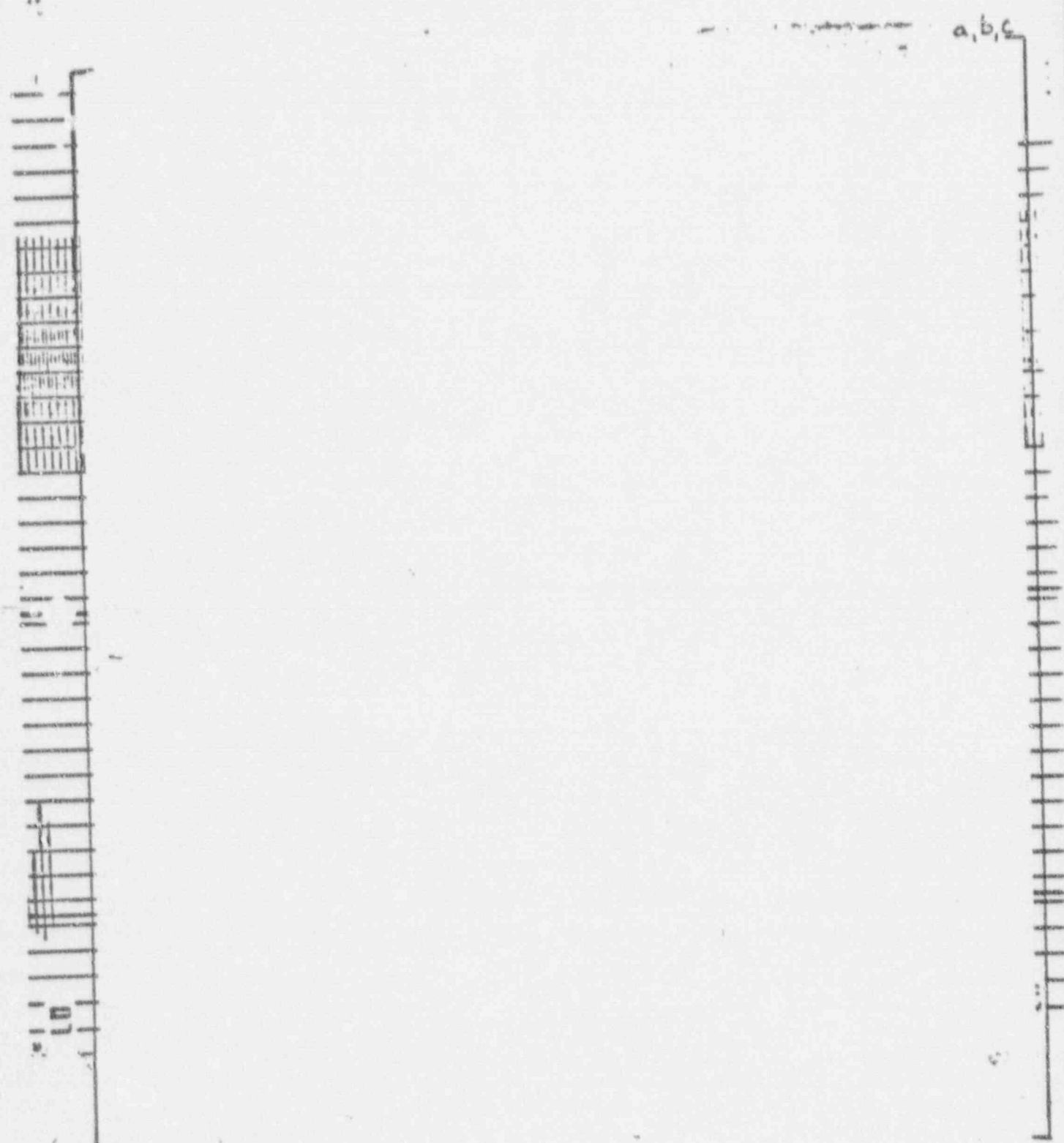


FIGURE 4.2.10 Typical vibration amplitude and tube/AVB impact force signals

Faint, illegible text or markings at the top center of the page.

a, b, c

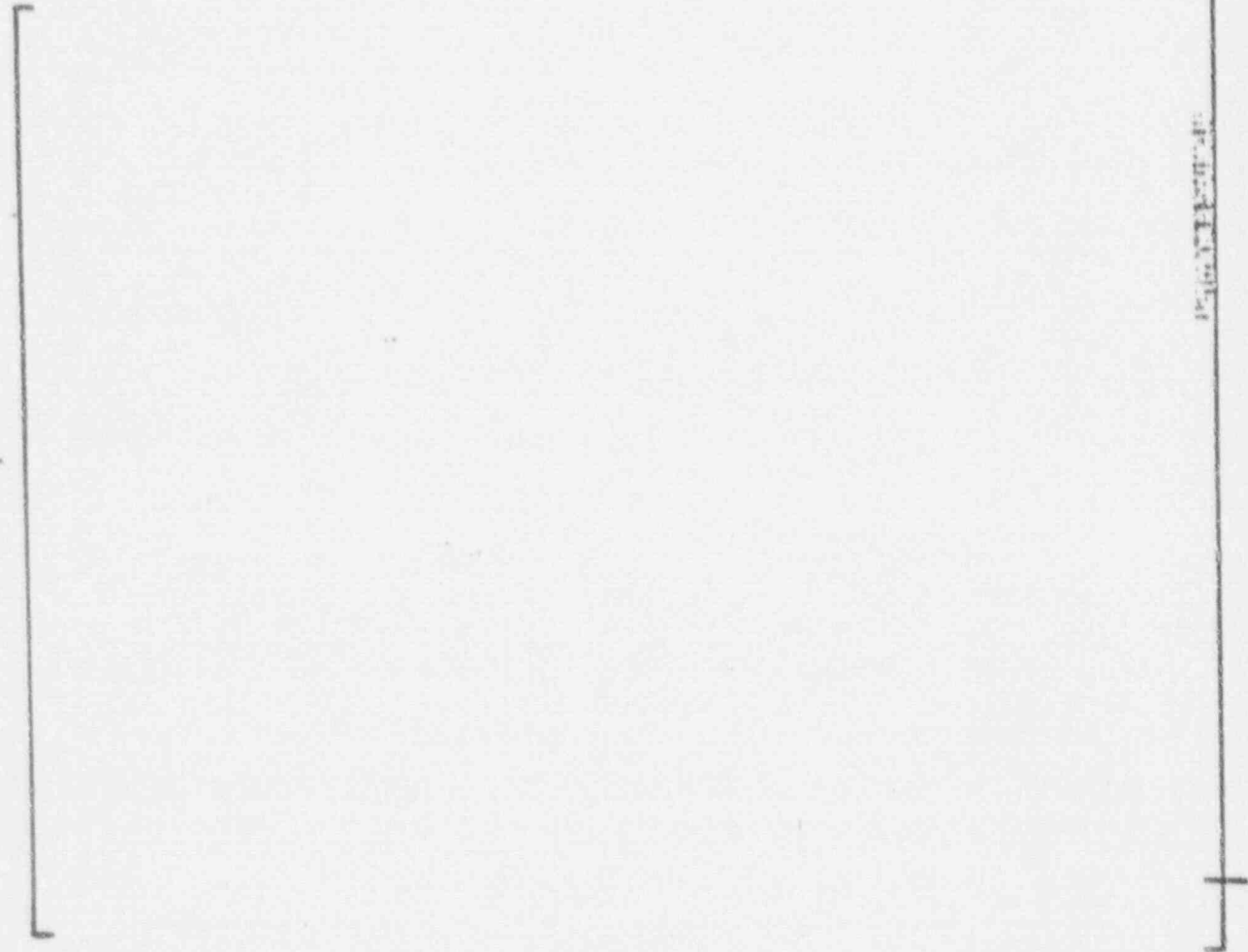


FIGURE 4.3.4E SINGLE AYB SUPPORT EVALUATION
AMPLITUDE VS. APPROACH VELOCITY

a, b, c

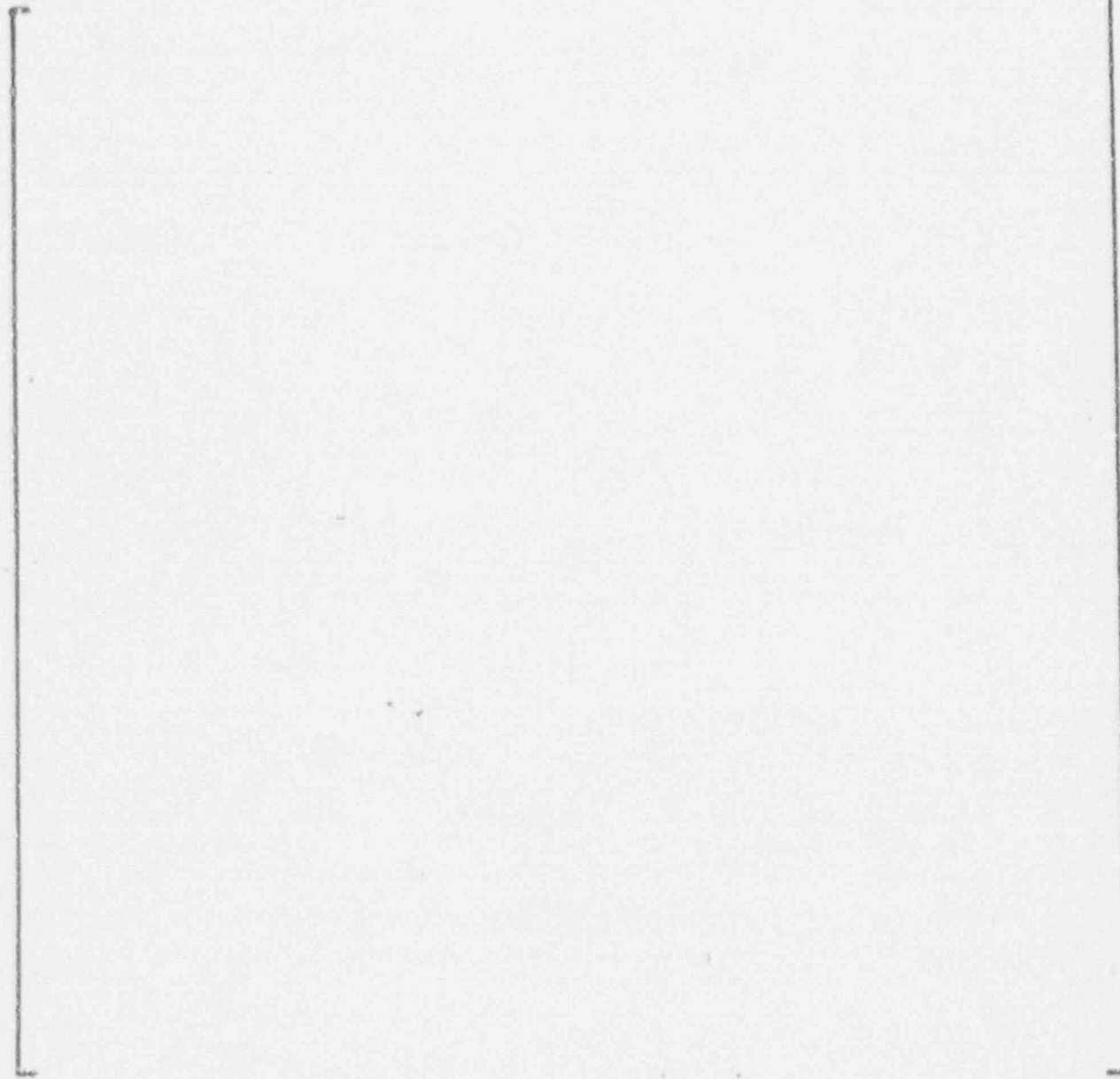


FIGURE 4.2.4F SINGLE AYB SUPPORT EVALUATION
AMPLITUDE RATIO VS. APPROACH VELOCITY

a, b, c

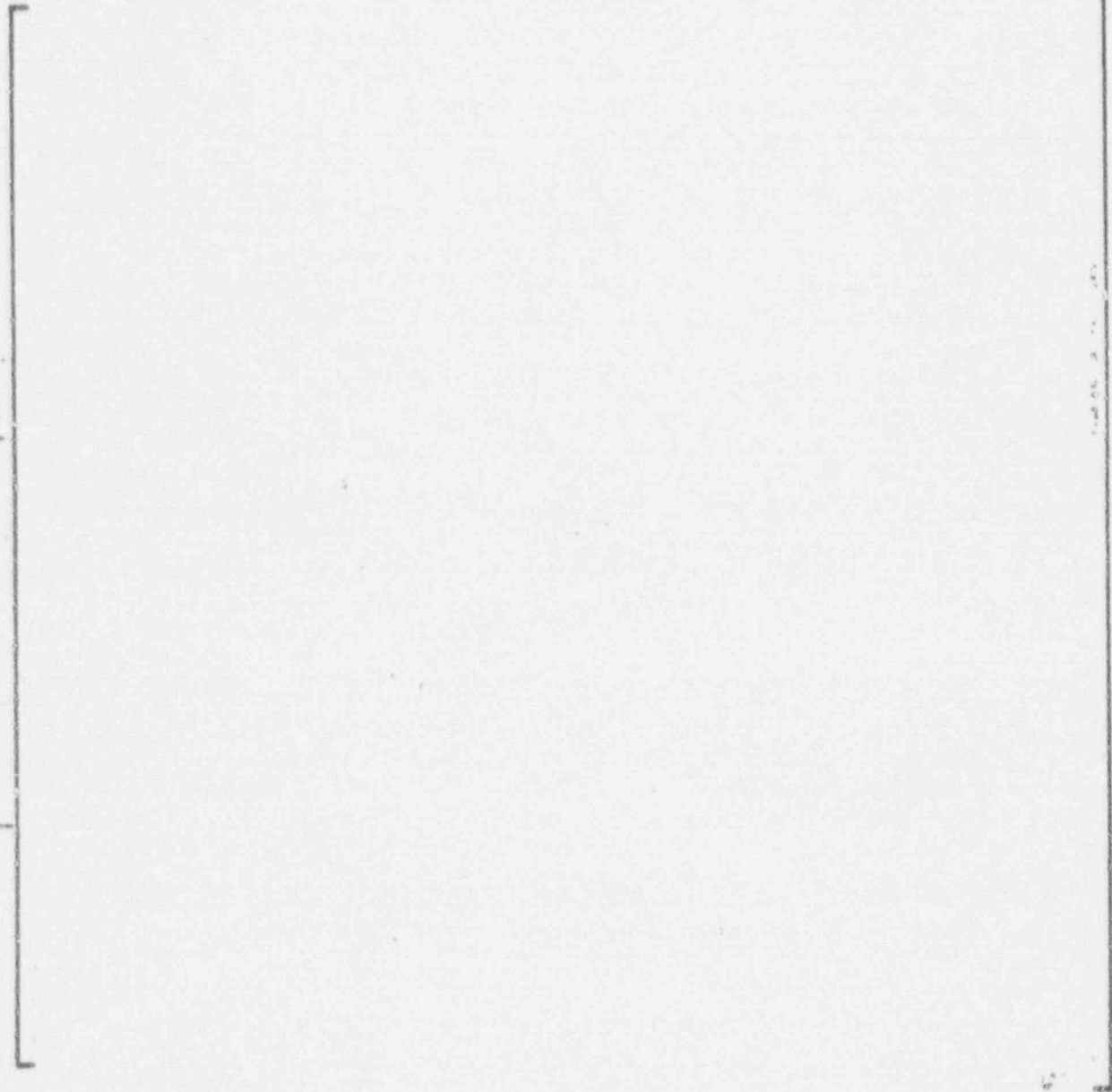
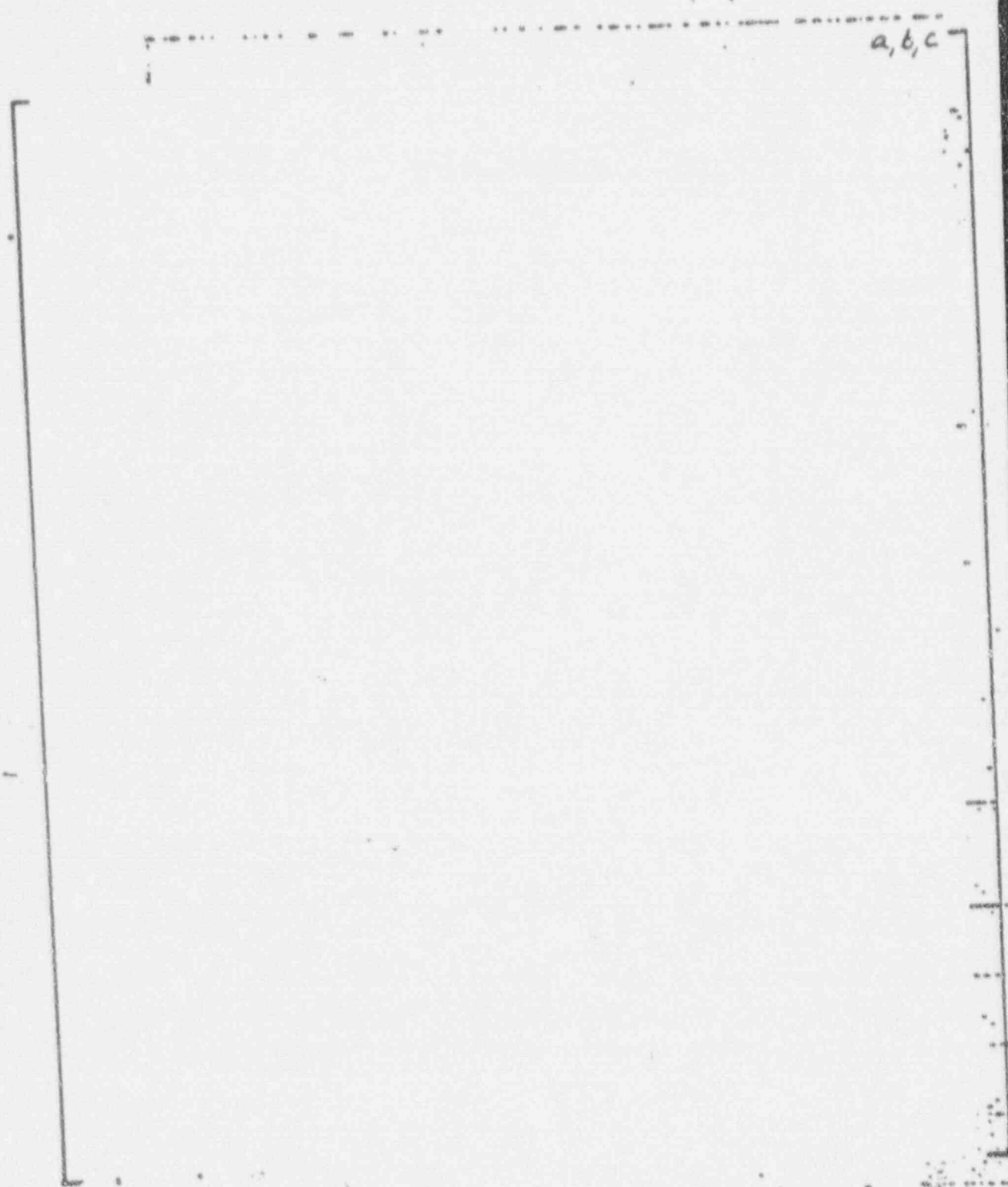


FIGURE 4.8.46 SINGLE AXIS SUPPORT EVALUATION
AMPLITUDE RATIO VS. CLEARANCE



a, b, c

FIGURE 4.2.4H Radial Velocity along U-Bend (Results from LEONARD Model Test with 2 Sets of Antivibration Bars)

7/20/84

a, b, c



FIGURE 4.2.4I

FIGURE 4.2.4-1
AVB Insertion Depth as Determined by ECT

- AVB Visible
- Plugged
- ⊖ Limit of Data (non-inclusive)

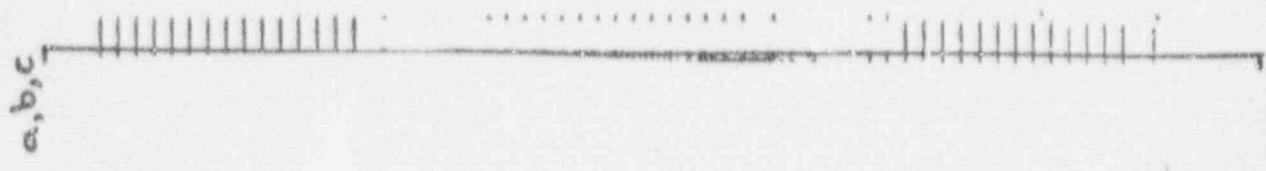
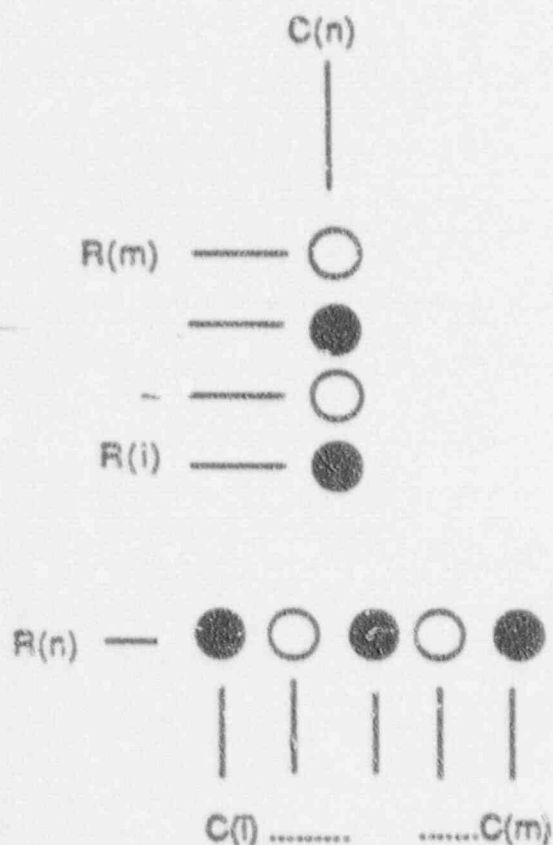


Figure 4.2.4 - 2

Interpretation of Tube Support Conditions



$k < m$: Indicated Unsupported Tubes must be Supported Because AVB is Seen at a Lower Row Number.

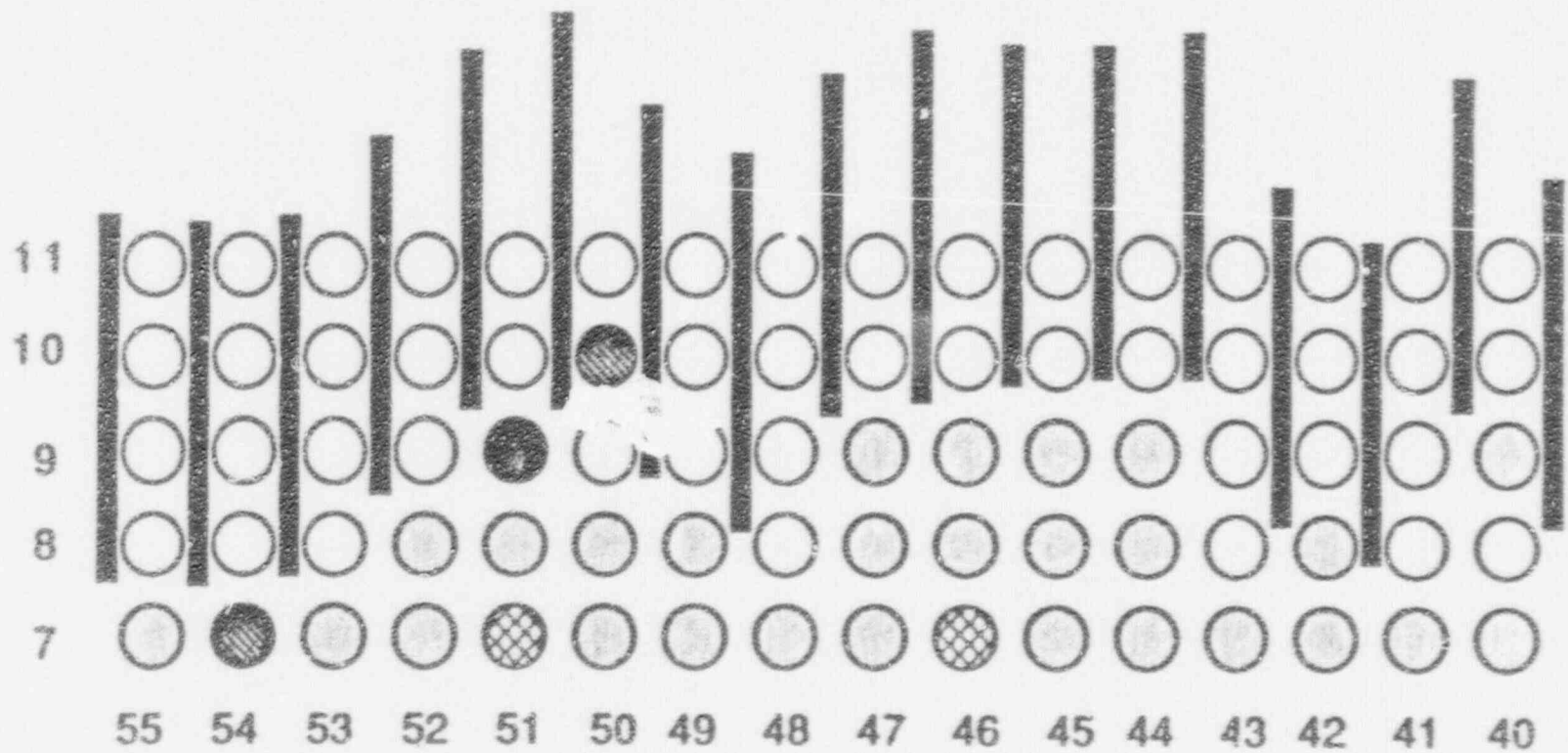
Example: S/G - A, Column 8, S/G - C, Column 40, etc.

At Least One of the Indicated Unsupported AVBs Must be Supported Because the AVB which Supports the Center Tube Must Also Support the Adjacent Tube.

Example: S/G - C; Row 10, Columns 24 - 32.

Figure 4.2.4 - 3

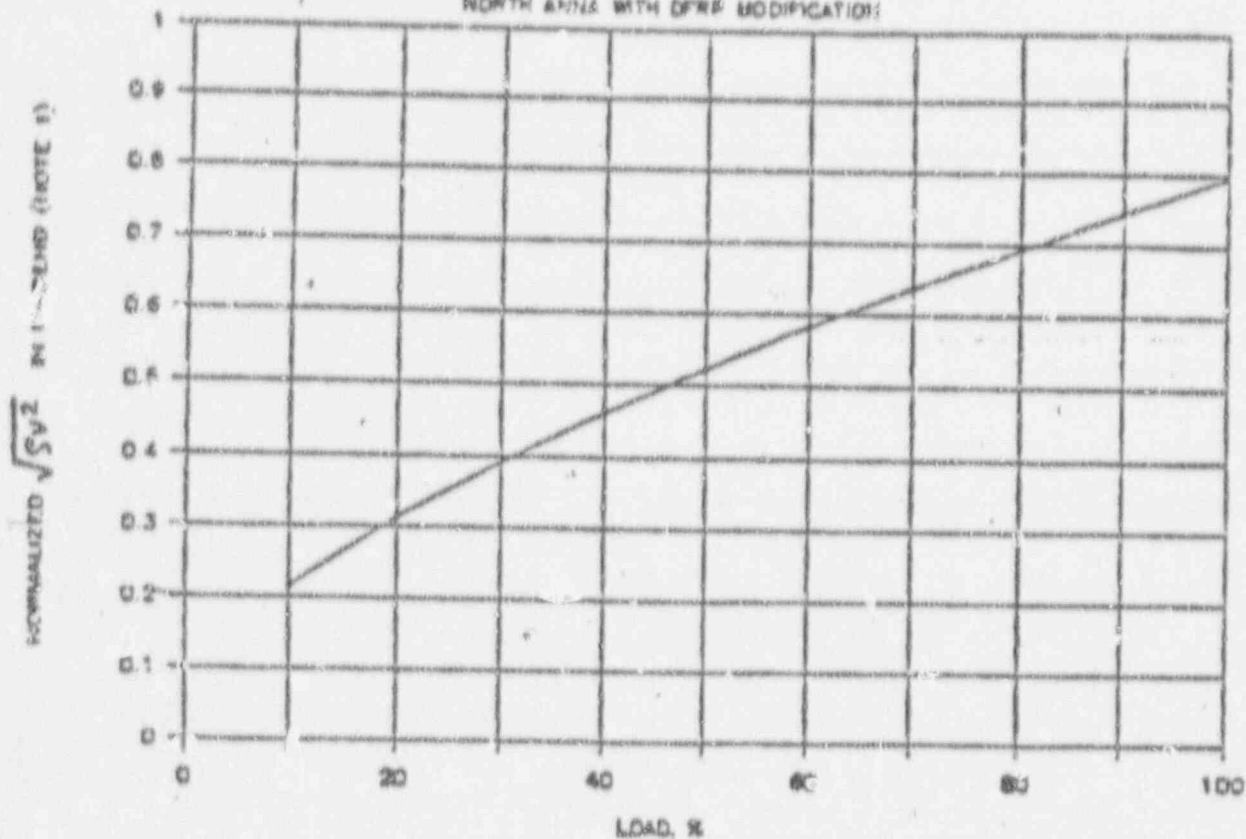
N. Anna : S/G - C
Tube Support Conditions



- AVB Visible
- AVB not Visible
- Previously Plugged
- ⊗ Not Inspected
- Failed Tube

Influence of Load on Stability Ratio

NORTH AXIS WITH DFRP MODIFICATION



Note 1. Normalized Relative to 100% Load Conditions Prior to the Downcomer Flow Resistance Plate (DFRP) Modification.

Figure 4.2.6-1

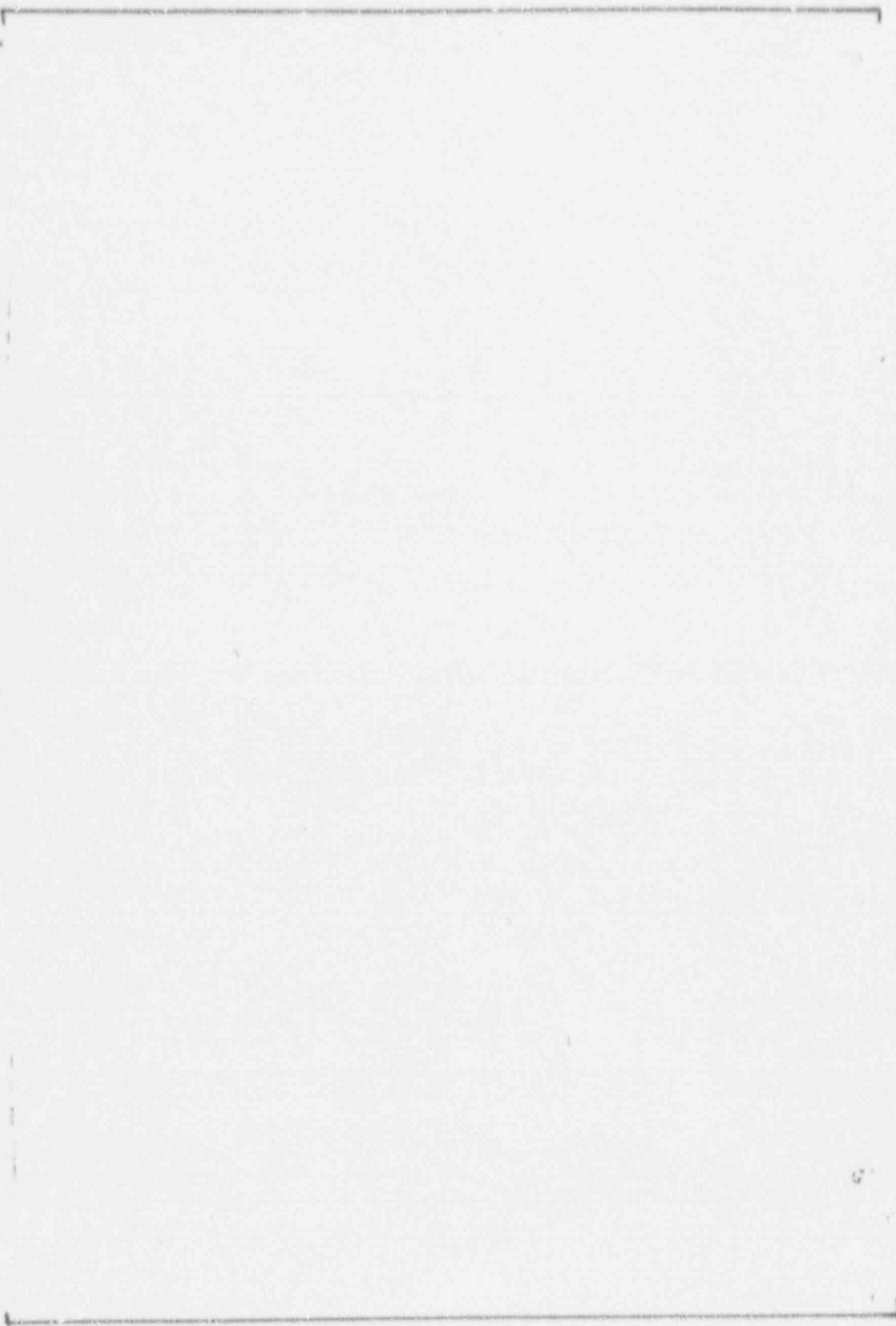
4.3 Post-Modification Leakage consideration.

The modification to be performed at North Anna Unit 1 is expected to substantially lessen the vibrational amplitudes of all tubes in the bundle. In addition, tubes with any opportunity for high cyclic stress amplitudes will be removed from service. Following these modifications, the development of a fatigue crack in a tube is considered unlikely. Should a crack develop, the stress amplitude is expected to be relatively small. The estimated worst case leak rate versus time relationship should therefore be similar to the history of the past event. Responding to the present administrative leak rate limit of 100 gpd would result in an orderly shutdown to zero power in approximately 6 hours. This would provide a factor of safety of four relative to time period observed during the past tube rupture. For convenience, the estimated leak rate versus time relationship in the unexpected circumstance of a tube fatigue event following plant modification is illustrated in figure 4.3.1.

FIGURE 4.3.1

Estimated leak rate versus time relationship
in the unlikely circumstance of a tube fatigue
event following plant modification.

a, b, c



4.4 STABILIZATION OF ROW 9, COLUMN 51

As a result of the steam generator tube rupture event, actions were taken at North Anna Unit 1 to remove the cold leg (CL) portion of the row 9, column 51 (R9C51) tube in steam generator C. The tube pull was performed to obtain one of the two tube fracture surfaces for investigation of the cause of the rupture event. The location of the tube separation was at the top surface of the seventh tube support plate (TSP 7) elevation on the CL side of the SG. This location was subsequently measured to be approximately 374.75 inches above the tube end. A vibration assessment of the remaining (U-bend) portion of the R9C51 tube indicated that it would be expected to be fluidelastically unstable in the steam generator flow field during plant operating conditions.

In view of the above, a combination spear and cable stabilizer system was designed for the remnant tube with the objective of preventing the tube remnant from interacting with adjacent tubes.

4.4.1 STABILIZATION OBJECTIVES

The objective for the design of the stabilizer system was that the installed configuration would be comparable to a plugged tube subjected to the same operational conditions. Thus, the vibration response characteristics of the design were to be equivalent or superior to those of a plugged tube, and the structural evaluation was in accordance with the requirements of the ASME Code, Section NG.

In addition, an installation objective was that the spear would not result in the R9C51 U-bend being in contact with its neighboring tubes.

4.4.2 DESIGN DESCRIPTION

The cold leg portion of the tube remnant stabilizer system is a "segmented spear" design. The design is segregated into three categories or types of segments. The uppermost segment is a [

The top [] of this segment has been machined to a [] for insertion in the free end of the U-bend remnant. The central section of the spear consists of six segments of [] tubing. The bottom section is []

The spear was inserted from the cold leg side by sliding the sections over a guide cable which was left in place following the tube pull. The eight individual sections of the spear are thread connected to form a continuous assembly. The threaded joints were assembled in the SG channelhead during installation. A locking feature precludes disassembly during subsequent plant operation.

Since the threaded ends of the spear sections [

] a.c

Following assembly and insertion, the spear was hydraulically expanded at each support plate elevation. At TSP's 1 through 6 the length of the expansion zone

is approximately four inches, which is longer than the thickness of the TSP's. The post-expansion clearance between the OD of the spear and the ID of the TSP hole is approximately [] At the seventh TSP the length of the expanded zone is approximately [] This was intended to result in contact with the TSP without the expansion extending beyond the edges of the plate. Finally, a hydraulic expansion joint connects the spear to the free-end of the tube remnant.

Eddy current inspection was used following the installation of the spear to verify the location of the expansions at each tube support plate. Following the ECT inspection, the bottom section of the stabilizer assembly is roll expanded into the tubesheet over a length of approximately [] The final pressure boundary closure on the cold leg was accomplished using a standard weld plug.

Considering that some degree of fatigue damage may have occurred to the tube at the seventh TSP elevation on the hot leg (HL) side, a cable type stabilizer was designed and installed, extending from the tubesheet through the seventh TSP and approximately 30 degrees over the u-bend. Stabilization of both sides of the u-bend is expected to reduce the potential for interaction with neighboring tubes if circumferential separation of either end were to occur.

The hot leg stabilizer consists of a series of [

] #,c

Finally, "sentinel" type, mechanical plugs were installed in each of the eight neighboring tubes to R9C51. "Tell tale" plugs are of the same design as standard mechanical plugs except that a small hole, approximately 0.012" in diameter, has been drilled into the top end. Should the tube wall become perforated during operation the plug will leak at a pre-determined rate of approximately 200 GPD. The purpose of the "tell tale" plugs is to allow monitoring of the integrity of the tube.

4.4.2.1 Verification Testing

4.4.2.1.1 Spear to U-bend Joint

The bending moment imposed on the spear to u-bend (upper) joint by flow-induced vibration forces was calculated to be on the order of 10-20 in.-lbs. for combined turbulence and fluidelastic mechanisms. The bending moment capability of the upper joint was determined by test and analysis involving axial torque tests and transverse bending tests.

Torque tests were performed on joints made in u-bend and straight length tubes. The rationale for testing u-bend sections, which involve more fabrication, was to determine if the tube bending process resulted in a work hardened zone which could affect the expansion and strength of the tube to u-bend joint. The tubing used for the joints was Inconel 600 MA with a yield strength of [] ksi. The field tube yield strength was determined to be approximately [] ksi based #,c reviewing the mill certification test results (before fabrication) and tensile tests performed on material from the pulled tube. The spear simulant was Inconel 690 TT from the same heat as used to fabricate the field spears. Since a minor heat treatment was specified for the spear tube-to-end blank weld, test sections included both the heat treated and non-heat treated condition.

The joints involved the four possible combinations of scale deposit on both the

spears and the tubes. The scaled surface on the spears resulted from the HT. Although the field spear tips have no scale, because the tips were machined after HT, the field u-bend may have light scale adhering to its surface (no significant scale was evident from the fiber-optic examinations and only very light scale was present in the pulled tube specimens), developed during operation.

The axial torque at which rotation first occurred ranged from 230 to over 600 in.-lbs. The effect of work hardening related to forming the u-bend did not result in any perceptible effect in the region where the upper joint was formed; straight and u-bend tube specimens exhibited comparable torques. The upper joint radial contact stress, acting over the interfacial contact area, and associated with the smallest found torque, 230 in.-lbs., conservatively assuming a coefficient of friction of 0.5, was calculated to be 533 psi. Using these results, a corresponding transverse static bending moment capability of the joint was calculated to be 227 in.-lbs. Therefore the calculated transverse strength of the joint is in excess of 11 (227/20) times the highest calculated dynamic transverse bending moment.

The torque testing was performed in the room temperature condition. Due to the slightly greater coefficient of linear expansion, of the [] spear versus that of the [] tube, the interfacial radial contact stress should increase at 525F, the operation temperature, and improve the resistance to bending moment.

Transverse static bending moment tests were also performed on simulated upper joints of the same configuration as for the torque tests. In all cases the limit bending moment of the spear was less than the bending moment to cause rotation of the joint, i.e., the spear bent before the joint rotated. Examination of the load-displacement records for the bending tests showed no effect of joint (bending) rotation, i.e., nonlinearity in the bending force-deflection relationship, at low moments and up to and including a bending moment sufficient to yield the spear. The maximum bending moment before spear bending yield was approximately 900 in.-lbs. By contrast, the structural analysis indicated that the maximum bending moment imposed on the joint by flow-induced forces is on the order of 10 to 20 in.-lbs. for combined turbulence and fluidelastic loads. Based on the static test results, and considering that other modes of vibration such as "ring" modes will not be excited, it was concluded that the dynamic loads will not loosen the joint.

Two axial-separation, pull tests were performed on simulated upper joint specimens. The applied forces for which non-linear behavior was first observed were 300 and 2100 lbs. respectively. Because the fluid drag loads acting on the u-bend are only of several pounds in magnitude, a large margin between actual strength and applied load exists. It is noted that the maximum load to cause separation of the joint in each test was in excess of 7000 lbs.

4.4.2.1.2 Spear Threaded Joint

The resistance to axial separation of the spear threaded joints (STJ's) was determined by a destructive uniaxial tensile test of a prototypical, properly torqued joint. It was also determined by a cyclic, axial-loading (tension-release) test, on a second STJ, in which the largest load, during any of the transients, 1360 lbs., was applied for the required number of times. This transient was heatup/cooldown and the remaining number of applications of this transient is approximately 150. The destructive tensile test showed that the STJ was elastic to a load of 4,500 lbs., approximately 3.3 times the largest axial load, 1,360 lbs. The cyclic application of the 1,360 lbs. 150

times had no apparent detrimental effect on the other prototypical STJ. Based on these most-stringent loading test results, the STJ's should perform reliably.

4.4.2.1.3 Spear-To-Tubesheet Joint

The spear-to-tubesheet joint (STSJ) is a []^{A.C} Such joints have been well characterized over many decades of use in the shell and tube heat exchanger industry. The []

[]^{A.C} Past tests have shown that, for I600 7/8" diameter tubing, expanded into the proper-sized tubesheet hole, []^{A.C} would satisfy the requirement to resist a pullout load of 1,360 lbs. The []^{A.C} provide a total axial length of approximately []^{A.C} (OK as is) in., thereby providing an adequate design margin. The tube and tubesheet surfaces will be adequately clean prior to expansion. The tube acquired essentially no scale during heat treat and the tubesheet hole will be brushed prior to spear insertion to remove hard scale.

4.4.2.2 Materials Evaluation

Spear

The mechanical configuration for the material in the metallurgical condition of the stabilized tube after expansion has been assessed. Specifically, the possibility of stress corrosion cracking (SCC) at the transition zone of the stabilizer expansion regions has been investigated at both the TSP elevations and at the expansion joint in the free end of the remaining portion of tube R9C51. Both nominal and off-nominal expansions (enveloping process parameters) have been evaluated. Based on previous laboratory testing (Reverse U-Bend, RUB, [] samples exposed to 750 F steam with equivalent strain to the expansion regions), geometric comparisons, and the absence of heat flux/corrosion concentrating environment, the expansion process implemented on the stabilizer at the TSP's and the insertion point in the remnant tube R9 C51 does not reduce the spear material margin to resist the occurrence of SCC.

Tube Remnant

Based on past Westinghouse testing, the I 600 tube hoop strain of up to approximately [] percent is judged to be acceptable, owing to the relatively low operating temperature (525 degrees F) and in the absence of heat-flux.

Cable Stabilizer

The installation of cable stabilizers (CS's) in degraded SG tubes is designed to maintain bundle structural integrity. The specific purpose of the CS is to reduce the amplitude of (bending) vibration which can cause or continue the tube degradation process.

In a contingency mode, the CS is designed, by strategic placement of the sleeve axial midpoints at the most likely severance locations, to prevent a severed tube from contacting adjacent tubes.

The design of the HL CS is based on analyses for installation in another location in a Model 51 SG and on extensive tests and analyses of CS's for SG's

containing tubes of two other sizes. Two of the three CS sizes are in use in Westinghouse SG's the third size was developed specifically for a competitor SG's one of the two sizes in use in Westinghouse SG's is also in use in another competitor's SG's. All three sizes involve the same design features, i.e., the sleeves, with relatively small clearances to the tube ID, contact the tube ID and thereby cause the cable to undergo bending vibration similar to that experienced by the tube. Although the CS decreases the vibrating system frequency, a detrimental effect, it produces a more-than-offsetting-effect of increasing system damping, a desirable effect.

A CS in the HL and extending into a portion of the u-bend of tube R9C51 serves the same two purposes as it does in the straight portions of tubes viz., to reduce vibration amplitude and, in a contingency mode, to reduce the effect on bundle integrity of a tube severance. Although the portion of the CS above the tube straight section-to-curved section tangent point contains no sleeves, it was concluded that the stiff cable will maintain adequate contact with the u-bend portion to perform an amplitude-reduction function. This conclusion was based on trial insertion of the cable in a Row 9 u-bend.

For the contingency mode, it was postulated that severance would occur at the same location on the HL as it did on the CL, i.e., at the top of TSP 7. For this reason, the top of the uppermost CS sleeve was designed to be located approximately 0.5 in. below the HL tangent joint. This positions the mechanical plug bottom at the proper location, flush, at the tube end. The 8.15 in.-long sleeve would therefore span the most likely severance point, the top of TSP 7. If the severed-on-the-HL u-bend rose approximately 0.5 in. as the CL end did, based upon both visual and ECT inspections, the HL u-bend straight length engagement after severance would still be approximately 2.3 in. The u-bend to sleeve engagement, along with the CL spear attachment, would limit the out-of-plane movement of the u-bend.

4.4.3 TUBE STABILIZER STRUCTURAL ANALYSIS

4.4.3.1 Vibration Analysis

In order to establish the acceptability of the spear-stabilized tube configuration, conservative non-linear single-tube finite element models were developed to compute the tube vibration response and wear potential under operating conditions. The reference (or base) configuration for evaluation comparison was chosen as a plugged tube. There are about 600 plugged tubes presently in operating Series 51 steam generators, in comparable rows, which have exhibited acceptable service to date. These tubes were removed from service for reasons unrelated to denting and would be expected to have boundary conditions similar to the stabilized tube. It is important to note, however, the stabilizer to TSP gaps are much smaller than for a tube, thus the stabilizer would be expected to be vibrationally supported at more locations than a plugged tube.

The tube vibration responses and implied stress and wear levels were determined using[

] a, c

Results from the above described analyses indicate that the wear time for the stabilizer at the plate with the highest work rate is 14% longer than the wear time for a plugged tube to reach a similar wear condition.

4.4.3.2 Structural Analysis

The analysis of the segmented spear stabilizer demonstrates structural acceptability for an operating period of 40 years. The analysis examines the expanded zones of the spear, the threaded spear joints, and the spear / tube remnant interface. Loading mechanisms which are evaluated include fatigue of the expansion and / or threaded joints, possible ratcheting of the threaded joints (slip - stick) under cyclic axial loads, and slippage and subsequent wear of the spear / tube remnant expansion zone. This analysis does not include vibrational loading mechanisms, which are treated above. The segmented spear is not part of the system pressure boundary and, therefore, is not subject to the criteria of the ASME Code. Where applicable, the criteria of Section III, Subsection NG, of the ASME Code is used as a guide in evaluating the design.

4.4.3.2.1 Loading Conditions

The spear is evaluated for a full duty cycle of events, as specified in the Model 51 Design Specification. A summary of the applicable duty cycle is provided in Table 4.4-1. Corresponding pressures and temperatures for each of the transients are summarized in Tables 4.4-2 and 4.4-3. The tube temperatures summarized in Table 4.4-3 represent the tube temperature in the first pass of the hot leg and the seventh pass of the cold leg. These temperatures are considered to be applicable to the straight leg portion of the tube in the hot and cold legs respectively. The tube temperature is based on the average of the primary and secondary side water temperatures. The plate temperatures correspond to the secondary side water temperatures. The transient times selected correspond to maximum and minimum values for the various temperatures and pressures being considered.

[
] o, c

[

]#.c

4.4.3.2.2 Spear Expansion Zones

Two expansion conditions for the spear are analyzed. The first condition corresponds to expansions in the first six support plates where the expansion is [] long, and is nominally centered within the support plate. For this expansion, the tube support plate hole is assumed to correspond to the maximum value within the tolerance range, 0.906 corresponds to a hole having a diameter equal to the tube outside diameter due to the dented condition at this plate, 0.875 inches.

To evaluate loading conditions where the beam response of the tube is involved, the [

]#.c

Analysis of the expanded zones to account for the local geometry of the expansions is performed using the finite element models shown in Figures 4.4-5 and 6. The model in Figure 4.4-5 corresponds to the expansion zones for tube support plates 1-6, and the model shown in Figure 4.4-6 corresponds to the expansion at the top support plate.

Analysis results show that the only significant loading experienced by the spear is due to differential axial growth between the stabilized tube and the surrounding active tubes. The differential radial growth between the spear and tube support plate is not sufficient to close the gap after expansion, approximately [] radial, and as a result, interference loads do not develop. Vibration loads at the top support plate are quite small for a nondegraded geometry and negligible stresses result. Stresses in the spear resulting from the remaining interactions with the tube support plates and tubesheet do not produce any significant stresses.

Using reference stresses for an axial load of 1000 lb., tube stresses are developed for each of the transient conditions. [

Summaries of the umbrella stresses are provided in Table 4.4-7 for the inside surface and in Table 4.4-8 for the outside surface. Fatigue calculations for both surfaces are provided in Table 4.4-9 during the expansion process and local concentrations in the expansion transition regions, a concentration factor of 2.0 is applied to the resulting alternating stresses.

4.4.3.2.3 Spear Threaded Joints

Hoop and axial stresses for the threaded joints are developed using conventional analysis techniques. [

The resulting fatigue usages are summarized in Table 11.

The pull-out capability of the threaded joint is demonstrated using a uniaxial tension test. The results of the test in the form of a load-deflection curve are provided in Figure 4. These results show the joint to behave in a linear (elastic) manner for a load up to 4500 any of the transient conditions is 1360 lb.. Thus, a factor of 3.3 exists between the applied load and the load capability of the joint.

4.4.3.2.4 Spear/Tube Remnant Joint

The contact pressure at the spear / tube remnant interface following expansion is determined using both analysis and test. Assuming the response of the tube and spear to be elastic - perfectly plastic, the contact pressure is calculated to be 1500 psi for an expansion of 45 a calibrated wrench the torque necessary to separate the spear and tube remnant, and then converting the torque to a friction force. The friction force is then converted to a corresponding normal

force or contact pressure. For expansions ranging from 9 to 50 mils the contact pressure is found to range from 500 - 1000 psi for a coefficient of friction ranging from 0.5 to 1.0. The static bending moment required to overcome contact pressures of 500 - 1000 psi is 230 - 470 in.-lb..

The bending moment imposed on the spear / tube remnant joint by flow induced forces is on the order of 10 - 20 in.-lb. for combined turbulence and fluid-elastic forces assuming that overall system modifications reduce bundle vibration to design basis levels. This is well below the required moment to initiate slippage. Dynamic aspects of this loading condition are being addressed by testing of this interface. Discussions regarding those tests are addressed in the section of the report dealing with the dynamic response of the spear and tube remnant.

4.4.3.2.5 Results & Conclusions

Based on the analysis results discussed above, the following conclusions can be drawn concerning the structural adequacy of the segmented spear stabilizer.

1. Fatigue usage of the spear expansion zones and the threaded joints is minimal.
2. The axial strength of the threaded joints is sufficient to preclude pull-out of a spear segment under a slip - stick ratcheting mechanism.
3. The contact pressure at the spear / tube remnant interface is sufficient to prevent slippage and wear in the joint on a static basis.

Overall, the segmented spear stabilizer is concluded to be structurally adequate for its intended mode of operation assuming that overall system modifications reduce bundle vibration to design basis levels.

4.4.4 INSTALLATION

Functional requirements were determined prior to the qualification program for installation of the stabilizer; these requirements were then used during qualification to demonstrate the adequacy of the installation process and procedure. The computer controlled hydraulic expansion process used in the installation of the spear has been qualified for the as-manufactured expected spear-to-TSP diametral clearance range. The personnel installing the segmented spear stabilizer have been qualified using prototypical mock-ups which simulate the steam generator.

4.4.4.1 Spear

[

] a, c

[

] a,c

4.4.4.2 Cable Stabilizer

The basic steps of the process involve:

[

] a,c

4.4.5 CONCLUSION

Analyses and/or testing of the tube remnant stabilization system have shown that the steam generator repair is structurally sound i.e., the spear remnant joint, the spear segment-to-segment joints and the spear-to-tubesheet joint can resist loadings due to: fluid drag, tube vibration mechanisms, tube differential thermal expansion and installation. Also, as the spear material is made of thermally treated [] the spear should be resistant to stress corrosion cracking during the remaining design objective life of the steam generators. Briefly, the performance integrity of the stabilized tube remnant is expected to be, at a minimum, equivalent to the integrity of a plugged tube.

It may be possible that some fatigue damage has also occurred in the hot leg of the failed tube. Therefore, to provide further assurance of maintenance of tube

bundle integrity during subsequent plant operation by precluding the potential for interaction with adjacent active tubes, the hot leg of the tube remnant will be cable stabilized.

Finally, all neighboring tubes will be plugged with "sentinel" (controlled leakage) plugs. This will prevent uncontrolled leakage in the event of spear failure of a type which would result in interaction with the neighboring tubes.

TABLE 4.4-1.
DUTY CYCLE SUMMARY

<u>TRANSIENT</u>	<u>Cycles</u>
PLANT HEAT UP / COOLDOWN	200
PLANT LOADING / UNLOADING	18,300
SMALL STEP LOAD INCREASE	2,000
SMALL STEP LOAD DECREASE	2,000
LARGE STEP LOAD DECREASE	200
HOT STANDBY OPERATION	18,300
LOSS OF LOAD	80
LOSS OF POWER	40
LOSS OF FLOW	80
REACTOR TRIP	400
FEEDWATER CYCLING	18,300
PRIMARY SIDE HYDRO	5
SECONDARY SIDE HYDRO	5
STEAM LINE BREAK	1*
LOSS OF COOLANT ACCIDENT	1*
FEED LINE BREAK	1*

* NOT CONSIDERED IN THE FATIGUE ANALYSIS

TABLE 4.4-2
TRANSIENT PRESSURES

TRANSIENT	TIME	PRIMARY PRESSURE	SECONDARY PRESSURE	PRESSURE GRADIENT
1 PLANT HEAT UP	0.0	0	0	0
	300.0	2250	1020	1230
2 PLANT COOLDOWN	0.0	2250	1020	1230
	300.0	0	0	0
3 PLANT LOADING	0.0	2250	1020	1230
	1200.0	2250	850	1400
4 PLANT UNLOADING	0.0	2250	850	1400
	1200.0	2250	1020	1230
5 SMALL STEP LOAD INCREASE	0.0	2250	850	1400
	25.0	2320	962	1358
	150.0	2125	886	1239
6 SMALL STEP LOAD DECREASE	0.0	2250	850	1400
	25.0	2190	746	1444
	180.0	2310	798	1512
7 LARGE STEP LOAD DECREASE	0.0	2250	850	1400
	60.0	2350	1180	1170
	540.0	1975	1106	869
	1200.0	2200	1089	1111
8 LOSS OF LOAD	0.0	2250	850	1400
	10.0	2600	1228	1372
	100.0	1630	1228	402
9 LOSS OF POWER	0.0	2250	850	1400
	10.0	2070	1238	832
10 LOSS OF FLOW	0.0	2250	850	1400
	140.0	1875	1047	828
11 REACTOR TRIP	0.0	2250	850	1400
	100.0	1870	1106	764
12 FEEDWATER CYCLING	0.0	2250	1020	1230
	540.0	2250	811	1439
13 PRIMARY HYDROTEST	---	3106	0	3106
14 SECONDARY HYDROTEST	---	0	1356	-1356

PRESSURES HAVE UNITS OF PSI
TIME HAS UNITS OF SECONDS

TABLE 4.4-3
TRANSIENT TEMPERATURES

TRANSIENT	TIME	PLATE TEMP	HOT LEG TUBE TEMP	CLD LEG TUBE TEMP
1 PLANT HEAT UP	0.0	70	70	70
	300.0	547	547	547
2 PLANT COOLDOWN	0.0	547	547	547
	300.0	70	70	70
3 PLANT LOADING	0.0	547	547	547
	1200.0	525	568	548
4 PLANT UNLOADING	0.0	525	568	548
	1200.0	547	547	547
5 SMALL STEP LOAD INCREASE	0.0	525	568	548
	25.0	540	579	560
	150.0	530	570	549
6 SMALL STEP LOAD DECREASE	0.0	525	568	548
	50.0	510	558	536
	180.0	518	567	544
7 LARGE STEP LOAD DECREASE	0.0	525	568	548
	60.0	565	590	572
	540.0	547	556	548
	1200.0	555	543	540
8 LOSS OF LOAD	0.0	525	568	548
	10.0	570	593	574
	100.0	570	560	555
9 LOSS OF POWER	0.0	525	568	548
	10.0	571	578	545
10 LOSS OF FLOW	0.0	525	568	548
	45.0	550	523	523
11 REACTOR TRIP	0.0	525	568	548
	100.0	557	544	542
12 FEEDWATER CYCLING	0.0	547	547	547
	540.0	520	534	534
13 PRIMARY HYDROTEST	---	70	70	70
14 SECONDARY HYDROTEST	---	70	70	70

TEMPERATURES ARE IN DEGREES FAHRENHEIT
TIME HAS UNITS OF SECONDS

TABLE 4.4-4
DIFFERENTIAL AXIAL EXPANSIONS

TRANSIENT	TIME	DL DUE TO PRESSURE	DL DUE TO TEMP	TOTAL DL
1 PLANT HEAT UP	0.0 300.0			a, b, c
2 PLANT COOLDOWN	0.0 300.0			
3 PLANT LOADING	0.0 1200.0			
4 PLANT UNLOADING	0.0 1200.0			
5 SMALL STEP LOAD INCREASE	0.0 25.0 150.0			
6 SMALL STEP LOAD DECREASE	0.0 50.0 180.0			
7 LARGE STEP LOAD DECREASE	0.0 60.0 540.0 1200.0			
8 LOSS OF LOAD	0.0 10.0 100.0			
9 LOSS OF POWER	0.0 10.0			
10 LOSS OF FLOW	0.0 45.0			
11 REACTOR TRIP	0.0 100.0			
12 FEEDWATER CYCLING	0.0 540.0			
13 PRIMARY HYDROTEST	---			
14 SECONDARY HYDROTEST	---			

INTERFERENCES ARE IN MILS
TIME HAS UNITS OF SECONDS

TABLE 4.4-5
DIFFERENTIAL RADIAL EXPANSIONS

TRANSIENT	TIME	DIFFERENTIAL EXPANSION TSP 7	DIFFERENTIAL EXPANSION TSP 1-6
1 PLANT HEAT UP	0.0 300.0	[]	[]
2 PLANT COOLDOWN	0.0 300.0		
3 PLANT LOADING	0.0 1200.0		
4 PLANT UNLOADING	0.0 1200.0		
5 SMALL STEP LOAD INCREASE	0.0 25.0 150.0		
6 SMALL STEP LOAD DECREASE	0.0 50.0 180.0		
7 LARGE STEP LOAD DECREASE	0.0 60.0 540.0 1200.0		
8 LOSS OF LOAD	0.0 10.0 100.0		
9 LOSS OF POWER	0.0 10.0		
10 LOSS OF FLOW	0.0 45.0		
11 REACTOR TRIP	0.0 100.0		
12 FEEDWATER CYCLING	0.0 540.0		
13 PRIMARY HYDROTEST	---		
14 SECONDARY HYDROTEST	---		

EXPANSIONS HAVE UNITS OF MILS
TIME HAS UNITS OF SECONDS

TABLE 4.4-7
SUMMARY OF UMBRELLA CONDITIONS
INSIDE SURFACE

CASE NO	TRANSIENT	CYCLES	SIG 1-2	SIG 2-3	SIG 3-1
1	PLANT HEAT UP	200			
2					
5	PLANT LOADING	18300			
6					
8	PLANT UNLOADING	18300			
12	SMALL STEP LOAD INCREASE	2000			
15	SMALL STEP LOAD DECREASE	2000			
19	LARGE STEP LOAD DECREASE	200			
22	LOSS OF LOAD	80			
24	LOSS OF POWER	40			
26	LOSS OF FLOW	80			
26	REACTOR TRIP	400			
29	FEEDWATER CYCLING	18300			
30					
31	PRIMARY HYDRO	5			

A.C

STRESSES HAVE UNITS OF PSI
TIME HAS UNITS OF SECONDS

TABLE 4.4-8
SUMMARY OF UMBRELLA STRESSES
OUTSIDE SURFACE

CASE NO	TRANSIENT	CYCLES	SIG 1-2	SIG 2-3	SIG 3-1
1	PLANT HEAT UP	200	}	}	}
2					
5	PLANT LOADING	18300			
6					
8	PLANT UNLOADING	18300			
12	SMALL STEP LOAD INCREASE	2000			
15	SMALL STEP LOAD DECREASE	2000			
19	LARGE STEP LOAD DECREASE	200			
22	LOSS OF LOAD	30			
24	LOSS OF POWER	40			
26	LOSS OF FLOW	80			
28	REACTOR TRIP	400			
29	FEEDWATER CYCLING	18300			
30					
31	PRIMARY HYDRO	5			

STRESSES HAVE UNITS OF PSI
TIME HAS UNITS OF SECONDS

TABLE 4.4-9
SUMMARY OF FATIGUE USAGES
SPEAR EXPANSION ZONES

INSIDE SURFACE

LOAD COND	Sr	Sa	K x Sa	n	N	n / N
1 - 15						
15 - 28						
15 - 26						
15 - 22						
15 - 24						
15 - 19						
31						
15 - 8						
5 - 6 - 8						
29 - 30						
10 - 12						

OUTSIDE SURFACE

LOAD COND	Sr	Sa	K x Sa	n	N	n / N
1 - 15						
15 - 28						
15 - 26						
15 - 22						
15 - 24						
15 - 19						
31						
15 - 8						
5 - 6 - 8						
29 - 30						
10 - 12						

YOUNG'S MODULUS RATIO = $26.0 / 29.0 = 0.897$
 CONCENTRATION FACTOR TO ACCOUNT FOR LOCAL EFFECTS = 2.0
 COMBINED FACTOR "K" = $0.897 \times 2.0 = 1.794$

TABLE 4.4-10
SUMMARY OF UMBRELLA CONDITIONS
THREADED JOINTS
EXTERNAL THREADS

CASE NO	TRANSIENT	CYCLES	SIG 1-2	SIG 2-3	SIG 3-1
1	PLANT HEAT UP	200			
2					
5	PLANT LOADING	18300			
6					
8	PLANT UNLOADING	18300			
12	SMALL STEP LOAD INCREASE	2000			
15	SMALL STEP LOAD DECREASE	2000			
19	LARGE STEP LOAD DECREASE	200			
22	LOSS OF LOAD	80			
24	LOSS OF POWER	40			
26	LOSS OF FLOW	80			
28	REACTOR TRIP	400			
29	FEEDWATER CYCLING	18300			
30					
31	PRIMARY HYDRO	5			

STRESSES HAVE UNITS OF PSI

TABLE 4.4-11
 FATIGUE CALCULATION SUMMARY
 SPEAR THREADED JOINTS

LOAD COND	Sr	Sa	K x Sa	n	N	n / N	A, C
1 - 15							
15 - 28							
15 - 26							
15 - 22							
15 - 24							
15 - 19							
31							
15 - 8							
5 - 6 - 8							
29 - 30							
10 - 12							

YOUNG'S MODULUS RATIO = 26.0 / 29.0 = 0.897

a, b, c

FIGURE 4.4-1

NORTH ANNA No.1 STEAM GENERATOR "C" TUBE R9C51
U-BEND TUBE REMNANT SPEAR STABILIZER
HYDRAULIC EXPANSION UPPER JOINT/ROLL EXPANDED LOWER JOINT



FIGURE 4.4-2

NORTH ANNA No.1 STEAM GENERATOR "C" TUBE RSCS1
U-BEND TUBE REMNANT SPEAR STABILIZER
THREADED JOINT BETWEEN SEGMENTS

a,b,c

FIGURE 4.4-3
NORTH ANNA No.1 STEAMGENERATOR 'C'
TUBE R9C51 HDT LEG CABLE STABILIZER

a, b, c

FIGURE 4.4-4 SEGMENTED SPEAR / TUBE REMNANT BEAM MODEL

a,b,c

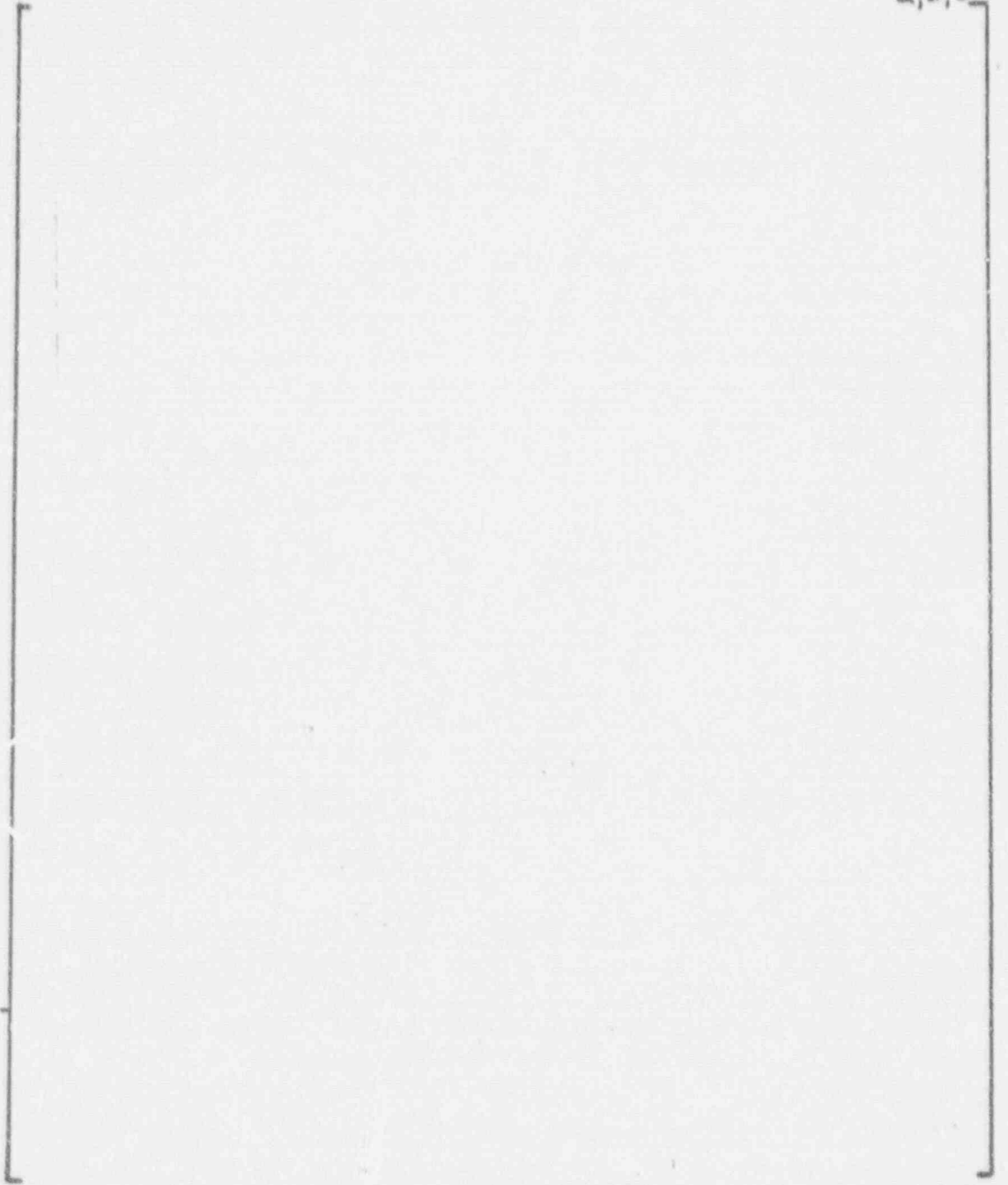


FIGURE 4.4-5 SPEAR EXPANSION ZONE MODEL
MAXIMUM TUBE SUPPORT PLATE HOLE

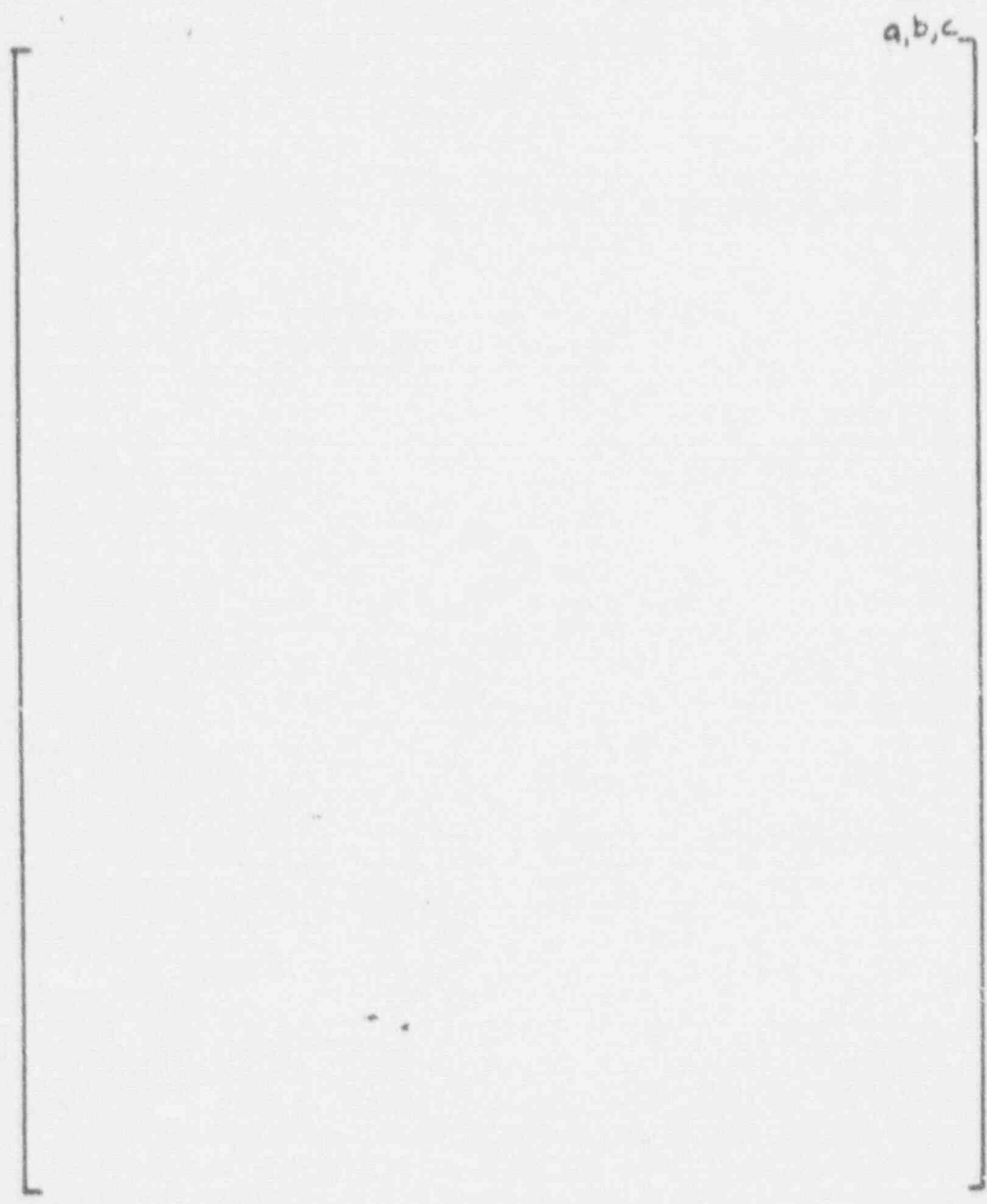


FIGURE 4.4-6 SPEAR EXPANSION ZONE MODI
TOP TUBE SUPPORT PLATE HOL

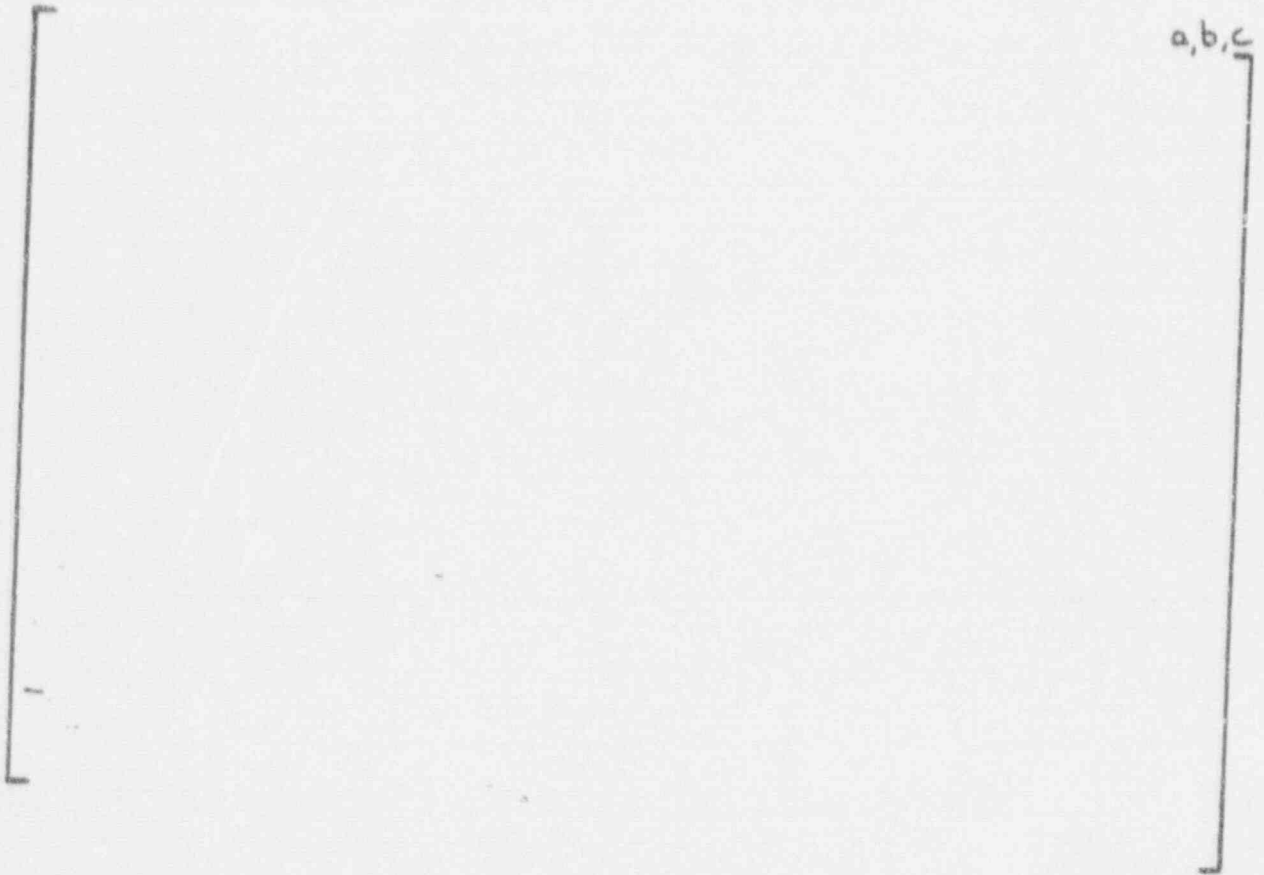


FIGURE 4.4-7 THREADED JOINT PULL-CUT FORCE TEST RESULTS

4.5 DOWNCOMER FLOW RESISTANCE PLATE (DFRP)

The DFRP assemblies comprise an annular, perforated plate located near the top of the downcomer annulus, between the wrapper and shell of the steam generator, as shown on Figure 4.5-1. Its function is to provide a hydraulic impedance to the recirculating coolant flow in the steam generator, thereby providing one of the hydraulic parameters used to establish the circulation ratio (CR). The purpose of this section of this report is to describe the design and analysis of the DFRP; the evaluation of the influence of the CR, and hence fluid velocities, on tube vibration is described elsewhere in this report.

4.5.1 DESIGN DESCRIPTION

The DFRP consists of a series of perforated plate assemblies, as shown on Figure 4.5-2. The assembly includes a []^{A.C.} perforated plate with two []^{A.C.} gusset plates welded thereto. The assembly comprises a nominal []^{A.C.} sector of the annulus, hence []^{A.C.} plates are to be installed in each generator. The size of the plate assemblies is compatible with installation through a 16 inch manway. The location of the DFRP in the steam generator, shown on Figure 4.5-3, is above the conical section of the wrapper and below the primary separator barrel.

The DFRP assemblies installation will position the plates snug against the wrapper (and its adjacent plate) while assuring a gap at the shell ID through the use of a removable gage. Installation will be performed by a crew of trained and qualified specialists. The major considerations during installation are fit-up of the assemblies to design requirements and loose parts management.

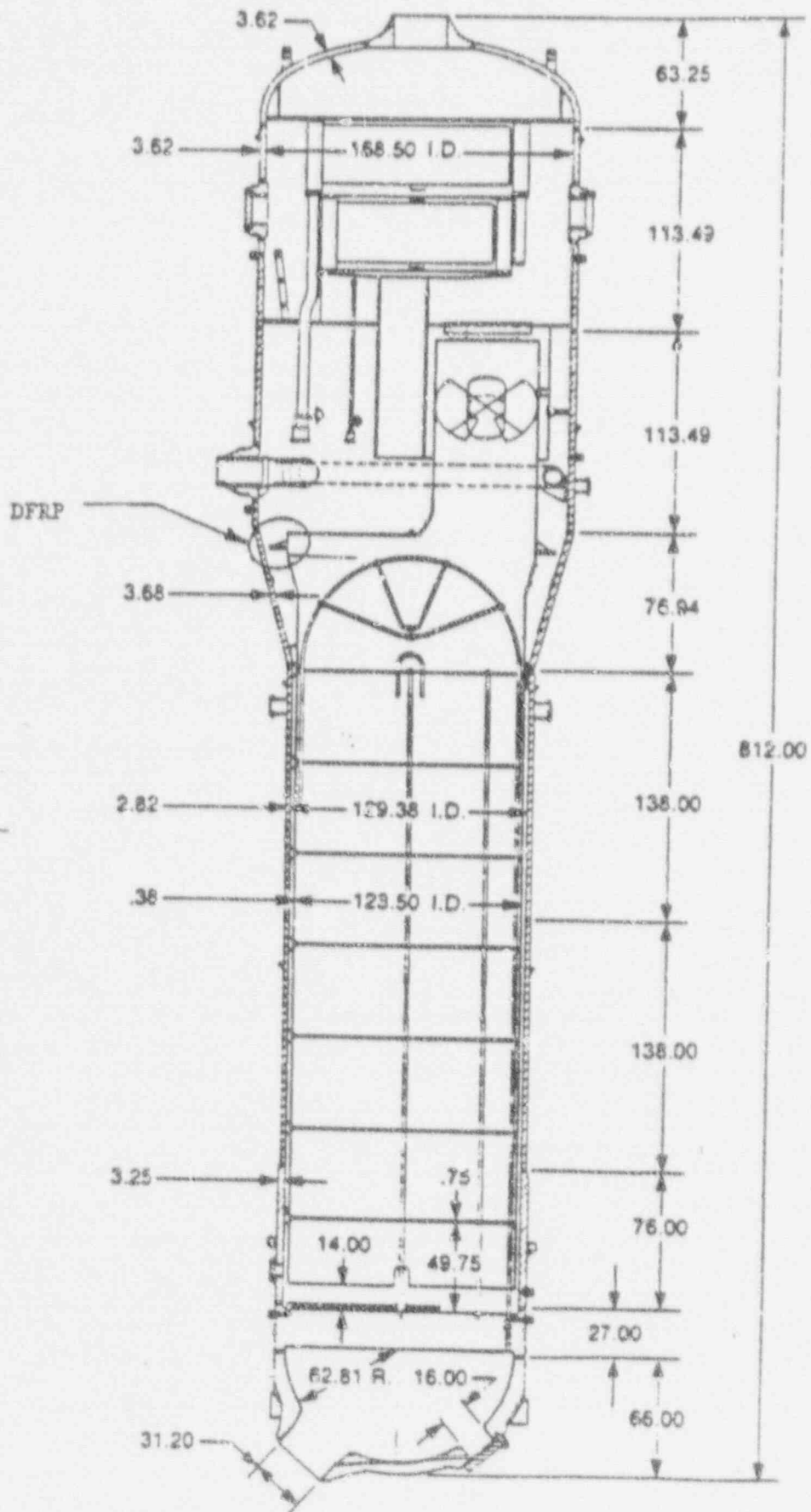


FIGURE 4.5-1



DOWNCOMER FLOW RESISTANCE PLATE

FIGURE 4.5-2

a, b, c

4.5.2 PERFORMANCE ANALYSIS

The objective of installing the downcomer flow resistance plate (DFRP) is to reduce the circulation ratio and thereby reduce the total secondary flow through the tube bundle. This in turn results in lowering the secondary side velocity in the U-bend region. The DFRP provides additional flow resistance in the circulation path. Since the driving force (gravity of water in the downcomer) remains unchanged, the circulation ratio is reduced.

4.5.2.1 Basis for Sizing

The sizing of the DFRP is based on first determining a target circulation ratio from tube vibration and other considerations and then calculating the plate geometry that will provide the flow resistance required to yield the circulation ratio.

In order to reduce the fluidelastic stability ratio significantly, it was decided that the circulation ratio should be reduced to below 3. The 51 Series steam generators in other operating plants currently have circulation ratios of 2.9. It was decided not to reduce circulation ratio too far below this value so as to stay within the operating experience of similar steam generators with respect to tube bundle void fraction, flow regime, etc. This yielded a target circulation ratio value of 2.9.

Having defined a target circulation ratio, it was relatively straight forward to determine the plate geometry needed to provide the flow resistance that will result in this circulation ratio. Given the location of the DFRP in the downcomer, flow area through the plate is the key geometric parameter that controls its flow resistance. The Westinghouse proprietary computer code GENF was used in the analysis to predict the circulation ratio. This verified code calculates the circulation ratio, steam pressure, fluid mass and other steady state operating characteristics of a feeding type steam generator. The effects of a DFRP on circulation ratio has been verified in field instrumented steam generators. This data has been used to confirm the calculational code.

4.5.3.5 Conclusions

Based on the results of this analysis the following conclusions can be drawn concerning the structural capability of the downcomer resistance plate assembly.

1. The fatigue usage for the gusset / wrapper weld is less than the ASME Code guideline.
2. The maximum stresses for the gusset / wrapper weld are less than the ASME Code guidelines.
3. The cooling capability of the steam generator is not impaired following a steamline break accident.
4. The wrapper support blocks meet appropriate limits for the steamline break accident.

Overall, the downcomer resistance ring is structurally acceptable for its intended mode of operation.

4.5.3 DFRP STRUCTURAL ANALYSIS

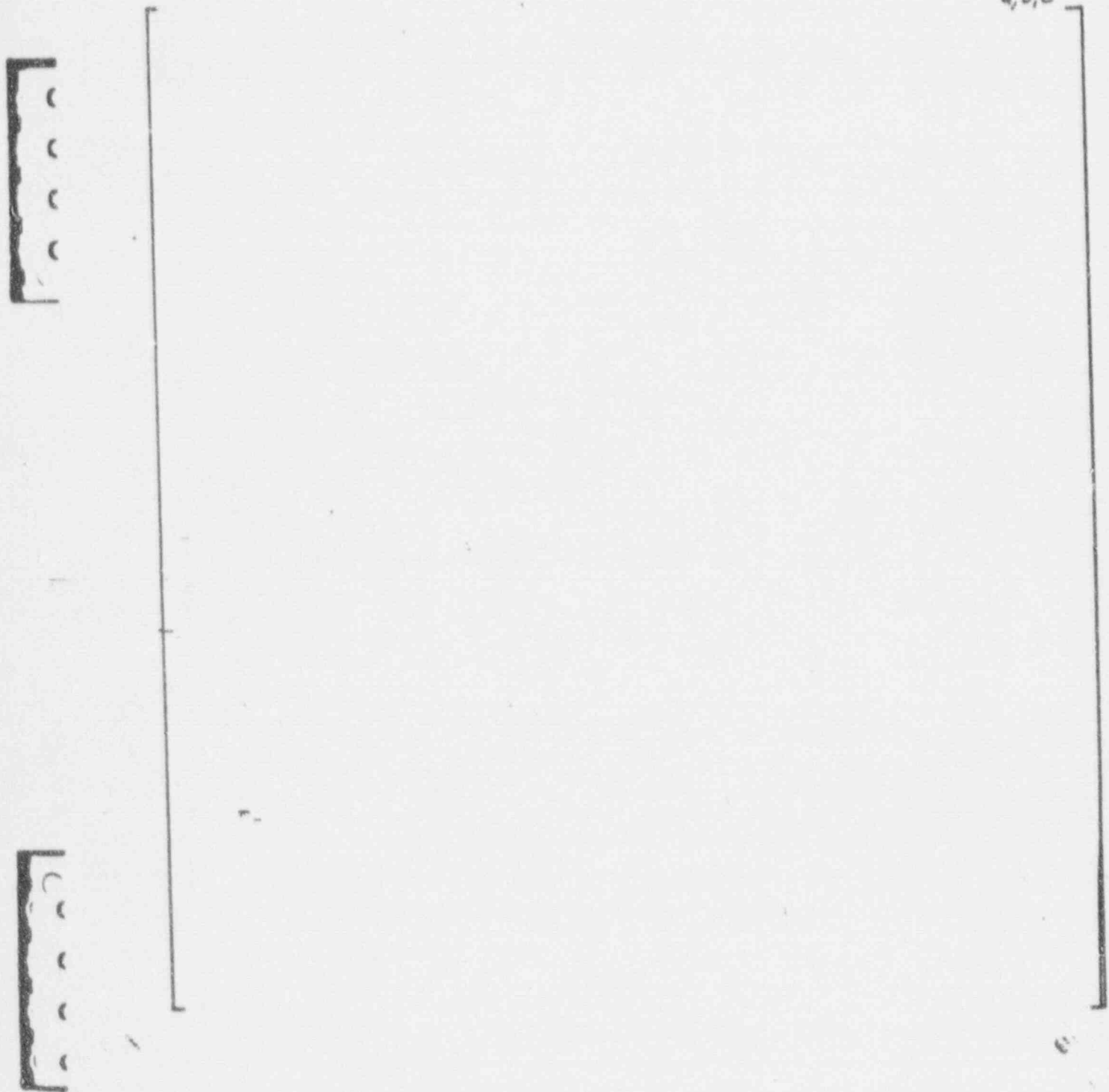
4.5.3.1 Introduction

The purpose of this analysis is to verify the structural adequacy of the downcomer ring assembly. The analysis considers fatigue loadings due to operating transients and pressure loadings from the steamline break analysis. Pressure loads during normal operation are not significant. The transients considered during the fatigue analysis include the Feedwater Cycling Transient and a De-Pressurization Transient which umbrellas those conditions which involve injection of cold auxiliary flow. A prior analysis of the shell girth weld has established that other normal, upset, and test conditions do not result in any significant fluctuations in the adjacent downcomer fluid or in the saturation temperature. The pressure drop across the resistance plate resulting from the steam line break loading is 60 psi.

The downcomer ring assembly and wrapper are non-pressure boundary components and are not subject to the criteria of the ASME Code. Where appropriate, however, Section III, Subsection NG, of the ASME Code has been used as a guide in establishing fatigue and stress limits.

4.5.3.2 Analysis Procedure

The analysis is performed using a combination of analysis tools. In considering the thermal transient analysis, the predominant loading mechanism is the relative temperature response of the various component parts, rather than a thermal shock concern which occurs for thicker members. Therefore, it is sufficient to determine the general average temperature response of the various component parts, the wrapper, gusset, and resistance plate. To establish the average temperature response of each component part, a one-dimensional heat transfer / thermal stress program is used.



DOWNCOMER RING FINITE ELEMENT SHELL MODEL

FIGURE 4.5.3-1

a, b, c

FEEDWATER CYCLING FLUID TEMPERATURES

FIGURE 4.5.3-2

2
7
3

abc

DE-PRESSURIZATION TRANSIENT FLUID TEMPERATURES

FIGURE 4.5.3-3

RTT



FEEDWATER CYCLING TRANSIENT RESPONSE
COMPARATIVE TEMPERATURE RESPONSE

FIGURE 4.5.3-4

a, b, c

DE-PRESSURIZATION TRANSIENT RESPONSE
COMPARATIVE TEMPERATURE RESPONSE

FIGURE 4.5.3-5

4.5.4 DOWNCOMER FLOW RESISTANCE PLATES SAFETY EVALUATION

4.5.4.1 Introduction

This evaluation is written to address the safety effects of the installation of flow resistance plate assemblies into the North Anna Unit 1 steam generators. The flow resistance plate assembly consists of segments of perforated plate positioned in the downcomer annulus between the tube bundle wrapper and the steam generator shell. The plate segments are supported by brackets welded to the wrapper. The resistance plate assembly adds a resistance in the flow path of the water flowing down the downcomer. The added resistance will reduce the circulation ratio and therefore the mass flow through the tube bundle.

The reduction in mass flow through the tube bundle is intended to reduce the potential for fluid elastic instability of the tubes in the U-bend portion of the tube bundle.

4.5.4.2 Evaluation

The original design of the Series 51 steam generators used at North Anna Unit 1 included a downcomer flow resistance plate. This plate was subsequently removed to increase the flow through the tube bundle. The increased tube bundle flow increases the crossflow into the bundle at the bottom of the wrapper and across the tubesheet. This increased crossflow was considered desirable to reduce the area of the tubesheet exposed to low velocity with the potential for sludge deposition.

Sludge accumulation currently does not have the level of concern as was the case at the time of the removal of the original downcomer flow resistance plates. The change in water chemistry from phosphate chemistry to all volatile treatment (AVT) has generally resulted in a sludge form

more mobile and less likely to become cemented together and has resulted in a smaller volume of sludge. Improved tubesheet cleaning methods, more frequent tubesheet cleaning, and increased attention to generation of corrosion product in the secondary system have typically resulted in operation of steam generators with a smaller inventory of sludge.

The potentially detrimental effect of sludge accumulation is the increased potential for corrosion of the tubes due to local superheat on the tube surface, chemical hideout, and concentration of chemical species in the sludge pile. This effect is not as likely in AVT type sludge as compared to phosphate type sludge.

Sludge deposition is an operational issue not a safety issue. The corrosion form typically associated with concentration of chemical species in the sludge does not result in a condition which changes the leak before break characteristics of the tube. That is, typical corrosion of the tube that could result in through wall degradation would result in leakage in excess of technical specification limits before the corrosion would reduce the structural integrity of the tube to less than what is required to resist postulated steamline break loads. The plant Technical Specifications require that the unit be shut down and leaking steam generator tubes be plugged before the leakage limit is exceeded. Existing analyses bound tube degradation up to a postulated tube rupture. Also, the normal eddy current inspection of the tubes would be expected to detect an unexpected increase in the corrosion rate due to increased sludge deposition.

A stress evaluation of the design of the resistance plate modification shows that stress levels in the plate segments, brackets, wrapper, and wrapper supports will not exceed appropriate limits for normal, and postulated accident conditions. For the most severe faulted load (steamline break) the resistance plate assembly and the wrapper near the welds of the bracket to the wrapper would be permanently deformed; but the

functional integrity of the wrapper and the attachment welds would be maintained. The downcomer flow resistance plate assembly is a non-pressure boundary component and is not subject to the criteria of the ASME Boiler and Pressure Vessel Code. Where appropriate the ASME Code, Section III, Subsection NG was used as a guide in establishing stress limits. The load on the plate is due to hydraulic forces resulting from the flow of water or steam through the resistance plate. The installation of the downcomer flow resistance plate assembly will not increase the loads on any other portion of the steam generator for normal and postulated accident condition loadings in excess of the original design loadings. The original design loadings included the effect of a similar downcomer flow resistance plate. The presence of the resistance plate alters slightly the structural load split among steam generator internals due to hydraulic forces in the steam line break analysis. This is bounded by previous analyses. A fatigue evaluation for the most critical location in the assembly results in a fatigue usage of less than 1. Therefore, the design is acceptable for design basis transients.

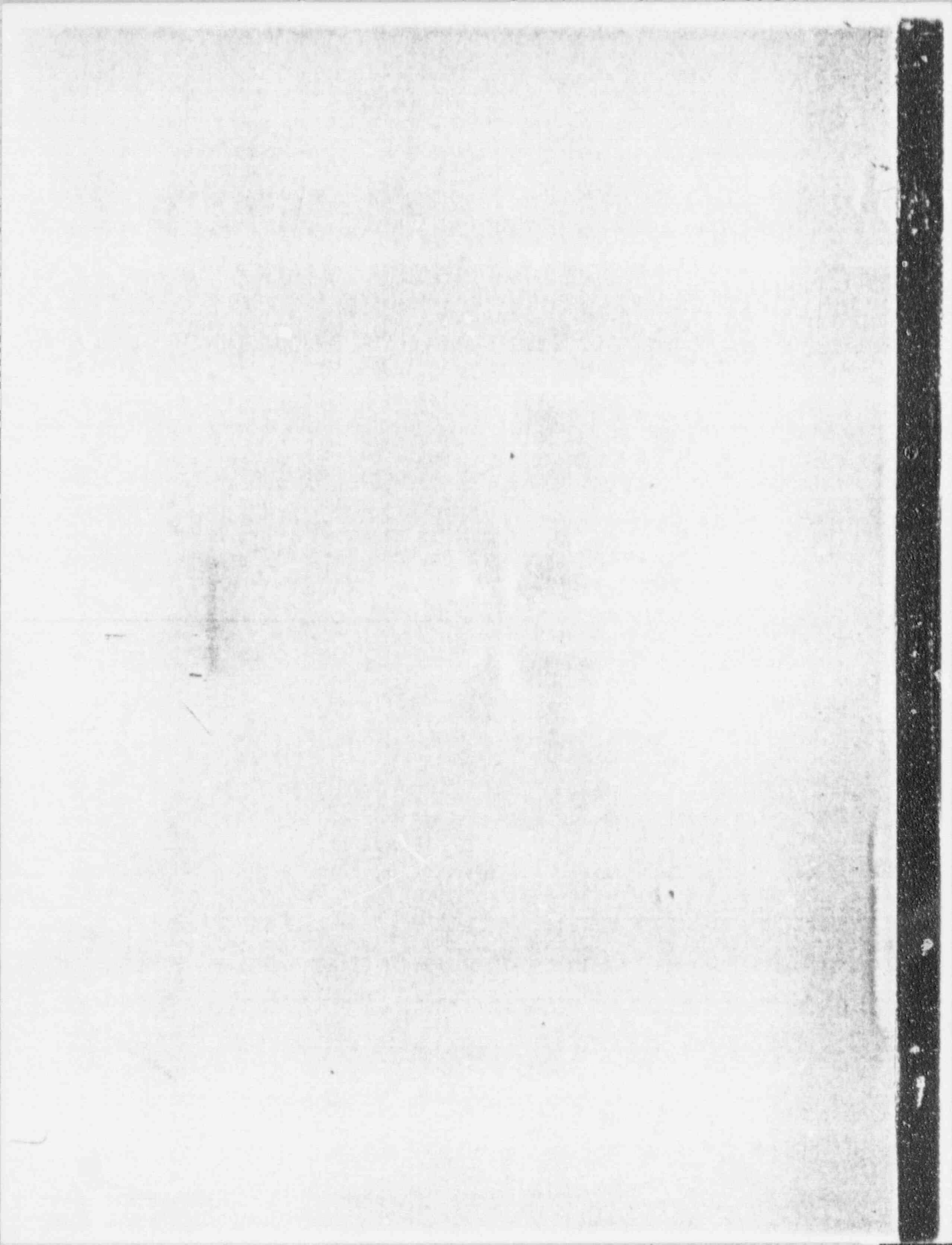
The purpose of the modification is to reduce the potential tube vibration due to fluid-elastic excitation. An evaluation of the fluid elastic stability of the tubes not supported by the anti-vibration bars (AVB'S) has shown that the reduction in flow will result in improved stability of the tubes to fluid elastic excitation in the U-bend region of the tube bundle. An evaluation of the steam generator hydraulics has shown that the installation of the resistance plate assembly will result in a significant reduction in the circulation ratio and mass flow through the tube bundle.

The relationship between the reduced flow area at the downcomer flow resistance plate and the circulation ratio was determined by a thermal-hydraulic analysis. The flow area includes the holes in the plate segments, the gap between the plate and the shell, the gap between subassemblies, and the gap between the plate and the wrapper. The

4.5.4.3 Conclusion

This evaluation has been written to consider the safety effects of installation of a downcomer flow resistance plate assembly into the steam generators of North Anna Unit 1. The installation of this modification is expected to improve the fluid elastic stability of tubes not supported by AVB's. This modification will reduce the circulation ratio which will result in a slightly larger low velocity area on the tubesheet with the potential for sludge deposition, however this is not expected to increase the potential for tube degradation. A stress evaluation has determined that stress levels will not exceed appropriate limits for normal and postulated accident conditions. The downcomer flow resistance plate assembly and the wrapper are Non-Nuclear Safety class components. Failure of either the resistance plate assembly or the wrapper at the attachment welds would not degrade the steam generator heat transfer capability below that required to safely cooldown the plant. The effect of the modification on the circulation ratio and the water inventory is not expected to change setpoints determined by previous analyses or to alter the response of the measurement instrumentation. The design of the modification includes provisions to minimize the potential for loose parts and occupational radiation exposure.

Therefore, the installation of the downcomer flow resistance plate assembly will not result in a previously unanalyzed accident or increase the probability of a previously analyzed accident. The margin of safety which, in part, is provided by the safety factors included in the ASME Code is not reduced. Based on the information outlined above, installation of downcomer flow resistance plate assemblies in the steam generators at North Anna Unit 1 will not result in an unreviewed safety question as defined in the criteria of 10CFR 50.59.



Sept. 1977

NONPROPRIETARY SAFETY EVALUATION

BY THE OFFICE OF NUCLEAR REACTOR REGULATION

NORTH ANNA POWER STATION, UNIT 1

DOCKET NO. 50-338

0/52

~~5912160396~~
1154P

SAFETY EVALUATION BY THE OFFICE OF NUCLEAR REACTOR REGULATION

FACILITY OPERATING LICENSE NO. NPF-4
VIRGINIA ELECTRIC AND POWER COMPANY
OLD DOMINION ELECTRIC COOPERATIVE
NORTH ANNA POWER STATION, UNIT NO. 1
DOCKET NO. 50-338

1 INTRODUCTION

On Wednesday, July 15, 1987, Unit 1 of the North Anna Power Station experienced a tube rupture in steam generator C, of tube R9-C51 at the top of the seventh support plate in the cold leg. This incident occurred after the reactor had returned to 100% power following the Spring 1987 refueling outage. The operators at the plant were able to bring the reactor to a cold shutdown mode without further damage to the plant or any significant radiation release to the environment.

By letters dated September 15, 1987 and September 25, 1987 (References 1 and 3), Virginia Electric and Power Company (the licensee) provided the document, "North Anna Unit 1 July 15, 1987 Steam Generator Tube Rupture Event Report" (Reference 2) describing its plan of action for returning the plant to full power operation. Also provided for our review was the Westinghouse Electric Corp. Report, "North Anna 1 S/G Tube Rupture and Remedial Actions Technical Evaluation" (Reference 4).

This Safety Evaluation (SE) presents the staff's evaluation of the adequacy of the licensee's identification of the major causal factors leading to this event and the adequacy of diagnostic and corrective measures implemented by the licensee to prevent a similar failure in the future. The staff's review was assisted by expert consultants from Oak Ridge National Laboratory in the field of eddy current testing; from Argonne National Laboratory in the field of flow-induced vibration; and from the Massachusetts Institute of Technology in the field of fatigue and fracture.

Section 2 of this SE provides a brief background of steam generator experience at North Anna prior to the rupture of tube R9-C51. The extensive steam generator (SG) inspection program conducted subsequent to the rupture event is discussed in Section 3. Section 4 details the comprehensive investigations and analyses conducted to establish the root causes of the rupture. Corrective actions implemented by the licensee to prevent a recurrence of the failure mechanism are discussed in Section 5. Staff findings and conclusions pertaining to the adequacy of the licensee's program to identify causes of the rupture event and of the diagnostic and corrective measures taken to prevent a recurrence of the event are presented in Sections 6 and 7, respectively.

2 SG EXPERIENCE PRIOR TO THE TUBE RUPTURE

The North Anna SGs are Westinghouse Model 51. These generators have 3388 tubes, each with an outside diameter of 0.875 inch and a wall thickness of 0.050 inch. The tubing material is Inconel 600 in the mill annealed condition. The tube support plates are carbon steel with drilled tube holes.

Since initial plant startup in 1978, North Anna Unit 1 has utilized an All Volatile Treatment (AVT) control of the secondary water chemistry. The unit experienced an inadvertent intrusion of powdex resin into the SGs during the first operating cycle. During the intrusion event, the resin decomposed to form sulfuric acid, resulting in reduced pH and increased cation activity.

A corrosion phenomenon known as "denting" was first observed at North Anna Unit 1 during the first refueling outage in 1979. "Denting" refers to the squeezing of tubes at tube-to-support plate intersections caused by a buildup of an iron oxide corrosion product (called magnetite) in the annulus between the tube and support plate as a result of corrosion of the carbon steel support plates.

A boric acid treatment was commenced in 1980 with the intention of arresting the progression of denting. From the time it was first observed in 1979, denting at North Anna 1 has been considered to be relatively minor in terms of the amount of diameter reduction induced at the tube to support plate intersections

(compared to what has been observed at other plants). In addition, eddy current inspections indicate that the progression of denting has been arrested since at least 1984.

Tube deformation accompanying denting leads to high tensile stresses at the surface of the tube. The most usual consequence of these high tensile stresses is stress corrosion cracking (SCC). These cracks generally have an axial orientation. Although the progression of denting has been arrested since at least 1984, the potential for SCC has continued to exist, since the high tensile stresses associated with denting continue to be present. Since 1985, hundreds of tubes have been plugged as a result of eddy current indications and/or leaks resulting from SCC at dented locations.

Apart from SCC, there are other potential consequences of denting which are now believed (after extensive failure analyses) to have created the conditions necessary for the rupture of tube R9-C51. This is discussed in detail in Section 4.

In addition to denting and SCC associated with denting, North Anna has also experienced non-denting-related SCC in the small radius, inner row U-bends and in the tube expansion transition region at the top of the tubesheet. Like the denting-related SCC flaws, the non-denting-related SCC flaws have been observed at numerous other plants besides North Anna Unit 1. The U-bend SCC cracks are attributable to high residual stresses in the U-bends caused by the original tube bending process during fabrication. The cracks in the expansion transition region near the top of the tubesheet are the result of the high residual stresses associated with the abrupt change in tube diameter formed when the tubes were explosively expanded against the tubesheet during SG fabrication.

North Anna Unit 1 has also recently begun to experience wear degradation as a result of the tubes interacting against the antivibration bar (AVB) supports in the U-bend region of the tube bundle. To date, the wear degradation, as indicated by eddy current test results, has been well within the Technical Specification plugging limits.

Prior to the rupture event on July 15, 1987, the North Anna Unit 1 SGs had most recently been inspected during the Spring 1987 refueling outage. The plant did not restart from this outage until June 29, 1987, and did not reach 100% power until July 14, 1987, the day before the event.

The Spring 1987 inspection had included a 100% inspection of the population of unplugged tubes in each SG. As a minimum, all tubes were inspected from the hot leg tube end to the seventh (i.e., uppermost) support plate on the hot leg side. However, some tubes were inspected around the U-bends, including some tubes which were inspected over their full length. In SG C (which contained the tube which subsequently ruptured), 24% of the tubes were inspected around the U-bend to at least the seventh support plate on the cold leg side; 16% of the tubes in SG C were inspected over their full length. This inspection program exceeded minimum plant Technical Specification requirements.

Tube R9-C51 in S/G C, which subsequently ruptured, had been inspected from the hot leg end to the seventh support plate on the hot leg side during the Spring 1987 outage, but had not been inspected at the seventh support on the cold leg side where the rupture occurred. Indeed, a review of past records indicates that this particular location had not been inspected since 1980. As will be explained later in this report, the failure mechanism associated with the rupture involves rapid crack propagation (i.e., no more than a few days) from the point of initiation to rupture. It is not clear that even if the upper support plate location on the cold leg side had been inspected during the Spring 1987 outage, that a detectable indication would have been present.

A total of 263 tubes were plugged during the Spring 1987 outage. Most of these were the result of SCC indications at dented support plate indications. Numerous other tubes were plugged as a result of SCC indications at the expansion transition location of the tubes near the top of the tubesheet.

3 POST-EVENT INSPECTION PROGRAM

Subsequent to the rupture event, the identity of the ruptured tube (i.e., R9-C51) was determined by observing leakage from the filled secondary side into the

drained primary side. This was followed by an eddy current examination of the tube to identify the failure location. A fiber optic-video device was then inserted to permit visual examination of the failure location. The failure was observed to involve a complete (360°) circumferential fracture of the tube at the upper edge of the seventh (uppermost) support plate on the cold leg side.

A portion of the ruptured tube on the cold leg side up to and including the fracture surface was removed from the SG for detailed examination. The results of these examinations and the determination of the tube failure mechanism are described in Section 4 of this report. In parallel with the assessment of the failure mechanism, the licensee commenced a comprehensive eddy current inspection program of all three SGs as described in Section 3.1 below.

3.1 Eddy Current Inspection Scope and Methodology

The eddy current test (ECT) inspection program consisted of three major elements. First, all portions of tubes not inspected during the Spring 1987 outage were inspected with a bobbin coil probe (with coils coaxial to the tube), which is the industry standard. (As noted earlier, the fracture location on tube R9-C51 had not been inspected during the Spring 1987 outage). Second, all tubes were inspected to the seventh (uppermost) support plate on both the hot leg and cold leg sides using a "pancake array" (8 x 1) probe. This probe consists of an overlapping array of 8 independent pancake coils spring-loaded against the inner surface of the tube. This probe is more sensitive to circumferential flaws (such as those associated with the rupture) than the standard bobbin probe. Third, a rotating pancake coil (RPC) probe was used to confirm signals from the bobbin and 8 x 1 inspections. The RPC probe gives better resolution to small defects, but is more time-consuming to employ.

The ECT inspection program was conducted utilizing state-of-the-art multifrequency eddy current test technology, including the use of digital data acquisition and analysis techniques. A Westinghouse Intelligent Eddy Current Data Analysis System (IEDA) was used as an aid in flagging suspect bobbin coil indications, which were then dispositioned by data analysts. The data from each tube was independently reviewed by two different analysts. One analyst

used the Westinghouse IEDA system and the other analyst used the Zetec Digital Data Analysis System. All data analysts were certified at least Level II in accordance with American Society of Nondestructive Testing (ASNT) requirements. The analysts were given additional training by Westinghouse and required to pass a test that covers the specific data analysis used for the North Anna eddy current tests.

The ECT inspection program, including the scope of inspections, and the procedures, equipment, and techniques employed were reviewed as part of the NRC Augmented Inspection Team (AIT), which was dispatched to the North Anna site shortly after the event. The team included staff members from the NRC Office of Nuclear Reactor Regulation and an expert consultant on ECT from Oak Ridge National Laboratory. Detailed findings of the AIT investigation are documented in Reference 5. In summary, the AIT report concluded that the overall test program, the extent of the examinations, the execution of the program, and the data analysis techniques were acceptable.

In addition to the AIT effort, NRC Inspectors from Region II visited the plant on August 10, 1987 and again on August 31, 1987 to evaluate the licensee's ECT inspection and training procedures. Their findings were also favorable and are contained in Inspection Reports 50-338/87-28 (Reference 6) and 87-31 (Reference 7). On September 10, 1987, an NRR staff member and the staff's ECT consultant visited North Anna to conduct an audit of the data analysis performed on a selected set of tubes at the seventh support plate location. Based on the limited sample, the licensee's data analysis results for the upper support plate were confirmed to be adequate.

3.2 ECT Inspection Results

The North Anna plugging limit, as specified in the plant Technical Specifications, is 40% of the tube wall thickness. However, consistent with past experience, the presence of competing signals from dents and from tube expansion transitions generally precluded making accurate depth estimates for indications located at the support plates and near the top of the tubesheet. The licensee therefore plugged all tubes containing such non-quantifiable indications.

Table 1 summarizes the number of tubes plugged by indication type. All indications identified were either present in the April 1987 refueling outage with no discernible change present, or were located in previously uninspected portions of each SG. Additionally, a review of the data from the last outage using the current analysis rules revealed several tubes that now had a pluggable call placed on them. This apparent, though not actual, change in the SG condition was due to the change in the analysis rules and increased awareness by the analysts of North Anna specific ECT signals. A review and comparison of SG C hot leg data demonstrated that there was essentially no change in tube condition from the April 1987 refueling outage to July 1987 (when the event occurred). Finally, there were no indications of a circumferential nature found at any tube support plate locations, including the seventh tube support plates.

In addition to tubes found to contain eddy current indications, other tubes were plugged for preventive reasons as indicated in Table 1. This "preventive plugging" activity is discussed in Sections 5.2 and 5.3.

4 FAILURE ANALYSIS

A detailed failure analysis program was conducted by Westinghouse to identify the causal factors leading to the tube rupture event and to provide a basis for determining the corrective actions necessary to prevent a recurrence of this event. As part of this program, a portion of the failed tube extending from the fracture surface to the tube end on the cold leg side was removed from the SG for detailed laboratory examination. Section 4.1 below provides a description of these examinations which indicate that the fracture occurred as a result of fatigue. The alternating stress level leading to fatigue crack initiation was determined on the basis of observed fatigue striation spacings on the fracture surface and is discussed in Section 4.2. Section 4.3 discusses the fatigue strength properties of Inconel 600 tubes in an AVT water environment. Section 4.4 provides an assessment of the potential loading mechanisms which could have led to fatigue crack initiation and propagation. As discussed in Section 4.4, a flow-induced vibration mechanism involving a fluidelastic instability is believed to have provided the driving

Table 1 Steam generator tubes plugged as result of SGTR event (by indication type)

S/G	Clear ¹ indications	Distorted ² indications	Tube ³ sheet indications	8x1 possible ⁴ indications	Preventively ⁵ plugged	Other ⁶	Total tubes plugged
A	0	6	6	11	80	2	105
B	0	3	5	12	12	1	33
C	2	2	20	11	58	19	112

¹Clear Indications (defective) - bobbin indications of greater than 40 percent "thru-wall" depth.

²Distorted Indications - bobbin indications of undetermined "thru-wall" depth at the tube support plates.

³Tubesheet Indications - bobbin indications of undetermined "thru-wall" depth at tubesheet.

⁴8x1 Possible Indications - indications identified by 8x1 probe.

⁵Tubes plugged as a preventative measure (see Sections 5.2 and 5.3).

⁶Tubes with broken probes or which would not pass 8x1 probe - includes failed tube.

force for initiating and propagating the fatigue crack. Section 4.5 discusses various factors which are believed to have contributed to the flow instability. Based on the above, Section 4.6 provides an overall summary of the necessary conditions for causing a fatigue failure such as occurred for tube R9-C51.

4.1 Laboratory Examination of Failed Tube Specimen

4.1.1 Destructive and Non-destructive Testing

The straight section of the failed tube (R9-C51) between the fracture surface and the cold leg end was removed from SG C without causing significant elongation or distortion.

The results of mechanical testing and chemical analysis established that the tube had mechanical properties that met all applicable requirements (e.g., ASME Code) and otherwise displayed the expected characteristics of Alloy 600 in the mill-annealed condition. Radiography, consisting of double-wall radiographs taken at four rotations 90° apart and of a single-wall radiograph using a "rociisserie" technique, revealed no indications in the seventh support plate region other than the fracture at the top edge of the support plate location. Eddy current examinations were also conducted on the seventh support plate region using bobbin, 8 x 1, RPC, and outer diameter (OD) pencil probes. No indications were observed below the fracture face in the support plate region.

4.1.2 Visual and Macroscopic Examinations

With reference to Figure 1 (taken from Reference 4), which summarizes the fractographic observations schematically, the 45° location corresponds to the plane of the U-bend. Multiple fracture initiation "origins" occurred between approximately 90° and 180°. The tubing between 90° and 180° is determined to have protruded approximately 0.07 inches above the top edge of the support plate. This location is the fracture region closest in elevation to the top edge of the support plate. The highest elevation of the fracture is located at 315° and is approximately 0.17 inches above the top edge of the support plate.

On the fracture face, a dark deposit was noted from approximately 90° to 150° . Typically, the deposit extends from the OD to 3/4 through-wall. An analysis of these deposits showed that they had a composition similar to adjacent OD deposits and that they contained elements which would be expected from secondary-side water-borne deposits. Fatigue cracks initiated in this location. The significance of these deposits is that they may show the shape of the early macro-crack before faster crack growth rates occurred which did not leave sufficient time for disposition of water-borne material. From the shape of the deposit, it is believed that the macro-crack initially broke through-wall over a 40° crack front that extended from 100° to 140° . Fatigue striation orientation data also support this hypothesis.

Oxidation and/or fretting was observed on most of the fracture surface but was most severe at about the 135° position. It was heavy throughout the region containing most of the crack origins and of diminishing severity at locations proceeding in the clockwise direction from about 170° and counter-clockwise from about 70° . This suggests that the oldest portion of the crack occurred at about the 135° position.

4.1.3 SEM and TEM Fracture Face Examination

A summary of fractographic features and striation spacing measurements is presented in Table 2 and in Figure 1, which also gives the estimates of cyclic stress levels that can be made from the striation spacing as described below. Replicas or "grids" of the fracture surface were examined in a transmission electron microscope (TEM). These TEM fractographic examinations were performed to provide the resolution needed to definitively determine if the striation-like markings observed during scanning electron microscope (SEM) fractography were indeed fatigue striations and to provide quantitative data pertaining to their spacing. The striations run perpendicular to the direction of local crack propagation. The striations develop as a consequence of repeated blunting and resharpening of the crack tip during the cyclic applications of load, so each striation marks the position of the crack tip at the time it was formed. The striation spacing provides a rough estimate of the crack growth rate per cycle.

Table 2 North Anna tube fracture-summary of striation spacing measurements and ΔK calculations

Grid	Distance from O.D. surface, in.	Average spacing μ -in.	Calculated* ΔK , ksi in.
A		6.04	29.2
B		3.39	21.5
C	0.014	1.00	11.7
	0.036	1.58	14.7
	0.046	1.85	15.9
E	0.24	1.60	14.8
	0.31	1.53	14.5
F		20.7	53.2

*The ΔK -values were calculated from striation spacing measurements using: $S = 6 (\Delta K/E)^2$. (Bates and Clark⁽⁷⁾ Correlation).

Bates and Clark (Reference 8), among others, have shown a correlation between the striation spacing and the cyclic stress intensity factor range (ΔK). Assuming that the overall vibrational loading of the tube is not significantly changed by the development and early growth of small fatigue cracks, then ΔK levels indicated from striation spacings can be used to estimate the cyclic stress range that led to fatigue crack initiation.

Scanning electron microscope (SEM) and transmission electro. microscope (TEM) fractographic examinations of the fracture surface confirmed the conclusions of the optical-microscopic examinations that the crack origins were located on the outside surface. A number of "origins" were identified from fracture surface markings (tear ridges) and contours on the outside surface, with four principal initiation sites found at approximately 110°, 120°, 135° and 150°. Fine fatigue striations were observed near the crack origins. Striation spacing increased from about 1.0 micro-in. near the OD surface to nearly 2.0 micro-in. near the inner diameter (ID) surface.

The region from about 90° to 155° is generally flat (orientation: normal to wall) throughout except for small portions that have shear orientations (45° to wall) adjacent to the OD and ID surfaces, with a fine fracture texture. Most

S = striation spacing

$S = 1.5/1.6 \mu \text{ in.}$

↖ indicates origin

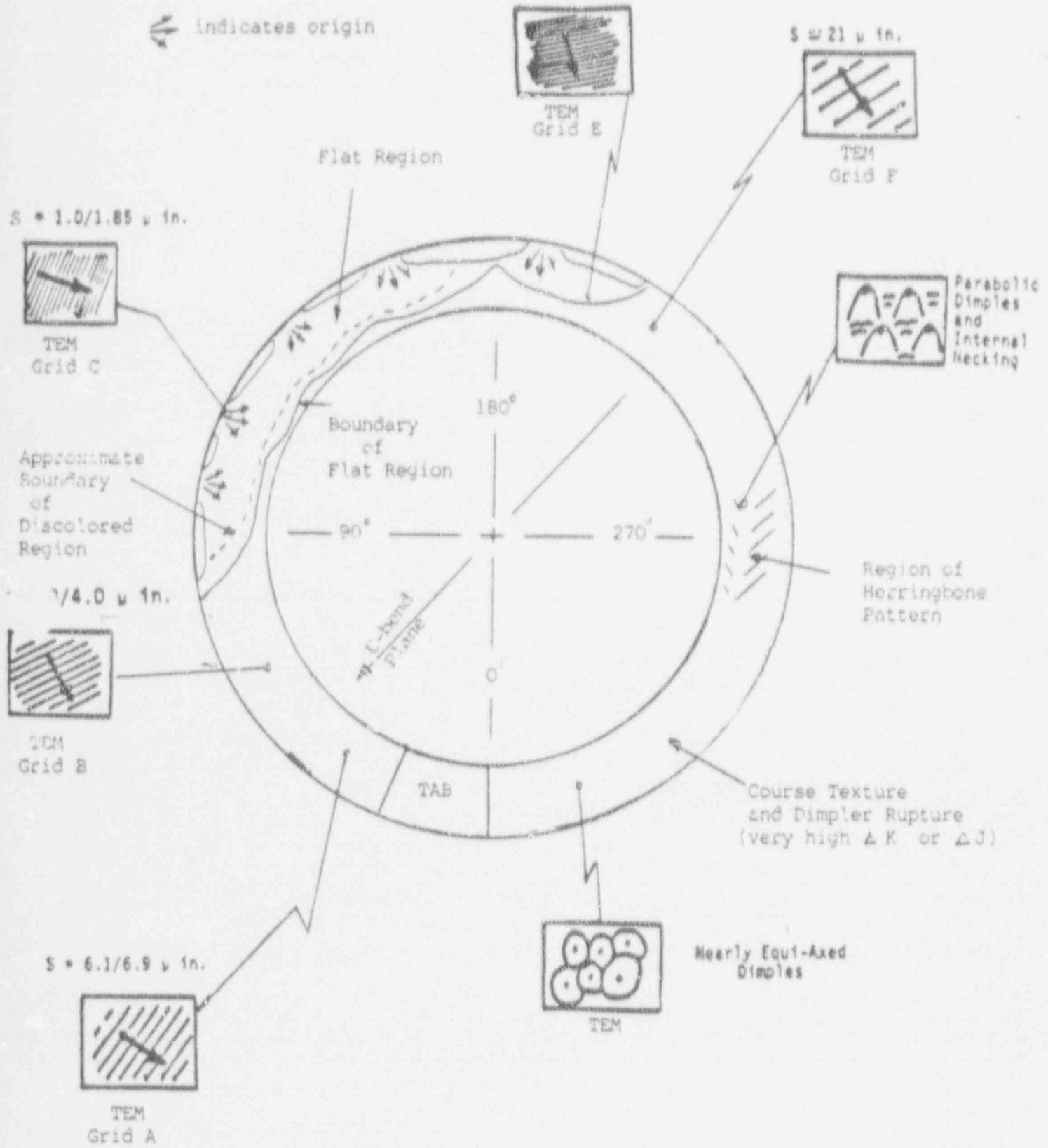


Figure 1 - Approximate mapping of fracture surface of tube R9-C51, S/G c

of the remainder of the fracture is oriented at about 45° to the wall surface except for a flat area surrounding a minor crack origin at about the 190° location. Clockwise from 180° , an initially fine texture becomes rougher with a "herringbone" pattern evident near the 270° region, indicating an accelerating rate of crack propagation.

Fine-to-coarse fatigue striations occur at locations from about 190° to 250° and from about 30° to 70° . The fatigue striation spacing increased (indicating higher propagation rates) as the crack propagated around the circumference of the tube in a clockwise direction from about the 190° position and counter-clockwise from about the 70° position. Higher propagation rates in the 190° to 300° positions than in the 70° to 15° regions indicates eccentric loading or a component of torsional loading.

Parabolic dimples with internal necking between dimples were the predominant fractographic features at about the 270° position. These features are indicative of very high fatigue propagation rates. This position is within the regions of herringbone pattern and coarse texture observed during visual examinations.

Within the region from about 280° clockwise 360° to 15° , there is a rough texture (fractographic examination revealed dimpled rupture in this region) indicative of overload fracture. Equiaxed dimples indicative of the overload portion of the fracture were observed at about the 310° position. These fractographic features coupled with the macroscopic features, indicate that the overload fracture occurred throughout the region defined above.

The tab-shaped area near region marked 0° has a rough fracture texture and orientation consistent with a final overload fracture.

4.1.4 Metallography of Seventh Support Plate Region

A series of longitudinal metallographic sections were made at the fracture location. Minor OD intergranular penetrations, as well as minor ID intergranular penetrations, were found in isolated, small zones within the support plate crevice region. The penetrations were typically 0.3 mils deep and approached a maximum depth of 1.0 mil. The closest distance to the fracture face, in which

an intergranular penetration approached the fracture face, was 4 mils. Although there was no direct evidence that intergranular penetrations were present at the exact fatigue initiation sites, Westinghouse notes that there remains the possibility that this could have occurred. However, Westinghouse concludes that this possibility does not change the observed data which supports fatigue as the mechanism for crack initiation and propagation.

4.2 Fatigue Crack Initiation Stress

Westinghouse estimates that an alternating stress amplitude of 4 to 10 ksi was necessary for crack initiation. Among the evidence cited by Westinghouse in support of this estimate was the following:

- (1) Use of a single-edge crack model indicates an alternating stress of 6.3 ksi for a crack penetrating 50% through-wall and assuming a ΔK of 13 ksi $\sqrt{\text{in.}}$ (see Table 2) and an R ratio (i.e., $K_{\text{min}}/K_{\text{max}}$) of 0.5 (Reference 4).
- (2) A cyclic fatigue test of a tube specimen was conducted at a known stress amplitude. Based on a comparison of the striation spacings between the test specimen and the fracture surface of tube R9-C51, an alternating stress of 8 ksi was estimated for R9-C51 (Reference 9).
- (3) Based on the observed striation spacings and use of the stress intensity expression taken from Section 33.2 of the Tada, Paris, Irwin handbook, the alternating stress level is estimated to have been about 5 to 7 ksi at the time the crack penetrated entirely through-wall and had begun to propagate around the tube circumference (Reference 4).

With respect to item 1 above, a Westinghouse representative indicated during a phone conversation with an NRC staff consultant that 4 ksi was judged to be a reasonable lower bound alternating stress to account for potential uncertainties in the use of the single-edge crack model and the assumed R ratio. With respect to item 3 above, the Westinghouse representative stated that 10 ksi was the

maximum possible value of alternating stress consistent with the $\Delta k = 53 \text{ ksi} \sqrt{\text{in.}}$ estimate shown in Table 2 (assumed to be located 90° relative to the point of crack initiation) without resulting in a physically impossible stress history during crack propagation (Reference 10).

4.3 Fatigue Strength

"S/N curves" are curves relating the magnitude of alternating stress to the number of alternating stress cycles necessary to initiate a fatigue crack. The S/N curves used by Westinghouse to evaluate conditions for crack initiation were taken from data in []. This data is based on fully reversed loading. As will be discussed in additional detail later in this report, a flow-induced, tube vibration mechanism is believed to be the driving mechanism for both fatigue crack initiation and crack propagation. The natural frequency of the row 9 tube U-bends is about []. Assuming that the fatigue crack initiated over a period ranging between 1 year and the 9 year lifetime of the plant to date, then the number of loading cycles leading to fatigue failure (assuming a plant availability factor of 75%) was between 1.4×10^9 cycles and 1.3×10^{10} cycles. The corresponding fatigue strengths are estimated by the staff to be 27 ksi and 22 ksi, utilizing a best fit S/N curve from the data in Reference 10 and 21 ksi and 16 ksi, respectively, when a 3 standard deviation (3σ) lower bound S/N curve is used. These fatigue strength estimates exceed the 4 to 10 ksi alternating stress believed by Westinghouse to have caused fatigue crack initiation (see Section 4.2), but do not include an adjustment for mean stress at the fracture location induced by denting of the tube at the seventh support plate.

The mean stress at the fracture location was evaluated by Westinghouse with an elastic-plastic finite element analysis utilizing an axisymmetric model. The assumed denting deflection profile from the bottom of the seventh support plate to the top was based on profilometry measurements conducted on the fractured tube and other adjacent tubes. The fractured tube had a maximum radial displacement of 2.5 mils. Steady-state pressure and thermal loadings were also

included in the model. The results of the analysis revealed a tensile mean stress level at the tube OD at the yield strength level.

The [] was used to make the mean stress adjustment to the S/N curves derived from the EPRI data. []

]

Table 3 provides a summary of alternating stress levels associated with assumed fatigue crack initiation over a 1 year and 9 year period, respectively, for a best fit, 2σ , and 3σ S/N curve incorporating the mean stress adjustment.

Table 3 Alternating Stress Levels Leading to Fatigue Crack Initiation

	1.4x10 ⁹ cycles (1 year)	1.3x10 ¹⁰ cycles (9 years)
Best fit S/N Curve	13.3 Ksi*	9.2 Ksi*
2 σ S/N Curve	10.5 Ksi	7 Ksi
3 σ S/N Curve	8.7 Ksi	5.6 Ksi

*These estimates were made by the NRC staff.

The tabulated stresses associated with fatigue crack initiation over a 9 year period are consistent with the Westinghouse-estimated range of 4 to 10 ksi required for crack initiation. The tabulated stresses associated with crack initiation over a 1 year period exceed this range if best fit or 2σ S/N properties are assumed. Thus, if best fit or 2σ S/N properties are assumed, then the cyclic loadings leading to crack initiation must have occurred during a period exceeding 1 year.

4.4 Potential Loading Mechanisms Leading to Fatigue Crack Initiation and Failure

It is evident from the observed striations on the R9-C51 fracture surface that at least 10^5 load cycles were required to propagate the crack to failure subsequent to crack initiation. Based on primary-to-secondary leak rates prior to the rupture event, it appears that the crack propagated rapidly to failure over just a few days. Potential loading mechanisms for crack initiation and/or propagation considered by Westinghouse are described below.

4.4.1 Duty Cycles Associated With Normal, Upset, and Test Conditions

Applicable duty cycles for normal, upset, and plant test conditions considered by Westinghouse were taken from the North Anna SG design specifications. Examples of the types of duty cycles considered include plant heatups and cooldowns, various plant loading transients, feedwater transients, reactor trips, steam line breaks, and plant hydrostatic tests. The various duty cycles included contributions from differential pressure loadings across the tube walls, interference loads from differential radial expansion between the tube and support plate, and through-wall thermal gradients in the tube.

These duty cycles were analyzed using an axisymmetric finite element model of the tube. Alternating stress levels ranged from [

] The total number of stress cycles, however, is estimated to be less than 40,000 cycles for the entire 40 year lifetime of the plant. Thus, the plant duty cycles were found to contribute very little to fatigue usage (i.e., usage factor = 0.04 over 40 year plant lifetime), and are not believed to have played a significant role in initiating or propagating the crack.

4.4.2 Flow-Induced Vibration

Potential flow induced vibration mechanisms considered by Westinghouse included vortex shedding, cross-flow turbulence, and fluid-elastic instability.

[

]

The Westinghouse analysis of linear turbulence and fluidelastic excitation of the tubing was conducted with a computer program called FLOVIB. FLOVIB incorporates a finite element model of the tube and tube support system and evaluates the dynamic response of the tube based on models for modal vibration amplitude in the turbulent and fluidelastic regimes.

-[

]

The above-mentioned model for evaluating tube response from the turbulence mechanism has reportedly been qualified against several series of tests, including prototypical two-phase tests. Turbulence-induced vibration amplitudes for tube RS-C51 are predicted to be on the order of less than [] at the tube apex. This order of amplitude would cause maximum stresses in the top of the uppermost support plate (where the rupture occurred) with peak-to-peak amplitudes of less than 1000 psi. Based on these low stress levels, Westinghouse believes it to be highly improbable that the turbulence mechanism is primarily responsible for the North Anna tube rupture.

The fluidelastic mechanism will have a significant effect on the tube response in cases where the fluidelastic stability ratio (SR) equals or exceeds 1.0. The stability ratio is defined as

$$SR = \frac{V_{eff}}{V_c}$$

where V_{eff} is the effective crossflow velocity and V_c is the critical velocity beyond which the displacement response increases rapidly.

The estimated stability ratio [] utilizing nominal estimates of parameters such as damping ratio, stability constant, and natural frequency is [] indicating no fluidelastic instability. As will be discussed later, these parameters are subject to significant uncertainties (particularly for damping ratio) such that depending on the actual values of the parameters, the stability ratio may substantially exceed 1.0.

Motions and corresponding stresses developed by a tube in the fluidelastically unstable mode are quite large in comparison to the other known mechanisms. For this reason, and because none of the other mechanisms discussed above appear to be a plausible mechanism for crack initiation, Westinghouse has concluded that the failed tube is most likely a result of its being fluidelastically unstable.

Given fluidelastic instability as the mechanism for fatigue crack initiation, the stability ratios for the failed tube can be inferred from []

]

To estimate the critical velocity and, hence, the stability ratios of the tube which failed, it is helpful to consider Figure 2. []

]

From experimental results, Westinghouse states that [

]

As can be seen from Figure 2, definition of points 1 and 2 and the slopes of the turbulence and fluidelastic response curves are sufficient to solve for V_c and thus for stability ratio (i.e., V_{oper}/V_c). On this basis, tube R9-C51 is estimated to have been operating (prior to crack initiation) at a stability ratio in the range of 1.22 (slope of 20) to 1.56 (slope of 10), assuming the tube to be vibrating with a displacement amplitude of 0.057 inches and a corresponding alternating stress level of 7 ksi.

It follows from Figure 2 that for a given reduction in stability ratio from SR_2 to SR_1 , the corresponding reduction in displacement (i.e., from D_2 to D_1) response and alternating stress can be expressed as follows:

[]

It can be seen from this equation that a small percentage reduction in stability ratio will lead to a much larger percentage reduction in displacement response and alternating stress. With a known reduction in alternating stress, the corresponding reduced value of fatigue usage factor can be estimated from the appropriate S/N curve.

It is useful for purposes of later discussion to tabulate reductions in alternating stress level and fatigue usage accumulation as a function of percentage

Figure 2

reduction in stability ratio. Tables 4 and 5 summarize these reductions for different S/N curve assumptions based on an assumed time to initiate a fatigue crack in R9-C51 of 1 year and 9 years, respectively. These reductions have been conservatively estimated assuming a slope of 10 for the fluidelastic response curve when the displacement response exceeds 40 mils, and a slope of 6 when the displacement response is less than 40 mils.

4.5 Causes of High Stability Ratios

As discussed in Section 4.4.2, the estimated stability ratio for tube R9-C51 is [] using nominal estimates of parameters such as stability constant, natural frequency, and damping ratio. Thus, the tube would have been expected to be stable with considerable margin. The following summarizes Westinghouse's assessment (Reference 4) of factors which may have caused the actual stability ratio to significantly exceed 1.

Average Flow Field, Stability Constant, and Natural Frequency Uncertainties

Westinghouse estimates that uncertainties in the average flow field, stability constant, and natural frequencies are essentially the same for units with dented or non-dented support plates. If these errors were large, Westinghouse believes that similar instabilities would be expected in the non-dented units with resulting wear at either the top support plate or inner row AVBs. Since such wear has not been observed in rows 8 to 10 in non-dented units, Westinghouse believes the potential uncertainties to be relatively small (about 15%) and, therefore, not a major contributor to the failure of R9-C51.

Local Flow Velocities

The eddy current test results revealed that the AVB supports generally extended as far as row 10, with most extending at least as far as row 9 and many as far as row 8. These non-uniform AVB penetrations are believed by Westinghouse to have channeled some of the flow to row 8 and row 9 tubes without adjacent AVB supports causing a "velocity peaking" effect for

Table 4 Alternating stress and fatigue usage sensitivity to stability ratio reductions (assuming 1.4×10^9 cycles to failure for R9-C51)

	S/N Curve Assumptions		
	Best Fit	2σ	3σ
Pre-mod alt. stress	13.3 ksi*	10.5 ksi	8.7 ksi
Post-mod alt. stress (10% reduction in SR)	NE	4.2 ksi	3.8 ksi
Additional accumulated usage factor over remaining 31 years of plant life	NE	0.20	0.52
Post-mod alt. stress (15% reduction in SR)	NE	3.0 ksi*	2.6 ksi*
Additional accumulated usage factor over remaining 31 years of plant life	NE	Negligible*	0.10*

*NRC staff estimates
 NE ~ Not estimated

Table 5 Alternating stress and fatigue usage sensitivity to stability ratio reductions (assuming 1.3×10^{10} cycles to failure for R9-C51)

	S/N Curve Assumptions		
	Best Fit	2 σ	3 σ
Pre-mod alt. stress	9.2 ksi*	7 ksi	5.6 ksi
Post-mod alt. stress (10% reduction in SR)	3.8 ksi*	3.2 ksi	2.8 ksi
Additional accumulated usage factor over remaining 31 years of plant life	Negligible*	0.06	0.10
Post-mod alt. stress (15% reduction in SR)	2.7 ksi*	2.3 ksi*	2.0 ksi*
Additional accumulated usage factor over remaining 31 years of plant life	Negligible*	Negligible*	Negligible*

*NRC staff estimates.

these tubes. Westinghouse has provided a preliminary estimate of a 15% velocity peaking factor for tube R9-C51 (Reference 4). However, a few row 8 to row 10 tubes were found to contain wall thinning indications (possibly wear from AVBs), which may have occurred as a result of fluid-elastic excitation. Some of these tubes were located in regions of relatively uniform AVB penetrations. Thus, Westinghouse concludes in Reference 3 that non-uniform AVBs and local flow effects are not the dominant factor for instability, although this effect at a 15% magnitude could have had a major contributing influence on the R9-C51 failure.

Tube Damping Uncertainties

Westinghouse concluded in Reference 3 that tube damping ratio uncertainties were the dominant factor affecting the stability ratio of the row 9 U-bends. Measurements of mechanical damping in air were performed using a U-bend shaker test facility. For [

] The measured mechanical damping was observed to increase substantially as the support conditions were gradually relaxed, reaching a value of 1.1% for preloaded, pinned-pinned supports typical of U-bend SG conditions without denting.

The above air tests do not consider the additional damping in a two-phase water/steam environment. Data cited by Westinghouse shows [

] However, Westinghouse concluded in Reference 4 that the effects of denting on tube

damping appear to be the major uncertainty factor leading to tube instabilities. Westinghouse estimates a 50% uncertainty factor associated with the assumed 0.82% damping ratio, which would contribute approximately 41% uncertainty to the nominal stability ratio estimate. Westinghouse further notes that an assumed lower bound damping ratio estimate of [] would double the nominal stability ratio estimate.

4.6 Required Conditions for Fatigue Cracking Initiation

Westinghouse has reached the following conclusions regarding the conditions necessary for fatigue crack initiation.

- (1) Denting at the top support plate is needed to (a) produce a high mean stress effect with an associated reduction in fatigue strength, (b) maximize bending stress at the upper support plate, and (c) minimize tube damping.
- (2) An absence of adjacent AVB supports is needed in order that tube displacements and, thus, alternating stress levels may be large enough to initiate a fatigue crack.
- (3) Stability ratios within 10% of that for tube R9-C51 (i.e., stability ratios \geq 90% of that for tube R9-C51) are needed since lower values are too small to initiate fatigue cracking.
- (4) Off-nominal conditions for fluid elastic vibrations are necessary including either or both of the following: (a) tube damping below test measurements [] approaching mechanical damping only [] and (b) locally high flow velocity regions.

5 CORRECTIVE ACTIONS AND COMPENSATORY MEASURES

The licensee has taken a two-fold approach to preclude future fatigue crack initiation; namely (1) installation of an SG downcomer flow resistance

plate as discussed in Section 5.1, and (2) implementation of preventive plugging of tubes with potentially high stability ratios as discussed in Section 5.2. Section 5.3 discusses actions taken to stabilize the remnant portion of tube R9-C51 (i.e., the ruptured tube) to ensure that it does not cause subsequent damage to adjacent tubes. Section 5.4 discusses the licensee's enhanced primary-to-secondary leak rate monitoring program which is intended to provide added assurance of SG tube integrity.

5.1 Downcomer Flow Resistance Plate (DFRP)

The DFRP is an annular, perforated plate located near the top of the downcomer annulus between the wrapper and shell of the SG. Installation of the DFRP will reduce the SG circulation ratio from 4.3 to 2.9 with an accompanying reduction in crossflow velocities and stability ratios for all tubes. As discussed in Section 4.6, low damping conditions are concluded by Westinghouse to be the primary contributor to fluid elastic instabilities. For tubes with low damping ratios, installation of the DFRP is calculated to produce between a 12% and 22% reduction in stability ratio, exceeding the 10% reduction objective set by Westinghouse. For tubes with nominal damping, an 8% reduction in stability ratio is estimated.

5.2 Preventive Plugging

Although installation of the DFRP is believed by Westinghouse to be a sufficient measure to preclude fatigue crack initiation in the future, preventive plugging of "susceptible" tubes in rows 9, 10, and 11 has been performed. A susceptible tube is one which is not supported by AVBs and is in a region of locally high flow velocities. All tubes above row 11 have AVB support. As discussed previously, many tubes down to row 8 are known from eddy current testing to be supported by AVBs. Tubes in row 8 and below, even if not supported by AVBs, have stability ratios at least 14% less than that of tube R9-C51 by virtue of their shorter span lengths (between supports) and associated higher natural frequency. Thus, tubes in rows 8 and below meet Westinghouse's 10% criterion (see Section 4.6), even without consideration of the additional reduction in stability ratio associated with the DFRP modification.

Based on the above, potentially susceptible tubes were considered by Westinghouse to be located in rows 9, 10, and 11. The detection of an AVB signal is considered by Westinghouse to be a firm indication of an AVB support on at least one side. Test data was presented demonstrating that the vibration amplitude for a given tube is controlled by the AVB exhibiting the minimum radial gap with respect to that tube. Thus, Westinghouse maintains that an AVB support on one side only will constitute a fully effective AVB support.

It is possible for eddy current testing to miss the presence of an effective AVB support due to background noise conditions such as from upper surface deposits. In some cases, however, the actual presence of an AVB support can be inferred from an AVB support detected for an adjacent tube. For example, it can reasonably be inferred from an AVB indication for a row 8 tube that the adjacent row 9 tube (in the same column) also has an AVB support, regardless of whether that tube exhibited a detectable AVB indication.

The plugging of all susceptible tubes in rows 9, 10, and 11 would have the effect of leaving tubes in row 8 as the tubes with the most limiting stability ratio. Therefore, this action by itself is estimated by Westinghouse to result in a 14% reduction in stability ratio relative to R9-C51. In addition, Westinghouse has estimated on the basis of a preliminary analysis of the local high flow velocity regions as affected by nonuniform AVB insertion that velocity peaking factors are lower for row 8 tubes than for the most limiting susceptible row 9 tubes. This effect is estimated by Westinghouse to produce an additional 6% reduction in stability ratio associated with the plugging of susceptible tubes in rows 9, 10, and 11.

The staff's review of the licensee's preventive plugging program identified two tubes in row 9 of SG A considered by the staff to be in the category of "susceptible tubes" (i.e., tubes R9-C38 and R9-C54), but which had not been preventively plugged. Neither of these tubes could be confirmed on the basis of the eddy current data to be supported by AVBs. In addition, the absence of AVB supports for these tubes could, in the staff's opinion, subject these tubes to locally high flow velocities due to channeling effects caused by nonuniform

AVB penetrations. At the staff's request, the licensee agreed to include these tubes in its preventive plugging program (Reference 7).

The staff also identified a concern to the licensee (during telephone conversations) that no criteria existed to ensure that an AVB signal represented an effective AVB support. The nominal radial clearance between the AVBs and adjacent tubes is about 10 mils. However, unless the AVB extends all the way down to at least the centerline of the tube, the tube will have additional freedom to displace laterally depending on exactly how far the AVB actually penetrates. Thus, a concern existed that AVBs may be sufficiently close to the tube to produce a detectable eddy current signal, but not be effective in limiting tube displacements to less than the estimated 0.032 to 0.080 inch range associated with fatigue crack initiation and failure of tube R9-C51.

In response to the staff's concern, the licensee reviewed the eddy current tapes for all row 9 tubes for which the adjacent row 8 tubes exhibited no detectable AVB indication. (In cases where row 8 tubes exhibited an AVB signal, it can be reasonably inferred that at least one AVB penetrates below the centerline of the adjacent row 9 tube, thus ensuring a fully effective AVB support). The presence of two discrete AVB signals (on the hot and cold leg side of the apex) was interpreted by the licensee to be indicative of at least one AVB intersecting the tube U-bend below the tube centerline at the apex, thus ensuring a fully effective (i.e., fully penetrated) AVB support. However, the review of the eddy current tapes for the subject tube revealed 41 tubes not exhibiting the two discrete AVB signals. In the absence of criteria for evaluating the acceptability of AVB indications for these tubes, the licensee conservatively elected to expand the preventive plugging program to include these 41 tubes.

Preventive plugging of susceptible tubes has been accomplished using a "sentinel plug" on the cold leg side and a standard mechanical plug on the hot leg side. The sentinel plug contains a hole to permit internal pressurization of the tube and low level primary-to-secondary leakage in the event that a through-wall crack develops in the tube. The hole is sized to permit detectable leakage in excess of the administratively imposed limit of 100 gallons per day

(gpd), but well under the 500 gpd Technical Specification limit. This plug is intended to serve as an early warning detection method of a circumferential break of the plugged tube prior to its potential interaction with adjacent tubes.

5.3 Stabilization of Severed Tube, R9-C51

After removing the cold leg section of tubing from the SG (see Section 4), only the hot leg remnant of the tube including the U-bend portion remained in the SG. Thermal-hydraulic analysis of the flow conditions surrounding tube R9-C51 indicated that the severed tube U-bend would be fluid elastically unstable during power operation. Once unstable, the remnant section could then impact neighboring tubes and over time cause wear on the neighboring tubes. Therefore, a stabilization technique was developed to secure the tube remnant from the cold leg side. Specifically, a threaded assembly (jointed spear) was designed and manufactured for insertion into the cold leg tubesheet and support plate hole. The assembly featured the following: (1) eight threaded sections, each assembled and inserted into the bare hole, (2) a locking feature to preclude separation of the threaded sections, (3) hydraulic expansions at each tube support plate and into the free end of remnant tube R9-C51, and (4) a roll expansion attachment of the spear to the tubesheet.

The design of the jointed spear components was verified by a combination of physical tests and computer analysis. These tests included torque and bending tests on the spear to remnant tube joint and axial separation (pull) tests and cyclic loading tests on both the threaded joint and on the spear to remnant joint. Analyses were performed to quantify the tube/spear vibrational characteristics. These analyses demonstrated that the critical components (threaded joints and spear to remnant joint) would withstand the design bases operational and transient-induced forces. Additionally, due to the small gap between the seventh support plate and the spear, damping would be higher and therefore reduce the loadings and susceptibility of the spear to a fatigue failure.

A full-scale mockup of tube R9-C51 was made at Westinghouse to ensure that the installation of the jointed spear on the cold leg side could be performed successfully.

Installation of the jointed spear was to be accomplished as follows:

[

]

As a preventive measure, it was determined to stabilize the hot leg portion of the remnant tube. Stabilization of the hot leg was to be performed by using a flexible [] cable with [

[] The stabilizer is then inserted into the remnant tube and extends over three inches above the top of the hot leg seventh support plate and slightly into the U-bend. [

]

No specific verification analyses were performed for the hot leg stabilizer to be used at North Anna Unit 1, since this type of design has been previously tested, qualified, and used by Westinghouse at other facilities.

After completing the installation process described above, the spear was then eddy-current tested to confirm the existence and proper positioning of the expansions.

The method of stabilization was modified from the above description to account for difficulties encountered during installation.

When the spear described above was expanded into the seventh tube support plate on the cold leg side, the expanding tool was slightly out of position and ruptured the spear wall over a length of about 1/2 inch. The crack was axial in nature and occurred near the top of the seventh tube support plate. Fracture and thermal-hydraulic analyses were conducted and it was then determined to install a sleeve inside the spear spanning the distance from the tube remnant to the seventh tube support plate. This sleeve was approximately 13 inches in length and extended from about 3 inches inside the tube remnant to about 9 inches below the seventh tube support plate. The bare hole in the tube sheet (cold leg) was sealed with a welded plug.

During installation of the cable stabilizer on the hot leg side, one of the cable sections was damaged when the stabilizer jammed on the base plate of the insertion tool. The damaged stabilizer was removed, the base plate was modified, and a second stabilizer, identical to the first, was then successfully installed. The cable stabilizer extends from the hot leg tube sheet to approximately 30° past the tangent point at the hot leg U-bend. The hot leg tube end was then sealed with a mechanical plug.

Finally, 12 adjacent tubes around tube R9-C51 were preventively plugged with sentinel plugs on the cold leg side. On the hot leg side, tube R9-C51 was plugged with a solid mechanical plug.

5.4 Leak-Before-Break Considerations

Prior to the failure of tube R9-C51 on July 15, 1987, the control room operators had no indication on the instrumentation normally used to detect primary-to-secondary leakage. However, a post-event analysis of air ejector radiation monitor count rate data and air ejector grab sample data did reveal indications of leakage prior to the event (Reference 4). These data were subject to some error because of the manner in which they were obtained, and the licensee has noted (in the context of discussion of the air ejector radiation monitor data) that the data should not be used to quantify a specific leak rate at a given point in time. However, these data give a positive indication that leakage was present for at least 48 hours prior to the event and that it was trending upward.

The licensee has taken a number of actions to ensure that similar precursor leakage in the future will be detected and monitored such that the plant will be shut down before a gross rupture of the tube can occur. These actions include:

- (1) primary-to-secondary leakage will be estimated every 4 hours using the air ejector radiation monitor, S/G blowdown monitor, and N-16 monitor; every 8 hours using the air ejector exhaust isotopic activity; and every 24 hours based on secondary coolant isotopic activity. The alarm setpoint for the air ejector monitor will be adjusted to respond if leakage increases and stays 10 to 20 gpd above the most recent leakage measurement.
- (2) N-16 monitors are being installed to provide a diverse indicator of primary-to-secondary leakage. The N-16 monitor will have a continuous readout (in gallons per day) in the control room and three pre-set alarms. The first alarm (S1) will be set consistent with the air ejector radiation monitor alarm above. The second alarm (S2) will be set at 60 gpd in order to detect the initial crack propagation associated with a fatigue failure. The third alarm (SE) will be set at the administratively imposed shutdown limit of 100 gpd.

As part of North Anna Power Station Standing Order #155 (Revision 1), dated October 9, 1987, the licensee has set the following administrative limits on primary-to-secondary leakage.

- a) 100 gpd per SG, 300 gpd total for all SGs. (This is substantially more conservative than the 500 gpd limit per SG and the 1 gallon per minute (gpm) (about 1430 gpd) limit for total primary-to-secondary leakage (i.e., for all SGs) in the Technical Specifications).
- b) 60 gpd increase during any 4 hour surveillance period (applies to leakage from each SG and total leakage from all SGs).
- c) An increasing trend based on the latest surveillance indicating that leakage will exceed 100 gpd within 90 minutes.

If any of the above limits are exceeded, then power will be reduced to less than 50% within 90 minutes. Analysis by the licensee indicates that this should be sufficient to cause further crack propagation to cease. In addition, the plant must be brought to a hot shutdown condition within 6 hours if the limits in items b) or c) above have been exceeded.

Analyses have been conducted by Westinghouse and the licensee to demonstrate that the 100 gpd administrative limit provides adequate assurance that crack propagation will be terminated and that the plant will be shut down before rupture occurs. Leakage rate versus time curves have been calculated on the basis of predicted crack growth rates and Westinghouse test data concerning leak rates as a function of crack arc-length. These curves vary as a function of alternating stress.

From the leak rate versus time curves, the licensee estimates that a 333 gpd limit would provide the approximately 90 minute period needed to identify excessive leakage and to reduce power to 50%, assuming an alternating stress level of 7 ksi, prior to rupture of the tube. Post-modification alternating stress levels, even assuming only a 10% reduction in stability ratio, are predicted to be less than 7 ksi. The 333 gpd limit would also allow for a $\pm 50\%$ error band

associated with the N-16 monitor reading, whereas the licensee estimates the actual error band to be between $\pm 10\%$ and $\pm 30\%$. Thus, the licensee concludes the 100 gpd administrative limit to be conservative.

Detailed procedures have been written for logging and trending data in accordance with the time schedules indicated above and for responding to the various alarms (S1, S2, and SE). Activation of the S1, S2, or SE alarms will cause the operator to be referred to the administrative limits in Standing Order 155. The staff notes that (in the event of an S1 or S2 alarm) this would include a new trending analysis to ensure that the 100 gpd administrative limits would not be exceeded over the next 90-minute period.

NRR staff representatives reviewed these procedures and witnessed (from the control room) implementation of the leak rate surveillance procedures for a typical 4-hour surveillance interval. This included the logging of the leak rate data provided directly and continuously by the N-16 monitor, the logging of count rate data from the air ejector and SG radiation monitors and calculation of corresponding leakage rates, and checking the setpoints of the various alarms. Trending plots were generated by computer. Based on its review, the staff concludes the leak rate surveillance schedules and procedures will be effective for purposes of early detection of low level primary-to-secondary leakage which could be a precursor to an impending fatigue failure. The administrative leak rate limits provide added assurance that the plant will be shut down in a timely fashion before a leaking through-wall crack can propagate to failure.

5.5 SG DFRP Installation and Resulting Increase in SGTR Accident Dose Rate

By letter dated September 25, 1987, the licensee provided an SE to assess the impact of the DFRP modifications on the North Anna Unit 1 and Unit 2 (NA-1&2) Updated Final Safety Analysis Report (UFSAR) Chapter 15 accident analyses. With the exception of the SGTR event, all accidents or events were not impacted because the limiting conditions or assumptions used in the analyses were unchanged by the modifications or the conclusions as stated in the NA-1&2 UFSAR and were within the guidelines of 10 CFR Part 100.

The one accident reanalyzed with a resulting increase in the consequences from those presented in the UFSAR was the SGTR accident for power levels in excess of 59 percent of rated thermal power. While the SG modifications are expected to have an insignificant impact on the overall thermal/hydraulic response of the plant, the offsite dose calculations were reperformed. This was done for two reasons: (1) calculations had demonstrated that, with the revised SG inventory, the secondary-side water level could drop below the top of the tubes for the first few minutes following a reactor trip for power levels in excess of about 59% of rated thermal power, and (2) the licensee's experience with the July 1987 NA-1 SGTR event had shown that the tube break location can be as high as the seventh support plate in the tube bundle.

The implication of the post-trip tube uncover for the SGTR is that the assumed conservative iodine partition factor (PF) could increase above the value used in the UFSAR analysis for power levels in excess of 59%. The present NA-1&2 UFSAR analysis uses a PF of 0.01 throughout the entire 30 minute interval of assumed releases from the faulted SG. This effectively assumes that the tubes remain covered with fluid. The licensee performed a conservative calculation to quantify the duration of post-trip tube uncover associated with the reduced initial mass in the modified SGs and concluded that this period could last up to 9 minutes. The offsite dose reanalysis assumed that the tubes were uncovered for the first 10 minutes of the event, with an associated PF of 1.0. Thereafter, the tubes were assumed to be covered with a resulting PF of 0.01.

Three cases were analyzed by the licensee: Case 1 included the revised assumptions concerning SG tube uncover, initial mass and Reactor Coolant System (RCS) break flow, but assumed RCS activity equivalent to 1% failed fuel. This is the same as the existing NA-1&2 UFSAR analysis, with the addition of including the SG DFRP modifications. Case 2 (the most limiting case) assumed that RCS and SG secondary-side activities equal the values set forth in the NA-1&2 Technical Specifications (TS), and includes the effects of a pre-accident iodine spike. Case 3 is the same as Case 2, except with an iodine spike concurrent with the accident.

In addition to those assumptions governed by SG initial conditions, the following additional major assumptions were made in performing the dose calculations: (1) the guidance of NUREG-0800 (Section 15.6.3) is used, (2) There is no failed fuel due to the tube rupture, (3) The radioactive releases from the three SGs are released directly to the environment and the faulted SG is isolated 30 minutes after initiation of the accident, (4) steam sump to the main condenser is not available, i.e., offsite power is unavailable, and (5) concurrent iodine spike appearance rates and duration are assumed which are bonding for the NA-1&2 uprated core conditions.

Models were used which separately track the release to the environment from each source of radioactive material. This includes the initial RCS coolant activity transferred to the faulted SG by way of the break and to the unfaulted SGs by way of primary-to-secondary leakage, the initial SG secondary coolant activity (liquid and vapor) and the iodine spike activity. Each source was followed along its path leading to ultimate release. Separate thyroid, gamma and beta doses were calculated from these sources for the Exclusion Area Boundary (EAB) and the Low Population Zone (LPZ). The results of the licensee's calculations are summarized in Tables 6 and 7.

Table 6. North Anna steam generator tube rupture (based on DFRP modifications) comparison of calculated dose to limits

Integrated thyroid dose at EAB (REM)			
	Calculated Result	SRP Section 15.6.3 Acceptance Guideline	10 CFR 100 Limit
UFSAR Case	0.38	Not Addressed	300
Case 1 - SGTR with 1% failed fuel/no iodine spike	1.77	Not Addressed	300
Case 2 - SGTR with pre-accident iodine spike (most limiting)	26.7	300	300
Case 3 - SGTR with concurrent iodine spike	1.52	30	300

Table 7 Integrated whole body dose at EAB (REM)

	Calculated Result	SRP Section 15.6.3 Acceptance Guideline	10 CFR 100 Limit
UFSAR Case	0.36	Not Addressed	25
Case 1 - SGTR with 1% failed fuel/no iodine spike	0.297	Not Addressed	25
Case 2 - SGTR with pre-accident iodine spike (most limiting)	0.119	25	15
Case 3 - SGTR with concurrent iodine spike	0.081	2.5	25

The staff has analyzed the SGTR event with DFRP modifications in accordance with Standard Review Plan Section 15.6.3. The pre-accident iodine spike case is most limiting; but even in this case the thyroid dose at the EAB is less than 30 rems, which is well below the acceptance criterion of 300 rems. In addition, the whole-body dose and the LPZ doses are less than 1 rem. The staff concludes that the acceptance criteria of NUREG-0800 and the requirements of 10 CFR Part 100 are met. Therefore, the SG DFRP design changes are acceptable for operation at all power levels.

6 STAFF FINDINGS

1. The eddy current test program encompassed all unplugged tubes in the SGs in both the hot and cold leg sides. The test equipment and probes and data analysis techniques were fully state-of-the-art and appropriate for the intended application; namely, the detection of cracks at the tube support plates and tubesheet and in particular, circumferential fatigue cracks at the seventh support plate. The additional training given to data evaluators (focusing on the North Anna circumstances) and the independent data analyses by different data evaluators using different data analysis equipment provide added assurance that the inspection program identified all tubes with potentially significant indications.

2. The presence of clearly identifiable fatigue striations as well as other features associated with fatigue leaves no doubt that the failure of R9-C51 was caused by fatigue.
3. The possibility that intergranular attack (IGA) may have contributed to fatigue crack initiation cannot be entirely discounted in view of small (1 or 2 grains) IGA penetrations observed as close as 4 mils from the fracture surface. Qualitatively, any such influence would be in the direction of reducing the alternating stress needed to initiate a fatigue crack over a given period time, but there is no data available to quantify this effect. Even if an IGA influence is assumed, however, it in no way detracts from the effectiveness of the corrective actions being taken to reduce alternating stress levels and the corresponding potential for fatigue, and thus does not affect the conclusions of this SE.
4. An independent calculation by one of the NRC staff consultants was consistent with Westinghouse's conclusion regarding the presence of a mean stress of approximately yield stress at the location of crack initiation. This calculation utilized a model for stress intensity factor (K) in a thin-walled tube containing a thumbnail crack initiating from the OD (Reference 10). The solution for K does not include the effects of bending, but is judged to be applicable to the conditions under consideration for very shallow crack depths where the axial stress gradient is small. Based on an assumed crack depth of 0.0025 inch and a K max equal to $4 \text{ Ksi} \sqrt{\text{in.}}$, this model predicts a "far field" stress of [], which is very close to the yield strength of the tube R9-C51 material. The K max assumption is consistent with the fractographic evidence observed by the consultant on the failed tube near the crack origin.
5. The 4 to 10 Ksi alternating stress estimate by Westinghouse for tube R9-C51 appears reasonable. The fatigue crack is estimated by the staff to have initiated over a period of between 3 and 9 years based on the length of time the requisite denting at the seventh support plate was present. (This is based on the fact that denting was first observed at North Anna Unit 1 in 1979 and reportedly has been arrested since at least

1984). Upon initiation, the crack propagated very rapidly (over a period of just a few days) to failure. Thus, the fact that eddy current testing revealed no other tubes with circumferential cracks at the seventh support plate is not surprising.

6. Fluidelastic instability has reasonably been established as the only credible mechanism for producing displacements of sufficient magnitude to cause a fatigue failure. Further, it has reasonably been demonstrated that such an instability is possible within the uncertainties of key parameters such as damping, velocity peaking factors, stability constant, and natural frequency cited by Westinghouse.
7. Given the complexity of the problem (e.g., two phase flow, U-tubes, denting) and the associated uncertainties, the Westinghouse analyses conducted with ATHOS AND FLOVIB provide only "ballpark estimates" of the response amplitudes and instability thresholds. Absolute values of predicted critical velocities and displacement amplitudes in the instability region incorporate significant uncertainty. However, the results of these analyses are appropriate for the use that Westinghouse has made of them; namely to examine trends, to develop relationships between changes in stability ratio and resulting changes in displacement and alternating stress response, and to evaluate relative improvements associated with installation of the downcomer flow resistance plate.
8. The predicted 8% to 22% reduction in stability ratio associated with the DFRP is judged to be reasonable since, again, it is the relative change in stability ratio that is of interest. Pertinent parameters, such as density and effective flow velocities, are calculated by the same method for both the pre-modification and post-modification conditions, thus minimizing the impact of any uncertainties regarding the values of these parameters. Predictions regarding the percent reduction in displacement and alternating stress are considered to be reasonable since they are based on conservative values of the fluidelastic response curve slopes.

9. Because the pre-modification stability ratio of tube R9-C51 is very uncertain, the 8% to 22% reduction in stability ratio associated with the DFRP and the additional 14% to 20% reduction associated with the preventive plugging of "susceptible tubes" in rows 9, 10, and 11 may or may not be sufficient to reduce the maximum stability ratio to less than 1.0. Even if the stability ratio exceeds 1.0, however, the expected reductions in displacement, alternating stress, and rate of fatigue usage accumulation are considered by the staff to be sufficient to preclude another fatigue failure in the future.

10. Apart from tube R9-C51 which failed, it is entirely possible that other tubes in row 9, 10, or 11 which may not have been effectively supported by AVBs and which may have been subject to locally high flow velocities may have developed significant fatigue usage factors at the time of the R9-C51 failure. Although installation of the DFRP is expected to significantly reduce the rate of future fatigue usage accumulation, it does nothing to mitigate fatigue usage which may have already have accumulated to date. Thus, actions taken to preventively plug susceptible tubes may be even more important than the DFRP in preventing future fatigue failures. Assuming that all susceptible tubes in rows 9, 10, and 11 have been plugged and considering that stability ratios for row 8 tubes are at least 14% to 20% less than that for R9-C51, the staff estimates that the fatigue usage factor for the most limiting row 8 tubes have not exceeded 0.03 to date, which is well within acceptable limits. Furthermore, assuming a stability ratio reduction of 8% as a result of the DFRP installation, the staff estimates that fatigue usage for row 8 tubes will exhibit negligible incremental increase during the remaining 31 years of plant life.

11. During a meeting with the staff on November 4, 1987 (Reference 13), Westinghouse reported that recent test results indicate that the flow peaking factor for tube R9-C51 may have exceeded 30%, compared to the 15% assumed in Reference 4. This information suggests that flow peaking factors may have played a more important role, and damping ratio uncertainties a less important role in contributing to the tube rupture than was indicated in Reference 4. This new information is currently being reviewed by the staff.

However, assuming this information to be valid, stability ratio reductions associated with preventive plugging would be expected by the staff to be higher than the 14% to 20% estimated by Westinghouse in Reference 4, since preventive plugging would be expected to significantly reduce flow peaking. The staff concludes that the overall stability ratio reductions estimated by Westinghouse in Reference 4, based on the corrective actions implemented by the licensee, are conservative.

12. Actions taken by the licensee to augment its preventive plugging program to address staff concerns, as discussed in Section 5.2, are considered acceptable by the staff and provide added assurance that tubes without fully effective AVB supports in rows 9, 10, and 11 have been removed from service.
13. The use of the sentinel plug for "susceptible tubes" precludes a recurrence of the Ginna syndrome (NUREG-916); namely, fracture of a tube subsequent to its being plugged, leading to damage and perhaps rupture of adjacent unplugged tubes without prior indication of primary-to-secondary leakage. Because the population of tubes with the sentinel plug includes the tubes in the bundle most susceptible to large amplitude vibration, any future fatigue cracks would likely affect tubes in this population producing detectable but small, controlled leakage before affecting non-plugged tubes. Thus, the tubes with sentinel plugs installed will also serve as a long-term indication of the effectiveness of DFRP minimizing large amplitude vibrations and alternating stress levels.
14. Stabilization of tube R9-C51 on the cold leg side has been determined to be acceptable based on physical tests and computer analyses. The analyses have determined that the jointed spear which was inserted in the R9-C51 cold leg remnant above the seventh support plate level meets design bases operational and transient-induced forces. In addition, damping will be higher and thus reduce the loadings and susceptibility of the spear stabilization mechanism to any fatigue failure. For the hot leg side, the design and use of the flexible steel cable design has previously been tested, qualified, and used at other facilities. Finally, for the cold leg side,

tubes adjacent to tube R9-C51 have been plugged with sentinel tubes to mitigate the impact of unlikely wear on neighboring tubes. Based on the above, the staff finds that the stabilization analyses and techniques used are acceptable to stabilize the R9-C51 tube remnant on both the cold and hot leg side.

15. The staff has evaluated licensee capabilities and procedures for monitoring primary-to-secondary leakage, and participated in an onsite walk-through of a 4 hour surveillance cycle and trending analysis. The staff finds that the licensee has substantially improved its capabilities to detect and monitor low level primary-to-secondary leakage, which could potentially be a precursor to a similar tube rupture in the future. The licensee has adopted an administrative limit of 100 gpd, which is significantly more restrictive than the standard Technical Specification limit of 500 gpd and which provides added assurance that the plant will be shut down in a timely fashion before a leaking through-wall crack can propagate to failure.
16. The SG DFRP design and installation have been performed in such a manner that there is no increase in the probability of accidents. The effects of this modification upon existing accident analyses have been investigated. Each accident continues to meet its applicable acceptance criteria. A reanalysis of the SGTR accident analysis has resulted in a calculated offsite dose greater than currently reported in the NA-1&2 UFSAR for core power greater than 59% of rated thermal power. This increase is not significant because the revised dose remains a small fraction of the 10 CFR Part 100 limits and meets the guidelines of NUREG-0800 (Section 15.6.3). No new accident types or equipment malfunction scenarios will be introduced as a result of the DFRP modification. The original design of the plant included such plates in the SGs. Therefore, operation with this modification does not create the possibility of an accident of a different type from any evaluated previously in the NA-1&2 UFSAR. There is no significant reduction in the margin of safety. An evaluation of NA-1&2 UFSAR accidents has concluded that the existing analyses continue to meet their acceptance criteria for operation with the SG modification. The

present margin of safety for the SGTR (as defined in the basis for the NA-1&2 TS 3/4.4.8) has also been maintained, since the revised dose remains a small fraction of the appropriate 10 CFR Part 100 limits. Therefore, based on all of the above, the staff finds the NA-1 SG DFRP modifications to be acceptable for operation at all power levels.

7 CONCLUSIONS

Based on the above evaluation, the staff finds that the licensee has (1) adequately demonstrated the primary failure mechanism leading to the July 15, 1987 SGTR event to be fatigue caused by flow-induced vibration, (2) adequately identified the major causal factors leading to this event, and (3) implemented acceptable diagnostic and corrective measures to prevent a similar fatigue failure in future. The staff concludes that the SGs have been restored to an acceptable condition from an SG tube integrity standpoint and that the plant can be operated at 100% power without undue risk to the public health and safety.

REFERENCES

1. Letter dated September 15, 1987, from W. L. Stewart, VEPCO, to Director of Nuclear Reactor Regulation, NRC, Accession No. 8709160239.
2. VEPCO Report, "North Anna Unit 1 July 15, 1987, Steam Generator Tube Rupture Event Report," September 15, 1987, Revision 1. (This report is docketed as part of Reference 1 above.)
3. Letter dated September 25, 1987 from W. L. Stewart, VEPCO, to Director of Nuclear Reactor Regulation, NRC, Accession No. 8709290377.
4. Westinghouse Report WCAP-11601 (Proprietary Version) and WCAP-11602 (Non-Proprietary Version), "North Anna Unit 1 Steam Generator Tube Rupture and Remedial Actions Technical Evaluation," September 1987. NRC Accession Nos. 8710050087 and 8710050084.

5. NRC Augmented Inspection Team (AIT) Report Nos. 50-338/87-24 and 50-339/87-24, Inspection Conducted July 15-August 14, 1987, NRC Accession No. 8709040277.
6. USNRC Inspection Report No. 50-338/87-28, August 10-14, 1987, NRC Accession No. 8709090321.
7. USNRC Inspection Report No. 50-338/87-31, August 31-September 4, 1987.
8. Bates, R. C. and Clark, W. G., Jr., Transactions of the American Society for Metals, Vol. 62, 1969, p. 380.
9. Westinghouse presentation to NRC staff and VEPCO on August 17, 1987, at Westinghouse Research Center, Pittsburgh.
10. NRC consultant's report authored by R. G. Ballinger, "North Anna #1, Steam Generator, Row 9, Column 51 Tube Failure Analysis," October 19, 1987.
11. [
- 12.
-].
13. Westinghouse letter NS-NRC-87-3285, dated November 2, 1987, to NRC. "Slide Presentation Material of November 4, 1987" (Proprietary Information).

Dated: December 11, 1987

Principal Contributors:

E. Murphy
 H. Conrad
 A. Gill
 C. Willis
 L. Engle